Receiving Basin Substrate Controls on Delta Morphodynamics

being a thesis submitted for the Degree of

Doctor of Philosophy

in the University of Hull

by

Joshua Edward Johnson, MSci.

June 2022

Abstract

Deltas are inhabited by hundreds of millions of people and are critical for food security, coastal defence, carbon sequestration and ecological diversity. These intrinsically vulnerable systems are threatened by an array of anthropogenic pressures, such as accelerated sea level rise, enhanced subsidence due to sub-surface fluid extraction, retention of sediment within upstream reservoirs and levee construction isolating the delta floodplain from sediment deposition. This study investigates how delta morphodynamics are influenced by the resistance of the sediment making up the receiving basin substrate, and how these effects evolve in the face of anthropogenic forcing of relative sea level and sediment supply loss.

Numerical modelling using Delft3d_flow found bed sediment erodibility w to be a strong driver of delta land area, elevation, distributary channel geometry and channel mobility, with the potential to overcome or modulate the effects of fluvial sediment. Substrate fine sediment content was found to be dominant in setting channel mobility, but the cohesive strength of the fine sediment was dominant in setting channel depth, width:depth ratio and subaerial land area. Fieldwork in the Wax Lake Delta, Louisiana, a sediment limited delta underlain by erosion resistant fine sediment, utilised multibeam echosounder and acoustic doppler current profiler to collect high resolution bathymetric and velocimetric data. This highlighted that substrate type and sediment supply could cause delta bifurcations to be stable under flow conditions different to those dictated to produce stable bifurcations by previous studies.

This work highlights that the effects of substrate sediment on delta morphodynamics cannot be neglected if their reaction to current and future anthropogenic forcing is to be accurately predicted and demonstrates the desperate need for further work constraining the effects of channel bed erodibility on bifurcation dynamics, as well as field studies to quantify the properties of sediment underlying modern and ancient deltas.

Acknowledgements

Firstly I would like to thank my supervisors: Dan Parsons, for providing the opportunities and encouragement to pursue the areas of research I found most interesting; Chris Hackney, for his valuable mentorship, and the many read-throughs of this Thesis; and Tom Coulthard, Doug Edmonds and Jim Best for their valuable insight and the illuminating discussions about this project we've had.

Secondly, I want to thank all my friends and colleagues, both current and past, in the EEI and Department of Geography, who have made the University an inspiring and enjoyable place to work over the last five years. In particular I would like to thank Josh Ahmed, for frequently getting me out of the office and into the field, and making sure I didn't spend too much time working on my PhD, and Flo Halstead, for the vital encouragement to keep going during the difficult final months of writing.

I would also like to thank those who organised, assisted or were otherwise vital to the 2018 and 2020 field trips to the Wax Lake delta; Chris Hackney (who organised and lead both campaigns), Doug Edmonds, Elizabeth Oliver and Connor Broadus.

I would like to thank Sophie Steward for her support, patience and understanding over the last four years. I'd like to thank my family, particularly my parents and sister, for providing a place to escape the world of academia when I needed it, and their constant encouragement and belief that I'd finish this Thesis. Finally, I'd wish to thank Heather Chung for her support and optimism that I'd finally finish the corrections for this thesis.

This project was funded as part of the Geostick project (European Research council grant - ERC-2016-COG, Project ID: 725955). The 2018 and 2020 field campaigns to Wax Lake Delta were funded through a Royal Society International Exchanges Grant (IES\R2\170218) gained by Chris Hackney.

List of symbols

$\mathbf{u,v}$	Horizontal velocity components
$\mathbf{x,y}$	Horizontal distance components
$\mathbf{t}$	Time
$\mathbf{\sigma}$	Vertical coordinate, normalised to depth (-1 to 0)
$\mathbf{h}$	Water depth
$\mathbf{\omega}$	Vertical velocity in σ coordinate system
$\mathbf{w}$	Vertical sediment settling velocity
$\mathbf{f}$	Coriolis Coefficient
$\mathbf{P}$	Pressure
$\mathbf{P_{x,y}}$	Horizontal pressure
$\mathbf{F_{x,y}}$	Horizontal Reynolds stresses
$\mathbf{M_{x,y}}$	Momentum from external sources or sinks
$\mathbf{\nu_V}$, $\mathbf{\nu_H}$	Vertical, Horizontal kinematic viscosity
$\mathbf{Q}$	Water Discharge
$\mathbf{q_b}$, $\mathbf{q_s}$	Sediment Discharge, Bedload and Suspended load
$\mathbf{\rho}$	Water density
$\mathbf{\rho_s}$	Sediment specific density
$\mathbf{g}$	Acceleration due to gravity
$\mathbf{\zeta}$	Water surface height
$\mathbf{S}$	External addition or removal of water (Precipitation, evaporation etc.) per unit area

$D_{V,H}$	Diffusivity, vertical and horizontal
c	Sediment concentration
d_{50}	Median grain diameter
D_*	Dimensionless particle size
τ	Bed shear stress
τ_{cr}	Critical shear stress for erosion
τ_{cs}	Critical shear stress for deposition
$\alpha_{1,2}$	Correction factors for sediment concentration

Table of Contents

1 Introduction

Deltas form a vital part of coastal environments, and are occupied by hundreds of millions of people worldwide (Syvitski et al., 2009; Syvitski and Saito, 2007). Deltas are highly agriculturally productive; for example the Mekong delta, which contains 40% of Vietnam's cultivated land and produces much of the countries food (>50% of its rice, 60% of its fish and shrimp and 80% of its fruit (Warner, 2010)), occupies only 49000 km^2 (Syvitski and Saito, 2007) which is less than 15% of Vietnam's land surface. The Nile delta compromises only 2% of Egypt's surface but hosts 63% of the country's agricultural land (Hereher, 2010). The seasonal flooding of these delta lands is known to enhance the fertility through delivering and depositing millions of dollars a year of nutrients attached to sediments carried by the floodwaters (Chapman et al., 2017).

Deltas also host significant areas of wetland (Wester et al., 2018) which are known to provide a range of important ecosystem services and supporting a range of biodiversity. Mitsch and Gossilink (2015) found that 95% of fish stocks in USA are dependent on wetlands. Greater wetland continuity provides flood protection through reducing storm surge levels (Barbier et al., 2013). Mangroves, a form of wetland present on many tropical deltas, increase the resilience of coastal settlements against the impacts of cyclones (Das and Vincent, 2009), and can reduce the power of tsunamis significantly if sufficiently dense (Danielsen et al., 2005).

In their study of thirty-three major deltas, Syvitski et al. (2009) found that there was a combined delta area of 26,000km^2 below mean sea level, and 96,000km^2 within 2m of sea level. Due to their low lying nature many delta areas are under threat from sea level rise (Van de Lageweg and Slangen, 2017) as well as human influences on flow, sediment flux and subsidence across the delta plain (Syvitski and Saito, 2007). Ericson et al. (2006) found that, across 40 studied deltas, current rates of subsidence and sea level rise could expose 28,000km^2 and 8.7 million people to coastal inundation and erosion by 2050.

Deltas are active, dynamic systems, with water and sediment entering and leaving constantly. The balance between these inward and outward fluxes is critical for the sustainability of the delta, and must be sufficiently positive to counter subsidence (Ericson et al., 2006). The mass balance of a delta is controlled primarily by the relationship between incoming and outgoing sediment:

$$\Delta \text{ Sediment stored} = \text{Fluvial sediment input} - \text{Sediment bypass} - \text{Sediment erosion} \pm \text{Longshore sediment transport} \quad \text{(Equation 1-1)}$$

Fluvial sediment input is the sediment supplied to the delta system by its feeder channel, sourced from erosion higher in the catchment, while sediment erosion is the removal of sediment from the delta front by basinal processes or

entrainment in the fluvial flow exported to the coastal sea. Sediment bypass represents the amount of the fluvial input that is never deposited in the system, but is instead washed out into deeper water. Longshore transport represents sediment fluxed to or from the delta from adjacent coastal sediment sources or sinks.

In many parts of the world sediment fluxed by rivers towards coastal areas has been significantly reduced by human actions such as sand mining (Hackney et al., 2020), reservoir construction (Dethier et al., 2022) and land use change. Together, Dunn *et al.* (2019) estimated that this could reduce sediment reaching deltas by an average of 38% by the end of the century. This is already resulting in loss of coastal land in some deltas for example the Mekong Delta (Liu et al., 2017) and the Nile (Frihy and Lawrence, 2004), and is likely to lead to even faster losses in the future (Ericson et al., 2006), particularly as a result of eustatic sea-level rise.

Even when sediment reaches a delta, a number of factors affect how much of that sediment is deposited and stored within the delta. Deltas with morphodynamic processes that enable sediment transport, such as channels that are large and stable, can deliver this sediment straight to deeper water where it is less effective at building land (Kim et al., 2009). On the other hand, deltas with morphodynamic processes conducive of deposition likely build more subaerial land with the same amount of sediment. Factors that increase the retention of sediment include diffuse river-mouth sediment plumes that deposit

sediment near the shore (Edmonds, 2012), and frequently avulsing channels with low and/or weak levees that enable overland flow which leads to subaerial deposition (Caldwell and Edmonds, 2014) on and across the delta top.

The vulnerability of delta systems to human influences on sediment delivery means it is important to have an understanding of how sediment that does reach the delta is stored, transported and eroded. The morphodynamics of deltas was categorized historically in terms of wave, tide, and fluvial end members (Galloway, 1975). While waves (Tamura et al., 2012; Bhattacharya and Giosan, 2003) and tides (McLachlan et al., 2017; Shaw and Mohrig, 2014; Geleynse et al., 2011) have effects on delta morphology, Wright (1977) found the dynamics of the fluvial effluent plume at a channel mouth to be a vital influence on how sediment was deposited. Edmonds and Slingerland (2007) studied how the dynamics of the river mouth jet effected the formation of mouth bars, and hence overall delta morphology. They found that greater channel depth caused the forming mouth bar to prograde (move basinward, with the flow direction) further before stagnating and aggrading vertically until it became a bifurcation. Canestrelli *et al.* (2014) also found channel geometry to be important to delta morphology. They argued that a higher stability number, *S*, (a function of channel W/D Ratio) made the formation of a mouth bar more likely, while a low *S* favours the formation of channel levees.

Orton and Reading (1993), where among the first to include sediment grain size into a three-way classification (**Figure 1-1**), arguing that sediment grain size

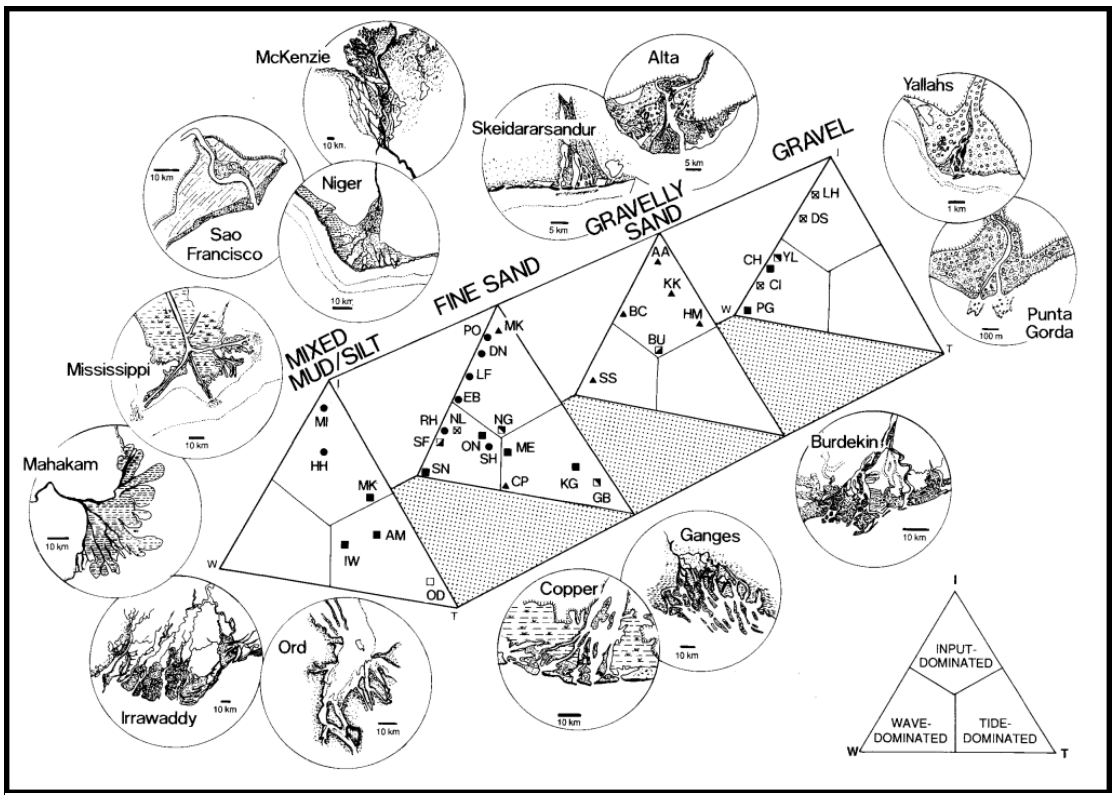

Figure 1-1: *Orton and Reading's (1993) extended ternary diagram, including sediment size as well as tidal, wave and fluvial influences. Example deltas are plotted on the diagrams with the following abrreviations: AA: Aalta, AM: Amazon, BC: Bella Coola, BU: Burdekin, CH: Chao Pharya, CI: Colorado, CP: Copper, DN: Danube, DS: Dead sea, EB: Ebro, GB: Ganges/ Brahmaputra, HH: Huanghe (Yellow), HM: Homathko, IW: Irrawaddy, KG: Klang, KK: Klinaklini, LF: Lafourche, LH: Liaohe, MA: Mahakam, ME: Mekong, MI: Mississippi, MK: MacKenzie, NG: Niger, NL: Nile, OD: Ord, ON: Orinoco, PG: Punta Gorda, PO: Po, RH: Rhene, SF: Sao Francisco, SH: Shoalhaven, SN: Senegal, SS: Skeidararsandur, YL: Yallahsi.*

modulates the effects of the above physical processes. Since then, multiple studies have focused on the role that grain size and the cohesivity of fluvial sediment play in determining on delta characteristics. Edmonds and Slingerland (2010) used a numerical model to show how a more cohesive fluvial sediment input could make delta coastlines more rugose by stabilising forming mouth bars and levees. Other numerical studies have found that sediment grain size and cohesivity can influence topset gradient, channel mobility and shoreline and topset rugosity (Burpee et al., 2015; Caldwell and Edmonds, 2014, discussed below in section 2.2.5). Additionally, the amount of fine cohesive sediment

within sediment has been shown to reduce the influence the height of bedforms in flows (Baas et al., 2013), and changing the nature of bedforms on the delta-top can go on to effect secondary flow characteristics and so the morphodynamics of bifurcations (Parsons et al., 2007).

As yet, however, little attention has been paid to the cohesivity and erodibility of the characteristics of the sediment on the bed of the receiving basin at the initiation of delta growth. Baas et al. (2013) identified that bedform dynamics can depend on both cohesivity within sediment beds and within sediment in the flow. Geleynse et al. (2011) found that delta channels incised more deeply into unconsolidated fine sediment. This would change the geometry of their channels which, as discussed above, is known to be important in determining morphodynamic processes and delta morphology. However, in the study of Geleynse et al. (2011), fine sediment was treated as unconsolidated (critical shear stress of erosion = 0.5 N m^{-1} and dry bed density of 500kg m^{-3}), meaning the effect of erosion resistant substrates was not investigated. Consolidated clay channel beds have been studied previously; Fola and Rennie (2010) investigated the hydraulic geometry of rivers forming over consolidated clay "bedrock", finding that *f*, the exponent relating channel depth to discharge, was higher than in alluvial channels, suggesting that the depth of channels with a consolidated bed substrate is more dependent on discharge. However, how these processes pertain to a prograding delta are unknown.

This study aims to investigate the effects of delta substrate sediment grain size and fine sediment erodibility (quantified in this study as critical shear stress of erosion, τ_{ce}, in N m^{-2}) on the morphology and morphodynamics of river deltas, as well as systematically explore how these characteristics will influence the way that deltas respond to ongoing a suite of changes in boundary conditions, including those impacted by anthropogenic driven changes such as sea-level rise and sediment supply.

1.1 Aims and Research Objectives

The overarching aim of this study is to constrain the influence that antecedent basin substrate has on morphodynamic processes in coastal river deltas. This will be achieved by exploring the following objectives:-

Objective 1: *Quantify the effect of receiving basin substrate erodibility on channel geometry, delta size and channel migration rates within prograding deltas.*

Objective 2: *Quantify how a decrease in fluvial sediment flux and changes in rates of sea level rise impact how delta distributaries interact and are influenced by their receiving basin substrates.*

Objective 3: *Assess the dynamics of deltaic channel incision and deltaic bifurcation stability in deltas with a cohesive substrates using the Wax Lake delta as a natural laboratory.*

The above objectives will be accomplished using a combination of numerical modelling in Delft3D and supporting field work to help validate model results against real world examples, as discussed below.

1.2 Thesis outline

Chapter 2 provides a literature review that summarises existing knowledge of sediment cohesivity and erodibility, and sediment controls on delta morphodynamics. This chapter also highlights the importance of the above

objectives, and the socio-economic importance, vulnerability and stability of deltas.

Chapter 3 will address Research Objective 1 using a series of modelled river deltas in Delft3D. The effects of bed erodibility is examined by changing the critical shear stress for erosion of cohesive sediment of the receiving basin substrate from 0.25 to 12.5 N m^{-2}. Morphological metrics such as channel geometry, channel mobility and delta top area are then extracted from model outputs by use of a series of algorithms in Matlab to directly quantify the how interacting with substrates of different erodibilities influences erosive processes and so the channel and macro-scale morphodynamics of the delta.

Chapter 4 addresses Research Objective 2. Further models in Delft3D, with differing bed resistances (consisting in this chapter of both the critical shear stress for erosion, and the proportion of cohesive sediment within the substrate) and fluvial sediment cohesivities are run to form a stable delta, which is then used as a baseline for studying how external forcing will affect these system's trajectories. These "base" deltas are then be exposed to varying degrees of sediment starvation from their upper boundary and/or sea level rise from their lower basin boundaries. As in chapter three, the changes in delta form and delta processes are explored by measuring channel geometries and motilities, as well as metrics representing larger scale morphology. From these, the impact of substrate composition on delta stability and resilience to anthropogenic sediment starvation are investigated.

Chapter 5 is a natural extension of Chapters 3 and 4, looking to substantiate the results of the models using the Wax Lake Delta (Louisiana, U.S.A.), which is an example of a delta that has formed over a cohesive sediment substrate. Multibeam echosounder and acoustic Doppler current profiler data are used alongside sediment samples to analyse flow and sediment partitioning and morphodynamic change. Alongside this, bedform distribution is analysed to investigate the locations of active erosion and deposition within the delta, and asses the sediment supply regime. These data are synthesised show to how the delta channels have interacted with the cohesive, resistant muds underlying the system to address Objective 3.

Chapter 6 presents a general discussion and provides a synthesis and thematic analysis of the overall findings from the thesis, drawing on the work of the above chapters and the literature.

Finally, Chapter 7 provides a short summary conclusions from the work and highlights possible future avenues for future research.

1.3 References

Barbier, E. B., Georgiou, I. Y., Enchelmeyer, B. and Reed, D. J. (2013) 'The Value of Wetlands in Protecting Southeast Louisiana from Hurricane Storm Surges', vol. 8, no. 3, pp. 1–7 [Online]. DOI: 10.1371/journal.pone.0058715.

Burpee, A. P., Slingerland, R. L., Edmonds, D. A., Parsons, D. R., Best, J. L., Cederberg, J., McGuffin, A., Caldwell, R. L., Nijhuis, A. and Royce, J. (2015) 'Grain-Size Controls On the Morphology and Internal Geometry of River-Dominated Deltas', *Journal of Sedimentary Research*, vol. 85, no. 6, pp. 699–714 [Online]. DOI: 10.2110/jsr.2015.39.

Caldwell, R. L. and Edmonds, D. A. (2014) 'The effects of sediment properties on deltaic processes and morphologies: A numerical modeling study', *Journal of Geophysical Research: Earth Surface*, vol. 119, no. 5, pp. 961–982 [Online]. DOI: 10.1002/2013JF002965.

Canestrelli, A., Nardin, W., Edmonds, D. A., Fagherazzi, S. and Slingerland, R. L. (2014) 'Importance of frictional effects and jet instability on the morphodynamics of river mouth bars and levees', *Journal of Geophysical Research: Oceans*, vol. 119, no. 1, pp. 509–522 [Online]. DOI: 10.1002/2013JC009312.

Chapman, A., Darby, S., Tompkins, E., Hackney, C., Leyland, J., Tri Van, P. D., Pham, T. V., Parsons, D. R., Aalto, R. and Nicholas, A. (2017) 'Sustainable rice cultivation in the deep flooded zones of the Vietnamese Mekong Delta', *Vietnam Journal of Science, Technology and Engineering*, vol. 59, no. 2, pp. 34–38 [Online]. DOI: 10.31276/vjste.59(2).34.

Danielsen, F., Sørensen, M. K., Olwig, M. F., Selvam, V., Burgess, N. D., Hiraishi, T., Karunagaran, V. M., Rasmussen, Michael S, Hansen, L. B., Quarto, A., Suryadiputra, N., Danielsen, F., Srensen, M. K., Olwig, M. F., Selvam, V., Parish, F., Burgess, N. D., Hiraishi, T., Karunagaran, V. M., Rasmussen, M S, Ha, B. and Qua, A. (2005) 'The Asian Tsunami: Role for Coastal Vegetation', vol. 310, p. 643.

Das, S. and Vincent, J. R. (2009) 'Mangroves protected villages and reduced death toll during Indian super cyclone SCIENCE',.

Dethier, E. N., Renshaw, C. E. and Magilligan, F. J. (2022) 'Rapid changes to global suspended sediment flux by humans', *Science*, vol. 376, pp. 1447–1452.

Dunn, F. E., Darby, S. E., Nicholls, R. J., Cohen, S., Zarfl, C. and Fekete, B. M. (2019) 'Projections of declining fluvial sediment delivery to major deltas worldwide in response to climate change and anthropogenic stress', *Environmental Research Letters*, vol. 14, no. 8 [Online]. DOI: 10.1088/1748-9326/ab304e.

Edmonds, D. A. (2012) 'Restoration sedimentology', *Nature Geoscience*, vol. 5, no. 11, pp. 758–759.

Edmonds, D. A. and Slingerland, R. L. (2007) 'Mechanics of river mouth bar formation: Implications for the morphodynamics of delta distributary networks', *Journal of Geophysical Research: Earth Surface*, vol. 112, no. 2, pp. 1–14 [Online]. DOI: 10.1029/2006JF000574.

Edmonds, D. A. and Slingerland, R. L. (2010) 'Significant effect of sediment cohesion on delta morphology', *Nature Geoscience*, vol. 3, no. 2, pp. 105–109 [Online]. DOI: 10.1038/ngeo730.

Ericson, J. P., Vörösmarty, C. J., Dingman, S. L., Ward, L. G. and Meybeck, M. (2006) 'Effective sea-level rise and deltas: Causes of change and human dimension implications', *Global and Planetary Change*, vol. 50, no. 1–2, pp. 63–82 [Online]. DOI: 10.1016/j.gloplacha.2005.07.004.

Fola, M. E. and Rennie, C. D. (2010) 'Downstream Hydraulic Geometry of Clay-Dominated Cohesive Bed Rivers', *Journal of Hydraulic Engineering*, vol. 136, no. 8, pp. 524–527 [Online]. DOI: 10.1061/(ASCE)HY.1943-7900.0000199.

Frihy, O. and Lawrence, Æ. D. (2004) 'Evolution of the modern Nile delta promontories : development of accretional features during shoreline retreat', pp. 914–931 [Online]. DOI: 10.1007/s00254-004-1103-3.

Galloway, W. E. (1975) 'Process Framework for Describing the Morphologic and

Stratigraphic Evolution of Deltaic Depositional Systems', in Broussard, M. L. (ed), *Deltas: Models for Exploration*, Houston, Texas, Houston Geological Society, pp. 87–98 [Online]. Available at http://archives.datapages.com/data/hgssp/data/022/022001/87_hgs0220087.htm.

Geleynse, N., Storms, J. E. A., Walstra, D. J. R., Jagers, H. R. A., Wang, Z. B. and Stive, M. J. F. (2011) 'Controls on river delta formation; insights from numerical modelling', *Earth and Planetary Science Letters*, Elsevier B.V., vol. 302, no. 1–2, pp. 217–226 [Online]. DOI: 10.1016/j.epsl.2010.12.013.

Hackney, C. R., Darby, S. E., Parsons, D. R., Leyland, J., Best, J. L., Aalto, R., Nicholas, A. P. and Houseago, R. C. (2020) 'River bank instability from unsustainable sand mining in the lower Mekong River', *Nature Sustainibility*, vol., no.

Hereher, M. E. (2010) 'Vulnerability of the Nile Delta to sea level rise : an assessment using remote sensing', vol. 5705 [Online]. DOI: 10.1080/19475705.2010.516912.

Kim, W., Mohrig, D., Twilley, R., Paola, C. and Parker, G. (2009) 'Is it feasible to build new land in the Mississippi River Delta?', *Eos*, vol. 90, no. 42, pp. 373–384.

Van de Lageweg, W. I. and Slangen, A. (2017) 'Predicting Dynamic Coastal Delta Change in Response to Sea-Level Rise', *Journal of Marine Science and Engineering*, vol. 5, no. 2, p. 24 [Online]. DOI: 10.3390/jmse5020024.

Liu, J. P., DeMaster, D. J., Nguyen, T. T. and Li, X. (2017) 'Stratigraphic Formation of the Mekong River Delta and Its Recent Shoreline Changes', *Oceanography*, vol. 30, no. 3, pp. 72–83 [Online]. Available at https://www.researchgate.net/publication/318351792_Stratigraphic_Formation_of_the_Mekong_River_Delta_and_Its_Recent_Shoreline_Changes.

Mitsch, W. J. and Gossilink, J. G. (2015) *Wetlands*, Fifth Edit. John Wiley & Sons.

Syvitski, J. P. M., Kettner, A. J., Overeem, I., Hutton, E. W. H., Hannon, M. T., Brakenridge, G. R., Day, J. W., Vörösmarty, C. J., Saito, Y., Giosan, L. and Nicholls, R. J. (2009) 'Sinking

deltas due to human activities', *Nature Geoscience*, vol. 2, no. 10, pp. 681–686 [Online]. DOI: 10.1038/ngeo629.

Syvitski, J. P. M. and Saito, Y. (2007) 'Morphodynamics of deltas under the influence of humans', *Global and Planetary Change*, vol. 57, no. 3–4, pp. 261–282 [Online]. DOI: 10.1016/j.gloplacha.2006.12.001.

Warner, K. (2010) 'Global environmental change and migration: Governance challenges', *Global Environmental Change*, Elsevier Ltd, vol. 20, no. 3, pp. 402–413 [Online]. DOI: 10.1016/j.gloenvcha.2009.12.001.

Wester, S. J., Grimson, R., Minotti, P. G., Booij, M. J. and Brugnach, M. (2018) 'Hydrodynamic modelling of a tidal delta wetland using an enhanced quasi-2D model', *Journal of Hydrology*, Elsevier B.V., vol. 559, pp. 315–326 [Online]. DOI: 10.1016/j.jhydrol.2018.02.014.

Wright, L. D. (1977) 'Sediment transport and deposition at river mouths: A synthesis', *Geological Soceity of America Bulletin*, vol. 88, no. 6, pp. 857–868.

2 Literature Review

2.1 Cohesivity and Erodibility

The process of erosion is fundamental to any fluvial system, even systems like deltas that were originally considered to be controlled mainly by deposition (Shaw and Mohrig, 2014a). Erosion dictates the rate at which sediment is removed from the system (see Equation 1-1) so plays a major part in determining the mass balance of a delta. The rate of erosion is dictated by a balance between the erosive power of the fluvial or wave system and the erodibility of the sediment bed.

Erodibility in sediments is commonly measured in terms of a minimum or critical shear stress (τ_{ce}) or velocity needed to mobilise the sediment into a flow. In non-cohesive sediment, the τ_{ce} of sediments in controlled by grain size and density, as well as the relative exposure of the of the particle to the flow, commonly quantified as protrusion above-, or 'hiding' behind- other grains (Andrews, 1983). These factors combine to influence the balance of forces acting on a single grain: lift, drag and gravity (Yang et al., 2010). These particles are assumed to initiate motion when the dimensionless bed shear stress exceeds the particle's dimensionless critical shear stress, τ_{c*}. τ_{c*} is usually derived empirically from the Shields Curve (Shields, 1936).

The way in which the grains are structured also influences the erodibility of a sediment; closely packed grains with a high area of contact between them are less erodible than those separated by water or finer sediments (Grabowski et al.,

2011). In sediment beds with multiple grain sizes, the surface can become 'armoured' or enriched in larger (hence less easily entrained) sediment, which protects the finer sediment below from being eroded through the hiding effect (Raudkivi, 1998), whereby large particles reduce the fluid forces acting on nearby smaller particles (Andrews, 1983).

Another way in which sediment beds resist erosion is the presence of cohesivity. In finer sediments, the grain size and weight are less important compared to electrochemical forces between grain surfaces (Raudkivi, 1998). Cohesive sediment has widely been defined as sediment with a diameter <64μm. However, Van Ledden et al. (2004) argued that sediment with diameter <4μm (clays) was a more useful distinction for determining the cohesivity of a sediment bed. Even in non-cohesive sediments, Van Ledden et al. (2004) found that a clay content of 5-10% is sufficient cause cohesive behaviour in entire substrates.

However, it is important to consider that many factors can affect the cohesivity of a sediment beyond clay content. The cohesivity of clay is variable between different clay minerals (Mitchell and Soga, 2005). The chemistry of the surrounding environment can also be an important factor in determining the potency of clay. Increasing salinity has been shown to make sediments with higher clay content harder to erode (more cohesive) (Aberle et al., 2004). The $\boldsymbol{\tau}_{ce}$ of clay has also been shown to respond other water chemistry factors, such as Sodium Adsorption Ratio (SAR), the ratio between Sodium cation and Calcium and Magnesium cation content of the water around the sediment. The clay minerals Montmorillonite and Illite were both found to have a $\boldsymbol{\tau}_{ce}$ that decreased with increasing SAR (Grabowski et al., 2011).

There are also a number of biological factors that can increase the cohesivity of a sediment. Land et al. (2012) showed that the presence of organic matter within fine sediment helped clay particles bind together into larger aggregates. In any kind of sediment, the presence of bacteria and other single-celled organisms can greatly enhance cohesion. Neumeier et al. (2006) found that biofilms on the surface of sediments can increase the τ_{ce} by 3-10 times. Bacterial extracellular polymeric substances (EPS) are also well known to increase cohesivity when they are dispersed throughout a sediment bed. Dade et al. (1990) found that even small concentrations (~100 nmol) was sufficient to almost double critical fluid velocity necessary for erosion. Similar effects have been replicated using isolated bacterial EPS in the form of Xanthan gum (Tolhurst et al., 2002).

Consolidation or compaction of sediments is the process by in which loose sediment expels pore fluids and decreases its pore space, resulting in an increased bulk density. The bulk density of sediments has been shown to have a positive correlation with τ_{ce} in both tidal flats (Amos et al., 2004) and estuaries (Bale et al., 2007). Because of this, τ_{ce} is commonly a function of depth, increasing quickly in the shallow layers before approaching an asymptote at depth (Rinehimer et al., 2008). As such, fine sediments that have undergone burial then been re-exposed will likely be less erodible then freshly deposited sediments. As with cohesivity, compressibility and reaction to compression vary between different clays (Mitchell and Soga, 2005).

As a result of this, τ_{ce} has been found to vary by a large amount in fine cohesive sediments. Lau and Droppo (2000) showed that freshly deposited clay sediment could have τ_{ce} as low as 0.031Nm^{-2}. Joensuu *et al.* (2018) found

sediments with τ_{ce} = 0.39-1.39Nm^{-2} in their survey of subtidal coastal sediments, and (Fola and Rennie, 2010) found glaciomarine deposits with τ_{ce} = 6-20 Nm^{-2} underlying rivers in western Ontario.

2.2 Effects of Sediment Qualities on Delta Morphodynamics

2.2.1 *Catchment and basin drivers*

The effects of erodible beds on river system morphodynamics have been studied in detail in inland rivers. Cohesivity in terrestrial river banks (Ferguson, 1987) and fluvial load (Van Dijk et al., 2013) has been shown to be important in controlling the transition from braided to meandering planform channel pattern behaviour. Ebisa-Fola and Rennie (2010) found that rivers incising into consolidated glaciomarine clay beds have higher depth exponents (i.e. depth increasing more strongly with greater discharge), than those flowing across erodible material.

The modelling study of Geleynse et al. (2011) showed fine unconsolidated sediment beds allow greater incision by channels that flow over them. The amount of incision can control flow dynamics at the channel mouth by changing the geometry of the channel; cross-sectional geometry is known to affect the stability of river mouth jets (Caldwell and Edmonds, 2014), and channel depth has been shown by Edmonds and Slingerland (2007) to be a fundamental control on the formation process of mouth bars (see section 2.2.3). These factors can both influence the overall planform of deltas (Caldwell and Edmonds, 2014) and their resistance to erosive forces (Fagherazzi et al., 2015).

2.2.2 *Behaviour of mouth jets*

The turbulent jets found at the mouths of most rivers are usually treated as wall bounded plane jets (Rowland et al., 2009) (i.e. a flattened jet bounded on two opposite sides by parallel impermeable walls). In the case of a river mouth jet, the two "walls" are the bed of the basin in contact with the bottom of the jet and the free surface of the water in contact with the top of the jet. These jets can be split into two zones; the Zone of Flow Establishment (ZoFE) and the Zone of Established Flow (ZoEF) (see Nardin *et al.* (2013) and *Figure 2-1*). Near the mouth, in the ZoFE, the centreline velocity is constant, and the turbulence generated from shearing at the jet boundaries doesn't affect the whole flow. Further away, in the ZOEF, flow velocity at the centreline begins to decrease and the whole width of the jet is turbulent.

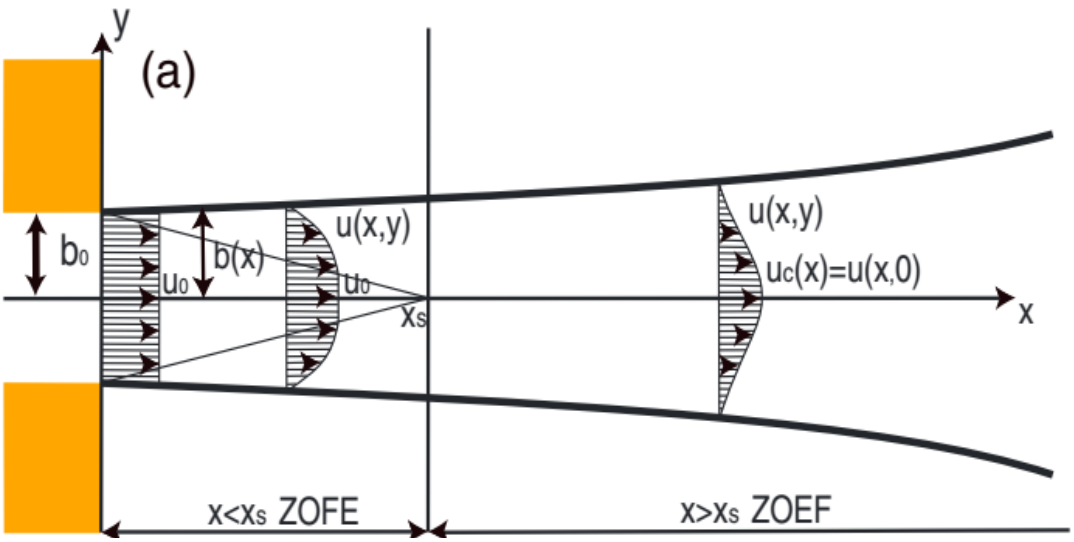

Figure 2-1: Diagram of a turbulent mouth jet [from Nardin et al. (2013)] showing transition constant centreline velocity (ZOFE) to decreasing centreline velocity (ZOEF).

Planar jets can be characterised as either stable (not changing significantly with time) or instable (changing significantly with time, commonly by

meandering) (Canestrelli et al., 2014). The stability of jets changes how sediment is deposited (see below, section 2.2.3).

The hydrodynamics at the mouth of a channel, and hence the morphological change that happens there, is controlled by the river's effluent plume, or river mouth jet (Wright, 1977), which is itself influenced by the morphology at the mouth of the channel. Due to the strong influence of mouth jets on the formation of mouth bars and levees, factors that affect their dynamics are likely to also affect overall delta morphodynamics.

Nardin et al. (2013) found that wind-waves could cause the mouth jet to spread further and the water velocity to decrease more steeply with distance from the river efflux. They also found that peak shear stresses at the bed increased as a result of the combination of wave orbital velocity and fluvial velocity. Tides have also been shown to have an effect on the mouth jet: during an ebbing tide, the combination of fluvial and tidal flow enhances the strength of the channel mouth jet, causing it to become more erosional even at low flows (Shaw and Mohrig, 2014a). Leonardi et al. (2013) found that even in weakly tidal systems, tidal energy caused more spreading of the river mouth jet, and so wider mouth bars. In more strongly tidal systems they found that the creation of trifurcations at channel mouths to be common, as the oscillating flow at the mouth prevents deposition, keeping a central channel open while depositing two bars either side of this channel that trifurcate the flow (Leonardi et al., 2013).

Sediment cohesivity from increased clay content (Baas et al., 2013) and biological polymers (Parsons et al., 2016) was found to reduce the height of bedforms in flows. This reduction in bedform height, and hence bed roughness

is likely to promote the formation of an stable, spreading jet at a river mouth (e.g. Fagherazzi et al., 2015).

2.2.3 *Mouth bar and levee formation*

River mouth bars form within the mouth jet of some channels, where sediment rich flowing water meets a still water body. The model for river mouth bar growth was formulated by (Edmonds and Slingerland, 2007). When the flow reaches a quiescent water body, the resulting spreading and reduction in flow speed of the jet causes the sediment to be deposited, and this deposition is most intense where the negative gradient in fluid velocity (hence sediment transport) is greatest. This is where the mouth bar begins to form. On the upstream bank of the forming bar effective flow depth is reduced, flow accelerates, and erosion is enhanced on the front of the bar. Meanwhile, the opposite process happens on the downstream bank of the bar: an increase in depth causes flow deceleration and enhances deposition. These processes combine to cause the mouth bar to prograde in the direction of the flow.

Edmonds and Slingerland (2007) found that when the water depth above the bar is reduced to around 40% of the original depth, the bar ceases to prograde but begins fast, runaway aggradation towards the surface. They attributed this to a sudden reduction in flow speed over the front of the bar as flow begins to divert around, rather than over it. This reduction in flow speed promotes rapid deposition on top of the bar. Esposito et al. (2013) studied these processes in the field and found them to be controlled by river stage. Systems that are at high flow can more easily deposit bedload sediment on large bars prograding them

effectively, while systems that where transitioning from high to low flow were found to drive the runaway aggradation of bars to above the water surface.

While the mouth bar is controlled strongly by the nature of the mouth jet, the nature of the sediment in the delta system has been shown to have a number of effects on mouth bar and levee evolution. The settling velocity of sediment has been shown to affect the deposition regime of a mouth jet (Mariotti et al., 2013). Sediments with settling timescales (the average time needed for a particle to settle to the bottom) much shorter than the mouth jet's eddy time scale (the average time needed for an eddy to make one half revolution), settle too fast to be moved out of the centre of the jet, so are principally deposited on the mouth bar. In jets where the sediment settling timescale is significantly longer than the eddy timescale, the turbulent eddies of the jet deposit the sediment over a wide, fan like area. Where the two timescales are close to the same, the sediment is transported out of the centre of the mouth jet, then deposited on the subaqueous levees. Settling velocity is dictated by grain size, but frequently changes for clay mineral as they flocculate (Khelifa and Hill, 2006).

Sediment cohesion is has been shown to stabilize river mouth bars and levees in the numerical modelling study of Edmonds and Slingerland (2010). They found that moderate cohesivity channels deposited mouth bars that the flow cannot erode or prograde easily, leading to frequent river bifurcations, while high cohesivity sediment led to the formation of narrow channels with focused mouth jets capable of easily eroding, and so prograding, the mouth bar with much less channel splitting. Both moderate and high cohesivity systems created levees capable of constraining the flow to channels and reducing overland flow. However in the moderate cohesivity deltas, cross-levee slopes where great

enough to cause avulsion of the channels. Esposito et al. (2013) found that fine sediment on bars could consolidate when they became subaerially exposed during periods of low flow, stabilising these features even further.

The nature of mouth bar and subaqueous levee formation has been shown to be a strong controlling factor on the large-scale morphology of a delta. Because in many cases bifurcations are fossilised mouth bars, the frequency of stable, subaerial mouth bar formation can dictate the number of bifurcations and hence the number of channels (Edmonds and Slingerland, 2010). If mouth bars prograde easily, rather than aggrading and stabilising, levees lengthen behind them to create long channels that give the delta an elongate form.

2.2.4 *Bifurcations*

Mouth bars that aggrade and stabilise sufficiently have been found to 'fossilise' and become the tips of islands around which the channel bifurcates (Edmonds and Slingerland, 2007). Delta channels with sufficient aggradation or backwater effects can also form bifurcations by partial avulsion (Kleinhans et al., 2013). Bifurcations are critical to the morphodynamics of deltas, as they can dictate how evenly sediment, especially bedload, is distributed across the delta front. The dynamics of a bifurcation are controlled by the sediment transport capabilities of each distributary (Kleinhans et al., 2013). If the distributaries are in sediment transport equilibrium (i.e., their sediment capacity is the same as the amount of sediment supplied to it) the bifurcation will stay in a stable equilibrium state. If capacity on one of the distributaries is greater than its sediment supply, it will erode, enlarge and hence increase its capacity. Inversely, if supply of sediment to a channel exceeds capacity, sediment will be deposited in that channel, reducing its size and hence its capacity. These two mechanisms

form a positive feedback that can lead to a distributary with a slight advantage increasing its capacity to capture all of the flow from the upstream channel, while the other silts up.

The distribution of sediment supply at a bifurcation can be influenced by a number of factors. A difference in upstream bed slope can cause the down-slope distributary to receive more sediment, as bed sediment is deflected down the transverse bed slope (Bolla Pittaluga et al., 2003). An upstream curve can also influence bedload distribution, as spiral flow induced by the channel curvature can deflect bed sediment towards the inside of the curve, causing the inner distributary to receive relatively more sediment and the outer to receive relatively more water (Kleinhans et al., 2008).

The stability of bifurcations is commonly assessed by comparing the upstream Shields stress (Θ, an indicator of sediment mobility) to the ratio of discharge between the two distributaries, Q_r. Bolla Pittaluga et al. (2003) used a 1-dimensional model to show that symmetrical bifurcations (where $Q_r=1$) where unstable at low Shield's stresses. Edmonds and Slingerland (2008) expanded this using a 3-dimensional model and found three different equilibrium solutions for bifurcations – one symmetric and two asymmetric – but established that only the asymmetric solutions where stable to small perturbations. (Iwantoro et al., 2021) used a 1-dimensional model to investigate the effects of channel bed slopes and sediment grainsize distribution, and found a larger range of stable conditions for asymmetric rivers than Edmonds and Slingerland (2008). The study also revealed the importance of bedload movement down transverse bed slopes to redistribute sediment towards the larger distributary.

Downstream deposition and accommodation space has also been shown to influence the stability of bifurcation. Edmonds et al. (2011) proposed a switching behaviour of some bifurcations, where reciprocating 'soft' avulsion switches the dominant flow path periodically between distributaries as channel lengthening and aggradation produce a backwater effect that makes the dominant distributary less favourable. Salter et al. (2017) found that bifurcations with very strong downstream sinks (such as a deep basin offshore) could remove the backwater effect and stop this switching behaviour. They also found that bifurcations would adjust their switching frequency to match the rate of accommodation space created by subsidence at the mouths of their distributaries.

2.2.5 *Macroscale processes*

Delta sediments naturally subside, due to unconsolidated sediments deposited on the delta becoming buried by further sedimentation and consolidating (as discussed in section 2). Even adding in the effects of tectonic subsidence in many basins, it is thought to be unlikely that subsidence rates commonly exceed a few millimetres per year (Ericson et al., 2006). However, certain anthropogenic effects can dramatically increase the rate of subsidence in deltas. Extraction of fluids from buried delta sediments reduces pore pressure and can accelerate consolidation and subsidence. Groundwater extraction is thought to be contributing 11 mm yr^{-1} of subsidence in the Mekong delta (Minderhoud et al., 2017), and in some, severe cases, 100 $mmyr^{-1}$ between 1978 and 1981 on the Chao Phraya delta in Bangkok (Lorphensri et al., 2011). Hydrocarbon extraction is also thought to be responsible for subsidence in some areas, with Liu et al. (2016) linking subsidence rates of up to 40 $mmyr^{-1}$ to

hydrocarbon exploitation on the Yellow river Delta. A similar link was also found in the Mississippi delta by Morton et al. (2006), who found subsidence rates of 8.2-18.9mm y^{-1} in areas of the Louisiana coast associated with hydrocarbon extraction.

Caldwell and Edmonds (2014), show that settling velocity of sediment is important for determining the gradient of a delta topset. Finer, slower settling sediment is deposited on average further from the channel mouth, leading to a shallower gradient. However, as the effects of clay flocculation were ignored in this study it is possible that salinity-induced flocculation and subsequent increase in settling velocity could partially counteract this, leading to steeper gradients than expected. These steeper gradients have been shown to increase the avulsion frequency of channels in deltas, which in turn increases delta front rugosity by leaving relict (inactive) channels and creating more active channel mouths though partial avulsion (Caldwell and Edmonds, 2014).

Increased sediment cohesivity is also known facilitate the formation of strong levees, which in turn limits out-of-bank overland flow (Caldwell and Edmonds, 2014; D. A. Edmonds and Slingerland, 2010). Overland flow is beneficial for deltas, as it is a mechanism in which sediment is deposited on top of otherwise subsiding delta tops. In the Mekong River Delta, this deposition of sediment has been found to deliver the nutrient equivalent of half the annually applied fertilizer to agricultural areas (Manh et al., 2014). However, in deltas with substantial levees, channels become long and stable, and so much of the sediment bypasses the delta topset (Kim, Mohrig, et al., 2009). Fine sediment is also more likely to bypass the delta topset because it is transported as suspended sediment rather than bedload (van der Vegt et al., 2016).

2.2.6 *Bedform Dynamics*

Deltas form over a variety of substrates, and while this is frequently poorly characterised in literature, some deltas are known to have their channel bottoms in direct contact with consolidated cohesive material that acts effectively as bedrock across most of their channel beds (Shaw and Mohrig, 2014a), while others flow over more mobile sand or gravel beds (Dong et al., 2019).

Deltaic channels often contain sand-mud mixtures of sediment which form bedforms over a range of flow conditions (Parsons et al., 2016). These alluvial channels (i.e. ones with loose sediment rather than bedrock on their beds) frequently develop bedforms as a result of the unstable interaction between the bed, sediment transport and water flow (Andreotti et al., 2012). Where a large part of the bed is immobile, sediment-starved bedforms such as barcan dunes and sand ribbons form (Kleinhans et al., 1999). This bed immobility could be a result of large grainsizes that are too large to be moved by flows, solid bedrock, or by material cohesive and/or consolidated enough to act as bedrock (Shaw and Mohrig, 2014). In channels with varying discharge, multiple size classes of bedforms can co-exist, with different size classes active at different discharges (Duţu et al., 2018)

Bedforms are present within meanders and bifurcations on delta tops, and can influence delta morphodynamics through changing the secondary flow characteristics of those bifurcations (Parsons et al., 2007) or meanders (Abad et al., 2013) and so are capable of changing the sediment and flow dynamics of the delta at these critical points. Equally, meanders can alter the shapes and sizes of bedforms moving through them, as the flow changes direction, speed and sediment transport capacity through the meander (Nittrouer et al., 2008).

Additionally, it is known that bifurcation stability can be influenced by upstream roughness, (Edmonds and Slingerland, 2008) which is commonly a result of bedforms. As such, the stability of symmetric bifurcations has been shown to increase at relatively small Shields stresses (as dunes grow in the bifurcation), whereas it decreases at high Shields stresses (as dunes shrink from erosion in the bifurcation; Jing and Qin, 2023)

As with larger scale delta processes and landforms, bedforms are known to be influenced by sediment cohesivity. Baas *et al.* (2013) identified that bedform dynamics depended on both cohesivity within the bed, and amount of cohesive sediment in the flow. Where cohesive forces in the bed dominate, erosional bedforms are common, fine sediment is winnowed out of the moving bedforms and bedforms tend to be smaller with increasing bed cohesive sediment (Baas et al., 2013). When the amount of cohesive sediment in the flow is high, however, depositional forces dominate, and bedforms increase in size with increasing cohesive content in the flow (Baas et al., 2009). Winnowing is also less common, so bedforms tend to be richer in fine sediment. (Baas et al., 2013)

2.3 The importance and vulnerabilities of deltas

2.3.1 *Ecological and Socio-Economic importance*

Many deltas, especially those that are less influenced by human alteration, are ecologically important. The wetlands present on deltas are important for a variety of wildlife including water birds (Herzka et al., 2013) and function as nurseries for fish and marine invertebrates (Zhang et al., 2016; Boesch and Turner, 1984).

Coastal wetlands common on deltas have also been found to increase the resilience the area to coastal natural hazards (Shepard et al., 2011). Coastal wetlands on US coast where estimated to provide USD23.2 billion yr^{-1} in storm protection services by Costanza et al. (2008), by absorbing the energy of storms, and hence the damage caused by them. Barbier et al. (2013) found that continuous wetland in the path of a storm surge could reduce surge height by 10^{-3} m/m, equivalent to a metre reduction in surge height from passing through a 1 km wide stretch of wetland. Some studies have also presented evidence for the attenuation of tsunamis by coastal mangroves (Danielsen et al., 2005; Kathiresan and Rajendran, 2005). Maintaining these natural coastal defences is especially important given that populations of delta are expected to be disproportionally affected by coastal flooding, especially in developing countries (Edmonds et al., 2020).

These coastal wetlands also function as effective traps for carbon, due to fast growing plants and quick burial of organic matter by sediment deposition. Due to this, mangroves, coastal marsh and seagrass areas can sequester carbon at a rate greater than 10 times that of terrestrial forest, and do not become carbon saturated due to their ability so aggrade with further sediment deposition (Warner et al., 2016; McLeod et al., 2011). Preservation of these ecosystems is especially important as their loss not only removes their ability to sequester carbon, but can cause emissions from their existing carbon store which were estimated to be as much at 1.02×10^9 tons of carbon dioxide per year worldwide by Pendleton et al. (2012).

While much of this study focuses on the vulnerabilities of deltas to coastal land loss, it is possible that these landforms are relatively resilient to coastal

erosion and inundation compared to other coastal landforms that do not receive strong inputs of sediment. For example, in the Gulf coast region of the US, where areas of coastal land are being lost at a between 28.01 and 83.5 km^2y^{-1} (Couvillion et al., 2016), both the Wax lake and Atchafalaya Deltas have gained land area (Kim, Mohrig, et al., 2009).

Deltas are commonly important for the food security of the extended region in which the delta sits (Foufoula-Georgiou, 2013) due to being hotspots of agriculture and aquaculture. This is the case in the Nile Delta, which hosts 63% of Egypt's agricultural land, while being only 2% of the country's overall land area (Hereher, 2010), or Vietnam's Mekong delta, which provides 40% of the country's cultivated land (Warner, 2010) despite occupying only 49000 km^2 (Syvitski and Saito, 2007), less than 15% of Vietnam's land surface. The Mekong Delta produces half of Vietnams rice (and 90% of its exported rice), 60% of its fish and shrimp, and 80% of its fruit, as well as being responsible for 25% of the country's GDP (Warner, 2010). Growing crops on the a delta allows the seasonal flooding of farming land, which can act as a natural pest control (Tong, 2017), as well as deposit large amounts of nutrients needed for crop growth (Manh et al., 2014).

In addition to land-based agriculture, deltaic wetlands can also benefit fisheries. These wetlands provide both food and shelter from predators to young marine animals (Boesch and Turner, 1984) which make up fish stocks. Over 95% of the USA's fish stocks are likely reliant on wetlands (Mitsch and Gossilink, 2015).

2.3.2 *Intrinsic vulnerabilities of deltas and social impact*

Nearly all active deltas form on the border a large water body, commonly the ocean, and have low elevations relative to this water body. For example, in a study of 33 deltas, Syvitski *et al.* (2009) found that there was a combined delta area of 26,000km^2 below mean sea level, and 96,000km^2 within 2m of sea level. This makes these systems vulnerable to inundation as a result of storm surges or high fluvial floods.

In addition, deltas naturally subside due to consolidation of recently deposited sediment. As freshly deposited, relatively porous sediment is compacted by the sediment deposited on top of it, it loses pore space and so compacts to take up less space, causing the delta to subside. This subsidence happens naturally at a rate ~0.001-0.01my^{-1} (Ericson et al., 2006), and is commonly balanced by sediment deposition.

Due to their socio-economic value, deltas are inhabited by hundreds of millions of people worldwide (Syvitski et al., 2009). Settlements on deltas are vulnerable to both short-term, weather-related flooding (Edmonds et al., 2020) and permanent inundation (Nienhuis and van de Wal, 2021), which will disproportionately impact populations in developing countries (Edmonds et al., 2020) and lead to widespread displacement of these people (Warner, 2010).

2.3.3 *Anthropogenic threats to deltas*

In most delta systems, human actions are now exacerbating the sources of vulnerability discussed above. Sediment input into a delta system is necessary to counteract natural subsidence, but the annual export of sediment to the coast is shown to have reduced by 1.4 billion metric tons compared pre-industrial levels (Syvitski et al., 2005). This reduction is due to a combination of sediment being

deposited and trapped in artificial reservoirs (for example, reservoir construction in the upper Mekong could reduce sediment discharge by 96% (Kondolf et al., 2014)), and sediment mining within the lower reaches of the river (for example, and extraction rate of 50 million tons yr^{-1} in the lower Mekong River (Hackney et al., 2020). This pattern is being repeated globally, with an average loss of 38% of sediment flux to deltas expected by the end of the century (Dunn et al., 2019)

Even when sediment does reach a delta, it is not necessarily deposited on the delta top where it can aggrade land and offset subsidence. In many cases extensive construction of levees for flood control have decreased the amount of sediment being deposited on the delta top (Vörösmarty et al., 2009). This lack of deposition has been shown to cause reductions in elevation on the scale of meters in the Ganges-Brahmaputra delta (Auerbach et al., 2015) as well as the loss of coastal wetlands surrounding the Mississippi Delta (Rutherford et al., 2018; Day et al., 2000).

Additionally, extraction of pore fluids from the sediment below deltas is decreasing pore pressures and so increasing the rate of compaction and subsidence. Morton et al. (2002) found subsidence of up to $9.4x10^{-3}$m y^{-1} linked to hydrocarbon extraction. Liu et al. (2016) found subsidence rates up to 0.04m y^{-1} linked oil extraction in the Yellow river delta. Minderhoud et al. (2017) found subsidence rates of 0.011 m y^{-1} with some areas as high as 0.025 m y^{-1} in the Mekong due to Hydrocarbon extraction.

In addition to subsidence, Sea Level Rise (SLR) as a result of global climate change raises the level of the surrounding basin water for coastal deltas. It has been shown that between 1993 and 2010, sea level rose at a rate of 2.8-3.6x10^{-}

^{3}m y^{-1} and could have reached a height of 0.98 m above 1998-2005 levels by 2100 (IPCC, 2013). Although eustatic SLR is not the dominant factor in relative SLR (Eustatic SLR + subsidence) in the case of most deltas (Ericson et al., 2006), it is still a significant and ubiquitous factor in all coastal deltas.

2.4 Modelling Delta Morphodynamics

2.4.1 *Predicting Stability and Resilience*

Modelling of the environment allows detailed analysis of a system that may otherwise be unsafe, impractical, or impossible to study. No model is a perfect representation of the real world, as simplifications have to be made to make the models both solvable and fast enough to run to completion within a feasible timescale. However, providing that the limitations of the model are known and accounted for, they can be used to study natural systems at spatial and temporal scales and resolutions that would be impossible otherwise. Conditions can be finely controlled to allow for the analysis of particular processes without interference from other processes. When supported by field observations, they are valuable tools in earth sciences, and have already been extensively applied to the study of river deltas.

Early physical models of deltas used only sand (e.g. Jopling, 1965) and commonly most closely represented non-cohesive, very coarse grained deltas with rapidly avulsing distributaries. Hoyal and Sheets (2009) managed to bypass this issue by using an artificial polymer to increase the cohesivity and hence bank stability, allowing them to model deltas with stable, branching channels.

Numerical fluid dynamics models work by solving a version of the Navier-Stokes equation for fluid movement, usually in a simplified form such as the 1-

dimensional Saint-Venant equations (as in Le et al., 2007) or the Shallow Water Equations (as in Lesser et al., 2004). Commonly, other processes are also included, such as sediment transport and wave action. Numerical models have been used to study deltas at a number of scales.

Numerical models can be used at a small scale to simulate single delta features. For example, Edmonds and Slingerland (2007) used Delft 3D to study the formation of river mouth bars forming in a still basin without waves or currents. Only a single grain size was simulated per model, but this was varied systematically, along with outlet width, depth and flow velocity, and basin bed slope. The study used a morphological scale factor, which multiplied the mass of erosion or deposition at every timestep to speed up morphological change and so reduce the model simulation time necessary to form mature morphological features. They found that the results of their models where consistent for morphological scale factors of up to 200.

At a much larger scale, numerical models can be used to study and predict the processes within and overall development of real-world deltas. For example, Martyr-Koller et al. (2017) developed a numerical model in Delft3D Flexible Mesh that encompassed the San Francisco Bay area, Sacramento-San Joaquim Delta and the channels of incoming rivers. The computational grid was fitted specifically to the bathymetry of the study area, and the model was then calibrated against 7 months of tidal, discharge and salinity data. The authors found that the model describes the dynamics of the delta well, allowing the model to be used to study sediment, plankton and habitat sustainability within the delta and bay area. Similar, region-specific models have been developed and

calibrated against other deltas, such as the Mekong (Thanh et al., 2017a; Manh et al., 2015; Le et al., 2007).

However, the focus of this study is around the simulation of a full scale, but generic deltas, such as those modelled by Edmonds and Slingerland (2010). In their study, they used Delft3D to simulate the formation of a delta in a basin without waves or tides. The proportion of cohesive sediment (in this case defined as sediment with D_{50}=30μm), and the τ_{ce} of the cohesive sediment where both varied. In this case, cohesive sediment deposition was assumed to be constant (by setting the critical shear stress for deposition, τ_{cd}, to 1000 N m^{-2}, far above any bed stress expected in the simulation), so equilibrium was reached when erosion became sufficient to exactly counteract the deposition. By using a model, the authors where able to study the temporal evolution of the delta in great detail, observing how the turbulent jet at stream mouths interacted with mouth bars of differing cohesivity.

Building on the above study, Caldwell and Edmonds (2014) utilised a similar model setup to study the effects of sediment grain size on delta morphologies. τ_{ce} was held constant at 1 Nm^{-2}. Use of numerical modelling allowed the authors to precisely define seven sediment fractions which were generated by discretising a log-normal distribution of grain sizes for each run, varying the mean grain size and the standard deviation and skewness of the distribution. From the model outputs, a representative timescale for the lifetime of channelised cells was calculated that represented "the average length of time that a channel stays in a given position" (pg.14, Caldwell and Edmonds, 2014).

A similar model has also been used to study the stratigraphic architecture of a delta. Burpee et al. (2015) used a model based on Caldwell and Edmonds (2014)

and Edmonds and Slingerland (2010) to create and record chronostratigraphic surfaces throughout nine modelled deltas, as well as to record the deposited sediment grain size in 0.2m thick layers. From these results, the author was able to characterise clinoform dips and concavity for deltas formed of different sediments, finding that sandier, less cohesive deltas created steeper, more concave clinoforms with more uniform dip directions.

2.4.2 *Delft3D-Flow*

As shown in Section 2.4.1, multiple approaches have been taken to modelling the dynamics of river deltas. In addition to those mentioned above, a number of modelling approaches are available. Examples of bespoke morphodynamic models developed for a study exist; Kim et al. (2009) used the Exner equations to model simple delta lobe advance. Wei and Wu (2014) combined the shallow water equations with the Engelund and Hansen sediment transport formulation to investigate the long term evolution of the Pearl River Delta.

Additionally, a number of modelling suites are available that have the ability to model the morphodynamics of river deltas. TELEMAC-MASCARET, is an open source hydraulic modelling system, which has been used with the SISYPHE module (which handles sediment transport and bed evolution) to model the effects of sand mining in the Vietnamese Mekong Delta (Ngoc Anh et al., 2022) as well as the estuarine morphology of the Modaomen branch of the Pearl River delta. MIKE21 and MIKE3 are 2-dimensional and 3-dimensional (respectively) morphodynamic models, also using the shallow-water equations, that have also seen significant use in research focusing on coastal delta fronts exposed to

waves (likely as wave dynamics are included within the model by default). Le Xuan et al. (2022) used MIKE21-FM to model the estuary mouths and surrounding coast of the Mekong Delta to investigate how breakwater structures influence sediment accumulation on the coastal areas. Another study also used MIKE21/3 to investigate sediment accumulation and removal, in this case at the mouth of the Sfântu Gheorghe branch of the Danube delta in the face of a range of flood discharges and storm wave events.

Delft3D-Flow[1] is a hydrological and morphological modelling package that also solves the unsteady shallow water equations (two-dimensional, Reynolds averaged versions of the Navier-Stokes equations) in two dimensions. These include a set of horizontal momentum equations and volume continuity equations (Lesser et al., 2004). In the shallow water equations, vertical acceleration (for example, due to buoyancy driven advection) is assumed to be small compared to horizontal acceleration, so is ignored. The modelled fluid is assumed to be incompressible. The equations are solved numerically using a finite difference model on a staggered grid. (For a more detailed description of the function of Delft3D, see Section 3.2.1.)

Delft3D is very widely used for the morphodynamic modelling of generic delta responses to sea level rise (Lageweg and Slangen, 2017), tides (Rossi et al., 2016; Leonardi et al., 2013)), waves (Nardin et al., 2013), and river discharge (Edmonds et al., 2010); for modelling the evolution of real world deltas, such as Wax Lake Delta (Olliver and Edmonds, 2017), the Mekong Delta (Thanh et al., 2017b) and the San Francisco Bay Delta (Martyr-Koller et al., 2017); and for

[1] For a more detailed description of the function of Delft3D, see Section 3.2.1.

investigating the morphodynamics of bifurcations (Edmonds and Slingerland, 2008) mouth jets and bars (Fagherazzi et al., 2015; Canestrelli et al., 2014; Mariotti et al., 2013) and sediment grainsize and cohesivity (Burpee et al., 2015; Caldwell and Edmonds, 2014; Geleynse et al., 2011; D. A. Edmonds and Slingerland, 2010).

In this study, Delft 3D was preferred for a variety of reasons. It has been proven in its ability to model mouth jets (Fagherazzi et al., 2015; Canestrelli et al., 2014), which are known to play important roles in the morphodynamics of deltas forming over resistant cohesive substrates (Shaw and Mohrig, 2014a). Allows use of the TRANSPOR2004 sediment predictor that is desired as it includes τ_{ce} (see below) as a factor in its handling of sediment transport and distinguishes between bed and suspended load (Baar et al., 2019), which is expected to be important in this study as the grain sizes used cover a range that will likely transition between travelling in bed and suspended load as flow conditions change. Delft3D's GUI also facilitates easy manipulation of sediment parameters, such as grainsize, bulk and dry-bed density, settling velocity and critical shear stress of erosion (τ_{ce}) and deposition (τ_{cd}). A potential downside to this is that sensible values or ranges for this array of sediment parameters need to be found, which is usually done from either calibration of field testing. Discussion of how these values are set can be found in Section 3.2.2.

However, some elements of Delft3D present challenges in its use for the modelling study attempted in this project. For example, to control sediment entrainment and deposition, Delft3D uses the Partheniades-Krone bed boundary condition, which may under- and over- estimate erosion in some conditions (see below). Additionally, Delft3D doesn't directly model subsidence, which is

considered in Section 4. However, even, domain-wide subsidence can be approximated by raising the water level at all boundaries at the desired rate of subsidence. While differential subsidence (not even across the domain) would be valuable to study, and could be a direction for future work, this study only aims to address constant subsidence, so this is not considered a big issue. Similarly, Delft3D does not directly model the height, shape or any other metric of bedforms, which would have been valuable for comparison to the fieldwork presented in Section 5, and the bedforms found there.

Ultimately, Delf3D was used as it is a fully featured 2-dimensional hydrodynamic and morphodynamic model, capable of fulfilling the majority of demands of this project as well or better than any other available modelling suite, without the need for additional modules or models, and its use for simulating delta morphodynamics across a range of scales is very well supported in previous studies. While a bespoke model made specifically for the aims of this study would likely have been more applicable, development of this would have been beyond the scope of this project. Additionally, it is open-source (increasing the repeatability of this work) and so is easily available as well as being compatible with VIPER, the High Performance Computer used for this research.

2.4.3 *Modelling Sediment, Cohesivity and Erosion*

A number of metrics used to quantify the erodibility of sediment beds, including critical shear stress for erosion ($\boldsymbol{\tau}_{ce}$; the lowest bed shear stress that will entrain sediment from the bed) and critical flow velocity (U_{crit}, the lowest flow velocity that will entrain sediment from the bed, used in studies such as (Sundborg, 1956), as well as non-dimensional derivatives of these such as shields parameter, which represents the overall force applied by the flow across the

surface of a grain relative to the balance of gravitational and buoyant forces acting on it (Shields, 1936). Here, the τ_{ce} is used as it is the factor most commonly supported by models (e.g. Braat et al., 2017; Geleynse et al., 2011; Douglas A. Edmonds and Slingerland, 2010), and is frequently quoted in what field studies exist (Cossette, 2016; Gaskin et al., 2003).

However, the use of τ_{ce} is not without its issues; a plethora of measurements techniques exist (for example, Shear flumes in both laboratory (Gaskin et al., 2003) and in-situ forms (He et al., 2021), Borehole Shear Testers (Lutenegger et al., 1978), in-situ impinging jet tests (Tolhurst et al., 1999) as well as laboratory based jet testing (Cossette, 2016) and shear vanes (Bryant et al., 1986)), but measured values of τ_{ce} can vary by orders of magnitude where different methods for measurement are used.

The shear vane method used by Bryant et al. (1986) reported shear strengths > 1kPa (1000 n m^{-2}) in marine sediments of the gulf of Mexico, even where sediments where 'underconsolidated' and had porosities >50%. This demonstrates that it is likely that Shear vane readings are not consistent with other measurements of τ_{ce}. This is supported by earlier studies, which conclude that 'macroscopic' shear strengths such as vane shear stress are 2-3 orders of magnitude higher than critical shear strength for fluvial erosion (Winterwerp et al., 2012).

Gaskin et al. (2003) used a laboratory-based flume to subject an undisturbed sample, collected in the field on the banks of the St Lawrence River, to unidirectional water flow, and measure sediment entrainment at a range of shear stresses to determine τ_{ce}. Similarly, Cossette (2016) presented how field samples for the Sawmill Creek, Ontario, Canada, where tested using a high pressure

impinging jet in a laboratory to measure τ_{ce}. In the study of Joensuu et al. (2018) sediment core samples were taken from the sea floor then their shear strength measured using a EROMES device, which used a propeller to induce turbulence at the sediment surface then measured the turbidity caused by this erosional force with an optical sensor.

The above publications, and their results (plotted on Figure 2-2) show that sediment bed τ_{ce} varies strongly between locations and across fine sediment contents. Different testing methodologies can also result in a wide range of

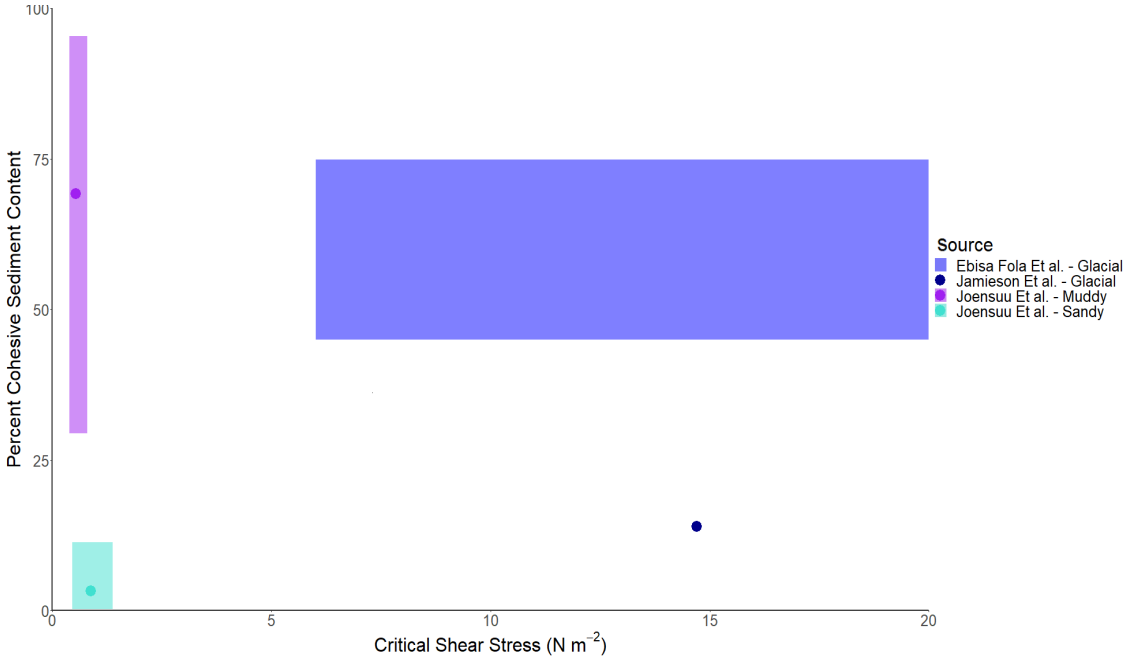

Figure 2-2: Estimated parameter space of real-world fluvial substrates. Examples consist of:- "Sandy" and "Muddy" type shallow coastal sediments described by Joensuu et al. (2018), Glaciomarine till described by Jamieson et al. (2013)*, and similar consolidated Champlain Sea clay described by (Gaskin et al., 2003). Model parameters for the previous chapter are included in grey for reference.

*Note that only percent clay content is given in Jamieson et al. (2013), and while this value has been used here as percent cohesive content, the actual value is likely higher when all cohesive material is included.

values, and due to a lack of comparative studies it is not clear how much of the variation in τ_{ce} is due to inconsistencies between methodologies. However, results from those methods that rely on fluid motion to cause entrainment, group together, with τ_{ce} between 0 and 20 n m-2. As such, τ_{ce} values used in this study are all within this range (substantially within the lower end of this range <= 12.5, as tests above this number were shown to have little difference from those > 12.5; see sections 3.2.2 and 4.2.1). Additionally, results from these methods are favoured in this study as their mechanisms for causing erosion most similar to the natural mechanism of fluvial erosion.

Within Delft3D, the transport of all suspended sediment is calculated by solving advection-diffusion equation consisting of flow velocity and sediment concentration terms (advection) and eddy diffusivity terms (diffusion). Bed load transport is calculated for "sand" fractions only, using the van Rijn method. In this method, bedload transport rate is calculated empirically based on sediment density and particle size and the shear stress and velocity at the bed.

Sediment in Delft3D must be defined in terms of discrete sediment fractions, which must be either fine (<64μm), cohesive "mud" or coarser, non-cohesive "sand". These two sediment types are handled differently by the model. For mud, erosion and deposition terms are calculated using the Partheniades-Krone bed boundary condition, and so are controlled primarily by the relationship between the critical shear stresses for erosion (τ_{ce}) or deposition (τ_{cd}) and the local maximum shear stress due to current. The critical shear stress for erosion, τ_{ce}, represents the minimum shear stress necessary to initiate erosion of a sediment fraction, while critical shear stress for deposition, τ_{cd}, sediment represents the maximum bed shear stress at which sediment will be deposited. For sand, any

cohesive forces holding the sediment to the bed are ignored, and erosion is controlled by shear stress, grain size and vertical diffusion of the sediment away from the bed. Deposition is controlled by the concentration of sediment in the water, the vertical diffusion and the sediment settling velocity.

Erosion in the Partheniades-Krone bed boundary condition, is based on experiments from Partheniades (1965) (see figure 1; Winterwerp et al., 2012), which was then parameterised into the erosion equation of the Partheniades-Krone condition (for example by Ariathurai and Arulanandan, 1978):

$$E = \begin{cases} M\left(\frac{\tau_{bed}}{\tau_{ce}} - 1\right), when\ \tau\_bed > \tau\_ce \\ 0 \qquad\qquad , when\ \tau\_bed \leq \tau\_ce \end{cases} \qquad \textbf{(Equation 2-1)}$$

In practice, fine cohesive sediments are eroded through a number of mechanisms. Where sediment resistance is very low and water content is high, such as in freshly deposited fine sediment, fluid mud can be entrained into the flow my fluid mixing (Gaskin et al., 2003). Where sediment resistance is higher, and bed shear is close to the threshold for erosion, surface erosion occurs in which single particles or flocs of sediment are eroded from a cohesive bed, (Pike et al., 2018). The rate of this process increases linearly with bed shear stress until forces become strong enough to initiate mass erosion of the bed (Krone, 1999). Mass erosion occurs when flow induced stress becomes sufficient to remove larger lumps of material from the bed, and is seen when bed resistances are high (Winterwerp et al., 2012). Partheniade's (1965)

original data showed low but non-zero erosion (identified as "floc erosion") at shear stresses below τ_{ce} and higher "mass erosion" at shear stresses higher than τ_{ce}. However, Equation 2-1 only represents one mode of erosion above a single threshold and no erosion below it. As Equation 2-1 is the only erosion formula implemented in Delft3D, it is used in this study, and it is acknowledged that the small amount of erosion at bed stresses < τ_{ce} will be neglected entirely, and mass erosion at very high bed stresses will likely be underrepresented.

For a more detailed description of the function of Delft3D, see Section 3.2.1.

2.5 Summary

As demonstrated above, cohesive sediment qualities can be crucial in determining delta morphology through the effects they have on the behaviour of mouth jets (Fagherazzi et al., 2015), how they influence the formation of sediment bars and levees at the channel mouths (Mariotti et al., 2015; Edmonds and Slingerland, 2007), and how they affect bifurcation dynamics (Edmonds and Slingerland, 2008), bedform formation (Baas et al., 2013), and hence the large-scale processes of the delta (Burpee et al., 2015; Caldwell and Edmonds, 2014). A thorough understanding of how sediment qualities affect deltas is critical due to the social and ecological importance of these land forms (Warner et al., 2016; Zhang et al., 2016; Barbier et al., 2013) and their intrinsic vulnerabilities to anthropogenic pressures such as sand mining (Hackney et al., 2020), sediment

impoundment in reservoirs (Syvitski et al., 2005) and the subsidence of the delta from pore-fluid extraction (Minderhoud et al., 2017). Many previous studies have successfully modelled delta morphodynamics through a variety of methods (Geleynse et al., 2011; Hoyal and Sheets, 2009; Le et al., 2007) and building on these previous studies, the chapters below attempt to investigate how the sediment underlying a delta can affect the morphodynamics of these landforms and influence how resilient they are to anthropogenic threats.

2.6 References

Abad, J. D., Frias, C. E., Buscaglia, G. C. and Garcia, M. H. (2013) 'Modulation of the flow structure by progressive bedforms in the Kinoshita meandering channel', *Earth Surface Processes and Landforms*, vol. 38, no. 13, pp. 1612–1622 [Online]. DOI: 10.1002/esp.3460.

Aberle, J., Nikora, V. and Walters, R. (2004) 'Effects of bed material properties on cohesive sediment erosion', *Marine Geology*, vol. 207, no. 1–4, pp. 83–93 [Online]. DOI: 10.1016/j.margeo.2004.03.012.

Amos, C. L., Bergamasco, A., Umgiesser, G., Cappucci, S., Cloutier, D., Denat, L., Flindt, M., Bonardi, M. and Cristante, S. (2004) 'The stability of tidal flats in Venice Lagoon - The results of in-situ measurements using two benthic, annular flumes', *Journal of Marine Systems*, vol. 51, no. 1-4 SPEC. ISS., pp. 211–241 [Online]. DOI: 10.1016/j.jmarsys.2004.05.013.

Andreotti, B., Claudin, P., Devauchelle, O., Durán, O. and Fourrière, A. (2012) 'Bedforms in a turbulent stream: Ripples, chevrons and antidunes', *Journal of Fluid Mechanics*, vol. 690, pp. 94–128 [Online]. DOI: 10.1017/jfm.2011.386.

Andrews, E. D. (1983) 'Entrainment of gravel from naturally sorted riverbed material.', *Geological Society of America Bulletin*, vol. 94, no. 10, pp. 1225–1231 [Online]. DOI: 10.1130/0016-7606(1983)94<1225:EOGFNS>2.0.CO;2.

Ariathurai, R. and Arulanandan, K. (1978) 'Erosion rates of cohesive siools', *Journal of the Hydraulics Division*, vol. 104, no. 2 [Online]. DOI: https://doi.org/10.1061/JYCEAJ.0004937.

Auerbach, L. W., Goodbred, S. L., Mondal, D. R., Wilson, C. A., Ahmed, K. R., Roy, K., Steckler, M. S., Small, C., Gilligan, J. M. and Ackerly, B. A. (2015) 'Flood risk of natural and embanked landscapes on the Ganges-Brahmaputra tidal delta plain', *Nature Climate Change*, vol. 5, no. 2, pp. 153–157 [Online]. DOI: 10.1038/nclimate2472.

Baar, A. W., Boechat Albernaz, M., van Dijk, W. M. and Kleinhans, M. G. (2019) 'Critical dependence of morphodynamic models of fluvial and tidal systems on empirical downslope sediment transport', *Nature Communications*, vol. 10, no. 1 [Online]. DOI: 10.1038/s41467-019-12753-x.

Baas, J. H., Best, J. L., Peakall, J. and Wang, M. (2009) 'A phase diagram for turbulent, transitional, and laminar clay suspension flows', *Journal of Sedimentary Research*, vol. 79, no. 4, pp. 162–183 [Online]. DOI: 10.2110/jsr.2009.025.

Baas, J. H., Davies, A. G. and Malarkey, J. (2013) 'Bedform development in mixed sand-mud: The contrasting role of cohesive forces in flow and bed', *Geomorphology*, Elsevier B.V., vol. 182, pp. 19–32 [Online]. DOI: 10.1016/j.geomorph.2012.10.025.

Bale, A. J., Stephens, J. A. and Harris, C. B. (2007) 'Critical erosion profiles in macro-tidal estuary sediments: Implications for the stability of intertidal mud and the slope of mud banks', *Continental Shelf Research*, vol. 27, no. 18, pp. 2303–2312 [Online]. DOI: 10.1016/j.csr.2007.05.015.

Barbier, E. B., Georgiou, I. Y., Enchelmeyer, B. and Reed, D. J. (2013) 'The Value of Wetlands in Protecting Southeast Louisiana from Hurricane Storm Surges', vol. 8, no. 3, pp. 1–7 [Online]. DOI: 10.1371/journal.pone.0058715.

Boesch, D. F. and Turner, R. E. (1984) 'Dependence of Fishery Species on Salt Marshes " The Role of Food and Refuge', vol. 7, no. 4, pp. 460–468.

Bolla Pittaluga, M., Repetto, R. and Tubino, M. (2003) 'Channel bifurcation in braided rivers: Equilibrium configurations and stability', *Water Resources Research*, vol. 39, no. 3, pp. 1–13 [Online]. DOI: 10.1029/2001WR001112.

Braat, L., van Kessel, T., Leuven, J. R. F. W. and Kleinhans, M. G. (2017) 'Effects of mud

supply on large-scale estuary morphology and development over centuries to millennia', *Earth Surface Dynamics Discussions*, pp. 1–47 [Online]. DOI: 10.5194/esurf-2017-14.

Bryant, W. R., Wetzel, A. and Sweet, W. (1986) 'Geotechnical properties of intraslope basin sediments, Gulf of Mexico, Deep Sea Drilling Project Leg 96, Site 619.', *Initial reports DSDP, Leg 96, Ft. Lauderdale to Galveston, Texas, 1983*, no. March, pp. 819–824 [Online]. DOI: 10.2973/dsdp.proc.96.153.1986.

Burpee, A. P., Slingerland, R. L., Edmonds, D. A., Parsons, D. R., Best, J. L., Cederberg, J., McGuffin, A., Caldwell, R. L., Nijhuis, A. and Royce, J. (2015) 'Grain-Size Controls On the Morphology and Internal Geometry of River-Dominated Deltas', *Journal of Sedimentary Research*, vol. 85, no. 6, pp. 699–714 [Online]. DOI: 10.2110/jsr.2015.39.

Caldwell, R. L. and Edmonds, D. A. (2014) 'The effects of sediment properties on deltaic processes and morphologies: A numerical modeling study', *Journal of Geophysical Research: Earth Surface*, vol. 119, no. 5, pp. 961–982 [Online]. DOI: 10.1002/2013JF002965.

Canestrelli, A., Nardin, W., Edmonds, D. A., Fagherazzi, S. and Slingerland, R. L. (2014) 'Importance of frictional effects and jet instability on the morphodynamics of river mouth bars and levees', *Journal of Geophysical Research: Oceans*, vol. 119, no. 1, pp. 509–522 [Online]. DOI: 10.1002/2013JC009312.

Cossette, D. (2016) 'Erodibility and Scour By a Vertical Submerged Circular Turbulent Impinging Jet in Cohesive Soils', p. 241.

Costanza, R., Pe´rez-Maqueo, O., Martinez, M. L., Sutton, P., Anderson, S. J. and Mulder, K. (2008) 'The Value of Coastal Wetlands for Hurricane Protection', *Journal of the Human Environment*, vol. 37, no. 4, pp. 241–248 [Online]. DOI: 10.1579/0044-7447(2008)37.

Couvillion, B. R., Beck, H., Schoolmaster, D. and Fischer, M. (2016) 'Land Area Change in Coastal Louisiana 1932 to 2016: U.S. Geological Survey Scientific Investigations Map 3381', US Department of the Interior, US Geological Survey [Online]. DOI: 10.3133/sim3381.

Dade, W. B., Davis, J. D., Nichols, P. D., Nowell, A. R. M., Thistle, D., Trexler, M. B., White, D. C. and Davis, J. D. (1990) 'Effects of bacterial exopolymer adhesion on the entrainment of sand', *Geomicrobiology Journal*, vol. 8, no. 1, pp. 1–16 [Online]. DOI: 10.1080/01490459009377874.

Danielsen, F., Sørensen, M. K., Olwig, M. F., Selvam, V., Burgess, N. D., Hiraishi, T., Karunagaran, V. M., Rasmussen, Michael S, Hansen, L. B., Quarto, A., Suryadiputra, N., Danielsen, F., Srensen, M. K., Olwig, M. F., Selvam, V., Parish, F., Burgess, N. D., Hiraishi, T., Karunagaran, V. M., Rasmussen, M S, Ha, B. and Qua, A. (2005) 'The Asian Tsunami: Role for Coastal Vegetation', vol. 310, p. 643.

Day, J. W., Shaffer, G. P., Britsch, L. D., Reed, D. J., Hawes, S. R. and Cahoon, D. (2000) 'Pattern and Process of Land Loss in the Mississippi Delta : A Spatial and Temporal Analysis of Wetland Habitat Change', *Estuaries*, vol. 23, no. 4, pp. 425–438.

Van Dijk, W. M., Van de Lageweg, W. I. and Kleinhans, M. G. (2013) 'Formation of a cohesive floodplain in a dynamic experimental meandering river', *Earth Surface Processes and Landforms*, vol. 38, no. 13, pp. 1550–1565 [Online]. DOI: 10.1002/esp.3400.

Dong, T. Y., Nittrouer, J. A., Czapiga, M. J., Ma, H., McElroy, B., Il'icheva, E., Pavlov, M., Chalov, S. and Parker, G. (2019) 'Roles of Bank Material in Setting Bankfull Hydraulic Geometry as Informed by the Selenga River Delta, Russia', *Water Resources Research*, vol. 55, no. 1, pp. 827–846 [Online]. DOI: 10.1029/2017WR021985.

Dunn, F. E., Darby, S. E., Nicholls, R. J., Cohen, S., Zarfl, C. and Fekete, B. M. (2019) 'Projections of declining fluvial sediment delivery to major deltas worldwide in response to climate change and anthropogenic stress', *Environmental Research Letters*, vol. 14, no. 8 [Online]. DOI: 10.1088/1748-9326/ab304e.

Duţu, F., Panin, N., Ion, G. and Duţu, L. T. (2018) 'Multibeam bathymetric investigations

of the morphology and associated bedforms, Sulina channel, Danube Delta', *Geosciences (Switzerland)*, vol. 8, no. 1, pp. 26–28 [Online]. DOI: 10.3390/geosciences8010007.

Edmonds, D. A., Caldwell, R. L., Brondizio, E. S. and Siani, S. M. O. (2020) 'Coastal flooding will disproportionately impact people on river deltas', *Nature Communications*, Springer US, vol. 11, pp. 1–8 [Online]. DOI: 10.1038/s41467-020-18531-4.

Edmonds, D. A., Paola, C., Hoyal, D. C. J. D. and Sheets, B. A. (2011) 'Quantitative metrics that describe river deltas and their channel networks', *Journal of Geophysical Research: Earth Surface*, vol. 116, no. 4, pp. 1–15 [Online]. DOI: 10.1029/2010JF001955.

Edmonds, D. A. and Slingerland, R. L. (2007) 'Mechanics of river mouth bar formation: Implications for the morphodynamics of delta distributary networks', *Journal of Geophysical Research: Earth Surface*, vol. 112, no. 2, pp. 1–14 [Online]. DOI: 10.1029/2006JF000574.

Edmonds, D. A. and Slingerland, R. L. (2008) 'Stability of delta distributary networks and their bifurcations', *Water Resources Research*, vol. 44, no. 9, pp. 1–13 [Online]. DOI: 10.1029/2008WR006992.

Edmonds, D. A. and Slingerland, R. L. (2010) 'Significant effect of sediment cohesion on delta morphology', *Nature Geoscience*, vol. 3, no. 2, pp. 105–109 [Online]. DOI: 10.1038/ngeo730.

Edmonds, Douglas A. and Slingerland, R. L. (2010) 'Significant effect of sediment cohesion on delta morphology', *Nature Geoscience*, vol. 3, no. 2, pp. 105–109 [Online]. DOI: 10.1038/ngeo730.

Edmonds, D. A., Slingerland, R. L., Best, J. L., Parsons, D. R. and Smith, N. (2010) 'Response of river- dominated delta channel networks to permanent changes in river discharge', *Geophys. Res. Lett.*, vol. 37, p. L12404.

Ericson, J. P., Vörösmarty, C. J., Dingman, S. L., Ward, L. G. and Meybeck, M. (2006) 'Effective sea-level rise and deltas: Causes of change and human dimension implications', *Global and Planetary Change*, vol. 50, no. 1–2, pp. 63–82 [Online]. DOI: 10.1016/j.gloplacha.2005.07.004.

Esposito, C. R., Georgiou, I. Y. and Kolker, A. S. (2013) 'Hydrodynamic and geomorphic controls on mouth bar evolution', *Geophysical Research Letters*, vol. 40, no. 8, pp. 1540–1545 [Online]. DOI: 10.1002/grl.50333.

Fagherazzi, S., Edmonds, D. A., Nardin, W., Leonardi, N., Canestrelli, A., Falcini, F., Jerolmack, D. J., Mariotti, G., Rowland, J. C. and Slingerland, R. L. (2015) 'Dynamics of river mouth deposits', *Reviews of Geophysics*, vol. 53, no. 3, pp. 642–672 [Online]. DOI: 10.1002/2014RG000451.

Ferguson, R. (1987) 'Hydraulic and Sedimentery controlls of Channel Pattern', in Richards, K. (ed), *River Channels: Environment and Process*, Oxford, Blackwell, pp. 129–158.

Fola, M. E. and Rennie, C. D. (2010) 'Downstream Hydraulic Geometry of Clay-Dominated Cohesive Bed Rivers', *Journal of Hydraulic Engineering*, vol. 136, no. 8, pp. 524–527 [Online]. DOI: 10.1061/(ASCE)HY.1943-7900.0000199.

Foufoula-Georgiou, E. (2013) 'A vision for a coordinated international effort on delta sustainability', *IAHS-AISH Proceedings and Reports*, vol. 358, no. July, pp. 3–11.

Gaskin, S. J., Pieterse, J., Al Shafie, A. and Lepage, S. (2003) 'Erosion of undisturbed clay samples from the banks of the St. Lawrence River', *Canadian Journal of Civil Engineering*, vol. 30, no. 3, pp. 585–595 [Online]. DOI: 10.1139/l03-008.

Geleynse, N., Storms, J. E. A., Walstra, D. J. R., Jagers, H. R. A., Wang, Z. B. and Stive, M. J. F. (2011) 'Controls on river delta formation; insights from numerical modelling', *Earth and Planetary Science Letters*, Elsevier B.V., vol. 302, no. 1–2, pp. 217–226 [Online]. DOI: 10.1016/j.epsl.2010.12.013.

Grabowski, R. C., Droppo, I. G. and Wharton, G. (2011) 'Erodibility of cohesive sediment: The importance of sediment properties', *Earth-Science Reviews*, Elsevier B.V., vol. 105, no. 3–4, pp. 101–120 [Online]. DOI: 10.1016/j.earscirev.2011.01.008.

Hackney, C. R., Darby, S. E., Parsons, D. R., Leyland, J., Best, J. L., Aalto, R., Nicholas, A. P. and Houseago, R. C. (2020) 'River bank instability from unsustainable sand mining in the lower Mekong River', *Nature Sustainibility*, vol., no.

He, C., Taylor, J. N., Rochfort, Q. and Nguyen, D. (2021) 'A new portable in situ flume for measuring critical shear stress on river beds', *International Journal of Sediment Research*, Elsevier Ltd, vol. 36, no. 2, pp. 235–242 [Online]. DOI: 10.1016/j.ijsrc.2020.08.004.

Hereher, M. E. (2010) 'Vulnerability of the Nile Delta to sea level rise : an assessment using remote sensing', vol. 5705 [Online]. DOI: 10.1080/19475705.2010.516912.

Herzka, S. Z., Mellink, E., Talley, D. M., Huxel, G. R. and Dayton, P. K. (2013) 'Stable isotope ratios of egg albumen of three waterbird species nesting in the Colorado River Delta indicate differences in foraging ground and isotopic niche breadth', *Aquatic Conservation: Marine and Freshwater Ecosystems*, vol. 23, no. 4, pp. 546–563 [Online]. DOI: 10.1002/aqc.2326.

Hoyal, D. C. J. D. and Sheets, B. A. (2009) 'Morphodynamic evolution of experimental cohesive deltas', *Journal of Geophysical Research: Earth Surface*, vol. 114, no. 2, pp. 1–18 [Online]. DOI: 10.1029/2007JF000882.

IPCC (2013) *Summary for Policymakers:*, *Climate Change 2013: The Physical Science Basis. Contribution of Working Group I to the Fifth Assessment Report of the Intergovernmental Panel on Climate Change*, Cambridge University Press, Cambridge, United Kingdom and New York, NY, USA. [Online]. DOI: 10.1260/095830507781076194.

Iwantoro, A. P., van der Vegt, M. and Kleinhans, M. G. (2021) 'Effects of sediment grain size and channel slope on the stability of river bifurcations', *Earth Surface Processes and Landforms*, pp. 1–15 [Online]. DOI: 10.1002/esp.5141.

Jamieson, E. C., Ruta, M. A., Rennie, C. D. and Townsend, R. D. (2013) 'Monitoring stream barb performance in a semi-alluvial meandering channel: Flow field dynamics and morphology', *Ecohydrology*, vol. 6, no. 4, pp. 611–626 [Online]. DOI: 10.1002/eco.1370.

Jing, Y. and Qin, J. (2023) 'The influence of the development of dunes on the stability of bifurcations in sand-bed rivers', *Earth Surface Processes and Landforms*, no. May 2022, pp. 1540–1556 [Online]. DOI: 10.1002/esp.5567.

Joensuu, M., Pilditch, C. A., Harris, R., Hietanen, S., Pettersson, H. and Norkko, A. (2018) 'Sediment properties, biota, and local habitat structure explain variation in the erodibility of coastal sediments', *Limnology and Oceanography*, vol. 63, no. 1, pp. 173–186 [Online]. DOI: 10.1002/lno.10622.

Jopling, A. V (1965) 'Hydraulic factors controlling the shape of laminae in laboratory deltas', *Journal of Sedimentary Research*, vol. 35, no. 4, pp. 777–791.

Kathiresan, K. and Rajendran, N. (2005) 'Coastal mangrove forests mitigated tsunami', *Estuarine, Coastal and Shelf Science*, vol. 65, no. 3, pp. 601–606 [Online]. DOI: 10.1016/j.ecss.2005.06.022.

Khelifa, A. and Hill, P. S. (2006) 'Models for effective density and settling velocity of flocs', *Journal of Hydraulic Research*, vol. 44, no. 3, pp. 390–401 [Online]. DOI: 10.1080/00221686.2006.9521690.

Kim, W., Dai, A., Muto, T. and Parker, G. (2009) 'Delta progradation driven by an advancing sediment source: Coupled theory and experiment describing the evolution of elongated deltas', *Water Resources Research*, vol. 45, no. 6, pp. 1–16 [Online]. DOI: 10.1029/2008WR007382.

Kim, W., Mohrig, D., Twilley, R., Paola, C. and Parker, G. (2009) 'Is it feasible to build

new land in the Mississippi River Delta?', *Eos*, vol. 90, no. 42, pp. 373–384.

Kleinhans, M. G., Ferguson, R. I., Lane, S. N. and Hardy, R. J. (2013) 'Splitting rivers at their seams: Bifurcations and avulsion', *Earth Surface Processes and Landforms*, vol. 38, no. 1, pp. 47–61 [Online]. DOI: 10.1002/esp.3268.

Kleinhans, M. G., Jagers, H. R. A., Mosselman, E. and Sloff, C. J. (2008) 'Bifurcation dynamics and avulsion duration in meandering rivers by one-dimensional and three-dimensional models', *Water Resour. Res.*, vol. 44, p. W08454.

Kleinhans, M. G., Wilbers, A. W. E., Swaaf, A. D. E. and Berg, J. H. V. A. N. D. E. N. (1999) 'Sediment Supply-Limited Bedforms In Sand-Gravel Bed Rivers', pp. 629–640.

Kondolf, G. M., Rubin, Z. K. and Minear, J. T. (2014) 'Dams on the Mekong: Cumulative sediment starvation', *Water Resources Research*, vol. 50, no. 6, pp. 5158–5169 [Online]. DOI: 10.1002/2013WR014651.

Krone, R. B. (1999) 'Effects of Bed Structure on Erosion of Cohesive Sediments', *Journal of Hydraulic Engineering*, vol. 125, pp. 1297–1301.

Lageweg, W. I. Van De and Slangen, B. A. (2017) 'Predicting Dynamic Coastal Delta Change in Response to Sea-Level Rise', [Online]. DOI: 10.3390/jmse5020024.

Land, L. E., Kolker, A. S. and Gambrell, R. P. (2012) 'Biotic and abiotic controls on sediment aggregation and consolidation: Implications for geochemical fluxes and coastal restoration', *Marine Environmental Research*, Elsevier Ltd, vol. 79, pp. 100–110 [Online]. DOI: 10.1016/j.marenvres.2012.05.012.

Lau, Y. L. and Droppo, I. G. (2000) 'Influence of antecedent conditions on critical shear stress of bed sediments', *Water Research*, vol. 34, no. 2, pp. 663–667 [Online]. DOI: 10.1016/S0043-1354(99)00164-5.

Le, T. V. H., Nguyen, H. N., Wolanski, E., Tran, T. C. and Haruyama, S. (2007) 'The combined impact on the flooding in Vietnam's Mekong River delta of local man-made structures, sea level rise, and dams upstream in the river catchment', *Estuarine, Coastal and Shelf Science*, vol. 71, no. 1–2, pp. 110–116 [Online]. DOI: 10.1016/j.ecss.2006.08.021.

Van Ledden, M., Van Kesteren, W. G. M. and Winterwerp, J. C. (2004) 'A conceptual framework for the erosion behaviour of sand-mud mixtures', *Continental Shelf Research*, vol. 24, no. 1, pp. 1–11 [Online]. DOI: 10.1016/j.csr.2003.09.002.

Leonardi, N., Canestrelli, A., Sun, T. and Fagherazzi, S. (2013) 'Effect of tides on mouth bar morphology and hydrodynamics', *Journal of Geophysical Research: Oceans*, vol. 118, no. 9, pp. 4169–4183 [Online]. DOI: 10.1002/jgrc.20302.

Lesser, G. R., Roelvink, J. A., van Kester, J. A. T. M. and Stelling, G. S. (2004) 'Development and validation of a three-dimensional morphological model', *Coastal Engineering*, vol. 51, no. 8–9, pp. 883–915 [Online]. DOI: 10.1016/j.coastaleng.2004.07.014.

Liu, Yilin, Huang, H., Liu, Yanxia and Bi, H. (2016) 'Linking land subsidence over the Yellow River delta, China, to hydrocarbon exploitation using multi-temporal InSAR', *Natural Hazards*, Springer Netherlands, vol. 84, no. 1, pp. 271–291 [Online]. DOI: 10.1007/s11069-016-2427-5.

Lorphensri, O., Ladawadee, A. and Dhammasarn, S. (2011) 'Review of Groundwater Management and Land Subsidence in Bangkok, Thailand', in Taniguchi, M. (ed), *Groundwater and Subsurface ENvironments*, Tokyo, Springer, pp. 127–142.

Lutenegger, A. J., Remmes, B. D. and Handy, R. L. (1978) 'Borehole Shear Test for Stiff Soil', *Journal of the Geotechnical Division*, vol. 104, no. 11 [Online]. Available at https://doi.org/10.1061/AJGEB6.0000718.

Manh, N. Van, Dung, N. V., Hung, N. N., Kummu, M., Merz, B. and Apel, H. (2015) 'Future sediment dynamics in the Mekong Delta floodplains: Impacts of hydropower development, climate change and sea level rise', *Global and Planetary Change*, Elsevier

B.V., vol. 127, pp. 22–33 [Online]. DOI: 10.1016/j.gloplacha.2015.01.001.

Manh, N. Van, Dung, N. V., Hung, N. N., Merz, B. and Apel, H. (2014) 'Large-scale suspended sediment transport and sediment deposition in the Mekong Delta', *Hydrology and Earth System Sciences*, vol. 18, no. 8, pp. 3033–3053 [Online]. DOI: 10.5194/hess-18-3033-2014.

Mariotti, G., Falcini, F., Geleynse, N., Guala, M., Sun, T. and Fagherazzi, S. (2013) 'Sediment eddy diffusivity in meandering turbulent jets: Implications for levee formation at river mouths', *Journal of Geophysical Research: Earth Surface*, vol. 118, no. 3, pp. 1908–1920 [Online]. DOI: 10.1002/jgrf.20134.

Mariotti, G., Valentine, K. and Fagherazzi, S. (2015) 'Time-dependent behavior of a placed bed of cohesive sediment subjected to erosion and deposition cycles', *Ocean Dynamics*, vol. 65, no. 2, pp. 287–294 [Online]. DOI: 10.1007/s10236-014-0798-2.

Martyr-Koller, R. C., Kernkamp, H. W. J., van Dam, A., van der Wegen, M., Lucas, L. V., Knowles, N., Jaffe, B. and Fregoso, T. A. (2017) 'Application of an unstructured 3D finite volume numerical model to flows and salinity dynamics in the San Francisco Bay-Delta', *Estuarine, Coastal and Shelf Science*, The Authors, vol. 192, pp. 86–107 [Online]. DOI: 10.1016/j.ecss.2017.04.024.

McLeod, E., Chmura, G. L., Bouillon, S., Salm, R., Björk, M., Duarte, C. M., Lovelock, C. E., Schlesinger, W. H. and Silliman, B. R. (2011) 'A blueprint for blue carbon: Toward an improved understanding of the role of vegetated coastal habitats in sequestering CO2', *Frontiers in Ecology and the Environment*, vol. 9, no. 10, pp. 552–560 [Online]. DOI: 10.1890/110004.

Minderhoud, P. S. J., Erkens, G., Pham, V. H., Bui, V. T., Erban, L. E., Kooi, H. and Stouthamer, E. (2017) 'Impacts of 25 years of groundwater extraction on subsidence in the Mekong delta, Vietnam', *Environmental Research Letters*, vol. 12 [Online]. DOI: 10.1088/1748-9326/aa7146.

Mitchell, J. K. and Soga, K. (2005) *Fundamentals of Soil Behavior*, 3rd ed. Hoboken, New Jersey, John Wiley & Sons.

Mitsch, W. J. and Gossilink, J. G. (2015) *Wetlands*, Fifth Edit. John Wiley & Sons.

Morton, R. A., Bernier, J. C. and Barras, J. A. (2006) 'Evidence of regional subsidence and associated interior wetland loss induced by hydrocarbon production, Gulf Coast region, USA', *Environmental Geology*, vol. 50, no. 2, pp. 261–274 [Online]. DOI: 10.1007/s00254-006-0207-3.

Morton, R. A., Buster, N. A. and Krohn, M. D. (2002) 'Subsurface Controls on Historical Subsidence Rates and Associated Wetland Loss in Southcentral Louisiana', *Transactions Gulf Coast Association of Geological Societies*, vol. 52, pp. 767–778.

Nardin, W., Mariotti, G., Edmonds, D. A., Guercio, R. and Fagherazzi, S. (2013) 'Growth of river mouth bars in sheltered bays in the presence of frontal waves', *Journal of Geophysical Research: Earth Surface*, vol. 118, no. 2, pp. 872–886 [Online]. DOI: 10.1002/jgrf.20057.

Neumeier, U., Lucas, C. L. and Collins, M. (2006) 'Erodibility and erosion patterns of mudflat sediments investigated using an annular flum', *Aquatic Ecology*, vol. 40, pp. 543–554 [Online]. DOI: 10.1007/s 10452-004-0189-8.

Ngoc Anh, L., Duc Tran, D., Thong, N., Thu Van, C., Hoa Vinh, D., Hai Au, N. and Park, E. (2022) 'Drastic variations in estuarine morphodynamics in Southern Vietnam: Investigating riverbed sand mining impact through hydrodynamic modelling and field controls', *Journal of Hydrology*, Elsevier B.V., vol. 608, no. January, p. 127572 [Online]. DOI: 10.1016/j.jhydrol.2022.127572.

Nienhuis, J. H. and van de Wal, R. S. W. (2021) 'Projections of Global Delta Land Loss

From Sea-Level Rise in the 21st Century', *Geophysical Research Letters*, vol. 48, no. 14, pp. 1–9 [Online]. DOI: 10.1029/2021GL093368.

Nittrouer, J. A., Allison, M. A. and Campanella, R. (2008) 'Bedform transport rates for the lowermost Mississippi River', *Journal of Geophysical Research: Earth Surface*, vol. 113, no. 3, pp. 1–16 [Online]. DOI: 10.1029/2007JF000795.

Olliver, E. A. and Edmonds, D. A. (2017) 'Defining the ecogeomorphic succession of land building for freshwater, intertidal wetlands in Wax Lake Delta, Louisiana', *Estuarine, Coastal and Shelf Science*, Elsevier Ltd, vol. 196, pp. 45–57 [Online]. DOI: 10.1016/j.ecss.2017.06.009.

Parsons, D. R., Best, J. L., Lane, S. N., Orfeo, O., Hardy, R. J. and Kostaschuk, R. (2007) 'Form roughness and the absence of secondary flow in a large confluence–diffluence, Rio Paraná, Argentina', *Earth Surface Processes and Landforms*, vol. 32, pp. 155–162 [Online]. DOI: 10.1002/esp.1457.

Parsons, D. R., Schindler, R. J., Hope, J. A., Malarkey, J., Baas, J. H., Peakall, J., Manning, A. J., Ye, L., Simmons, S., Paterson, D. M., Aspden, R. J., Bass, S. J., Davies, A. G., Lichtman, I. D. and Thorne, P. D. (2016) 'The role of biophysical cohesion on subaqueous bed form size', *Geophysical Research Letters*, vol. 43, no. 4, pp. 1566–1573 [Online]. DOI: 10.1002/2016GL067667.

Pendleton, L., Donato, D. C., Murray, B. C., Crooks, S., Jenkins, W. A., Sifleet, S., Craft, C., Fourqurean, J. W., Kauffman, J. B., Marbà, N., Megonigal, P., Pidgeon, E., Herr, D., Gordon, D. and Baldera, A. (2012) 'Estimating Global "Blue Carbon" Emissions from Conversion and Degradation of Vegetated Coastal Ecosystems', *PLoS ONE*, vol. 7, no. 9 [Online]. DOI: 10.1371/journal.pone.0043542.

Pike, L., Gaskin, S. and Ashmore, P. (2018) 'Flume tests on fluvial erosion mechanisms in till-bed channels', *Earth Surface Processes and Landforms*, vol. 43, no. 1, pp. 259–270 [Online]. DOI: 10.1002/esp.4240.

Raudkivi, A. J. (1998) *Loose Boundary Hydraulics*, 4th ed. Rotterdam, A.A. Balkema.

Rinehimer, J. P., Harris, C. K., Sherwood, C. R. and Sanford, L. P. (2008) 'Estimating Cohesive Sediment Erosion and Consolidation in a Muddy, Tidally-Dominated Environment: Model Behavior and Sensitivity', *Estuarine and Coastal Modeling (2007)*, vol. 40990, no. March 2018, pp. 819–838 [Online]. DOI: 10.1061/40990(324)44.

Rossi, V. M., Kim, W., López, J. L., Edmonds, D. A., Geleynse, N., Olariu, C., Steel, R. J., Hiatt, M. and Passalacqua, P. (2016) 'Impact of tidal currents on delta-channel deepening, stratigraphic architecture, and sediment bypass beyond the shoreline', *Geology*, vol. 44, no. 11, pp. 927–930 [Online]. DOI: 10.1130/G38334.1.

Rowland, J. C., Stacey, M. T. and Dietrich, W. E. (2009) 'Turbulent characteristics of a shallow wall-bounded plane jet: Experimental implications for river mouth hydrodynamics', *Journal of Fluid Mechanics*, vol. 627, pp. 423–449 [Online]. DOI: 10.1017/S0022112009006107.

Rutherford, J. S., Day, J. W., D'Elia, C. F., Wiegman, A. R. H., Willson, C. S., Caffey, R. H., Shaffer, G. P., Lane, R. R. and Batker, D. (2018) 'Evaluating trade-offs of a large, infrequent sediment diversion for restoration of a forested wetland in the Mississippi delta', *Estuarine, Coastal and Shelf Science*, Elsevier Ltd, vol. 203, pp. 80–89 [Online]. DOI: 10.1016/j.ecss.2018.01.016.

Salter, G., Paola, C. and Voller, V. R. (2017) 'Control of delta avulsion by downstream sediment sinks', *Journal of Geophysical Research: Earth Surface* [Online]. DOI: 10.1002/2017JF004350.

Shaw, J. B. and Mohrig, D. (2014a) 'The importance of erosion in distributary channel network growth, Wax Lake Delta, Louisiana, USA', *Geology*, vol. 42, no. 1, pp. 31–34

[Online]. DOI: 10.1130/G34751.1.

Shaw, J. B. and Mohrig, D. (2014b) 'The importance of erosion in distributary channel network growth, Wax Lake Delta, Louisiana, USA', *Geology*, vol. 42, no. 1, pp. 31–34 [Online]. DOI: 10.1130/G34751.1.

Shepard, C. C., Crain, C. M. and Beck, M. W. (2011) 'The protective role of coastal marshes: A systematic review and meta-analysis', *PLoS ONE*, vol. 6, no. 11 [Online]. DOI: 10.1371/journal.pone.0027374.

Shields, A. (1936) *Appllication of similarity principles and turbulence research to bed-load movement [Translated]*, [Online]. Available at http://resolver.tudelft.nl/uuid:a66ea380-ffa3-449b-b59f-38a35b2c6658.

Sundborg, Å. (1956) 'The River Klarälven : A Study of Fluvial Processes Author (s): Åke Sundborg Published by : Taylor & Francis , Ltd . on behalf of Swedish Society for Anthropology and Geography Stable URL : https://www.jstor.org/stable/520140', *Geografiska annaler*, vol. 38, no. 2, pp. 125–237.

Syvitski, J. P. M., Kettner, A. J., Overeem, I., Hutton, E. W. H., Hannon, M. T., Brakenridge, G. R., Day, J. W., Vörösmarty, C. J., Saito, Y., Giosan, L. and Nicholls, R. J. (2009) 'Sinking deltas due to human activities', *Nature Geoscience*, vol. 2, no. 10, pp. 681–686 [Online]. DOI: 10.1038/ngeo629.

Syvitski, J. P. M. and Saito, Y. (2007) 'Morphodynamics of deltas under the influence of humans', *Global and Planetary Change*, vol. 57, no. 3–4, pp. 261–282 [Online]. DOI: 10.1016/j.gloplacha.2006.12.001.

Syvitski, J. P. M., Vörösmarty, C. J., Kettner, A. J. and Green, P. (2005) 'Impact of Humans on the Flux of Terrestrial Sediment to the Global Coastal Ocean', *Science*, vol. 308, no. 5720, pp. 376–380 [Online]. DOI: 10.1126/science.1109454.

Thanh, V. Q., Reyns, J., Wackerman, C., Eidam, E. F. and Roelvink, D. (2017a) 'Modelling suspended sediment dynamics on the subaqueous delta of the Mekong River', *Continental Shelf Research*, Elsevier Ltd, vol. 147, no. July, pp. 213–230 [Online]. DOI: 10.1016/j.csr.2017.07.013.

Thanh, V. Q., Reyns, J., Wackerman, C., Eidam, E. F. and Roelvink, D. (2017b) 'Modelling suspended sediment dynamics on the subaqueous delta of the Mekong River', *Continental Shelf Research*, Elsevier Ltd, vol. 147, no. August, pp. 213–230 [Online]. DOI: 10.1016/j.csr.2017.07.013.

Tolhurst, T. J., Black, K. S., Shayler, S. A., Mather, S., Black, I., Baker, K. and Paterson, D. M. (1999) 'Measuring the in situ erosion shear stress of intertidal sediments with the cohesive strength meter (CSM)', *Estuarine, Coastal and Shelf Science*, vol. 49, no. 2, pp. 281–294 [Online]. DOI: 10.1006/ecss.1999.0512.

Tolhurst, T. J., Gust, G. and Paterson, D. M. (2002) 'The influence of an extracellular polymeric substance (EPS) on cohesive sediment stability', *Proceedings in Marine Science*, vol. 5, no. C, pp. 409–425 [Online]. DOI: 10.1016/S1568-2692(02)80030-4.

Tong, Y. D. (2017) 'Rice Intensive Cropping and Balanced Cropping in the Mekong Delta , Vietnam — Economic and Ecological Considerations', *Ecological Economics*, Elsevier B.V., vol. 132, pp. 205–212 [Online]. DOI: 10.1016/j.ecolecon.2016.10.013.

van der Vegt, H., Storms, J. E. A., Walstra, D. J. R. and Howes, N. C. (2016) 'Can bed load transport drive varying depositional behaviour in river delta environments?', *Sedimentary Geology*, Elsevier B.V., vol. 345, pp. 19–32 [Online]. DOI: 10.1016/j.sedgeo.2016.08.009.

Vörösmarty, C. J., Syvitski, J. P. M., Day, J. W., de Sherbinin, A., Giosan, L. and Paola, C. (2009) 'Battling to save the world's river deltas', *Bulletin of the atomic scientists*, vol. 65, no. 2, pp. 31–43 [Online]. DOI: 10.2968/065002005.

Warner, K. (2010) 'Global environmental change and migration: Governance

challenges', *Global Environmental Change*, Elsevier Ltd, vol. 20, no. 3, pp. 402–413 [Online]. DOI: 10.1016/j.gloenvcha.2009.12.001.

Warner, R., Kaidonis, M., Dun, O., Rogers, K., Shi, Y., Nguyen, T. T. X. and Woodroffe, C. D. (2016) 'Opportunities and challenges for mangrove carbon sequestration in the Mekong River Delta in Vietnam', *Sustainability Science*, Springer Japan, vol. 11, no. 4, pp. 661–677 [Online]. DOI: 10.1007/s11625-016-0359-3.

Wei, X. and Wu, C. (2014) 'Long-term process-based morphodynamic modeling of the Pearl River Delta', *Ocean Dynamics*, vol. 64, no. 12, pp. 1753–1765 [Online]. DOI: 10.1007/s10236-014-0785-7.

Winterwerp, J. C., van Kesteren, W. G. M., van Prooijen, B. and Jacobs, W. (2012) 'A conceptual framework for shear flow–induced erosion of soft cohesive sediment beds', *Journal of Geophysical Research: Oceans*, vol. 117, no. October, pp. 1–17 [Online]. DOI: 10.1029/2012JC008072.

Wright, L. D. (1977) 'Sediment transport and deposition at river mouths: A synthesis', *Geological Soceity of America Bulletin*, vol. 88, no. 6, pp. 857–868.

Le Xuan, T., Nguyen Cong, P., Vo Quoc, T., Tran, Q. Q., Wright, D. P. and Tran Anh, D. (2022) 'Multi-scale modelling for hydrodynamic and morphological changes of breakwater in coastal Mekong Delta in Vietnam', *Journal of Coastal Conservation*, Springer Netherlands, vol. 26, no. 3, pp. 1–18 [Online]. DOI: 10.1007/s11852-022-00866-3.

Yang, F., Liu, X., Cao, S. and Huang, E. (2010) 'Bed load transport rates during scouring and armoring processes', *Journal of Mountain Science*, vol. 7, no. 3, pp. 215–225 [Online]. DOI: 10.1007/s11629-010-2013-3.

Zhang, H., Chen, X. and Luo, Y. (2016) 'An overview of ecohydrology of the Yellow River delta wetland', *Ecohydrology and Hydrobiology*, European Regional Centre for Ecohydrology of Polish Academy of Sciences, vol. 16, no. 1, pp. 39–44 [Online]. DOI: 10.1016/j.ecohyd.2015.10.001.

3 The effects of substrate erodibility on delta morphodynamics

3.1 Introduction

Globally, river deltas are home to more than 300 million people (Syvitski et al., 2009; Syvitski and Saito, 2007) and commonly host important areas of productive agricultural land (Warner, 2010), especially in countries that otherwise have unsuitable climates for food production (such as in Egypt, where the Nile Delta compromises 63% of the country's agricultural land despite being only 2% of its total land area; Hereher, 2010). The wetlands present on many deltas have been shown to provide valuable ecosystem services, including resilience to storm surges (Barbier et al., 2013) and sequestration of carbon at a far greater rate than terrestrial forests (McLeod et al., 2011). However, these systems are vulnerable to coastal erosion and inundation, as large areas of delta tops are below or near sea level (Syvitski et al., 2009), and they naturally subside due to consolidation of deposited sediment. This natural subsidence is compounded by anthropogenic subsidence due to subsurface fluid extraction (Morton et al., 2002), sediment extraction (Hackney et al., 2020) and sea level rise, with projections suggesting that globally up to 5% of delta area could be lost by then end of the century (Nienhuis and van de Wal, 2021).

It has become clear that, when averaged globally, the volumes of sediment reaching river mouths has decreased significantly from pre-Anthropocene levels (Dethier et al., 2022; Syvitski et al., 2005) and is projected to continue to decline by an average of 38% by 2099 (Dunn et al., 2019). Deltas need constant deposition of sediment to counteract subsidence and sea level rise, so anthropogenic

sediment reduction impairs the ability of deltas to respond to changes. In the face of decreasing sediment discharge, the efficiency with which deltas build subaerially exposed land with the sediment that is delivered to the coast is critical. Studying the morphology of these systems can give us an insight in to how morphodynamics distribute sediment to build land and how resilient these areas are to inundation and coastal erosion.

Sediment grain size has been shown to effect delta morphology, with increasing grain size leading to an increase of topset slope as greater slopes are needed to transport larger sediment (Caldwell and Edmonds, 2014). Deltas formed from finer sediment commonly have fewer (Burpee et al., 2015), more stable (Caldwell and Edmonds, 2014) channels. This is likely because of the lower topset slope reducing avulsion potential (Caldwell and Edmonds, 2014) as well as levees becoming more resistant due to increased cohesivity inherent to finer grains (Edmonds and Slingerland, 2010). Deltas with fewer channels that migrate less tend to deposit sediment at a limited number of locations on their coast, meaning that these delta coastlines tend to be more rugose (Burpee et al., 2015). Large, competent channels can also extend outward into a basin and deposit sediment into deeper waters some distance from shore where land building is less efficient (Kim et al., 2009).

While fine, erodible basin sediment has been shown to lead to more incisive delta channels (Geleynse et al., 2011), no research has been conducted into how the basin sediment erodibility impacts delta morphology. The geomorphology of deltas has previously been understood to be predominantly driven by depositional processes (Edmonds and Slingerland, 2007), and interaction with their receiving basin substrate has been largely marginalised, but multiple recent

studies have identified deltas as being more erosional than previously thought (Shaw and Mohrig, 2014a; Hoyal and Sheets, 2009), suggesting that the qualities of the underlying sediment may play a bigger role than previously thought in determining the mechanisms that influence delta morphology. This is especially the case in examples such as Wax Lake Delta (Louisiana, USA), which is known to interact with underlying resistant, consolidated muds in its receiving basin (e.g. Shaw et al., 2013).

The aim of the work herein is to explore the impact that the erodibility of the underlying basin substrate has on the morphological evolution of river deltas as they grow from initiation. As deltas are becoming more vulnerable due to anthropogenic impacts (Nienhuis and van de Wal, 2021; Dunn et al., 2019), it is also important to consider how they will react to a range of ongoing and future pressures, such as reductions in sediment supply and relative sea-level rise. Previously unstudied and otherwise "hidden" metrics such as the composition of the receiving basin substrate could compromise predictions where these impacts are ignored. While higher cohesivity fluvial sediment is known to cause deltas to form with fewer, more stable channels, more rugose shorelines and shallower topset gradient, (Burpee et al., 2015; Caldwell and Edmonds, 2014; Edmonds and Slingerland, 2010) more resistant substrate sediments are hypothesised to reduce incision, without increasing the strength of deposited levees or mouth bars. As such, channel stability is hypothesised to decrease rather increase as substrate strength increases, leading to more equitable sediment distribution and hence less rugose shorelines.

3.2 Methodology

3.2.1 *Delft3D*

Delft3D is a hydrological and morphological model that has been widely used in the past to study coastal fluvial landforms such as deltas (van de Lageweg et al., 2018; Burpee et al., 2015; Caldwell and Edmonds, 2014; Geleynse et al., 2011; Edmonds and Slingerland, 2010), river mouth bars (Fagherazzi et al., 2015) and estuaries in confined basins (Van de Lageweg and Feldman, 2018).

Water flow is solved through 2D unsteady shallow-water equations. These equations are derived from the 3D Navier-Stokes equations for incompressible fluid by assuming vertical accelerations (due to buoyancy or variations in bed topography) are negligible compared to gravity, hence reducing the vertical momentum components to a hydrostatic pressure relation (Lesser et al., 2004):

Horizontal U Component

$$\frac{\partial u}{\partial t} + u\frac{\partial u}{\partial x} + v\frac{\partial u}{\partial y} + \frac{\omega}{h}\frac{\partial u}{\partial \sigma} - fv = -\frac{1}{\rho_0}P_x + F_x + M_x + \frac{1}{h^2}\frac{\partial}{\partial \sigma}\left(\nu_V \frac{\partial u}{\partial \sigma}\right) \quad \textit{(3-1)}$$

Horizontal V Component

$$\frac{\partial v}{\partial t} + u\frac{\partial v}{\partial x} + v\frac{\partial v}{\partial y} + \frac{\omega}{h}\frac{\partial v}{\partial \sigma} - fu = -\frac{1}{\rho_0}P_y + F_y + M_y + \frac{1}{h^2}\frac{\partial}{\partial \sigma}\left(\nu_V \frac{\partial v}{\partial \sigma}\right) \quad \textit{(3-2)}$$

Vertical

$$\frac{\partial P}{\partial \sigma} = -\rho g h \tag{3-3}$$

A continuity equation for conservation of mass is also used, which equates fluid entering and leaving an area with a change in surface height:

$$\frac{\zeta}{t} + \frac{\partial hu}{\partial x} + \frac{\partial hv}{\partial y} = S \tag{3-4}$$

Delft3D distinguishes between coarse, non-cohesive sediment (D_{50}>64μm) and fine cohesive sediment (D_{50}<64μm), and treats these two types differently in some situations. Both cohesive and non-cohesive fractions are transported in suspension using an advection-diffusion equation:

$$\frac{\partial hc}{\partial t} + \frac{\partial huc}{\partial x} + \frac{\partial hvc}{\partial y} + \frac{\partial wc}{\partial s} = h\left[\frac{\partial}{\partial x}\left(D_H \frac{\partial c}{\partial x}\right) + \frac{\partial}{\partial y}\left(D_H \frac{\partial c}{\partial y}\right)\right] + \frac{1}{h}\frac{\partial}{\partial \sigma}\left(D_V \frac{\partial c}{\partial \sigma}\right) + hS \tag{3-5}$$

Deposition and erosion of suspended cohesive sediment is controlled by the Partheniades-Krone formulation, consisting of two step functions for erosion and deposition:

Erosion is controlled by equation 2-1, as shown in Section 2.4.3:

$$E = \begin{cases} M\left(\frac{\tau_{bed}}{\tau_{ce}} - 1\right), & when\ \tau_{bed} > \tau_{ce} \\ 0, & when\ \tau_{bed} \leq \tau_{ce} \end{cases} \tag{2-1}$$

Along with the step function for deposition of a cohesive sediment fraction:

$$D = \begin{cases} \omega_s c \left(1 - \frac{\tau_{bed}}{\tau_{cd}}\right), & when\ \tau_{bed} < \tau_{cd} \\ 0 & , \ when\ \tau_{bed} \geq \tau_{cd} \end{cases} \qquad \textit{(3-6)}$$

Deposition and erosion of suspended non-cohesive sediment is calculated in terms of separate erosive 'source' and depositional 'sink' terms acting between the bed and the *kmx* layer (the lowest hydrodynamic layer that is entirely above van Rijns reference height, a):

$$\boldsymbol{Source} = \ \boldsymbol{\alpha_2 c_a \left(\frac{\varepsilon_s}{\Delta z}\right)}$$

$$\boldsymbol{Sink} = \ \left[\boldsymbol{\alpha_2 \left(\frac{\varepsilon_s}{\Delta z}\right) + \alpha_1 w_s}\right] \boldsymbol{c_{kmx}} \qquad \textit{(3-7)}$$

As discussed in section 2.4.3, equation 2-1 simplifies the erosion of cohesive material, and neglects the differences between fluid mud mixing, surface and mass erosion (Krone, 1999) that would happen . Here it is assumed that τ_{ce} represents the critical shear stress for the onset of surface erosion, and acknowledge the model will neglect any small amounts of erosion that happen where $0 > \tau_{bed} > \tau_{ce}$ and will underestimate the mass erosion that may happen when both τ_{ce} and τ_{bed} are high. This is necessary as Delft3D does not support erosion with multiple shear stress thresholds, and this also simplifies the considerations for setting these thresholds in the study's parameter space.

In addition to this, non-cohesive sediment is transported as bedload. In this study, the TRANSPOR04 model (van Rijn et al., 2004) is used to simulate bedload transport, $\boldsymbol{q_b}$:

$$\boldsymbol{q_b = 0.5 \rho_s d_{50} D_*^{-0.3} \left(\frac{\tau}{\rho}\right)^{0.5} \left(\frac{\max(0, \tau - \tau_{cr})}{\tau_{cr}}\right)} \qquad \textit{(3-8)}$$

3.2.2 *Model setup*

Delft3D-FLOW was used to simulate a series of generic deltas, with the model domain consisting of a 300x225 grid of 30x30m cells, giving a total domain size of 9.0 x 6.9 km (see supplementary figure 1). A domain of this size was chosen as it gave enough space in which to form a mature delta without compromising cell size or lengthening run-time to more than would be manageable. The bed of the basin deepened towards the north with a gradient of 0.000375, based on similar Delft modelling studies (Caldwell and Edmonds, 2014; Edmonds and Slingerland, 2010). Flowing into this basin was a fluvial inlet 300 m wide with an average discharge of 880 $m^3 s^{-1}$ and a constant sediment concentration of 0.2 kg m^{-3}, made up of 60% non-cohesive sand and 40% cohesive fluvial mud by mass. Channel geometry was chosen to be large enough to easily accommodate peak flows, even in high τ_{ce} runs where channel deepening was likely to be precluded.

The inlet channel had a temporally varying, synthetic discharge made from the product of two sine waves, one with a period of 1 morphological year and one with a period of 41 morphological days (simulating a storm rainfall) to represent both seasonal and higher frequency variations in flow. Flow variation and the inclusion of inter-flood base flow periods been shown to be important in constructing realistic deltas in physical models (Piliouras et al., 2017). While small fluctuations in discharge are likely to happen at higher frequency this, the frequency used here was limited by the temporal resolution with which this data could be supplied to the model. The synthetic hydrograph was intended to give this flow variation in a simple and broadly realistic way, without attempting to recreate specific flow events or the discharge regimes of specific deltas. This generated hydrograph varied between 500 and 3,500 m^{-3} s^{-1}, with a mean

discharge of 1,476 m3s-1 (Figure 3-1), meaning the deltas modelled here most closely align with smaller deltas about half the size of Wax Lake Delta, Louisiana, (10 year mean; 3382 m3s-1, 10 year median annual maximum; 6315 m3s-1) or the lobes of larger deltas. A discharge of approximately twice this was originally tested but was reduced to this to a) slow the filling of the basin to allow analysis of the delta over longer morphological time and c) increase model stability by decreasing peak flow speeds. The overall shape of the hydrograph is likely to have a considerable effect on delta morphodynamics, but in the absence of detailed studies quantifying this effect, this study keeps the hydrograph constant across all models for consistency.

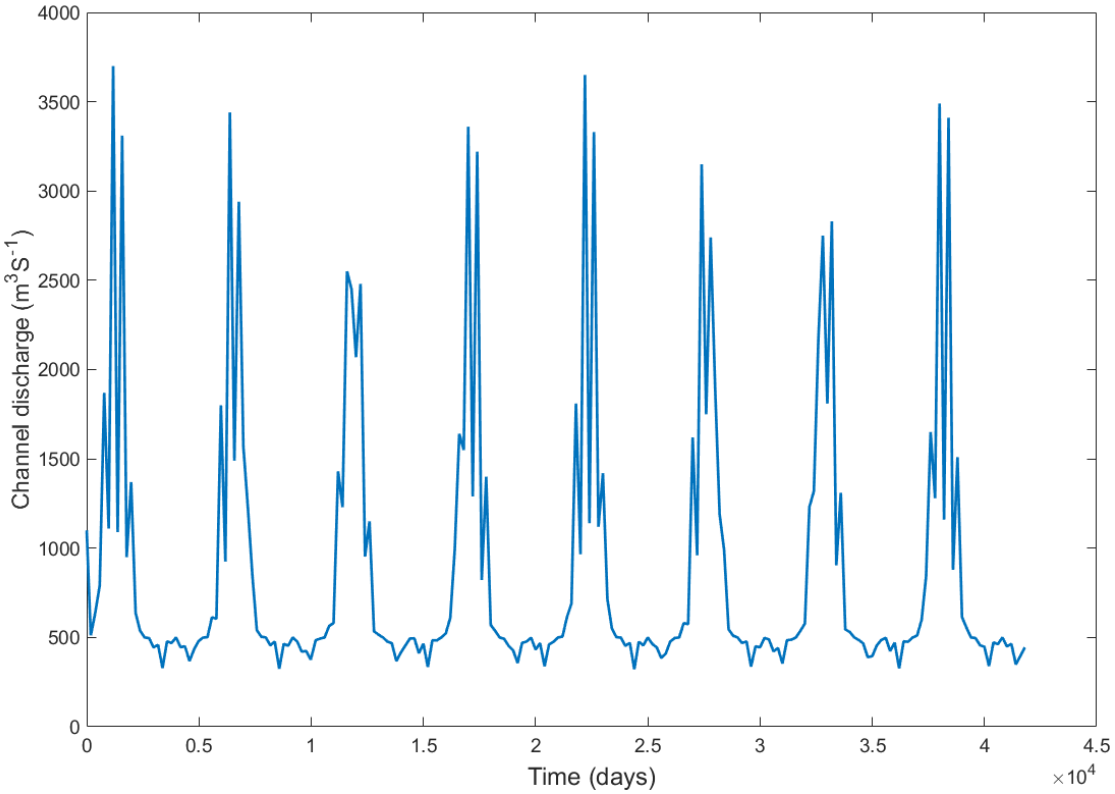

Figure 3-1: Discharge hydrograph used to provide the fluvial input at the inlet boundary.

The substrate of the receiving basin comprised a 20 m thick layer of sediment consisting of 20% fine sand and 80% mud (see Table 3.1). The critical shear stress (τ_{ce}) for erosion for the mud fraction was varied between runs from

0.25 - 12.5 N m^{-2}, which represents a wide range of sediment resistances. Lower τ_{ce} values (<2 N m^{-2}) may represent shallow marine sediments (which deltas are likely to form over) whereas higher values are intended to represent stiff clays that some deltas are known to interact with (e.g. Wax Lake Delta, Louisianna; Shaw and Mohrig, 2014a). The highest values of τ_{ce}, (>6 N m^{-2}) are known to be found in compacted clays, such as those forming in glacio-marine settings (Cossette, 2016; Gaskin et al., 2003; see figure 2-2). While some sediment beds may resistances higher than the upper τ_{ce} limit of this study (12.5 N m^{-2}), models whish higher values where not investigated as initial investigative model runs showed that model instability was common at these values and delta morphology was not dramatically different above τ_{ce} = 10 N m^{-2}.

Erosion is also controlled within Delft3D by an erosion parameter (M, see equation 2-1), which, similarly to τ_{ce} controls the rate at which erosion happens at a given bed shear stress, but unlike τ_{ce}, does not dictate a minimum threshold for erosion. The M parameter in known to vary widely in value across sediment types (Winterwerp et al., 2012), but in other studies that use Delft3D-flow to investigate similar environments, this value is frequently unexplained or neglected entirely (Burpee et al., 2015; Caldwell and Edmonds, 2014; Hanegan and Georgiou, 2014), but where it is quoted, a value of 0.0001 is frequently used (Braat et al., 2017). Ideally this value would be determined experimentally (Winterwerp et al., 2012), but this process was outside of the scope of this study. As such, similar to other studies, a value of M = 0.0001 is used here, and kept constant between runs and chapters to minimise its effect on the results.

Sediment deposition is controlled by the critical shear stress of deposition, τ_{cd}, the maximum bed shear stress at which sediment deposition happened.

However, studies have shown that sediment deposition happens continuously, and that continuous deposition was more effective for recreating full scale field conditions (Sanford, 2008). As such, as with many previous modelling studies (Braat et al., 2017; Caldwell and Edmonds, 2014), τ_{cd} was kept constant at 1,000 N m^{-2}, to cause constant deposition of fine sediment. This means that for erosion to happen, the erosive flux, E_m, must be large enough to exceed the depositional flux D_m.

Non-Cohesive sediment	**Specific Density (kg m^{-3})**	**Dry-bed Density (kg m^{-3})**	**Sediment D50 (µm)**	
Fine sand	2,650	1,600	225	
Cohesive sediment	**Specific Density (kg m^{-3})**	**Dry-bed Density (kg m^{-3})**	**τ_{ce} (N m^{-2})**	**τ_{cs} (N m^{-2})**
Fluvial Mud	2,650	500	1	1,000
Basin Mud	2,650	500	0.5–12.5	1,000

Table 3-1: List of sediment properties used by Delft3D.

A time step of was originally set to 9 seconds after similar modelling studies (Edmonds and Slingerland, 2010) but was later reduced to 3 seconds after the original timestep was found to cause instability in initial test runs of the model. All morphological change was multiplied by a factor of 75 to shorten model run times, again following previous studies (Edmonds and Slingerland, 2010). For each critical shear stress, three separate models were run with different white noise filters applied to the initial bed elevation, consisting of a randomly distributed addition of 0-0.05m to each cell. This was done to give 3 repetitions of each setup, an ensure that small changes in initial conditions did not lead to differences in model results greater than the differences caused by varying the control variable, $\boldsymbol{\tau}_{cs}$.

3.2.3 *Active Channel identification*

To investigate the effect that bed sediment has on delta morphodynamics, data on channel geometry, morphological change and flow velocity was collected from model outputs. Methods of automatic channel centreline identification have been shown to be effective in previous studies (Isikdogan et al., 2017; Passalacqua et al., 2010) to estimate channel geometries in situations where manual identification would be restrictively time consuming. Due to the large number of model outputs produced in this study, an algorithm (See Appendix 1), implemented in Matlab, was used to define "active" channels using threshold values for flow velocity, sediment transport and water depth. These values were then used to extract in-channel flow velocities, channel widths and channel lifetimes. Centrelines were defined from these active channels and used to extract channel depth measurements.

The algorithm used to identify active cells used four inputs taken directly from the Delft3D outputs; flow velocity magnitude (ms^{-1}, extracted from model files as $\sqrt{\boldsymbol{u}^2 + \boldsymbol{v}^2}$), total bed and suspended sediment transport magnitude (m^2s^{-1}, extracted from model files as $\sqrt{\left(\boldsymbol{q}_{b,u} + \boldsymbol{q}_{s,u}\right)^2 + \left(\boldsymbol{q}_{b,v} + \boldsymbol{q}_{s,v}\right)^2}$), bed elevation (m, extracted directly) and water depth (m, extracted as *water level - bed elevation*).

Flow velocity, sediment transport and water depth (Figure 3-2 a, b, and c,) are used to select a set of cells, by taking all cells that are i) higher than the 95th quartile of flow velocity, ii) higher than the 95th quartile of sediment transport and iii) shallower than 0.5m in depth to generate a raw map of active cells (*Figure 3-2e*). Separately, bed elevation (*Figure 3-2d*) was selected for cells below 0m

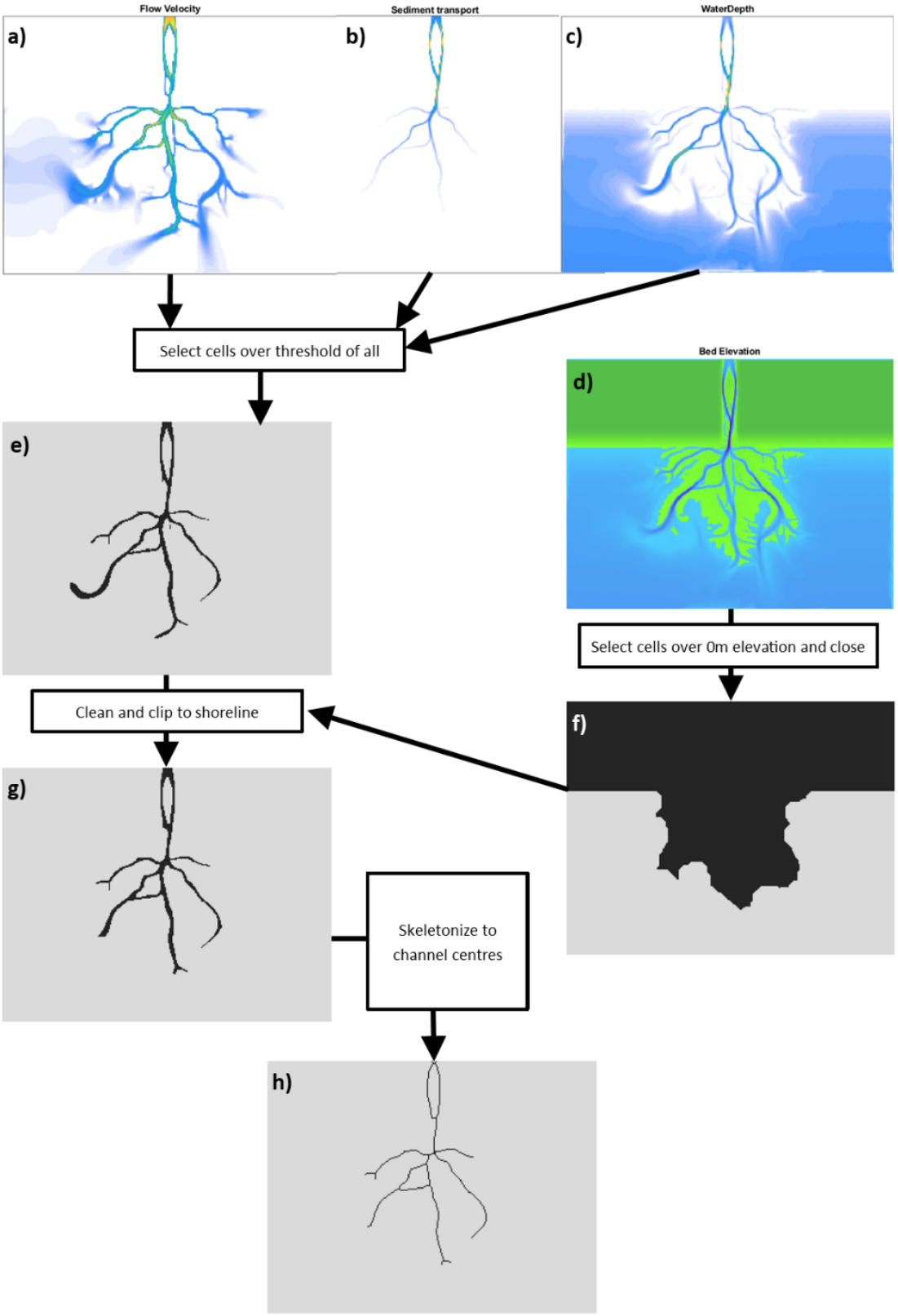

Figure 3-2: Process of the channel finding algorithm

elevation, then a closing operation was used to remove isolated gaps in the selected cells with a width less than 10 cells.

Morphological closing and opening are operations in mathematical morphology that are widely used in image analysis for removing noise from a binary image. These operations use two simpler operations; erosion and dilation, both of which use a structuring element (for example, element ***a*** on Figures 3-3 and 3-*4*) which is applied to a binary image (an image matrix consisting only of 1's and 0's). Dilation makes groups of 1's (referred to as objects) larger, and works

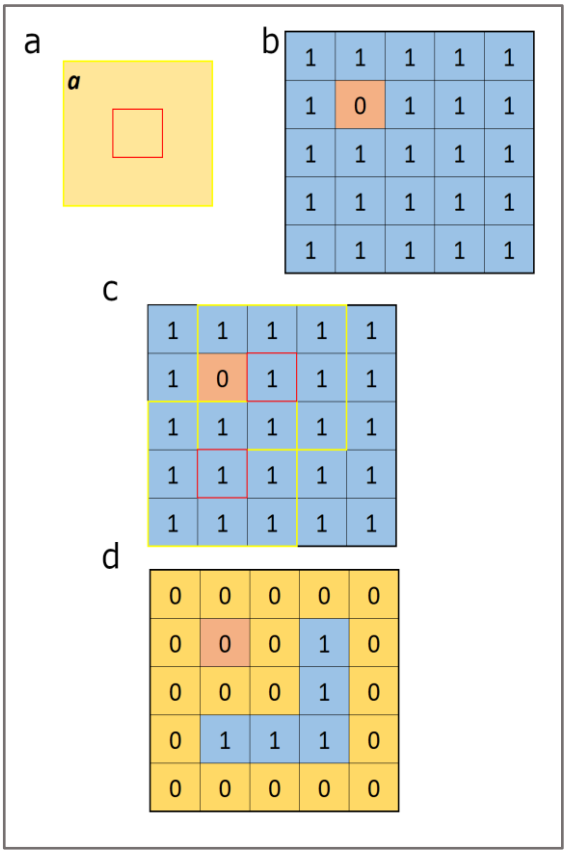

Figure 3-4: *Erosion of a binary image. In the top-right structuring element (c), one of the cells is a 0, so the centre cell is set to 0. In the bottom-left structuring element, all cells are 1's, so the centre cell remains 1.*

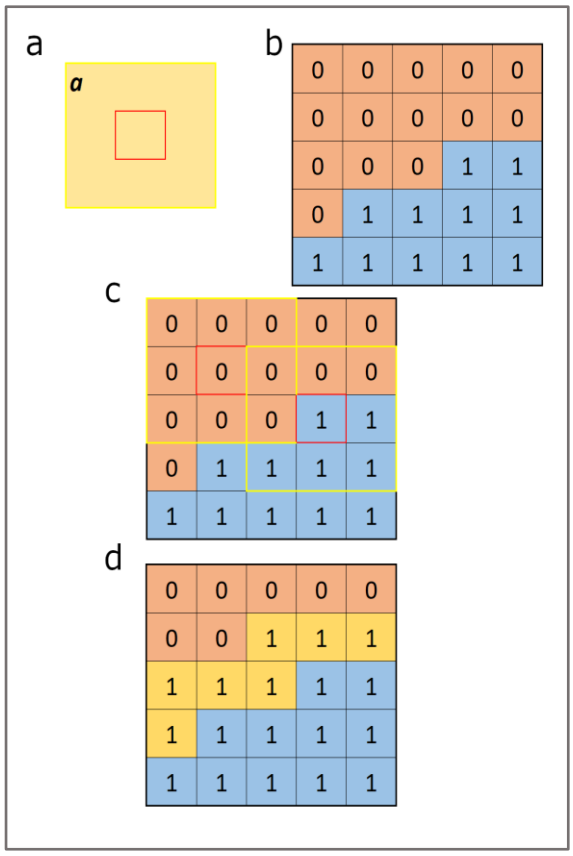

Figure 3-3: *Dilation of a binary image. For the top-left structuring element, the centre cell is 0 so no changes are made. For the bottom-right structuring element, the centre cell is 1 so all cells in the structuring element are set to 1*

by iteratively positioning the structuring element with its centre over each cell, and making all cells in the structuring element 1 if the cell at the centre is a 1 (see *Figure 3-3*). Erosion makes objects smaller, and works by iteratively positioning the structuring element with its centre cell over each cell of the input image, then marking that cell as a 1 if all cells within the structuring element contain 1's or marking it as a 0 otherwise (see Figure 3-4).

Binary closing and opening are performed by dilating and eroding a binary image. Closing an image removes any gaps (small groups of 0's surrounded by 1's) which are smaller than the width of the structuring element (see Appendix 2-fig.1), and is performed by first dilating then eroding an image. Opening does the opposite, removing small objects or parts of objects that are smaller than the structuring elements (groups of 0's surrounded by 1's) (see Appendix 2-fig.1).

A closing operation using a circular structuring element with a diameter of 20 model grid cells (30x30 m) is applied to the thesholded bed elevation map, the result of which is an approximate map of the delta shoreline (*Figure 3-2*f), without channels. These two matrices of selected (1) and unselected (0) cells are them multiplied by each other to create a map of active cells that are within the delta shoreline.

The rough map of active cells is then cleaned using a number of image processing operations. First, a bridging operation is used that sets any cell to 1 if it has two neighbouring 1's that aren't connected, to re-connect any channels that have become disconnected form the channel network due to gaps. Next, the whole map is closed with a 2x2 cell square structuring element to remove any small 'islands' in channels that can be generated by the above bridging operation.

Finally, all non-connected objects with an area less than 1% of the total area of channelised cells are removed to give a final map of major channels on the delta top (*Figure 3-2g*). This map is used over all recorded model timesteps to quantify channel stability (see below).

The channels are then reduced to a width of one cell to give a map of channel centrelines (see *Figure 3-2h*). This was done using a 'Skeletonizing' operation, which works by removing cells from the boundaries of objects without breaking them apart, until the objects are one cell wide. While this finds only the geometric centre of the channel rather than the true thalweg, no thalweg finding process could be found that was significantly more accurate than this operation, so the simpler 'Skeletonize' operation was used to keep reduce the computational intensity of the analysis.

3.2.4 *Measuring delta morphology*

Depths are recorded at each cell of the channel skeleton for the final timestep of each model run, and the mean of these then taken. Channel widths were approximated by taking the width in the X and Y directions at each point and using a function to convert these into the cross-channel width. If the X and Y components of the width are as below (Figure 3-5):

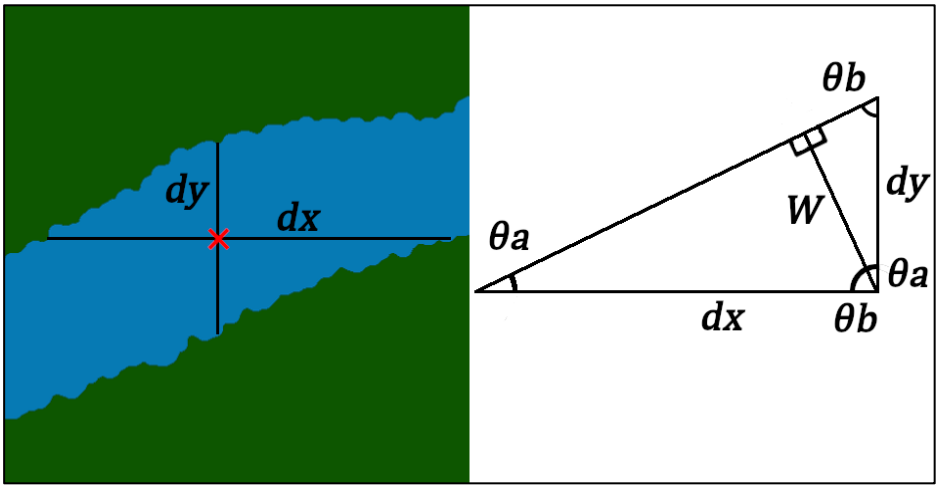

Figure 3-5: Schematic of the method used for channel width measurement method

Then:

$$\boldsymbol{W = dx\ \sin(\theta a) = dy\ \sin(\theta b)} \qquad \textbf{(3-9)}$$

$$\boldsymbol{\theta a = \tan^{-1}\left(\frac{dy}{dx}\right)}$$

$$\boldsymbol{\theta b = \tan^{-1}\left(\frac{dx}{dy}\right)}$$

(3-10)

Substituting **3-11** into $\boldsymbol{W = dx\ \sin(\theta a) = dy\ \sin(\theta b)}$ **(3-9**

gives:

$$\boldsymbol{W = dx\ \sin\left(\tan^{-1}\left(\frac{dy}{dx}\right)\right) = dy\ \sin\left(\tan^{-1}\left(\frac{dx}{dy}\right)\right)}$$

(3-11)

Substituting $\boldsymbol{\sin(\tan^{-1} x) = \frac{x}{\sqrt{1+x^2}}}$ gives:

$$W = \cancel{dx}\frac{\frac{dy}{\cancel{dx}}}{\sqrt{1+\left(\frac{dy}{dx}\right)^2}} = \cancel{dy}\frac{\frac{dx}{\cancel{dy}}}{\sqrt{1+\left(\frac{dx}{dy}\right)^2}}$$

$$= \frac{dy}{\sqrt{1+\left(\frac{dy}{dx}\right)^2}} = \frac{dx}{\sqrt{1+\left(\frac{dx}{dy}\right)^2}}$$

(3-12)

And so width is calculated as:

$$W = \frac{dx}{\sqrt{1+\left(\frac{dx}{dy}\right)^2}} \quad (3\text{-}13)$$

Where $\mathbf{dx}$ and $\mathbf{dy}$ are measured in cells, then W is multiplied by the cell width (30m) after calculations have been made. Channel geometry was recorded to analyse how equilibrium channel shape were reacting to different substrate erodibilities, and to identify deltas where extreme vertical incision or bank erosion was happening.

The volume of sediment eroded from the pre-delta bay was calculated by taking a Digital Elevation Model (DEM) of difference between the pre-run bathymetry and the basin bathymetry at the end of the run. Only grid cells that where negative (i.e., below the level of the pre-delta basin bed) where used, and their depths below the original bathymetry where multiplied by the area of the cell (600m^2) to give an overall volume of sediment removed, which was then summed across the whole domain. The area of erosion was calculated similarly, except the number of cells with that where deeper than pre-delta levels were counted and multiplied by the area of a cell.

Mean flow velocity in active channels was calculated by clipping the velocity magnitude matrix to include only cells identified as active by the algorithm (see above). The mean and maximum values of velocity where then calculated.

To attempt to quantify the larger-scale morphology of the delta top, three more morphometric coefficients were also calculated. 'Delta-top channel coverage' was calculated by calculating the total area occupied by active channel cells and dividing this by the total area of the delta top (effectively dividing *Figure 3-2*g by *Figure 3-2*f) to give a proportion (m^2/m^2) of the delta top occupied by channels. Additionally, a measurement of channel sinuosity was sought but, due to the highly complex nature of delta channel networks, the existing method for calculating sinuosity (e.g., total length/direct length) cannot be applied here. As such, two indicators of channel density and complexity were proposed. Firstly, 'network density' (D_n) was calculated by first measuring the total length of channel centrelines (see *Figure 3-2*h), then dividing this by the total area of the delta top (see *Figure 3-2*f). Secondly, to calculate 'network sinuosity' (S_n), the boundary of the delta top area was identified by running an edge finding algorithm on the delta shoreline map (*Figure 3-2*f), then calculating the average distance to every point on this boundary from the delta apex. The total length of channel centrelines was then divided by this average to give network sinuosity. These two metrics give a length-per-area and length-per-distance indicator (respectively) of how channelised the delta top is, and would be expected to be low in deltas with few, straight channels and high in deltas with many, sinuous and branching channels.

3.2.5 *Channel mobility analysis*

To investigate the mobility of channels, an algorithm in MATLAB used the active cell maps (above) for all recorded model timesteps to calculate an average descriptive channel residence time per cell. A residence time (T_{ch}) for each model cell was calculated by recording the time between it first becoming an active cell and the next time was no longer active. The lifetime was recorded, then that cell was reset so that if it was re-occupied a new residency time would be calculated. Following the a similar method to Caldwell and Edmonds (2014), these residence times were plotted as a cumulative distribution function of channel survival (i.e.,

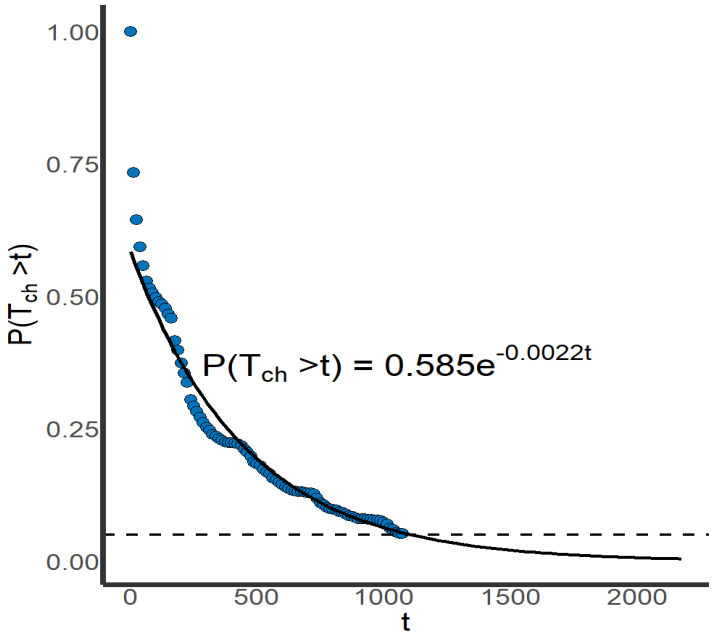

Figure 3-6: An example log curve $P(T_{ch}>t) = \alpha e^{-\lambda t}$ fitted to a survival plot of channel residence times

$P(T_{ch} > t)$, the proportion of channelised cells that survived longer than a time (t)) for each model run (Figure 3-6).

The lm (linear model) operation in R was then used to fit a curve to these plots with the generic equation:

$$P(T_{ch} > t) = \alpha e^{-\lambda t} \quad \textbf{(3-14)}$$

The α and λ coefficients where extracted, and the decay constant, λ, was then used to calculate the mean T_{ch} of channelised cells in that system:

$$\overline{T_{ch}} = \lambda^{-1} \quad \textbf{(3-15)}$$

This method of calculating mean channel lifetime was used, rather than taking an arithmetic mean of recorded lifetimes, as the distribution function can predict lifetimes greater than the length of the model run, and as such should be unaffected by the run length chosen for the study (Caldwell and Edmonds, 2014).

3.3 Results

Delta bathymetry plots (*Figure 3-7*) show change in morphology across the $\boldsymbol{\tau}_{ce}$ range, but this change is most dramatic at lower $\boldsymbol{\tau}_{ce}$ values. In general, deltas forming over lower $\boldsymbol{\tau}_{ce}$ substrates have wider channels, more shallow subaqueous deposition, and a lower elevation delta top. These morphologies are investigated below in more detail by applying the above methods to each of the model outputs from the 84 Delft3D runs. Channel residence time used every recorded model timestep, whereas delta top area and elevation, channel geometry and incision and flow velocity were calculated for the final timestep of the model run.

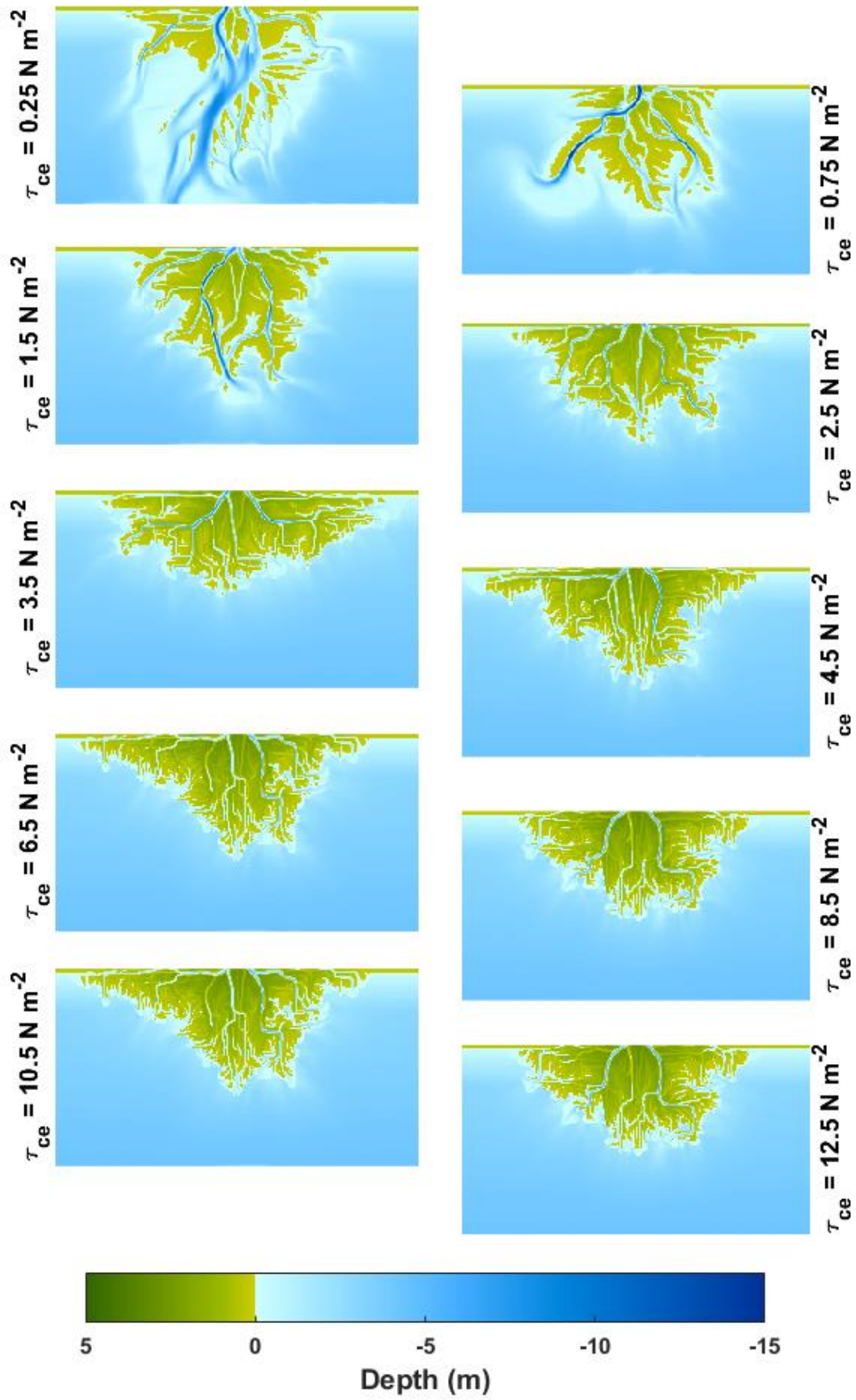

Figure 3-7: Bathymetries of sample deltas formed over different basin substrates. For Bathymetries of all deltas see Appendix 2 figures ii-vi

3.3.1 *Channel Geometry*

To support the analysis of channel geometry trends, the amount of erosion into the pre-existing substate was first quantified. The volume of sediment eroded from the substrate was found to decrease dramatically with increasing $\boldsymbol{\tau}_{ce}$ (by a factor of ~15, see Figure 3-8), demonstrating that receiving basin substrates that are more resistant results in more limited vertical erosion and hence shallower channels. The area over which incision occurs into the existing substrate decreases sharply between deltas with substrate $\boldsymbol{\tau}_{ce}$ = 0.25 and those with substrate $\boldsymbol{\tau}_{ce}$ 1 N m^{-2}, (*Figure 3-8*), as in very erodible (low $\boldsymbol{\tau}_{ce}$) sediments, even wide channels are able to easily incise into the erodible substrate across their

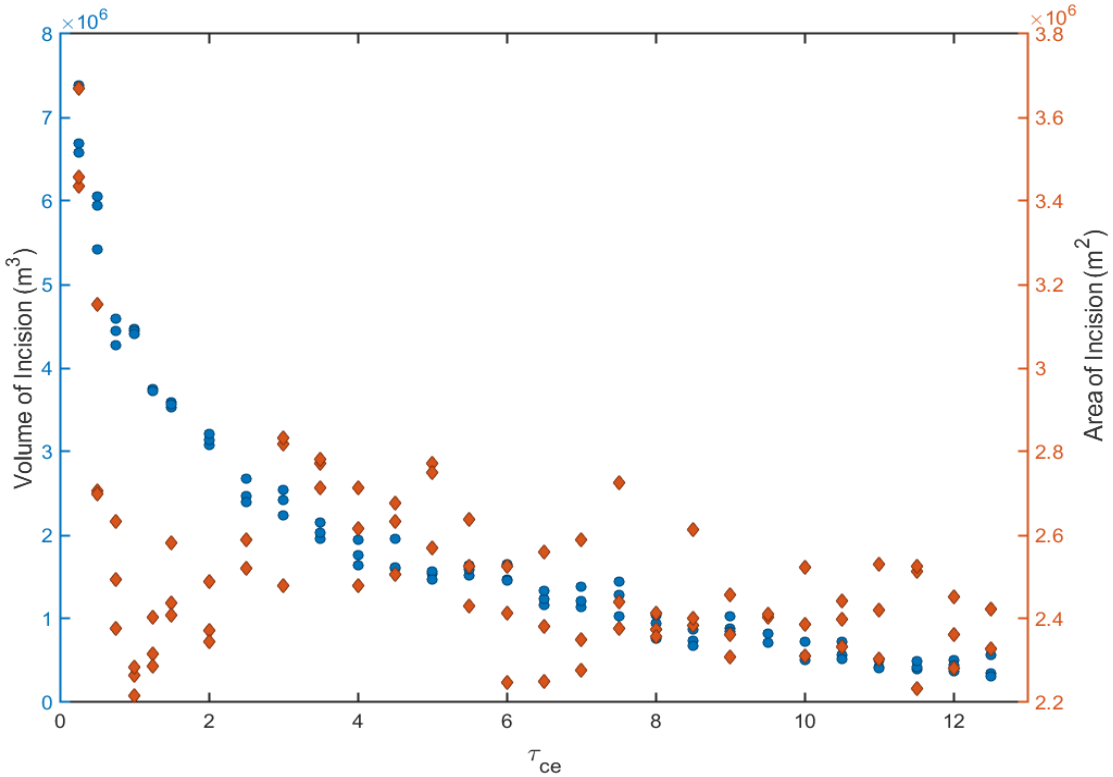

Figure 3-8: Volume of sediment eroded from the pre-delta bed and the area over which this erosion has happened

whole width, but a small increase in $\boldsymbol{\tau}_{ce}$ restricts incision to the centre of the channel where erosive power is greatest.

At low $\boldsymbol{\tau}_{ce}$, mean channel depth and width decrease rapidly with increasing $\boldsymbol{\tau}_{ce}$, but change very little above $\boldsymbol{\tau}_{ce}$ = *c.* 4 N m^{-2} (*Figure 3-9*). This reduction in channel depth can be attributed to a decreased ability to erode into more resistant basin substrates, with an increasing width:depth ratio at greater τ_{ce} (*Figure 3-10*) revealing shallower, relatively wider channels at higher τ_{ce} driven by lateral erosion rather than vertical incision into a resistant bed. At critical shear stresses above 4 N m^{-2}, channel depth stabilises around 2.5m (*Figure 3-9*), a value similar to the depth of the basin, suggesting that above this $\boldsymbol{\tau}_{ce}$, channels are not sufficiently erosional to significantly deepen channels. Note that despite this increasing width:depth ratio, channel width is not actually increasing, but is decreasing with τ_{ce} at a lower rate than channel depth is decreasing (*Figure 3-9*). Because of the trends in width and depth, channels decrease dramatically in size

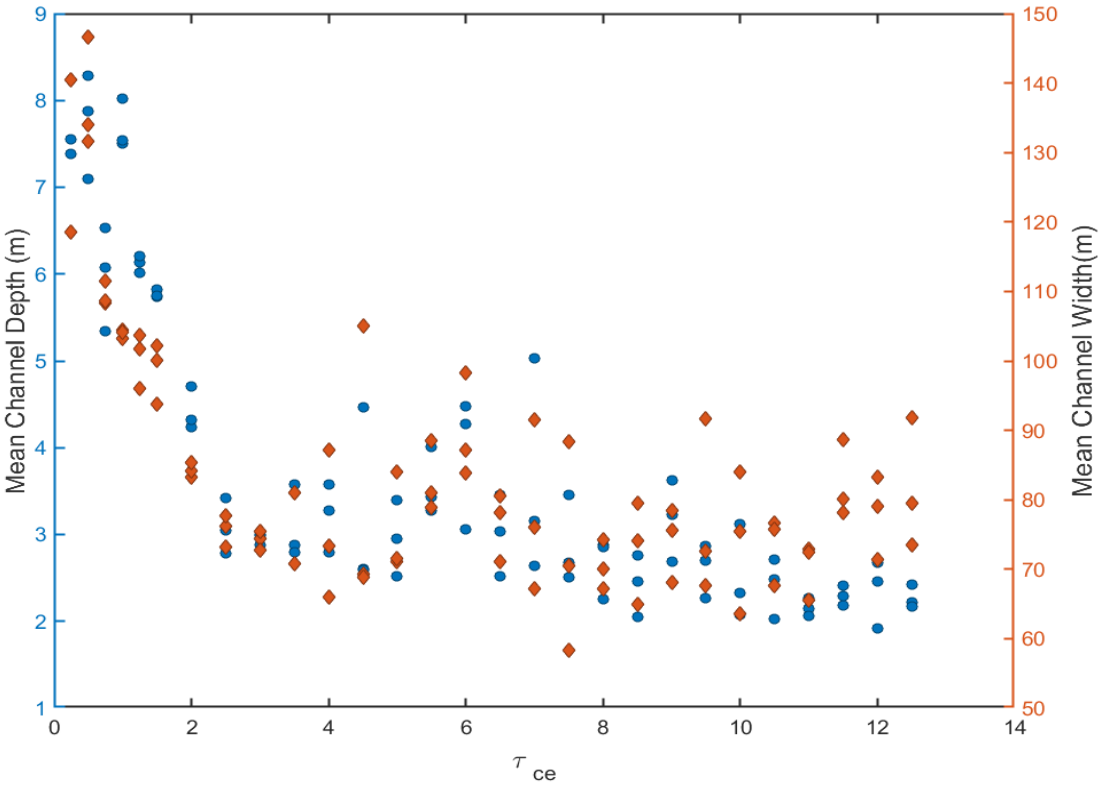

Figure 3-9: Mean width and depth of delta channels

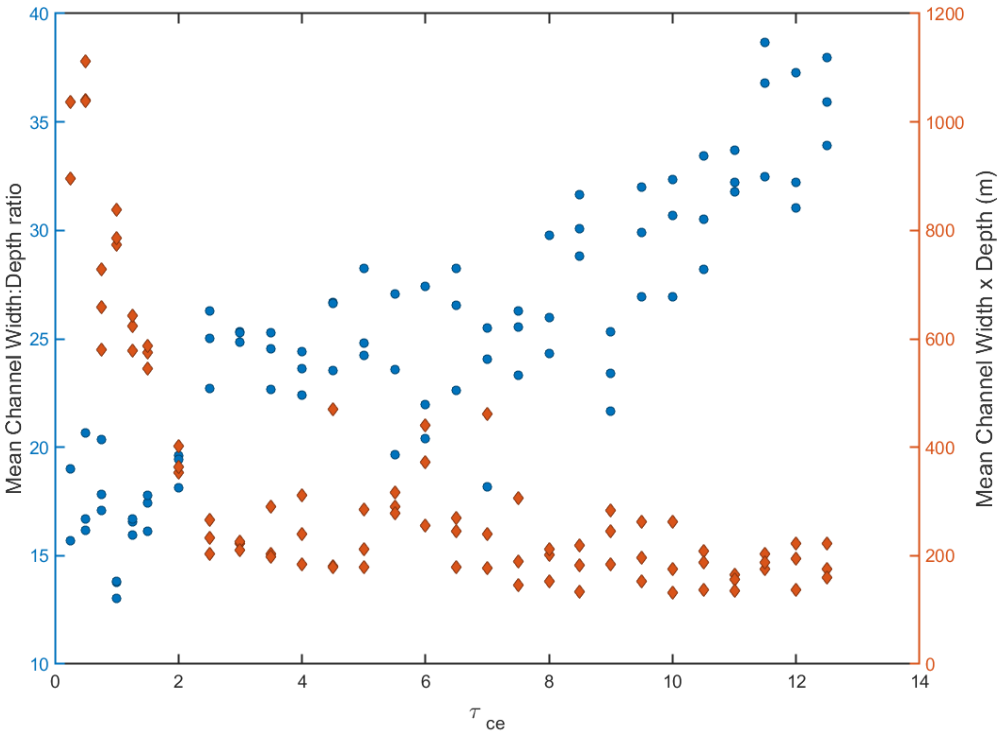

Figure 3-10: Mean Channel W:D ratio and indicative channel cross section area (Width multiplied by depth)

between $\boldsymbol{\tau}_{ce}$ = 0.25 and 3 N m^{-2} (*Figure 3-10*). These trends show that substrate resistance is a strong controlling factor in determining channel geometry.

Figure *3-11* a) shows that delta top channel coverage decreases from ~35% to 10% as $\boldsymbol{\tau}_{ce}$ is increased between 0.25 and 5 N m^{-1}. The dominant factor causing this was the decrease in channel area over that range, rather than any effect of delta-top area, which does not change significantly with $\boldsymbol{\tau}_{ce}$ (*Figure 3-11* b). Further, this increase in channelised area is likely due to an increase in channel width (*Figure 3-9*) rather than an increase in the number of channels on the delta top, as total channel length also does not change significantly with $\boldsymbol{\tau}_{ce}$ (*Figure 3-12*a). Similarly, network density (*Figure 3-11*b) and network sinuosity (*Figure 3-11*c) do not change significantly with increasing $\boldsymbol{\tau}_{ce}$. This suggests that while the layout of the channel network obviously changes with $\boldsymbol{\tau}_{ce}$ (see *Figure 3-7*), the

density of this network remains largely unaffected by the underlying sediment, at least as far as the metrics presented here can show.

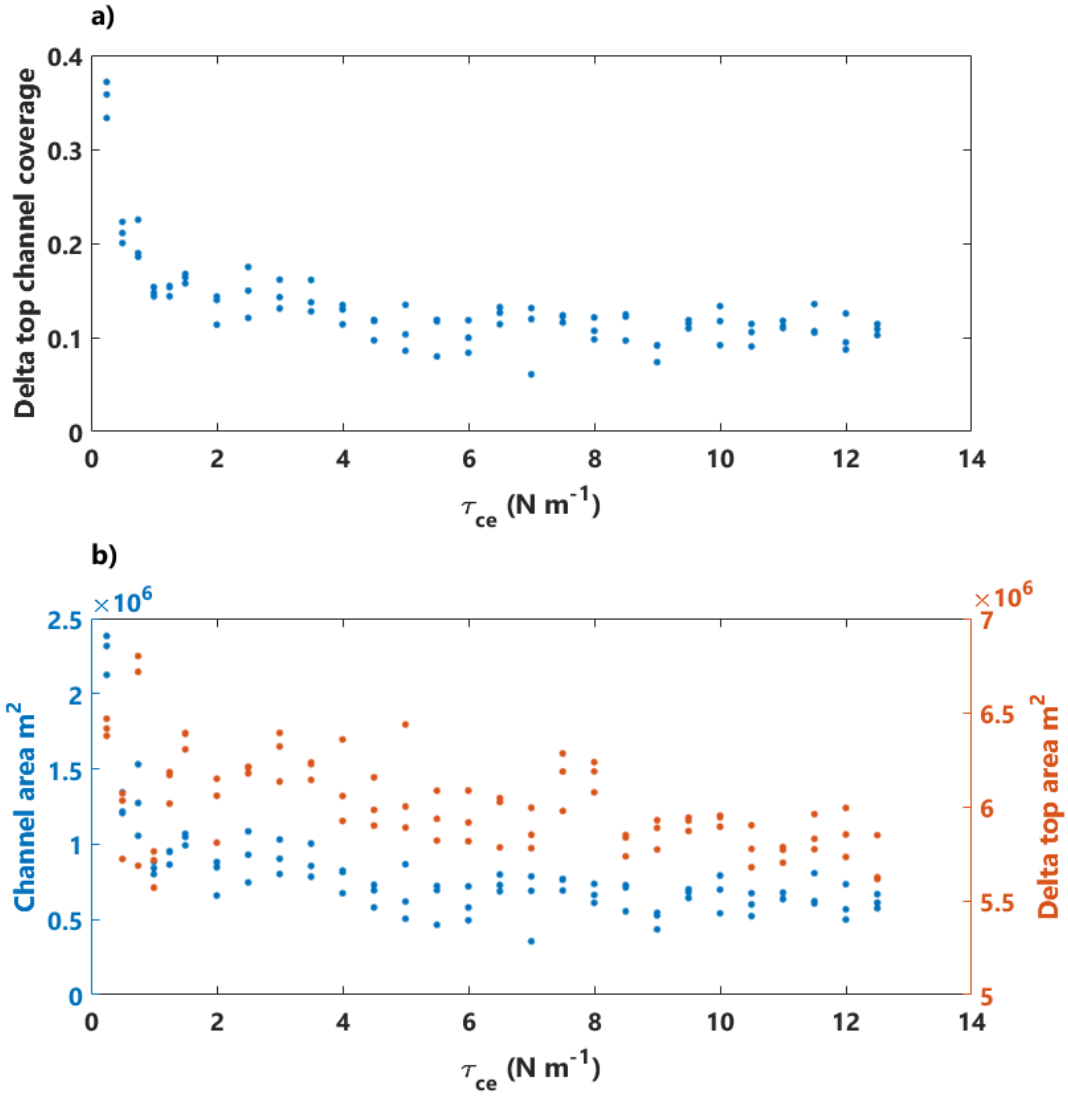

Figure 3-11: a) Delta top channel coverage proportion (m^2/m^2) and b) Total area of channelised cells (m^2; blue) and total delta top area, including channels (m^2; orange), all plotted against bed critical shear stress of erosion

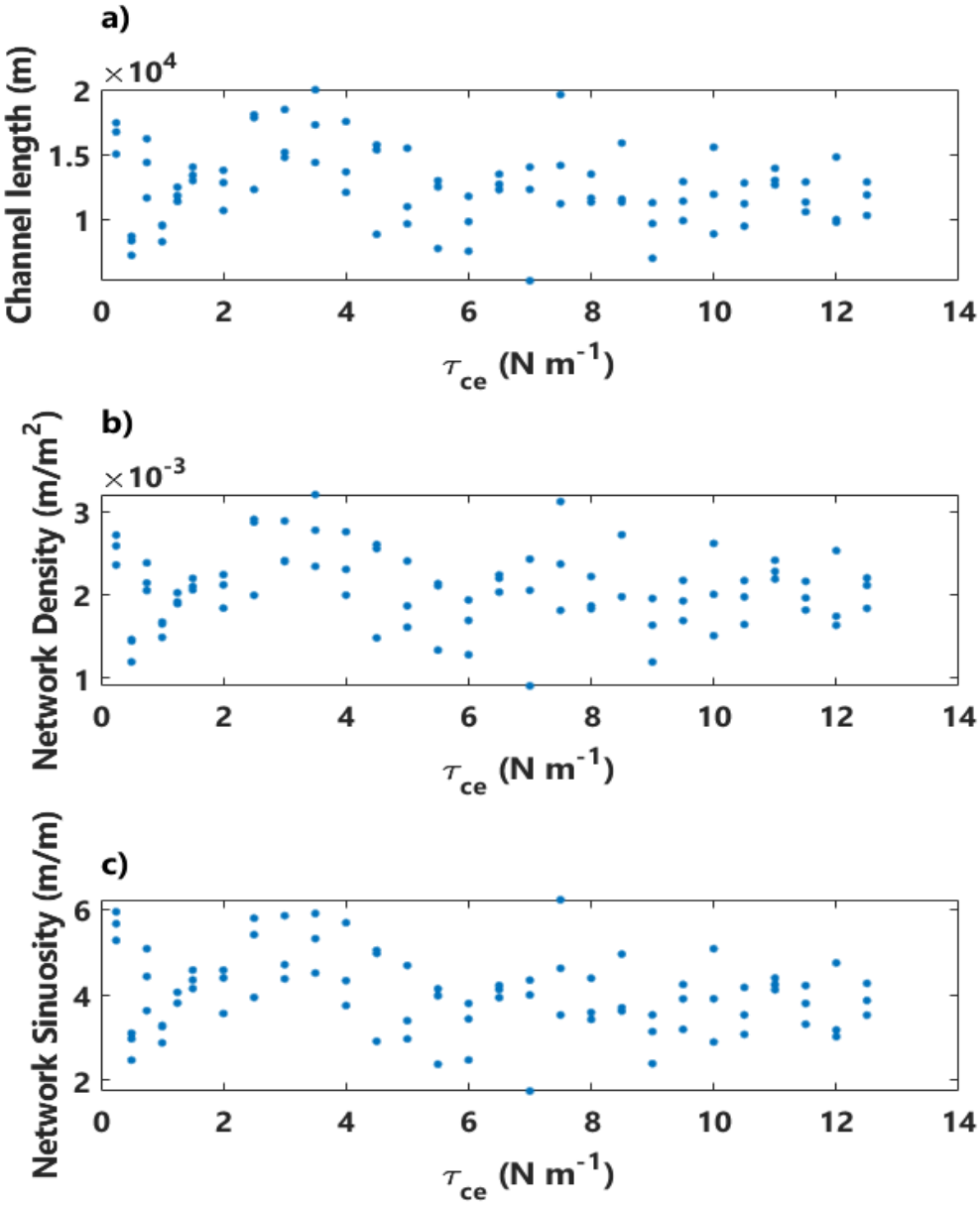

*Figure 3-12: a) T*otal channel length (m) b) Network density (total channel length per channel area) and c) Network sinuosity (total channel length divided by average distance from the delta apex to the edge of the delta top, both plotted against bed critical shear stress of erosion.

3.3.2 *Channel Mobility*

Next, the mobility of channels was assessed by relating mean channel residence times to substrate cohesive strength. Mean channel lifetime changes behaviour dramatically at ~1.5 N m^{-2}, from a steep positive trend in $\boldsymbol{\tau}_{ce}$, below this value to shallower negative trend above it (*Figure 3-13*). The trend below $\boldsymbol{\tau}_{ce}$, = 1.5 N m^{-2} is likely due to the delay in the initiation of channel formation (or at least the formation of channels that can be accurately identified by the channel detection algorithm) limiting the highest possible residence time of cells. Initial channel formation can be seen in *Figure 3-14* as a sudden jump in channelized cells, usually suggesting that subaqueous levees have become sufficiently large to shape the flow into a coherent channel rather than a diffuse plume (such as in Appendix 2 – fig. vii.b). Lower $\boldsymbol{\tau}_{ce}$, results in a later formation of channels, as in these deltas as the soft underlying sediment allows a much larger channel to form in the outlet. This causes the mouth jet to become wide and diffuse, and deposit

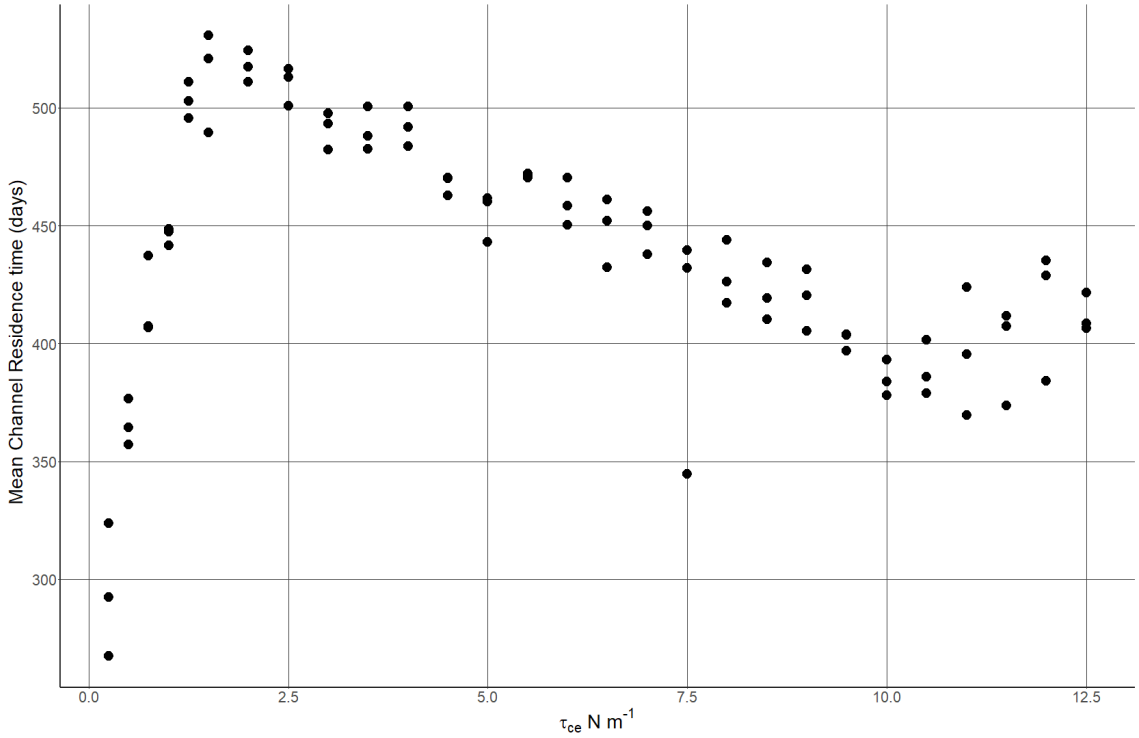

Figure 3-13: Calculated mean channel cell residence times

a wide, crescent-shaped mouth bar (See Appendix 2 - fig. vii), which continually progrades into the basin, and does not form topography that the algorithm can identify as a channel. In contrast, higher $\boldsymbol{\tau}_{ce}$, deltas allow these bars to aggrade to the surface earlier, where they become bifurcations (as described in Canestrelli *et al.*, 2014) and deposit levees which creates lower width:depth ratio channels, which are easily identified.

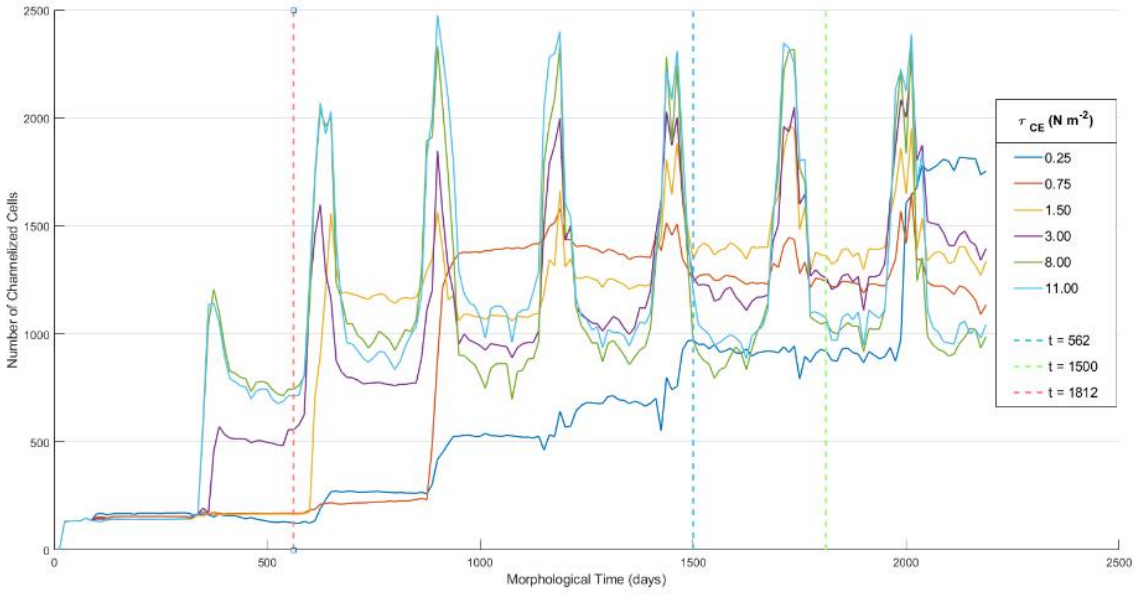

Figure 3-14: Figure showing the number of model cells recognised as being part of a channel at each recorded timestep, for deltas forming a range of substrates, plotted against morphological time (model time x morphological scale factor). Times at which later analyses were started are shown as dashed lines. Note how the appearance of large numbers of channel cells gets later with decreasing τ_{ce}, especially in those with τ_{ce} <1.5

If the same lifetime analysis is performed on the data, but starting at a later time (see *Figure Figure 3-14*) this inflection point is moved towards lower $\boldsymbol{\tau}_{ce}$ (*Figure 3-15*), as a later analysis start time means that low $\boldsymbol{\tau}_{ce}$ deltas will have developed channels by (or sooner after) the start of analysis, and hence deltas are mature, with recognisable channels, for a larger proportion of the analysed runtime. However, running the analysis only on the time period in which all deltas

had formed channels would reduce the analysed run time to such a short period (less than a quarter of the total run time) that it may reduce the accuracy of the analysis, so instead the full run was analysed and this effect was taken in to account when interpreting the channel mobility data.

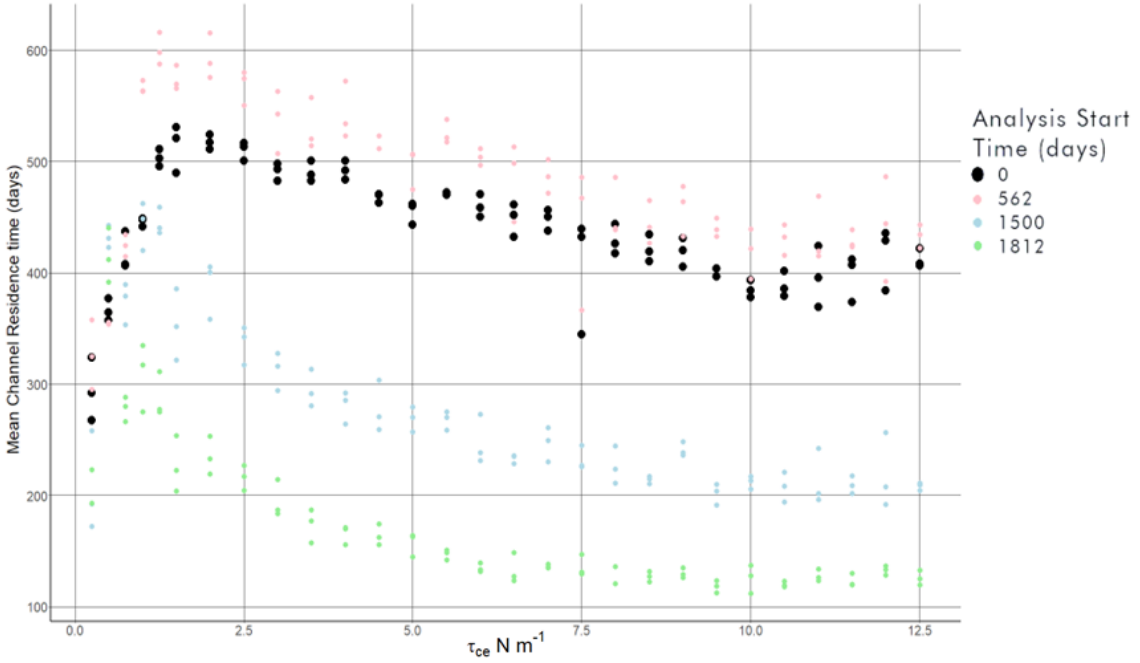

Figure 3-15: Comparison plot showing differences in mean lifetimes curves when processing is started later into the run. Note how the section of the curve with a positive trend (likely influences by late channelization) becomes smaller as analysis is started later.

At higher $\boldsymbol{\tau}_{ce}$, channel residence times start to decline with increasing $\boldsymbol{\tau}_{ce}$. As shown above, channels flowing over more resistant sediment cannot erode to the same depth, leading channels with higher width:depth ratios (*Figure 3-10*). Channels have been shown to avulse as the ratio of super elevation above the surrounding area to flow depth increases (Mohrig et al., 2000). Vertical incision will lower the bed of the river, decreasing this ratio by either increasing flow depth or decreasing superelevation, which will lead to a decrease in the likelihood of channel avulsion. As shown above, a more resistant substrate leads to decreased

incision, decreased depth, and hence increased water surface superelevation, which will encourage avulsion and thus decrease mean channel residence times.

The increasing width:depth ratio will also increase the stability of jets forming at the mouths of these channels, which has been shown to lead to the deposition of mouth bars (Fagherazzi et al., 2015), rather than subaqueous levees. The increased size and frequency of these bars could cause an enhanced morphodynamic backwater effect (Hoyal and Sheets, 2009), which will also drive channels to avulse more often.

3.3.3 *Subaerial Land*

Finally, this section investigates if the changes in channel geometry and mobility are affecting the size and height of the delta top. The area of subaerial land built at the end of the runs increases strongly with τ_{ce} up to around 3.5 N m^{-2} (Figure 3-16), after which land area is invariant to further increases in τ_{ce}. Mean delta top height also increases with τ_{ce} (*Figure 3-16*), most strongly below 5 N m^{-2}. This increase in land building is possibly due to the enhanced out of bank overland flow from more frequent avulsions seen in high τ_{ce} deltas. Frequent avulsions and crevasse splays enhance sediment deposition on the delta top and frequently changing channel paths also allows a more equal growth of land around the whole delta front (Burpee et al., 2015), increasing delta top elevation and land area respectively. In contrast, large stable channels present on low τ_{ce} deltas could route sediment to deeper water, preferentially depositing on the delta toe rather than the delta top (*Figure 3-7*) and leaving large bays between these channels. Additionally, the wide channels seen in low τ_{ce} deltas (*Figure 3-9*) occupy large fractions (of the delta top *Figure 3-11*), decreasing the amount of the delta top that is above water. Through these differences in sediment transport

dynamics, caused by changes in channel geometry and mobility, it is clear that delta substrate resistance is influencing the large-scale form of the delta top.

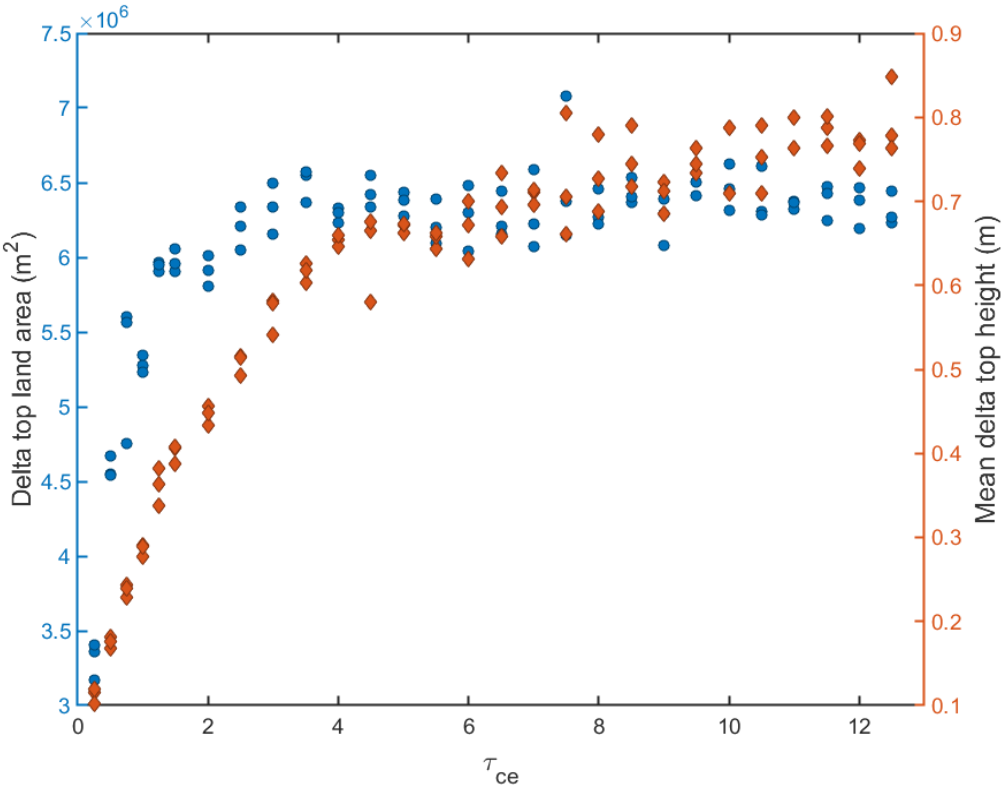

Figure 3-16: Delta top land area (Surface >0m) at end of run, and mean delta top elevation.

Frequent avulsion also leaves relict channels on the delta top (as can be seen in high τ_{ce} runs in Figure 3-7). *Figure 3-17* shows again that deltas forming over more resistant substrates grow faster. This figure also demonstrates that while deltas forming over less resistant substrate grow in pulses related to times of high discharge, growth in deltas forming on more resistant substrate is via a more continuous process. In addition, it has been shown that frequencies of change in depositional sedimentary systems such as deltas can determine which environmental signals are recorded in stratigraphy, and which are lost completely, or 'shredded', (Jerolmack and Paola, 2010). Jerolmack and Paola (2010), showed that signals with a timescale less than a critical timescale of the system (related to

avulsion frequency in deltas) would be shredded, and so the reduction of this frequency seen in deltas forming over high $\boldsymbol{\tau}_{ce}$ substrates could result in more, shorter timescale signals would potentially be recorded.

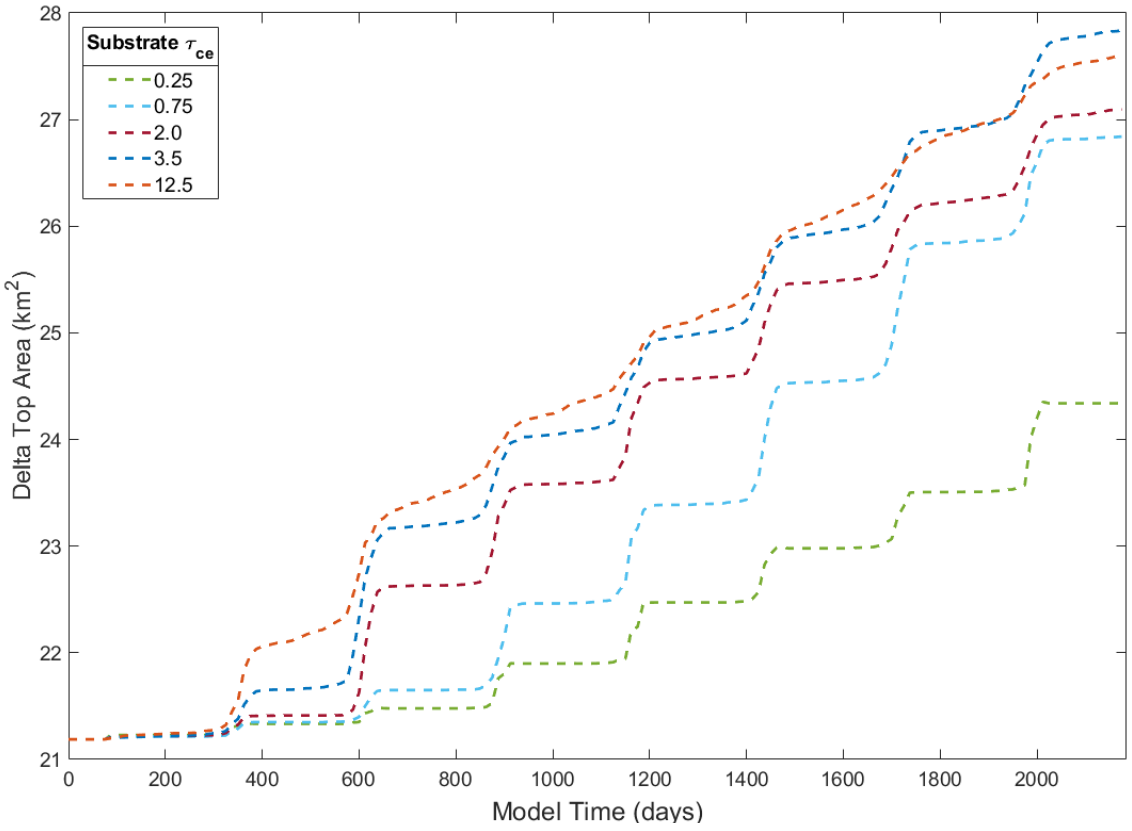

Figure 3-17: Delta top area growth over the whole model run

3.4 Discussion

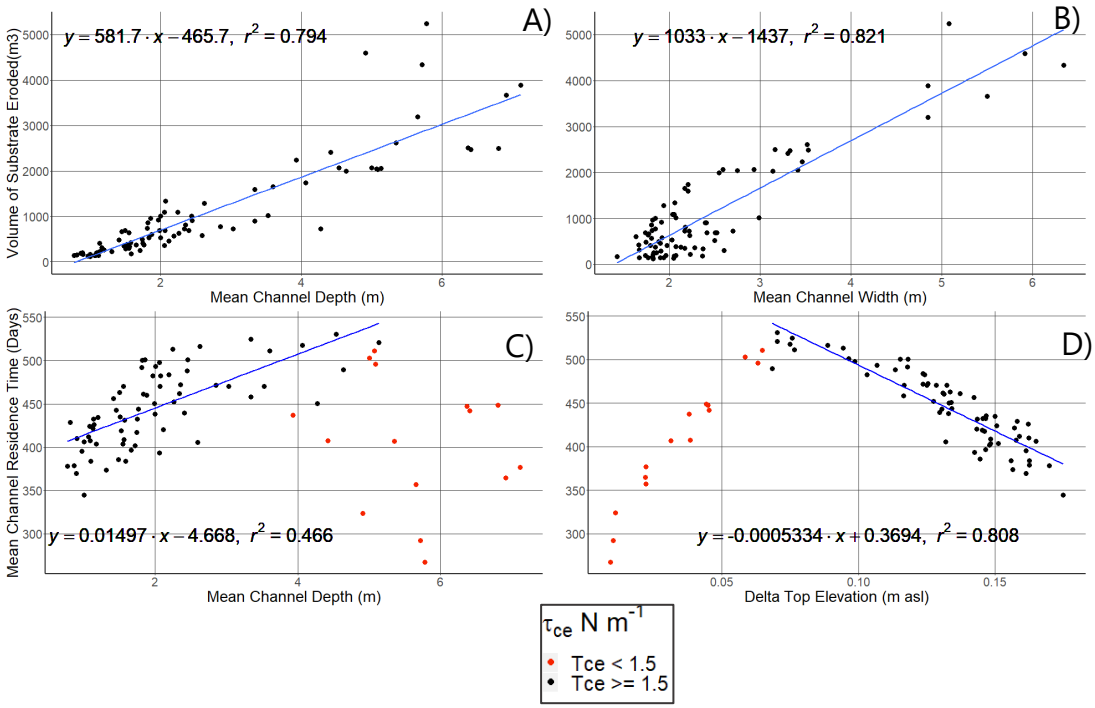

Figure 3-18: A) mean channel depths of modelled deltas at the end of the run, plotted against the volume of sediment eroded from the pre-delta substrate B) mean channel width plotted against the volume of sediment eroded from the pre-delta substrate C) mean channel residence time plotted against mean delta channel depth D) mean channel residence time plotted against mean delta top elevation. Note that runs with τ_{ce} <1.5 are neglected from trend line calculations for channel residence time plots (see text).

3.4.1 *Morphodynamic effects of delta substrates*

The results show that channel depth and width, delta top land area and delta top elevation are all distributed as horizontal asymptotes (see Figures 3-8, 3-9 and 3-13). All of these measures are controlled in some way by the delta's ability to incise into the receiving basin substrate as it progrades. The channel width and depth (*Figure 3-18 A & B*) are both linearly related to volume of incision, channel mobility is linearly related to channel depth (for deltas with $\boldsymbol{\tau}_{ce}$ > 1.5 Nm^{-2}: see

Figure 3-18 C) and delta top elevation is linearly related to channel mobility (again for deltas with > 1.5 Nm^{-2}: *Figure 3-18 D*), which would support the hypothesis that substrate erodibility has a considerable control on channel mobility, expressed via controls on channel geometry.

The strong linear, physical relationship between these characteristics and incision causes them for follow the same trend. Cohesive sediment erosion in the model was controlled entirely by the source (bed to flow) equations of the sediment model, as was set to a very high value to cause constant deposition, meaning erosion happened only when erosive flux was sufficient to overcome this deposition. As such, the volume of incision is expected to be asymptotically distributed, as the Partheniedes-Krone equation (*equation 2-1*) for erosion controls it:

$$\boldsymbol{E_m = M_m\left(\frac{\tau_{cw}}{\tau_{ce}} - 1\right)} \qquad \textbf{2-1}$$

Where E_m is the erosional flux, M_m is an erosional parameter and $\boldsymbol{\tau}_{cw}$ is the maximum shear stress due to flow. If M_m is constant (M_m is a model parameter so is held constant between model runs), then for a given $\boldsymbol{\tau}_{cw}$, E_m plots as an asymptote against $\boldsymbol{\tau}_{ce}$. This is likely the driver behind the distribution of channel geometries and delta top land characteristics.

The evolution of these systems is closely tied to the distribution of erosive power capable of overcoming the resistance of the substrate sediment and so initiate erosion. As such, factors which change this distribution will modulate the

effects of substrate on delta morphodynamics. Tidal ebb flows can increase erosive power at sub-aqueous channel tips (Shaw and Mohrig, 2014a), possibly allowing incision into harder bed sediment regardless of the magnitude of flood peaks. The deltas modelled here incise into their beds primarily in channels close to the river efflux, but in deltas where erosive power is concentrated around channel tips, the erosion may be focused more towards the distal areas of the delta. This could increase channel depth there, and increase the power of the mouth jet, potentially leading to stronger erosion of mouth bars and reduction in morphodynamic backwater effects and hence avulsion rates (Rossi et al., 2016; Edmonds and Slingerland, 2010; Hoyal and Sheets, 2009).

In some real-world cases, it is likely that substrate qualities, such as grain size, minerology, and cohesion, are not homogenous. In such cases, the difference in avulsion frequency could guide channels towards lower parts of the basin. Channels would likely avulse away from high $\boldsymbol{\tau}_{ce}$ areas faster than they would avulse away from low $\boldsymbol{\tau}_{ce}$ areas, causing areas with low $\boldsymbol{\tau}_{ce}$ to "collect" channels. This could result in the formation of deltaic land being steered towards areas with more erodible sediment substrate.

Finally, the results show how different amplitude pulses in delta morphodynamics area also related to the resistance of the substrate. How intrinsic processes can dampen or shred extrinsic signals in sedimentary systems has received significant attention over the recent past (Jerolmack and Paola, 2010). Interestingly the examples herein demonstrate how receiving basin characteristics

can amplify these morphodynamic responses, which has a range of implications on how variability impacts delta stability and longer-term sedimentological characteristics. For example, more resistant substrates could better record variability in the incoming sediment load through amplification of the morphodynamic processes as the delta top is built. Such impacts suggest that underlying basin characteristics should be considered when interpreting morphodynamics from delta deposits in the sedimentary record.

3.4.2 *Uncertainties with morphodynamic models*

Due to the model's use of the Partheneides-Krone bed boundary condition (see sections 2.4.3 and 3.2.1) it is likely that erosion in low $\boldsymbol{\tau}_{ce}$ environments at low bed shear stresses (caused by fluid mud mixing (Gaskin et al., 2003)) is underestimated, and so even the high values seen in deltas forming over soft substrates may under-represent what would be found in real world deltas. Similarly, the Partheneides-Krone bed boundary condition does not model the increased rate of sediment entrainment caused by mass erosion (when high shear stress acts on the bed), and so the erosion happening at peak flows may be higher across all deltas. This may have an effect on the overall morphology of the delta; low but non-zero erosion rates of low $\boldsymbol{\tau}_{ce}$ material in low bed shear environments, caused by fluid mud mixing, may lead to higher erosion rates than estimated by the model at the channel margins, where erosional power is usually too low to entrain sediment. This would suggest that in the real world, channel widths in the lowest $\boldsymbol{\tau}_{ce}$ deltas would be even higher than estimated here. This suggests that the negative trend seen in width (see *Figure 3-9:* Mean width and depth of delta channels) is likely to be even stronger in real world deltas.

Equally, mass erosion at high shear stresses may lead to increased channel depth in real world examples compared to the models here, as the fastest flows and highest bed shear stresses will be focused at the channel centre. This effect will likely be most relevant in areas of low to mid $\boldsymbol{\tau}_{ce}$ deltas where erosion is happening but is limited to peak flows, where it will potentially increase otherwise low volumes of sediment erosion and shallow channel depth. At the highest $\boldsymbol{\tau}_{ce}$ deltas, both of the above effects will likely have little influence, as sediment bed resistances would be high enough to preclude nearly all substrate erosion. As depth is key in the explanation of the trend of increasing channel mobility with increasing $\boldsymbol{\tau}_{ce}$, channel mobility could also be expected to be reduced at these mid-range $\boldsymbol{\tau}_{ce}$ values in real systems.

To simplify this first set of model runs, only the $\boldsymbol{\tau}_{ce}$ of the substrate was varied between runs. As such, these models do not account for variations in non-cohesive sediment content, nor for the inclusion of sediment coarser than the 225μm fine sand used here. Therefore, this study best represents deltas forming over silty-mud mixtures that may be expected to constitute the beds of shallow, quiescent basins. While this means that deltas formed from courser material, such as those in small, high relief catchments are not represented in these models, those forming at the mouths of large rivers (which tend to have finer sediment loads; Syvitski and Saito, 2007) are represented here, making this study most relevant to more heavily populated deltas.

3.5 Conclusion

The results of this study show that deltas forming over basin substrates of higher cohesivity (higher $\boldsymbol{\tau}_{ce}$) sediment build channels that migrate more frequently. While these systems could be interpreted as being unstable on a human scale, recent studies have argued that avulsion is crucial for long term delta stability and should be accounted for in management strategies (Passalacqua and Moodie, 2022; Passalacqua et al., 2021). This suggests that channel migration speed and avulsion frequency is not a good analogue for long term stability, but an indicator of the morphodynamic rate at which the system changes. Faster channel migration also acts to make the delta front less rugose (*Figure 3-7*) which has been equated to delta stratigraphy with a less variable foreset dip directions. As such, higher $\boldsymbol{\tau}_{ce}$ substrates could affect the interpretation of ancient deltas in the same way as sandier fluvial sediment supplies, providing the delta is topset dominated (i.e., the basin is shallow enough delta channels interact with the basin substrate).

Deltas are increasingly impacted by eustatic sea level rise, with sea level rise estimated between 0.26 and 0.98m before 2100 (IPCC, 2014), as well as enhanced subsidence from extraction of water and hydrocarbons, leading to an estimated ESLR of up to 12.5mm yr^{-1} (Ericson et al., 2006). As well as effecting delta systems by altering water base level at the river mouth (Investigated in Chapter 4), this will expose low lying areas of deltas to coastal erosion and inundation, which can only be counteracted by sediment deposition on the delta top and shoreline. The numerical models described herein show that deltas that form over high $\boldsymbol{\tau}_{ce}$ substrates have higher altitude delta tops and larger areas of subaerial land for

the same supplied catchment sediment fluxes. This will be particularly important consideration given reductions in sediment supply resultant from anthropogenic impacts (Hackney et al., 2020; Dunn et al., 2019). Accurate characterisation of the substrate of the delta is important to predictions of how deltas will respond to anthropogenic forcing.

In this chapter, numerical models in Delft3D have been used to quantify how the $\boldsymbol{\tau}_{ce}$ of the substrate underlying a forming delta affects the channel geometry and mobility of channels on that delta. Higher substrate cohesivity (quantified as $\boldsymbol{\tau}_{ce}$), lead to shallower, smaller channels that migrated from their positions more often, likely due to being relatively superelevated above the surrounding delta when compared to channels on deltas formed over less cohesive (lower $\boldsymbol{\tau}_{ce}$) substrates. This demonstrates that the nature of the underlying sediment can have a critical effect on the morphology and dynamics of deltas.

3.6 References

Barbier, E. B., Georgiou, I. Y., Enchelmeyer, B. and Reed, D. J. (2013) 'The Value of Wetlands in Protecting Southeast Louisiana from Hurricane Storm Surges', vol. 8, no. 3, pp. 1–7 [Online]. DOI: 10.1371/journal.pone.0058715.

Braat, L., van Kessel, T., Leuven, J. R. F. W. and Kleinhans, M. G. (2017) 'Effects of mud supply on large-scale estuary morphology and development over centuries to millennia', *Earth Surface Dynamics Discussions*, pp. 1–47 [Online]. DOI: 10.5194/esurf-2017-14.

Burpee, A. P., Slingerland, R. L., Edmonds, D. A., Parsons, D. R., Best, J. L., Cederberg, J., McGuffin, A., Caldwell, R. L., Nijhuis, A. and Royce, J. (2015) 'Grain-Size Controls On the Morphology and Internal Geometry of River-Dominated Deltas', *Journal of Sedimentary Research*, vol. 85, no. 6, pp. 699–714 [Online]. DOI: 10.2110/jsr.2015.39.

Caldwell, R. L. and Edmonds, D. A. (2014) 'The effects of sediment properties on deltaic processes and morphologies: A numerical modeling study', *Journal of Geophysical Research: Earth Surface*, vol. 119, no. 5, pp. 961–982 [Online]. DOI: 10.1002/2013JF002965.

Canestrelli, A., Nardin, W., Edmonds, D. A., Fagherazzi, S. and Slingerland, R. L. (2014) 'Importance of frictional effects and jet instability on the morphodynamics of river mouth bars and levees', *Journal of Geophysical Research: Oceans*, vol. 119, no. 1, pp. 509–522 [Online]. DOI: 10.1002/2013JC009312.

Cossette, D. (2016) 'Erodibility and Scour By a Vertical Submerged Circular Turbulent Impinging Jet in Cohesive Soils', p. 241.

Dethier, E. N., Renshaw, C. E. and Magilligan, F. J. (2022) 'Rapid changes to global suspended sediment flux by humans', *Science*, vol. 376, pp. 1447–1452.

Dunn, F. E., Darby, S. E., Nicholls, R. J., Cohen, S., Zarfl, C. and Fekete, B. M. (2019) 'Projections of declining fluvial sediment delivery to major deltas worldwide in response to climate change and anthropogenic stress', *Environmental Research Letters*, vol. 14, no. 8 [Online]. DOI: 10.1088/1748-9326/ab304e.

Edmonds, D. A. and Slingerland, R. L. (2007) 'Mechanics of river mouth bar formation: Implications for the morphodynamics of delta distributary networks', *Journal of Geophysical Research: Earth Surface*, vol. 112, no. 2, pp. 1–14 [Online]. DOI: 10.1029/2006JF000574.

Edmonds, D. A. and Slingerland, R. L. (2010) 'Significant effect of sediment cohesion on delta morphology', *Nature Geoscience*, vol. 3, no. 2, pp. 105–109 [Online]. DOI: 10.1038/ngeo730.

Ericson, J. P., Vörösmarty, C. J., Dingman, S. L., Ward, L. G. and Meybeck, M. (2006) 'Effective sea-level rise and deltas: Causes of change and human dimension implications', *Global and Planetary Change*, vol. 50, no. 1–2, pp. 63–82 [Online]. DOI: 10.1016/j.gloplacha.2005.07.004.

Fagherazzi, S., Edmonds, D. A., Nardin, W., Leonardi, N., Canestrelli, A., Falcini, F., Jerolmack, D. J., Mariotti, G., Rowland, J. C. and Slingerland, R. L. (2015) 'Dynamics of river mouth deposits', *Reviews of Geophysics*, vol. 53, no. 3, pp. 642–672 [Online]. DOI: 10.1002/2014RG000451.

Gaskin, S. J., Pieterse, J., Al Shafie, A. and Lepage, S. (2003) 'Erosion of undisturbed clay samples from the banks of the St. Lawrence River', *Canadian Journal of Civil Engineering*, vol. 30, no. 3, pp. 585–595 [Online]. DOI: 10.1139/l03-008.

Geleynse, N., Storms, J. E. A., Walstra, D. J. R., Jagers, H. R. A., Wang, Z. B. and Stive, M. J. F. (2011) 'Controls on river delta formation; insights from numerical modelling', *Earth and Planetary Science Letters*, Elsevier B.V., vol. 302, no. 1–2, pp. 217–226 [Online]. DOI: 10.1016/j.epsl.2010.12.013.

Hackney, C. R., Darby, S. E., Parsons, D. R., Leyland, J., Best, J. L., Aalto, R., Nicholas, A. P. and Houseago, R. C. (2020) 'River bank instability from unsustainable sand mining in the lower Mekong River', *Nature Sustainibility*, vol., no.

Hanegan, K. and Georgiou, I. (2014) 'Tidal modulated flow and sediment flux through Wax Lake Delta distributary channels: Implications for delta development', *IAHS-AISH Proceedings and Reports*, vol. 367, no. December 2014, pp. 391–398 [Online]. DOI: 10.5194/piahs-367-391-2015.

Hereher, M. E. (2010) 'Vulnerability of the Nile Delta to sea level rise : an assessment using remote sensing', vol. 5705 [Online]. DOI: 10.1080/19475705.2010.516912.

Hoyal, D. C. J. D. and Sheets, B. A. (2009) 'Morphodynamic evolution of experimental cohesive deltas', *Journal of Geophysical Research: Earth Surface*, vol. 114, no. 2, pp. 1–18 [Online]. DOI: 10.1029/2007JF000882.

IPCC (2014) *Summary for Policymakers:*, *Climate Change 2014: Impacts, Adaptation and Vulnerability -Contributions of the Working Group II to the Fifth Assessment Report* [Online]. DOI: 10.1016/j.renene.2009.11.012.

Isikdogan, F., Bovik, A. and Passalacqua, P. (2017) 'RivaMap: An automated river analysis and mapping engine', *Remote Sensing of Environment*, Elsevier Inc., vol. 202, pp. 88–97 [Online]. DOI: 10.1016/j.rse.2017.03.044.

Jerolmack, D. J. and Paola, C. (2010) 'Shredding of environmental signals by sediment transport', *Geophysical Research Letters*, vol. 37, no. 19, pp. 1–5 [Online]. DOI: 10.1029/2010GL044638.

Kim, W., Mohrig, D., Twilley, R., Paola, C. and Parker, G. (2009) 'Is it feasible to build new land in the Mississippi River Delta?', *Eos*, vol. 90, no. 42, pp. 373–384.

Krone, R. B. (1999) 'Effects of Bed Structure on Erosion of Cohesive Sediments', *Journal of Hydraulic Engineering*, vol. 125, pp. 1297–1301.

van de Lageweg, W. I., Braat, L., Parsons, D. R. and Kirwan, M. L. (2018) 'Controls on mud distribution and architecture along the fluvialto- marine transition', *Geology*, vol. 46, no. 11, pp. 971–974 [Online]. DOI: 10.1130/G45504.1.

Van de Lageweg, W. I. and Feldman, H. (2018) 'Process-based modelling of morphodynamics and bar architecture in confined basins with fluvial and tidal currents', *Marine Geology*, Elsevier, vol. 398, no. December 2016, pp. 35–47 [Online]. DOI: 10.1016/j.margeo.2018.01.002.

Lesser, G. R., Roelvink, J. A., van Kester, J. A. T. M. and Stelling, G. S. (2004) 'Development and validation of a three-dimensional morphological model', *Coastal Engineering*, vol. 51, no. 8–9, pp. 883–915 [Online]. DOI: 10.1016/j.coastaleng.2004.07.014.

McLeod, E., Chmura, G. L., Bouillon, S., Salm, R., Björk, M., Duarte, C. M., Lovelock, C. E., Schlesinger, W. H. and Silliman, B. R. (2011) 'A blueprint for blue carbon: Toward an improved understanding of the role of vegetated coastal habitats in sequestering CO2', *Frontiers in Ecology and the Environment*, vol. 9, no. 10, pp. 552–560 [Online]. DOI: 10.1890/110004.

Mohrig, D., Heller, P. L. and Lyons, W. J. (2000) 'Interpreting avulsion process from

ancient alluvial sequences: Guadalope-Matarranya system (northern Spain) and Wasatch Formation (western Colorado)', *Geological Soceity of America Bulletin*, vol. 112, no. 12, pp. 1787–1803 [Online]. DOI: 10.1130/0016-7606(2000)112<1787:IAPFAA>2.0.CO;2.

Morton, R. A., Buster, N. A. and Krohn, M. D. (2002) 'Subsurface Controls on Historical Subsidence Rates and Associated Wetland Loss in Southcentral Louisiana', *Transactions Gulf Coast Association of Geological Societies*, vol. 52, pp. 767–778.

Nienhuis, J. H. and van de Wal, R. S. W. (2021) 'Projections of Global Delta Land Loss From Sea-Level Rise in the 21st Century', *Geophysical Research Letters*, vol. 48, no. 14, pp. 1–9 [Online]. DOI: 10.1029/2021GL093368.

Passalacqua, P., Giosan, L., Goodbred, S. and Overeem, I. (2021) 'Stable ≠ Sustainable: Delta Dynamics Versus the Human Need for Stability', *Earth's Future*, vol. 9, no. 7 [Online]. DOI: 10.1029/2021EF002121.

Passalacqua, P. and Moodie, A. J. (2022) 'Delta-scale solutions for human-scale needs', *Science*, vol. 376, no. 6596, pp. 916–917.

Passalacqua, P., Tarolli, P. and Foufoula-Georgiou, E. (2010) 'Testing space-scale methodologies for automatic geomorphic feature extraction from lidar in a complex mountainous landscape', *Water Resources Research*, vol. 46, no. 11, pp. 1–17 [Online]. DOI: 10.1029/2009WR008812.

Piliouras, A., Kim, W. and Carlson, B. (2017) 'Balancing Aggradation and Progradation on a Vegetated Delta: The Importance of Fluctuating Discharge in Depositional Systems', *Journal of Geophysical Research: Earth Surface*, vol. 122, no. 10, pp. 1882–1900 [Online]. DOI: 10.1002/2017JF004378.

van Rijn, L. C., Walstra, D. J. R. and van Ormondt, M. (2004) *Description of TRANSPOR2004 and Implementation in Delft3D-ONLINE*,.

Rossi, V. M., Kim, W., López, J. L., Edmonds, D. A., Geleynse, N., Olariu, C., Steel, R. J., Hiatt, M. and Passalacqua, P. (2016) 'Impact of tidal currents on delta-channel deepening, stratigraphic architecture, and sediment bypass beyond the shoreline', *Geology*, vol. 44, no. 11, pp. 927–930 [Online]. DOI: 10.1130/G38334.1.

Sanford, L. P. (2008) 'Modeling a dynamically varying mixed sediment bed with erosion, deposition, bioturbation, consolidation, and armoring', *Computers and Geosciences*, vol. 34, no. 10, pp. 1263–1283 [Online]. DOI: 10.1016/j.cageo.2008.02.011.

Shaw, J. B. and Mohrig, D. (2014a) 'The importance of erosion in distributary channel network growth, Wax Lake Delta, Louisiana, USA', *Geology*, vol. 42, no. 1, pp. 31–34 [Online]. DOI: 10.1130/G34751.1.

Shaw, J. B. and Mohrig, D. (2014b) 'The importance of erosion in distributary channel network growth, Wax Lake Delta, Louisiana, USA', *Geology*, vol. 42, no. 1, pp. 31–34 [Online]. DOI: 10.1130/G34751.1.

Shaw, J. B., Mohrig, D. and Whitman, S. K. (2013) 'The morphology and evolution of channels on the Wax Lake Delta, Louisiana, USA', *Journal of Geophysical Research: Earth Surface*, vol. 118, no. 3, pp. 1562–1584 [Online]. DOI: 10.1002/jgrf.20123.

Syvitski, J. P. M., Kettner, A. J., Overeem, I., Hutton, E. W. H., Hannon, M. T., Brakenridge, G. R., Day, J. W., Vörösmarty, C. J., Saito, Y., Giosan, L. and Nicholls, R. J. (2009) 'Sinking deltas due to human activities', *Nature Geoscience*, vol. 2, no. 10, pp. 681–686 [Online]. DOI: 10.1038/ngeo629.

Syvitski, J. P. M. and Saito, Y. (2007) 'Morphodynamics of deltas under the influence

of humans', *Global and Planetary Change*, vol. 57, no. 3–4, pp. 261–282 [Online]. DOI: 10.1016/j.gloplacha.2006.12.001.

Syvitski, J. P. M., Vörösmarty, C. J., Kettner, A. J. and Green, P. (2005) 'Impact of Humans on the Flux of Terrestrial Sediment to the Global Coastal Ocean', *Science*, vol. 308, no. 5720, pp. 376–380 [Online]. DOI: 10.1126/science.1109454.

Warner, K. (2010) 'Global environmental change and migration: Governance challenges', *Global Environmental Change*, Elsevier Ltd, vol. 20, no. 3, pp. 402–413 [Online]. DOI: 10.1016/j.gloenvcha.2009.12.001.

Winterwerp, J. C., van Kesteren, W. G. M., van Prooijen, B. and Jacobs, W. (2012) 'A conceptual framework for shear flow–induced erosion of soft cohesive sediment beds', *Journal of Geophysical Research: Oceans*, vol. 117, no. October, pp. 1–17 [Online]. DOI: 10.1029/2012JC008072.

4 Relative controls on delta morpho-dynamics and stability in the face of modern stresses

4.1 Introduction

Deltas have considerable value ecologically (Zhang et al., 2016; Herzka et al., 2013) and economically (Warner, 2010). They are critical landforms that are home to hundreds of millions (Syvitski et al., 2009) of people. However, deltas are increasingly under pressure from human influences on the environment. The vast majority of deltas form in the ocean, so are under pressure from eustatic sea level rise as a result of global warming, expected to total between 0.26 (RCP2.6) and 0.82m (RCP8.5) between the period from 1986-2005 to 2081-2100 (IPCC, 2013).

In addition to this eustatic sea-level rise, both natural sediment compaction and ground fluid extraction (Liu et al., 2016; Morton et al., 2002) is also causing subsidence of these delta landscapes (Waltham, 2002). For example, (Morton et al., 2006) found subsidence rates of 8.2-18.9mm y^{-1} in areas of the Louisiana coast associated with hydrocarbon extraction, which they linked to extensive wetland loss on the Mississippi delta. Similarly, Minderhoud *et al.* (2017) used a 3D hydrogeological model to estimate an average subsidence rate of 11 mm y^{-1}, across the Mekong Delta, while the satellite-based synthetic aperture radar data analysed by Erban et al. (2014) indicated subsidence rates of 2.8 to 31mm y^{-1} in the same area. Both studies attributed this subsidence to sediment compaction from groundwater extraction, and highlighted that this movement was an order of magnitude greater than sea level rise.

The combination of eustatic sea level rise and subsidence on deltas will likely result in a combined Relative Sea Level Rise (RSLR) of tens of millimetres a year, and could lead to the inundation of 4.9% of delta area by 2050, affecting 8.7 million people (Ericson et al., 2006). A more recent study by Nienhuis and van de Wal (2021) estimated an annual loss of 1026 $km^2\ y^{-1}$ and a total loss of 5% of delta land by 2100 under the IPCC RCP8.5 scenario. The former study uses a sediment balance equation, and the latter a simple morphodynamic model, meaning that both of these neglect complex morphological mechanics, including the effects of delta substrate on the resistance and resilience of deltas to imposed changes.

RSLR is expected to have numerous effects beyond permanent inundation. On the Red River delta in northern Vietnam for example, Neumann *et al.* (2015) found that by 2050 sea level rise could increase the height of storm surges, effectively increasing the frequency of a given height of storm surge. The authors estimated that due to this effect, a storm surge with a height currently expected with a 100 year return period under current conditions could occur every 49 years by 2050. Similarly, Jisan et al. (2018) estimated that a category-1 tropical storm affecting the Ganges-Brahmaputra-Meghna delta would inundate 28% more land if sea level was increased by 0.26m (a mid-21st century estimate for sea level rise) than if it made landfall with current (2007) sea level. Furthermore, Bhuiyan and Dutta (2012) used numerical modelling to predict saline intrusion in the Gorai River network, a distributary of the Ganges in Bangladesh, and showed that the 10 ppt (Parts Per Thousand) salt concentration point moved 21 km upstream as a result of 59 cm of relative sea level rise. They also predicted that salinity 80 km north of the river mouth would increase by 1.5 ppt per m of sea level rise. More saline water in deltaic rivers is less suitable for agriculture and drinking. As well as

this, it has been shown that higher water level in delta channels could increase sediment flow on to floodplains (Manh et al., 2015), decreasing the amount of sediment that reaches the sea, but increasing sedimentation on floodplains.

In addition to this, human activity has led to a reduction in the amount of sediment reaching coastal systems by approximately 1.4 billion tons per year (Syvitski et al., 2005). Globally, reservoirs retain 20% of river discharge (Syvitski et al., 2005), though sediment trapping in some catchments could be significantly higher if dam construction continues as planned (Kondolf et al., 2014). In a study of 47 deltas, Dunn et al. (2019) estimated that sediment supply could be reduced by an average of 38% due to dam building and socioeconomic factors (channel engineering and land use change), but found this number to be as high as 83% for individual deltas.

In some cases, reservoir construction could effectively cut off sediment supply entirely. For example, Kondolf et al. (2014) estimated that 96% of the Mekong Delta's sediment supply (estimated to be 160 Mt y^{-1} before dam construction) could be lost if all planned upstream dams are built, though with extensive strategic planning and trans-national cooperation the delta's supply could be stabilized around 50 Mt y^{-1} (Schmitt et al., 2019). The same percentage loss was estimated for the Ebro delta after the construction of the Ribarroja-Mequinenza dam (Sanchez-Arcilla et al., 1998). In fact, 5 of the 17 globally distributed river basins studied by Vörösmarty *et al.* (2003) where observed to have a trapping efficiency of more than 95%, indicating that river systems supplying a very reduced amounts of sediment to their mouths are not isolated cases.

Human extraction of sediment from channels exacerbates this by removing the limited sediment that does reach a delta. For example, sediment mining in the Mekong Delta, Vietnam, has been found to remove around seven times more sediment than is supplied by the river (Hackney et al., 2020). Sediment removal from channels, either by sediment mining or erosion by sediment deficient water, lowers the river bed and hence increases bank height, which was found by Hackney et al. (2020) to increase bank instability, with a 3 m drop in the bed level of channels causing 57% of unvegetated banks to become unstable. This bank lowering could also reduce water levels, reducing the connection between the river and its floodplain, as well as reducing the avulsion frequency (as discussed in Section 3.3.2). The construction of river levees on deltas also reduces flooding and channel avulsion, halting the deposition of sediment on delta tops and preventing aggradation of land (Kim et al., 2009). While none of the above studies reference this, more resilient substrates would likely reduce the amount that the river bed is lowered (mainly where sediment poor channels are eroding vertically, though mud-clay channel beds would also be less attractive as a resource for construction sand), and so reduce this effect in deltas forming over them.

The channel deepening resulting from sand mining and sediment starvation has been shown to increase the area of saltwater intrusion, with the numerical surface water modelling study of the Mekong Delta conducted by Eslami *et al.* (2021) indicating a 10-30% increase in the area affected by saltwater intrusion by 2050 due to a continuation of current bed erosion rates. Another numerical modelling study, by Vasilopoulos *et al.* (2021), predicted that the extent of tidal influence in the Mekong had moved upstream by 13.2km between 1998 and 2018, and that it could move inland a further 35.7km if channel erosion was not

stopped. Similarly to above, while substrate type is not referenced in the above studies, a resistant substrate may be able to limit channel depth and slow the described effects. While extensive coring of the Mekong delta plain has taken place, the substrate of "Undifferentiated Pleistocene Deposits" found in the distal parts of the delta are frequently neglected from investigations (Liu et al., 2017; Ta et al., 2002). Hanebuth et al. (2012) did find consolidated, stiff clay in the more proximal delta plains of the Mekong, but it is unclear whether this is interacting with the channels in a meaningful way.

The above studies outline that sediment supply to many of the world's deltas is decreasing and has functionally ceased in some cases, and that this loss of sediment is having effects on the hydrodynamics and morphology of these important systems. It has also been shown how other anthropogenic stresses, such as RSLR are affecting these systems. However, these parameters have not yet been fully explored in relation to how deltas forming over different substrates will react to these anthropogenic forces, and the material that underlies the delta is frequently neglected in both field and numerical morphological studies of delta systems.

As already shown in this study (Chapter 3), the sediment comprising the receiving basin's bed can influence the morphodynamics of the delta that forms on top of it; resistant beds lead to less channel incision, decreased channel stability and hence more frequent avulsions (Chapter 3, figure 3-12) and greater deposition of sediment on the delta topset (Chapter 3, figure 3-15). Given the vulnerability of these systems to anthropogenic sea level rise and sediment starvation, it is important to constrain how systems with different substrate

sedimentology will react to these stressors. In this chapter, the morphodynamic change that results from both fluvial and receiving basin substrate sediment properties will be assessed and the resulting influence on delta responses to anthropogenic sediment removal and relative sea level rise will be quantified.

4.2 Methodology

4.2.1 *Model Setup*

In this section, numerical models in Delft3D-Flow are used to quantify how a decrease in fluvial sediment flux and changes in rates of sea level rise impact how delta distributaries interact with their receiving basin substrates. To do this, a series of 'baseline' deltas with varying fluvial sediment and bed erodibility boundary conditions are run to maturity, then exposed to combinations of sea level and sediment starvation forcings. As in the previous chapter, the resulting deltas are analysed algorithmically to investigate changes in channel and delta top geometry and channel mobility.

Delta formation was modelled in Delft3D-flow (described in Section 3.2.1). As discussed in sections 2.4.3 and 3.2.1, the Partheniedes-Krone equation (2-1) neglects the differences between different modes of cohesive sediment erosion (e.g., fluid mud mixing, surface and mass erosion; Krone, 1999). As models implementing other formulations were not practical to use in this project (Section 2.4.2), this study uses the Partheniedes-Krone bed boundary formulation, assumes that τ_{ce} represents the critical shear stress for the onset of surface erosion, and acknowledges the model will underestimate mass erosion that happens when τ_{ce} and τ_{bed} are high, and will neglect the small amount of erosion that happens at $0 > \tau_{bed} > \tau_{ce}$ and. This is necessary as Delft3D does not support

erosion with multiple shear stress thresholds, and this also simplifies the considerations for setting these thresholds in the study's parameter space.

All models were run on a 400x280 cell computational grid with 25m square cells, as this was found to be a good compromise between providing detailed model outputs, maintaining model stability and keeping computational times manageably small. The deltas were formed in a 5,750m by 10,000m basin devoid of non-fluvial currents and waves (*Figure 4-1*) (an increase in size from Chapter 3 to try and more fully utilize computational resources). Water and sediment were supplied to the basin by a 500m wide, 4m deep, 1,250m long inlet channel, which was expanded from that used in chapter three because early test runs showed the thinner channel to be a source of instability in some of the runs. This basin setup therefore most closely represents lakes, or micro-tidal, low wave energy settings such as the Gulf of Mexico, but was chosen for its simplicity, which would

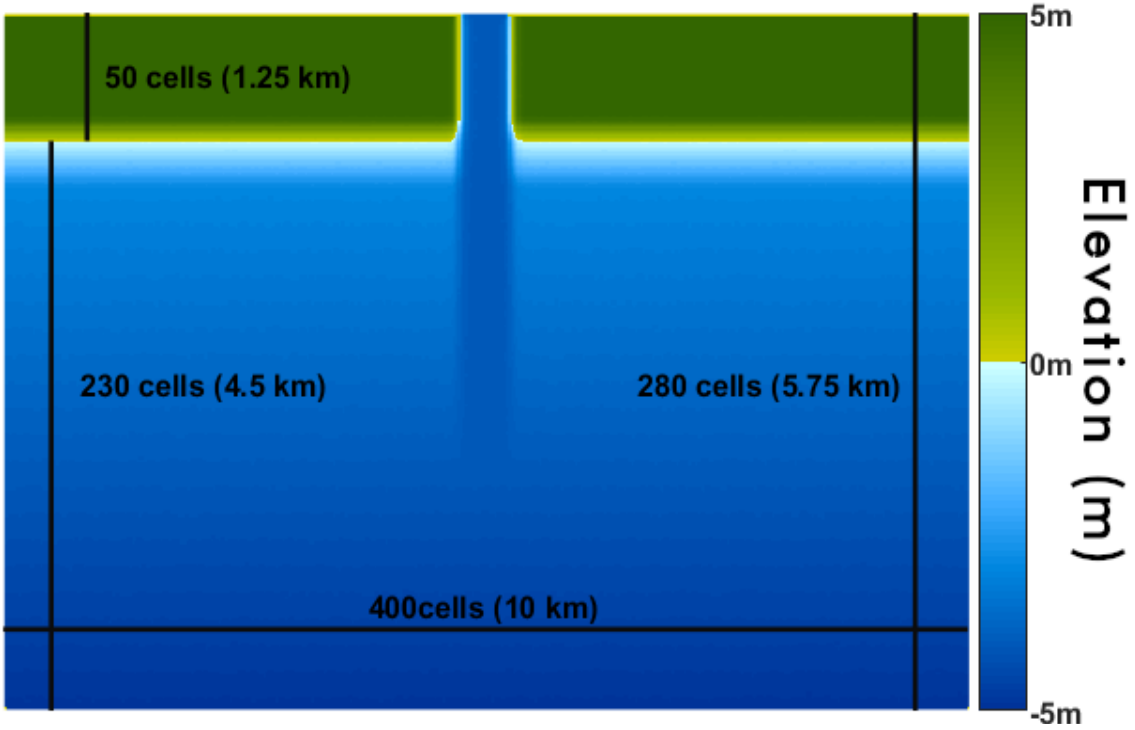

Figure 4-1: Schematic of model set up and bathymetry initial conditions

allow clearer identification of the effects of input parameters on end results, rather than to model any specific environment.

As in chapter 3 (see 3.2.2 for details), the inlet channel had a temporally varying, synthetic discharge made from the of the multiple of two sine waves to maintain simplicity while providing a varying discharge to the model, which has been found to be important to replicate channel incision and lateral migration in physical models (Piliouras et al., 2017). One sine wave had a period of one year to represent seasonal variation and one had a period of 1/42 of a morphological year, simulating a rainfall mediated peak in discharge every 8 to 9 days). This generated a hydrograph with discharges varying between 240 and 3,830 m^3s^{-1}, with a mean discharge of 1,476 m^3s^{-1} (*Figure 4-2*). The discharged water carried a mixture of cohesive and non-cohesive sediment at a constant concentration of 0.05 km m^{-3}.

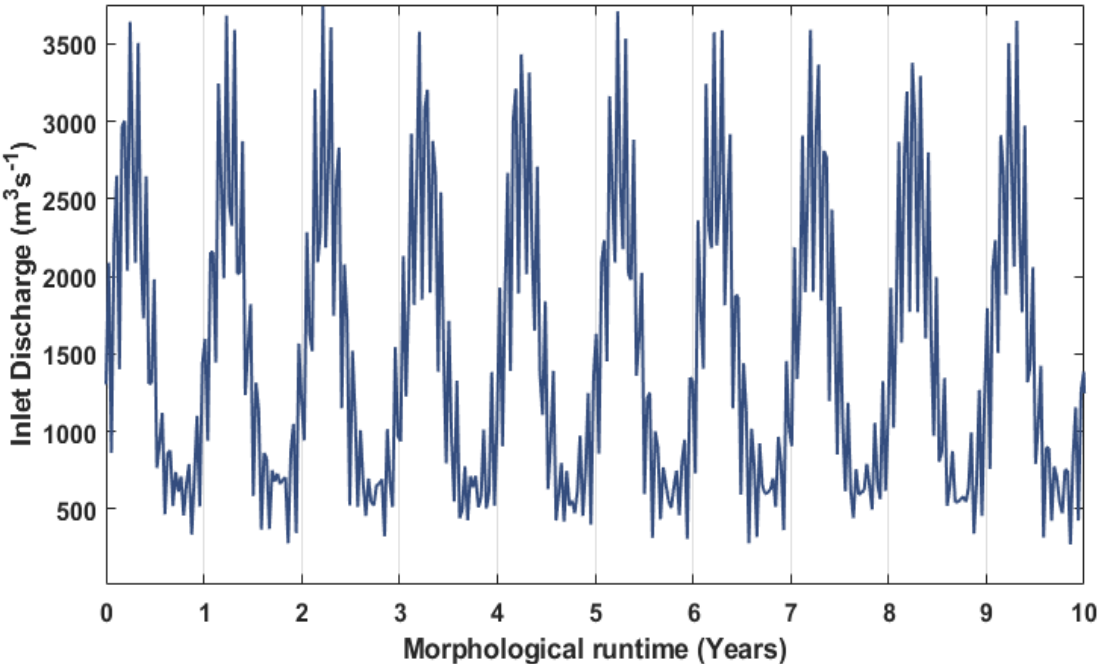

Figure 4-2: The first 10 morphological years of the hydrograph used to drive the models for this chapter

The fluvial sediment supplied to the basin consisted of cohesive and non-cohesive sediment in three different proportions: 20%:80% for low cohesivity runs, 50%:50% for medium cohesivity runs and 80%:20% for high cohesivity runs. Cohesive sediment is treated as mud with no specified grain size (grain size is not used by Delft3D-flow for sediment with grainsize<64 μm), but a settling velocity of $9.0x10^{-4}$ ms^{-1} (within the range found by Tan *et al.* (2012) for both pure clay and clay-exopolymer flocs), a specific density of 2,650 kg m^{-3}, and a dry bed density of 500 kg m^{-3} (after Burpee *et al.* (2015)). Erosion and deposition of cohesive sediment is controlled by critical shear stresses (i.e. the maximum or minimum shear stress needed to initiate erosion and deposition). The cohesive sediment in the fluvial inflow has a critical shear stress for erosion of 1 N m^{-2} (a value within the bounds found by Black *et al.*, (2002) for estuarine mud, and already used in delta models by Caldwell and Edmonds (2014). Following the methods of previous modelling studies (Caldwell and Edmonds, 2014; Edmonds and Slingerland, 2010), all cohesive sediment was given a critical shear stress for deposition (i.e., the shear stress under which deposition will happen) of 1,000 N m^{-2}, causing it to deposited constantly unless erosive power was sufficient to cause erosive flux to exceed depositional flux.

Noncohesive sediment is treated in Delft3D as any sediment with a grain size over 64 μm. In these models, the noncohesive sediment was sand grains with a D_{50} of 225 microns, a specific density of 2,650 kg m^{-3} and a dry bed density of 1,600 kg m^{-3} (standard values, used in several similar studies, e.g. Burpee et al. (2015), and Edmonds and Slingerland (2010)). These sediment inputs simulate a delta with a fluvial sediment input that is dominantly fine, even in the low cohesivity runs. As such, the deltas simulated here most closely represent coastal

deltas generated by large, long rivers with fine sediment load (correlating to most of the worlds largest river deltas (Syvitski et al., 2009)) as opposed to deltas forming from shorter, upper coarse rivers that may form deltas with much coarser material.

The basin substrate was made of evenly mixed cohesive and non-cohesive sediment to a depth of 20 m. As possible basin substrates in the real world are widely varied (*Figure 4-3*), three different generic substrates where used to give a cross-section of possible conditions without overly complicating model setup; Low resistance, Medium resistance and High resistance (see *TABLE 4-1*: Properties and makeup of bed sediment for sediment proportions and cohesive sediment τ_{ce}). These three categories neglect certain delta substrates (such as those with high sand content *and* cohesive sediment τ_{ce}, or very muddy substrates with low τ_{ce}), as well as substrates made from coarser material than 225 µm fine sand, but only a limited number of substrates could be tested without the number of model runs becoming unmanageable, so three varied substrate types where chosen that constitute end members of the values seen on *Figure 4-3*, with one intermediate value. These substrates broadly represent deltas forming over fine costal sand (low resistance), consolidated mud (such as that found underlying Wax Lake Delta (Shaw and Mohrig, 2014); High resistance) and an intermediate substrate. Substrate noncohesive sediment had identical properties to fluvial noncohesive sediment (D_{50} = 225 µm, specific density = 2,650 kg m^{-3}, dry bed density of 1,600 kg m^{-3}). Substrate cohesive sediment was similar to fluvial cohesive sediment, except where noted in *TABLE 4-1*: Properties and makeup of bed sediment.

TABLE 4-1: Properties and makeup of bed sediment

Bed sediment	Cohesive sediment proportion	Cohesive sediment τ_{ce} (Nm^{-2})
Soft	20%	1.5
Medium	50%	4
Hard	80%	10

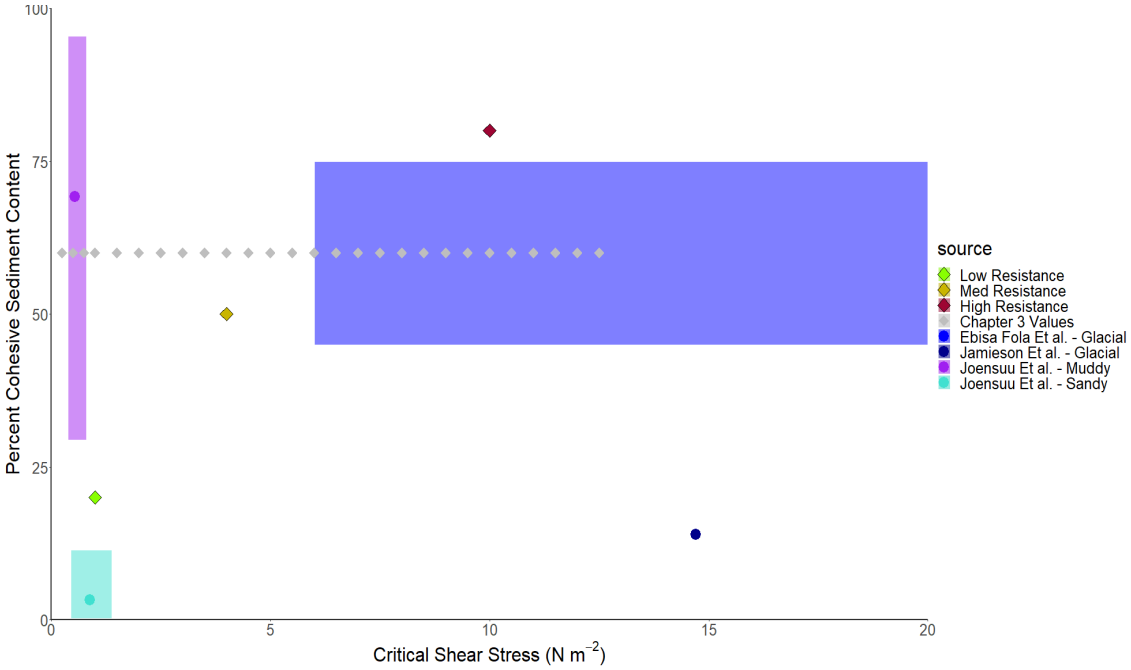

Figure 4-3: (Modified from Figure 2-2.) Estimated parameter space of real-world delta substrates, and modelled substrate conditions. Real world examples consist of:- "Sandy" and "Muddy" type shallow coastal sediments described by Joensuu et al. (2018), Glaciomarine till described by Jamieson et al. (2013)*, and similar consolidated Champlain Sea clay described by Ebisa Fola and Rennie, (2010). Model parameters for the previous chapter are included in grey for reference.

**Note that only percent clay content is given in Jamieson et al. (2013), and while this value has been used here as percent cohesive content, the actual value is likely higher when all cohesive material is included.*

Each model was run three times, with an initial bed elevation modified with a 0.05 m amplitude random noise filter. This was done to give three repeats of each test, as well as to check that small variances in initial conditions did not lead to large variations in the resulting morphometric analysis. Combined with bed and fluvial sediment, this gave 27 (3x3x3) initial model runs (Appendix 3 – Table A1), which were allowed to run until they had all formed "mature" deltas which could act as good start points for further runs.

What constituted a mature delta was found to be difficult to define objectively, and so a number of methods were tested in an attempt to do this. Originally, a threshold of the mass of sediment imported into the model was used, but this was found to be insufficient as model runs supplied with high amounts of fine sediment transported much of the supplied sediment out of the open water boundaries rather than depositing it, meaning that the remaining deltas where much smaller and less developed than the equivalent, coarser sediment deltas. To alleviate this, another method was tried that defined the maturity of deltas by the volume of sediment deposited, but this was also found to be limited as some deltas (mainly ones supplied with more cohesive sediment forming over high resistance substrate) could consist of large subaqueous deposits with very little subaerial land, when other deltas had much larger subaerial island and channel networks. As a result, a method of defining a mature delta by morphodynamic processes rather than sediment or time thresholds was sought. The method arrived at was to define the model runs as mature when they had at least three channels with a length greater than their width, separated by subaerial islands. This was based on the idea that two channels only constituted a bifurcation, but for three channels to exist, at least one of the bifurcation

distributaries must have bifurcated as well, or otherwise avulsed or breached one of its levees, suggesting that large scale morphodynamic processes associated with deltas are beginning to take place. While this method is not flawless, and involves some subjectivity in defining channels, it was used as it identified mature deltas more consistently than other methods tried.

Once all deltas had achieved this threshold, their delta top area (A_t, = the area of land with elevation greater than 0 m from the model datum, i.e. above the open-water boundary water level) was measured, and a single A_t was found at which all deltas had matured (A_{t0} = 12,203 m^2). For each run, the recorded timestep with A_t closest to the chosen A_{t0} was used as the "base" delta (see *Figure 4-4*). These 27 base deltas where then used as initial conditions for the next stage

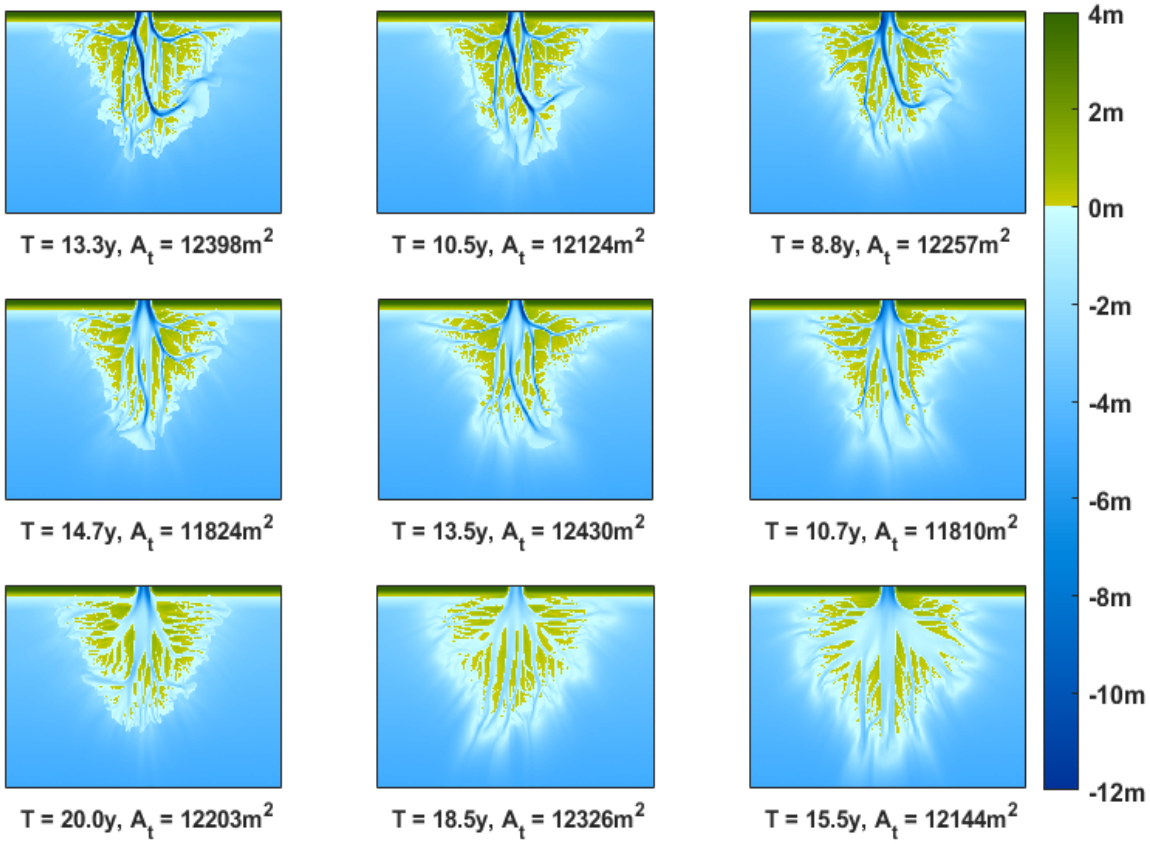

Figure 4-4: Bathymetry of base deltas at the timestep used as initial conditions for continuing model runs

of modelling, and their evolution was continued under influence of four different regimes of external forcing factors. For one test, these deltas where exposed to sea level rise consisting of a 15 mm y^{-1} linear increase in the water level at the three open-water model boundaries. This rate of relative sea level rise is justified as a combination of basin subsidence and eustatic sea level rise, estimated at 10 mm y^{-1} and 5mm y^{-1} respectively.

While these are both high values designed to simulate the end member effects of RSLR, neither are unrealistic compared to ESLR values for the IPCC's RCP6.0 scenario (5.05 mm y^{-1}) (IPCC, 2013), and ground subsidence seen in some coastal areas where large scale groundwater extraction is occurring (Erban et al., 2014). Additionally, this assumes that both sea level rise and basin subsidence are happening evenly across the whole model domain. While this is not always the case in real world examples, especially concerning subsidence (Paola et al., 2009) where faults and differential subsurface fluid extraction (Morton et al., 2006) can lead to large spatial and temporal variation in subsidence rates. A constant and uniform rate was used as Delft3D (as with other applicable, freely available morphodynamic models known to the author) doesn't support the implementation of differential subsidence, and a consistent subsidence rate would make interpretation of the results more straightforward.

In a second test, the 27 base scenarios (*Figure 4-4:* Bathymetry of base deltas at the timestep used as initial conditions for continuing model runs) were exposed to a series of fluvial sediment starvation scenarios, which were modelled by entirely stopping sediment import in to the model by the inlet by setting the concentration of all sediment fractions to 0 kg m^{-3}. While 100% cut-off of

sediment is unlikely in the real world, this was used for simplicity as an end-member to show the maximum possible effects of sediment starvation, and as discussed in Section 4, observed sediment losses greater than 95% are not uncommon. The sediment supply was cut off instantaneously which, while it would represent an extreme end member scenario of a single large impoundment being constructed directly upstream of the delta such that sediment could neither pass it nor be reintroduced into the feeder channel by erosion of the upstream bed, was done to simplify model setup and interpretation, and keep the overall run time of the models short and the number of different model runs manageable.

For the third test, the deltas where exposed to both the RSLR and sediment decline scenarios simultaneously. In addition to this, there was also a control run which experienced no sea level rise, received normal sediment input, and in all ways continued to run as they had in the base runs. This gave a total of 108 final models (Appendix 3 – Table A2)

4.2.2 *Channelised cell finding algorithm*

The channel finding algorithm described in Chapter 3 is used here to identify active channels within the delta, although some small changes have been made to reflect the scenarios run here which do not contain incoming sediment. The active cell identification process was adjusted to use only water depth and flow velocity, rather than water depth (see Appendix 4), flow velocity and sediment transport magnitude to avoid the possibility of the detection algorithm unfairly favouring channel detection in continuous sediment supply runs, where channel sediment transport was expected to be much higher.

4.2.3 *Statistical analysis and checking*

Once active channel cells had been identified at each recorded time step, the lifetimes of cell channelization for each cell was calculated by counting the number of time steps that each cell was continuously identified as active. Once the cell is abandoned (no longer identified as active) its lifetime is recorded and that cell is reset, so that if it becomes active again that lifetime is recorded separately. These lifetimes are plotted in an inverse cumulative frequency graph (*Figure 4-5*) and a curve is fitted them. The fitted curve has the generic equation:

$$P(t_{ch} > t) = \alpha \boldsymbol{e}^{-\boldsymbol{\lambda}} \quad \textbf{(4-1)}$$

The α and λ terms of the curve are then extracted and recorded, and the λ term is inverted to give a mean channelization lifetime, $\overline{t_{ch}}$ (years), which can be used to compare the mobility of channels between model runs:

$$\overline{t_{ch}} = \frac{1}{\lambda} \quad \textbf{(4-2)}$$

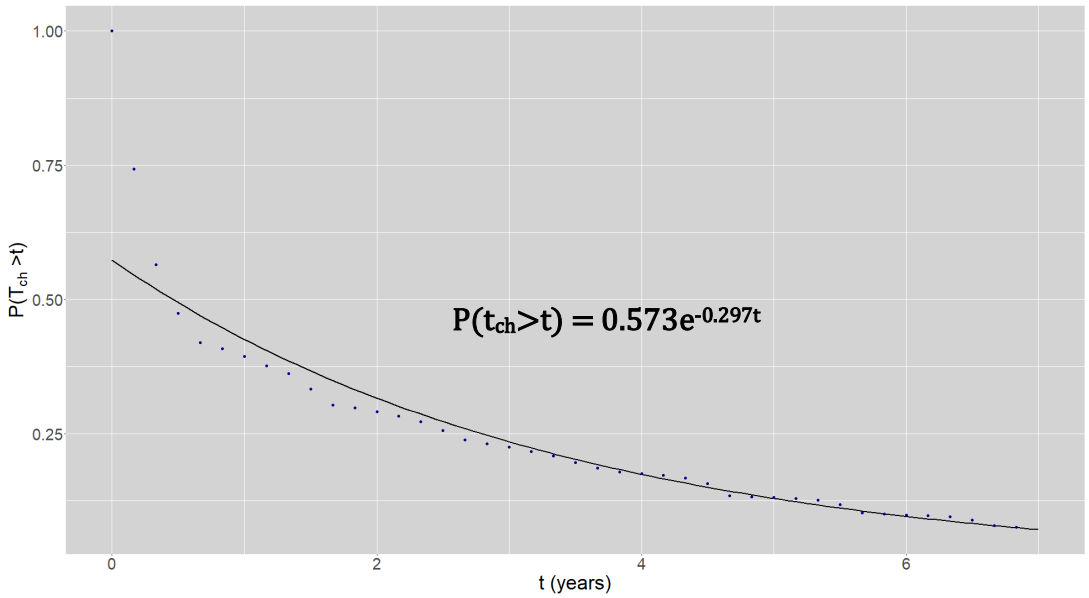

Figure 4-5: An example P(Tch>t) (the proportion of channelised cells with residence time >t) plot, with the curve fitted to all lifetimes >1 year.

In addition to this, the maps of active cells were used to calculate, mean channel width (m), mean channel depth (m) and mean width:depth ratio (dimensionless) using the same methods described in Section 3.2.3. This was done when morphological time, T_{morph} = 7 years, as after this point, delta channel's reached the edge of the model domain, and became stuck in place due to the effect of the infinite sink that the model boundary acted as (See appendix figure 1). Bed elevation outputs were used to calculate subaerial area (m^2) and mean delta top elevation (m) as in Section 3.2.3, and also to create a difference map between initial and final bed which represented the morphological change (deposition and erosion) between these two times. The same method used in Section 3.2.3 to calculate mean centreline channel depths (clipping to the 'skeletonized' channel centreline, then averaging across the remaining cells) was used on this morphological change map to give the average channel centreline incision (m).

As in Section 3, three other morphometric coefficients were also calculated in an attempt to quantify the larger-scale morphology of the delta top (see Section 3.2.4 for more detailed methodology). 'Delta-top channel coverage' was calculated by algorithmically counting the total area of model cells containing an active channel and dividing this by the total delta top area to give a proportion of the delta top occupied by channels. Additionally, two indicators of channel density and complexity are calculated: 'network density' (D_n) calculated by dividing the total length of channel centrelines by the total delta top area; and 'network sinuosity' (S_n), calculated by dividing the total length of channel centrelines by the average distance from the delta apex to the coast. All of metrics indicate the overall density of channels on the delta top, and would be expected

to be low in deltas with few, straight channels and high in deltas with many, sinuous and branching channels.

The collected delta metrics where all fitted with generalised linear models (GLMs) in R, with the predictor variables Sea Level Rise (m, 0 or 0.105), Sediment Starvation (Boolean, true/false), fluvial sediment cohesive fraction (proportion, 0.2-0.8) and substrate sediment resistance (ordered categorical data, low resistance < med resistance < high resistance). These predictors, and their higher order interactions, where then eliminated using a stepwise model development method, in which the statistical significance (p-value calculated by an analysis of deviance "F" test in R) of each term is evaluated, the term with lowest significance is dropped, and then the test is repeated with the new GLM. This is done until all terms are found to be statistically significant ($P<0.01$). The remaining correlations where then considered in terms of the physical relationship they represented.

4.3 Results

4.3.1 River Sediment cohesivity and substrate erodibility

To evaluate the effects of the basin substrate on delta top morphology (found to be important in the previous chapter) metrics of delta top shape and channel geometry, as well as more complex morphometrics are analysed with respect to variations in fluvial and substrate sediment regime. Delta top area was calculated as the area of land above the sea level set at model open water boundaries. This was 0 m for runs not exposed to sea level rise and 0 m + (RSLR rate x model time) for runs that were. For deltas receiving sufficient sediment, delta top area increases with increasing fluvial sediment cohesivity (*Figure 4-6*), at a rate of 106.2

m^2 (for deltas growing without SLR) and 129.5 m^2 (for deltas growing with SLR) per percent increase in fluvial cohesivity. However, no significant correlation between substrate resistance and delta top areas was found.

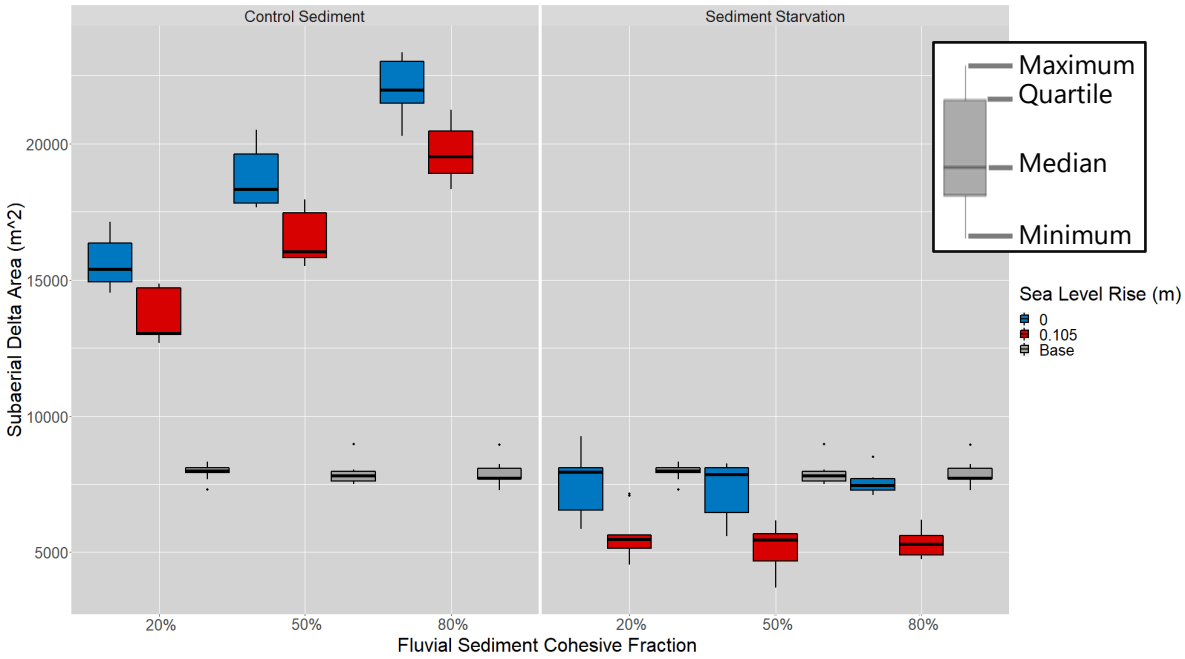

Figure 4-6: Boxplots of subaerial delta top area. Base models that were used as initial conditions are shown in grey on both panels.

For deltas with a continuous sediment supply, higher resistance substrates increase mean elevations (0.28m for low resistance substrate, 0.33m for medium resistance and 0.40m for high resistance) (*Figure 4-7*). For lower resistance substrates, delta-top elevation increases with increasing fluvial sediment cohesivity at a rate of 0.092m per percentage increase in fluvial cohesive fraction but is not significantly different to the initial conditions. However, on deltas forming over high resistance substrates, delta-top elevation decreases with increasing fluvial sediment cohesivity at a rate of -0.185m per percentage increase in fluvial cohesive fraction. Deltas forming over medium resistance sediment have no strong trend with fluvial cohesivity, possibly as they are in a transitional state between the states seen in deltas forming over low and high resistance substrates

(*Figure 4-7*). This shows that fluvial and basin substrate sedimentology influence delta tops in different ways.

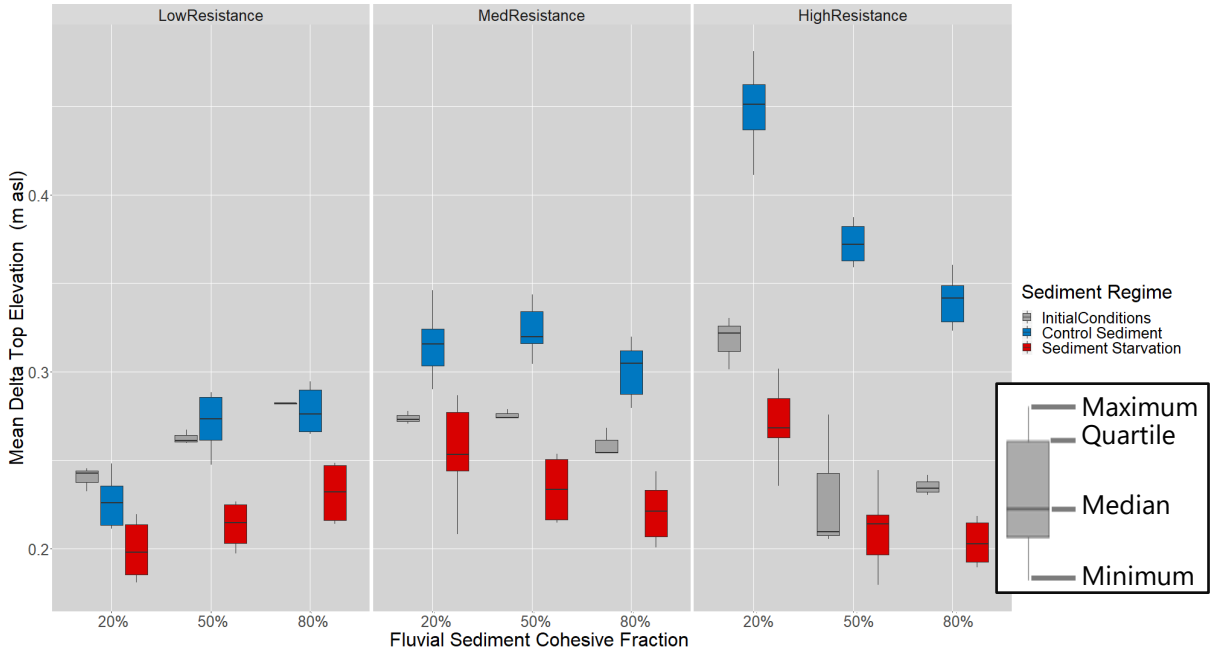

Figure 4-7: Mean delta top elevation for final deltas, plotted against fluvial cohesive proportion, sediment regime and substrate resistance. Top and bottom box edges indicate 3rd and 1st quartiles respectively, and whiskers indicate maximum and minimum values. Central bar indicates medium.

The mean depth of delta channels decreases slightly between low and medium resistance substrates (from an average of 3.67 m to 3.36 m), then much more dramatically between medium and high resistance substrate (to 1.83m) (*Figure 4-9*). In deltas forming over the hardest substrates, the highest mean channel depth is 2.17 m. Channel depth decreases at a rate of 0.0063 m per percent increase in cohesive sediment fraction, for all substrate types.

When supplied with constant sediment, channels forming over high resistance sediments have an average width of 221 m (*Figure 4-8*), universally wider than those formed over less resistant substrates. In runs with low and medium resistance substrate, increasing fluvial cohesivity decreases channel

width from 154.6 m and 166.9 m respectively for 20% fluvial sediment cohesivity to 135.4 m and 150.7 m for 80% fluvial sediment cohesivity.

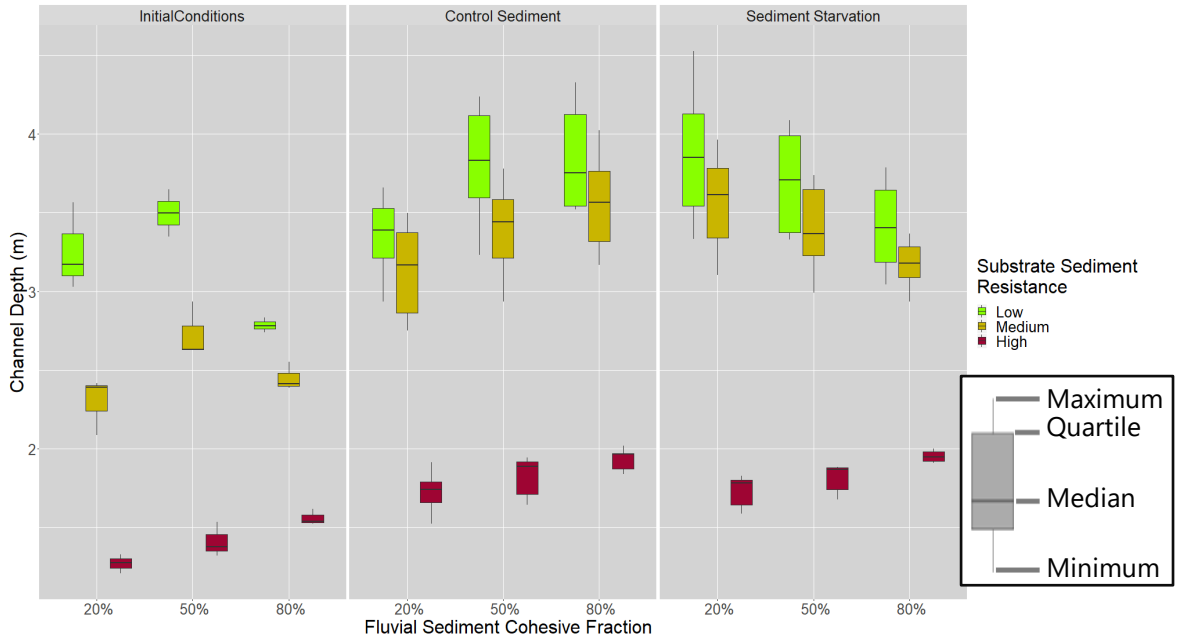

Figure 4-9: Boxplot of mean channel centreline depth against fluvial sediment cohesive fraction, substrate sediment resistance and sediment supply regime.

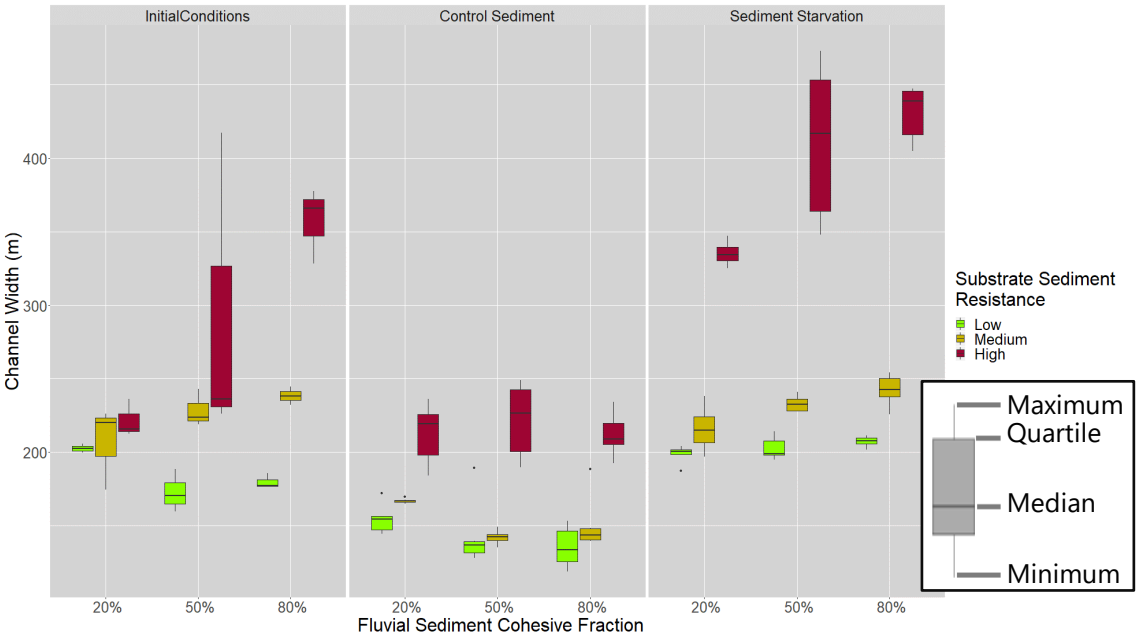

Figure 4-8: Boxplot of mean channel widths against fluvial sediment cohesive fraction, substrate sediment resistance and sediment supply regime.

Deltas forming over high resistance substrates with a constant sediment supply have significantly higher width:depth ratios (118 on average; *Figure 4-10*) than those forming over low or medium cohesivity sediment substrates (averages of 40 and 46 respectively), a difference that is largely caused by the channels being significantly shallower, rather than much wider (see *Figures Figure 4-9* and *Figure 4-8*). Increasing fluvial cohesivity leads to decreased width:depth ratios across all substrate types when sediment supply is constant. Taken together, the above results demonstrate that while fluvial and substrate sedimentology affect channel geometry, in most cases, the presence of particularly resistant substrate is the dominant influence.

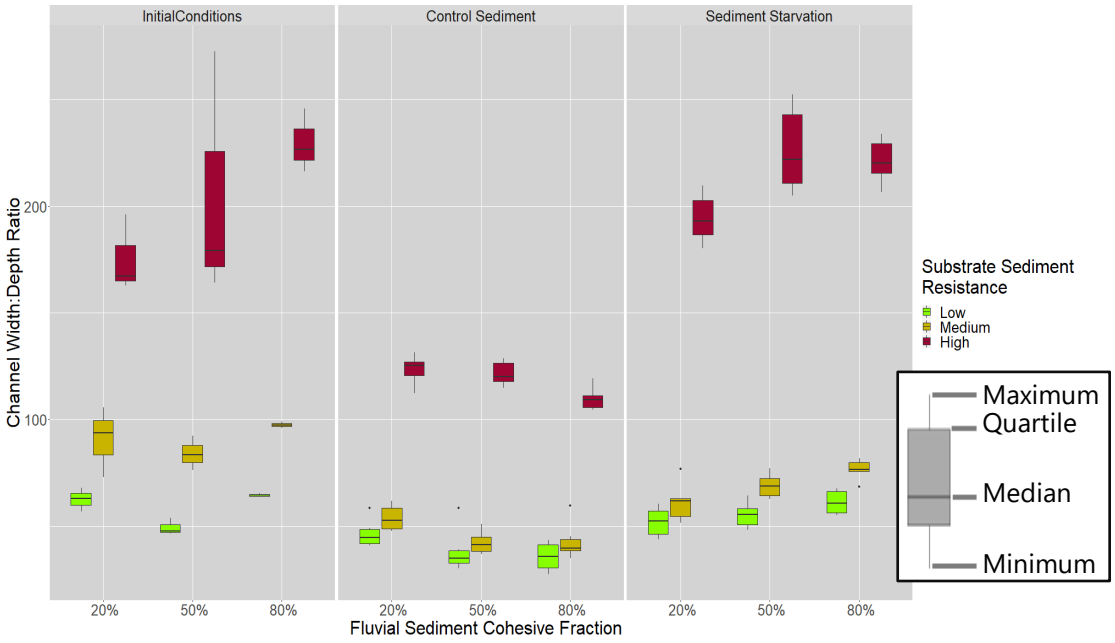

Figure 4-10: Boxplot of width:depth ratios for deltas formed with different substrates and fluvial load cohesivities.

In deltas with a constant sediment supply the channels have an average residence time of 3.9 years (*Figure 4-11*). The effect of fluvial cohesive sediment proportion on channel residence times is modulated by substrate resistance; when deltas form over low resistance substrates, increasing fluvial cohesivity causes a decrease in channel residence time, from an average of 3.8 years for

those supplied with 20% cohesive fluvial sediment, to 3.2 years for those supplied with 80% cohesive fluvial sediment (*Figure 4-11*). However, when forming over high resistance substrates, the same change in fluvial sediment cohesivity causes residence times to increase from 3.8 to 5.5 years.

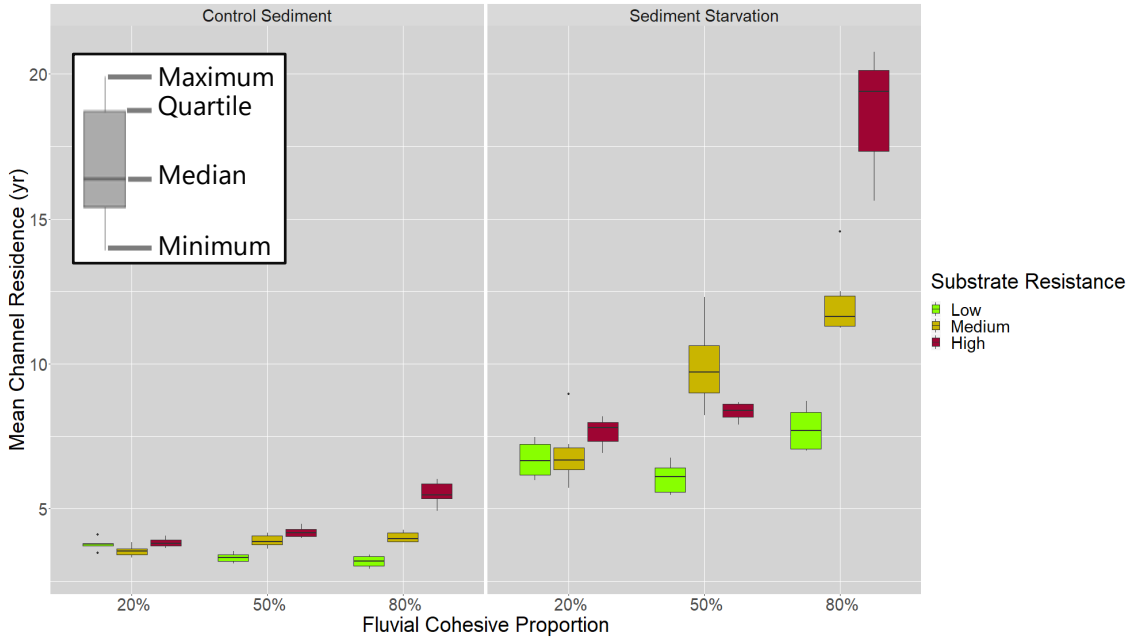

Figure 4-11: Boxplots of mean channel residence time against substrate resistance, fluvial sediment cohesivity and sediment supply regime.

Figure 4-12 shows that in all cases, more resistant substrates lead to higher delta top channelised cell density, as wider channels take up a larger proportion of the delta top. Fluvial sediment type has a less strong effect, however, and decreases the channel density, likely due to more cohesive flows building relatively fewer, thinner channels.

For deltas with healthy sediment supplies, increasing cohesivity of the fluvial sediment decreases the channel network density (Figure 4-13), as less channels a smaller number of channels build larger delta tops (see Figure 4-6). Substrate type does not strongly affect network density. With healthy sediment supply, and without the influence of sea level rise, network sinuosity increases with

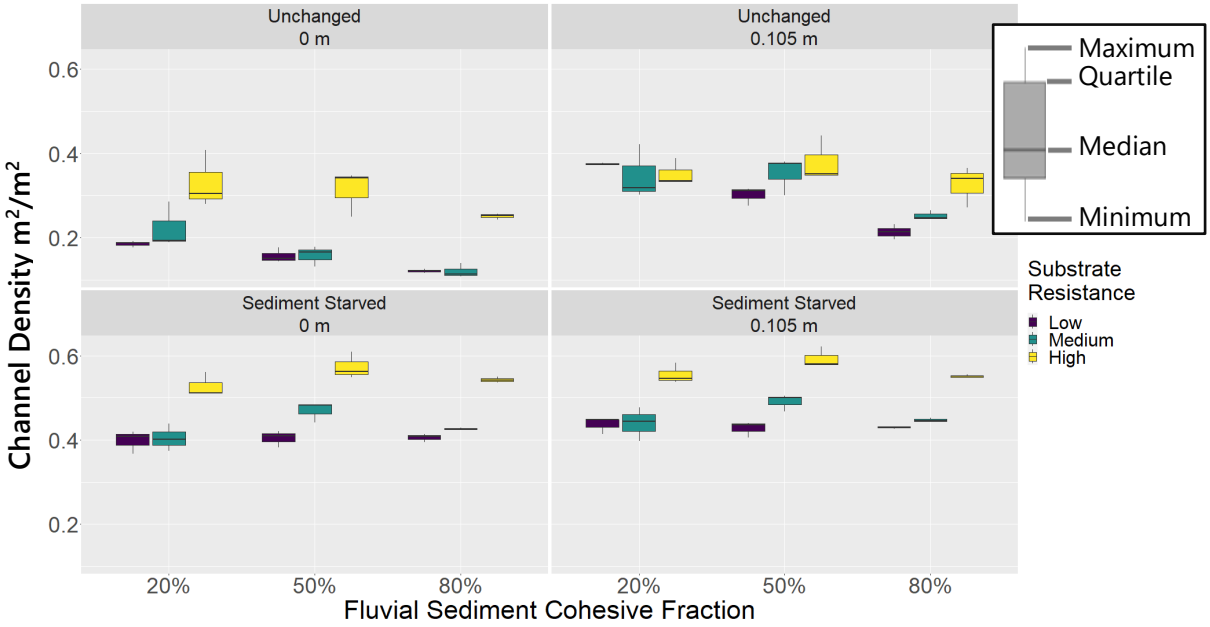

Figure 4-12: Channel density (i.e. the area of active channels as a proportion of delta top area) plotted against fluvial sediment cohesivity and substrate resistance, with subplots for different sea level and sediment supply regimes.

substrate resistance (*Figure* 4-14), potentially as a result of there being greater number of connected channels on delta tops formed over resistant substrates, than on those formed over less resistant substrates. Fluvial sediment cohesivity has little or no effect network sinuosity.

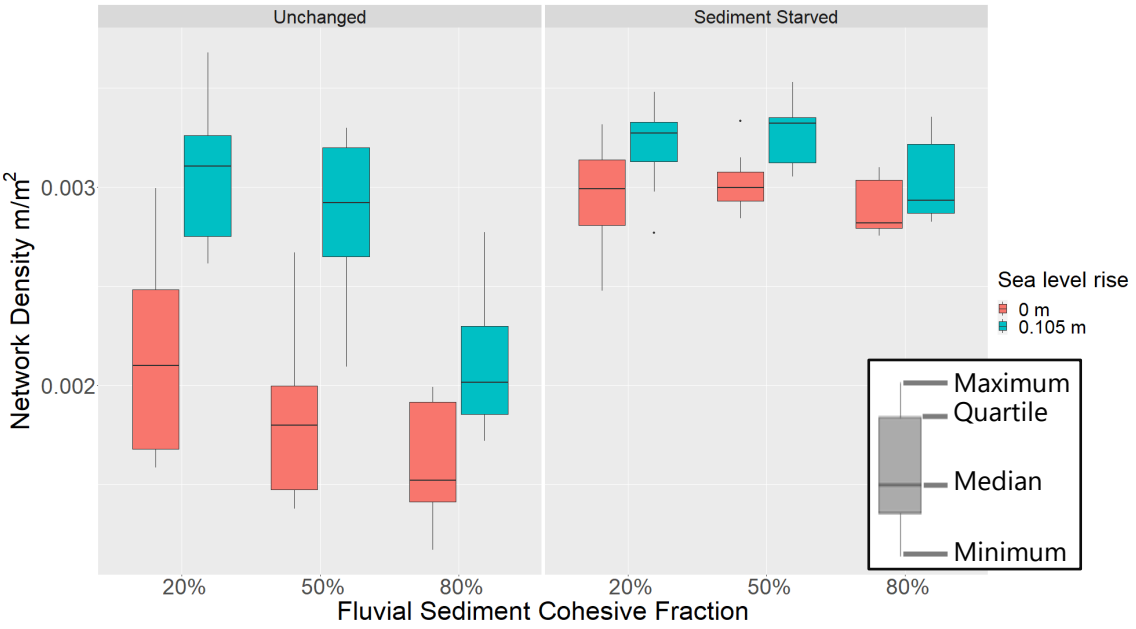

Figure 4-13: Network density (total length of active channels per delta top area) plotted against fluvial sediment cohesivity and sea level, with subplots for different sediment supply regimes.

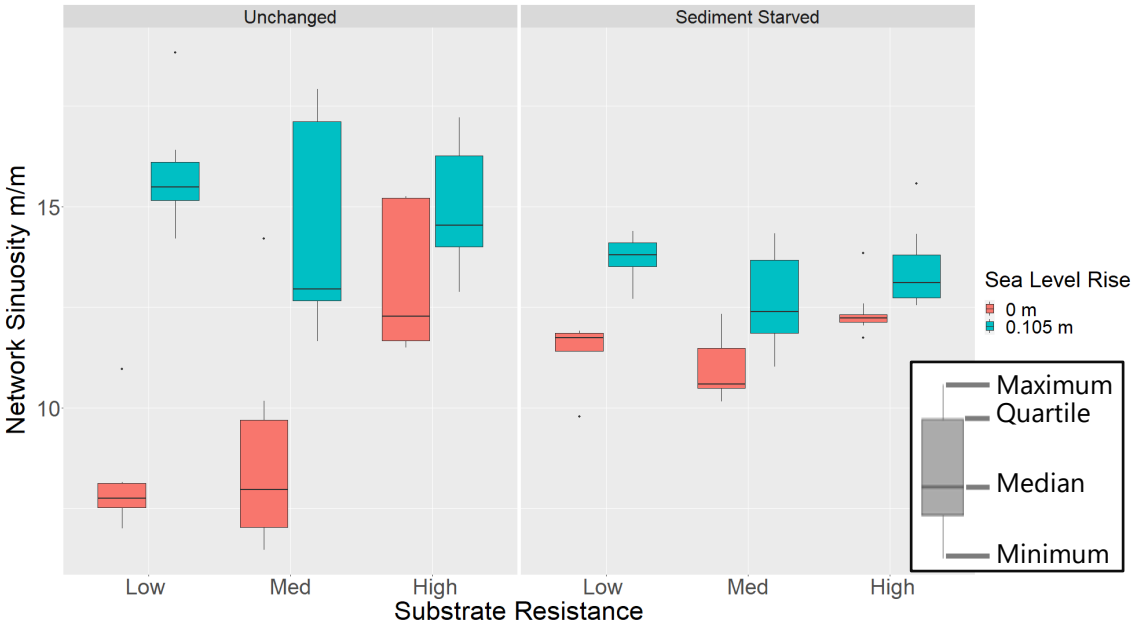

Figure 4-14: Network sinuosity (total length of active channels divided by the average length from the delta apex to the coast) plotted against fluvial sediment cohesivity and sea level, with subplots for different sediment supply regimes

4.3.2 *Sediment starvation and Sea level Rise*

The central aim of this chapter is to address the effects of sea level rise on delta morphodynamic, and so all of the above metrics were also analysed with respect to the four combinations of relative sea level rise and sediment shutoff. Sea level rise decreases delta-top area consistently by c.2135 m^2 for all delta types (Figure 4-6). However, the sediment starvation scenario imposed here decreases delta area much more dramatically than sea level rise (by between 48-66%) and removes the influence of fluvial sediment (as no fluvial sediment is reaching the delta) (*Figure 4-6*). Sediment starvation decreases delta elevation, by 0.038 m, 0.082 m and 0.155 m for low, medium and hard substrates respectively (*Figure 4-7*). These differences effectively remove the trend between substrate resistance and elevation seen in deltas with constant sediment supply (*Figure 4-7*). Sediment

starved deltas forming over medium resistance substrate transition from the transient state seen in sediment-rich deltas (in which there is no trend between fluvial sediment cohesivity and delta-top elevation) to being inversely correlated to fluvial sediment cohesivity. This suggests that the threshold between delta elevation increasing or decreasing with fluvial sediment cohesivity shifts towards less resistant beds. Overall, these results indicate that in all cases, the extreme sediment starvation scenario modelled here influences the form of delta tops more strongly than sea level rise.

Sea level rise does not greatly affect the depth of channels over the high resistance substrate (*Figure 4-15)*. In channels forming over medium and low resistance substrate however, sea level rise results in mean channel depth decreasing by 0.4 m and 0.7 m respectively, possibly as reduced water level gradients cause enhanced deposition in the channels. All deltas show deeper channels than they had in their initial conditions (*Figure 4-15*), indicating that they

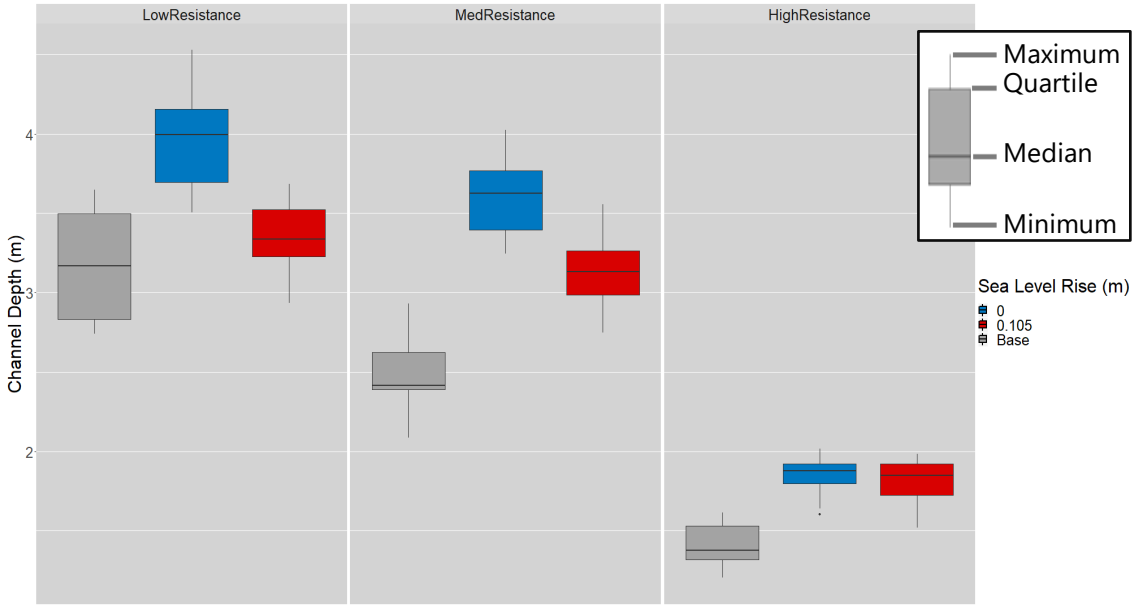

Figure 4-15: Mean channel centreline depth plotted against substrate resistance and sea level rise. Initial conditions plotted in grey for comparison.

either erode downwards into their substrate as they prograde or extend channels into the deeper waters distally.

In deltas forming over low and medium resistance substrates, sediment starvation inverts the relationship between fluvial sediment cohesivity and channel depth, meaning that for these deltas increasing fluvial sediment cohesivity decreases channel depth (*Figure 4-9*). This leads to channels in some delta channels (those forming from 80% cohesive sediment over low and medium resistance substrates, and those forming from 50% cohesive sediment over low resistance substrates) being shallower on average in deltas undergoing sediment starvation. However, deltas forming over hard substrates retain their positive correlation with fluvial cohesivity, and do not become noticeably deeper or shallower. When channel depths are compared to the depth of incision into the substrate, it can be seen that even in cases where channels are not getting deeper or even becoming shallower on average (*Figure 4-9*) the incision depth increases (*Figure 4-16*). As such, incision depth for deltas formed from high and medium cohesivity is high even though mean channel depth is low.

Sediment starvation increases channel width by >103% in the case of deltas with a 80% cohesive sediment supply forming over high resistance substrates (*Figure 4-8*) though less dramatically for deltas forming over low and medium resistance substrates, which saw average width increases of 40% and 50% respectively. Additionally, under sediment starvation the relationship between fluvial cohesivity and channel width becomes more positive for all substrate types, transitioning from decreasing or not changing with increasing fluvial sediment cohesivity to increasing (*Figure 4-8*). As sediment starvation removes the direct

effect of the fluvial sediment properties (as none reaches the delta), this trend is likely to do with how sediment starved channels rework delta tops composed of different sediment, rather than how the supplied sediment is deposited through the network (See Section 4.4.1).

Figure 4-16: Plots of mean channel centre depth against mean channel incision for modelled deltas experiencing both constant and shutoff fluvial sediment supply. Individual chart titles indicate substrate resistance and fluvial sediment cohesive fraction.

Similarly, the negative trend between width:depth ratio and fluvial cohesivity seen in sediment rich deltas is inverted in sediment starved deltas, where increasing fluvial cohesivity leads to higher width:depth ratios (*Figure 4-10*). Sediment starvation also increases the width:depth ratio of delta channels

forming over high resistance substrate, largely due to increased widths (*Figure 4-8*) rather than decreased depths (*Figure 4-9*).

Sea level rise also increases channel density in deltas forming over low and medium resistance substrate when sediment supply is unchanged (Figure 4-12). This is likely caused by higher water levels flooding the deeper relict channels left in the softer substrates. Sediment starvation also increased channel density in all situations (Figure 4-12), as sediment loss causes channels to widen and deltas to grow more slowly, leading to smaller subaerial delta tops dominated by wide channels.

Network density is increased by sea level rise, especially in deltas with healthy sediment supplies (Figure 4-13). This is likely caused by smaller delta top areas as land is inundated by higher water levels. Fluvial sediment reduction dramatically increases network density and decreases the strength of the trend in sea level rise, as the strong reduction in delta top area caused by sediment loss overpowers the smaller reduction from sea level rise (see *Figure 4-6*). Additionally, while the smaller deltas may also contain fewer channels, it is possible that the lack of sediment may be reducing the deposition that would usually cut off the smaller distributaries of unstable bifurcations on the delta, and so keep relatively more channels open. Sediment starvation also removes the negative correlation between network density and fluvial sediment cohesivity (Section 4.3.1), which was expected, as no fluvial sediment in delivered in there runs.

Sea level rise greatly increases network sinuosity in all cases (*Figure 4-14*) and removes the influence of substrate resistance seen initially (see section 4.3.2). This change is caused by higher sea levels reducing overall delta top size by

inundation, and potentially also by the heightened downstream water level immersing otherwise dry relict channels on the delta top. Sediment starvation also leads to higher network sinuosity in most cases (Figure 4-14), as the lack of sediment decreases delta top growth, while also increasing erosion, potentially keeping mor channels open. When sea level rise and sediment starvation effect the same delta, network sinuosity rises to higher than with sediment starvation alone, as higher sea levels inundate low lying coastal land, reducing the radius of the delta top without dramatically reducing the overall length of channels on the delta (Figure 4-14). These results demonstrate that sediment starvation has a strong effect on both local channel geometry and larger scale morphometrics. This effect is also frequently modulated by the fluvial cohesivity and substrate resistance of the delta, highlighting the importance of considering sedimentology when evaluating the effects of external stresses.

In deltas undergoing sediment starvation, channel residence times are much longer, increasing by at least 77% (from 3.78 to 6.7 years in the case of low fluvial sediment cohesivity and low substrate resistance deltas) to as much as 238% (for high fluvial sediment cohesivity, high substrate resistance deltas). For deltas flowing over hard and medium resistance substrates, the effect of fluvial sediment cohesivity on residence times is stronger in sediment poor deltas than in sediment rich deltas. For those forming over low resistance substrates, the trend changes from being negative to weakly positive (*Figure 4-11*). As above, this demonstrates the considerable effect of the sediment loss scenario modelled here, and how sedimentology is modulating this impact.

4.4 Discussion

4.4.1 *Morphodynamic effects of substrate type and sediment starvation*

Deltas forming with consistent sediment supplies over low resistance substrate have mean elevations very similar to the initial conditions, suggesting that these modelled deltas have reached an equilibrium in which they only prograde, rather than growing vertically (*Figure 4-7*). These deltas are also the ones that have the smallest subaerial delta top areas, (see *Figure 4-6*) suggesting that deltas with low substrate resistance don't deposit much of their sediment above sea level, instead depositing it sub-aqueously over a wider area. When subaerial deposition does occur, it is close to sea level, indicating that these deltas would be more vulnerable to storm surges and other inundation events. Increasing fluvial cohesivity increases both elevation and area, and hence the overall amount of sediment that is being retained on the delta top.

However, in deltas forming over high resistance substrates, delta-top elevation decreases with increasing fluvial sediment cohesivity, while delta-top area increases with increasing fluvial sediment cohesivity. This suggests that for these substrates, fluvial cohesivity determines whether sediment is deposited on levees and already subaerial land (low cohesivity) or transported to more distal areas and deposited to form new land (high cohesivity). Deltas forming over medium resistance sediment have no strong trend with fluvial cohesivity, possibly resultant from a balance between erodibility and channel constrains.

All deltas modelled in this study show large decreases in area and smaller decreases in elevation when growing without a sediment supply. This suggests

that sediment starvation effects delta land of all elevations mostly equally. An exception here is land forming over hard substrates. Higher delta tops are not seen at all under sediment starved conditions, as without the sediment supply high inter-channel islands or levees cannot be built. Also of note is that the topset elevation of all deltas grown without a continuous sediment supply is moderately lower than the initial condition deltas, while their land area is only slightly lower. This indicates that land lost due to sediment starvation is mainly of higher elevation, suggesting that the proximal levees are eroded by sediment-poor channels, rather than lower lying distal land. This is supported by the dramatic widening of channels seen in *Figure 4-8*.

Deltas forming over high resistance substrates have noticeably shallower channels than those forming over softer substrates. In fact, they don't exceed 3.5 metres (the depth of the basin) suggesting that channels are unable to erode into the harder substrate. The only method of deepening for these channels is levee building, which is consistent with deltas forming over hard substrates tending to have higher delta top elevations, as long as they are supplied with sediment to build the levees.

The decrease in channel depth in many deltas experiencing SLR is likely due to a shallower water surface gradient slowing flow speed and causing enhanced deposition. However, in deltas forming over a high resistance substrate, SLR seemingly does not alter the depth. This is likely because the channels are already so shallow that deposition cannot occur, and so channel depth is forced by the elevation of the high resistance substrate, rather than being controlled by an erosion-deposition balance modulated by hydrology.

Deltas forming over resistant substrates also seem to be resilient to depth changes in the face of sediment starvation. Where delta channels forming over low and (some) medium resistance substrates deepen as a result of the shut-off of fluvially supplied sediment, delta channels forming over more resistant substrates do not get deeper. Instead, channel depth remains the same, but channels widen dramatically. This leads to channels occupying a higher fraction of the delta top, increasing channel density in these cases.

In high fluvial cohesivity deltas, sediment starvation tends to decrease channel depth. This may be due to the lack of supplied sediment precluding the deposition of large levees, which have shown to be important in the morphology of high cohesivity deltas (Edmonds and Slingerland, 2010). The weakening of these levees may cause lateral erosion and levee overtopping to become more favourable than vertical erosion, decreasing channel deepening when compared to high cohesivity deltas with large levees.

These findings highlight that total sediment shut off of deltas is a more serious threat to deltaic lands than sea level rise, at least at levels presented here and across these delta timescales. The loss of fluvial sediment slows the growth of deltas, and causes a greater proportion of the subaerial delta to be occupied by wide channels. The difference is sufficiently pronounced that even with only a partial shut off of sediment flux and more rapid sea level rise, sediment starvation is likely to remain the primary driver of delta land loss.

In as-normal sediment regimes, channels become thinner and deeper with increasing fluvial sediment cohesivity, as is found in a number of previous studies (Caldwell and Edmonds, 2014; Edmonds and Slingerland, 2010). This is associated

with high cohesivity channels being able to build strong levees to confine the channels, while low cohesivity channels only build weak, easily eroded levees. However, when these same deltas form under conditions of sediment starvation, the opposite is true; increasing fluvial cohesivity leads to wider channels with higher width:depth ratios. While all deltas have higher average channel widths when growing under sediment starvation (due to enhanced erosion by sediment poor channels), this difference is highest for deltas where the original fluvial sediment supply was more cohesive. This is likely due to the sediment poor channels being able to erode fine sediment from the bed, with the excess erosive power being sufficient to wash this fine sediment out of the delta and into deeper water, rather than depositing this sediment near channel mouths. This leads to channels and any deposited subaqueous mouth bars or levees becoming relatively enriched in sand as finer sediment is winnowed out. As a result, in deltas that were built by mostly cohesive fluvial sediment, the delta top is contains less sand that can be reworked, leading to smaller, weaker subaqueous levees that cannot laterally confine channels as effectively.

Sediment starvation also decreases channel mobility universally, which is expected as avulsion is mainly driven by deposition and channel accretion. This slows or stops when sediment starvation precludes deposition. Under the influence of sediment starvation, deltas with substrates made softer sediment or delta tops made of sandier sediment may be able to maintain the morphodynamic processes that lead to channel movement by reworking this material. However, those with harder substrates or more cohesive delta tops see their channel mobility decrease dramatically. In deltas forming over hard substrates, this could be due to their substrate being difficult to erode, reducing

the amount of re-workable sediment that can be liberated from the bed. Similarly, in deltas formed of highly cohesive sediment, strong levees may help to reduce horizontal erosion, and when the cohesive sediment is entrained, the sediment poor flow is less likely to redeposit it. Delta systems that can maintain morphodynamic processes by reworking already present sediment may be able to better adapt to sediment starvation by adjusting channel geometries and overall delta size to fit a new equilibrium.

Sediment starvation also increases network density, suggesting a greater *number* of channels are present per area of the delta top (as opposed to channel density, which could be increased purely by the same number of channels widening to take up more space.) This increase in the number of channels combined with the decreased mobility of channels found in sediment starved deltas, could both be caused by increased bifurcation stability, which would decrease the number of avulsion events (increasing channel stability and hence mean channel life time) as well as increasing the number of channels as compared to a similar delta with less stable bifurcations by keeping both distributaries open. In sediment starved conditions, less sediment would be present to drive deposition in the non-dominant channel of a bifurcation, potentially causing otherwise unstable bifurcations that would cut off one of their channels to become effectively more stable.

A similar, trend can be seen in network sinuosity (though in this case the change from sediment starvation is smaller than the change caused through sea level rise) and sediment starvation also decreases the size of the change in network sinuosity when both sea level rise and sediment starvation occur

together. It is unclear why these otherwise similar morphometrics respond to sea level rise and sediment starvation differently, as the only difference between these morphometrics is that network density is influenced by delta top area, while network sinuosity is influenced by average delta-top radius (i.e., the average distance from the delta apex to the shoreline). As such, the cause of this discrepancy is likely related to delta shape. Sediment starvation causes deltas to remain small and generally semi-circular in shape, as compared to deltas with competent sediment supplies, with largely prograde forward into the basin, becoming more elongated and increasing area while the *average* radius remains relatively small (though some parts of the shore are far from the apex, a large extent of the shoreline on the lateral edges of the delta remains close to the apex) meaning that sediment starvation decreases area more dramatically than delta radius. Sea level rise, however, effects delta shorelines evenly, along their length, meaning that the radius is decreased relatively more than it is in sediment starvation.

Much of the evidence here suggests that fluvial sediment delivery modulates many of the morphodynamic effects of sediment type. Channels carrying water rich in a particular sediment type may act very differently from sediment poor channels flowing through a delta top composed of that sediment type. This results in trends in channel depth and width with fluvial cohesive sediment inverting when exposed to sediment starvation. An implication of this is that the sediment supply axis of the expanded ternary diagram (Orton and Reading, 1993), may not capture the full complexity of sediment's role within a delta system, as it doesn't distinguish between sediment supplied to a delta, and the sediment that was deposited as the delta top. While these two categories are likely the same

when studying delta systems with sediment supplies that are stable for hundreds or thousands of years, this assumption may fail when studying modern and future deltas, many of which already are (Syvitski et al., 2005) or will soon be (Dunn et al., 2019) severely sediment limited.

It is worth noting, however, that anthropogenic intervention may have already be controlling some of the morphodynamics discussed above. In many fluvial settings, human built levees have reduced or precluded complete avulsions, and so the effects of substrate and sediment qualities may be less important in determining channel mobility. Similarly, the dredging of channels for navigation purposes may be able to deepen channels even where substrate is very hard, and could dictate which delta channels become dominant in the transport of water and sediment by increasing the flow and sediment accommodation space in dredged channels.

4.4.2 *Uncertainty*

Within the models presented here, there are a number of sources of uncertainty. A known source of possible uncertainty within Delft3D-FLOW is the use of the Partheniades-Krone bed-boundary condition to calculate the erosion of cohesive sediment. This formulation simplifies all of the processes that control fine sediment erosion (Fluid mud mixing, surface erosion and mass erosion) into a linear relationship controlled by a single co-efficient τ_{ce} (for further details see sections 4.2.1 and 2.4.3).

Low resistance substrates primarily consist of non-cohesive fine sand, the erosion of which is not controlled by the Partheniades-Krone formulation. As

such, the limitations of this formulation are unlikely to have a strong effect on how deltas forming over low resistance substrates behave. Equally, high resistance substrates have very high τ_{ce}, and the conditions for either fluid mud mixing (which happens when τ_{ce} is low) and mass erosion (which happens when $\tau_{bed} > \tau_{ce}$) are unlikely to be met. Because of this, use of the Partheniades-Krone formulation which neglects these processes may not lead to results that differ significantly from results from different formulation.

However, as mid-resistance substrates contain more cohesive sediment (50%) than low resistance substrates, and this sediment has a lower τ_{ce} (4 N m^{-2}), these substrates may be more likely to experience mass erosion in the real world or in other formulations, and so it is possible that erosion in these model runs has been underestimated by Delft3D. Moreover, in modelled deltas with high fluvial sediment cohesivity, which have likely built delta-tops composed of a higher amount of low τ_{ce} cohesive sediment than other deltas, the Partheniades-Krone formulation may again underestimate the amount of erosion that would happen, especially channel widening from mass erosion of banks. These effects would mean that channels on deltas forming over medium resistance substrates would likely be both wider and deeper if a more advanced cohesive sediment erosion formulation was used. Additionally, the trend of channel width increasing with fluvial cohesivity seen in deltas forming over high resistance substrates (*Figure 4-8*) would likely be even stronger than when the Partheniades-Krone formulation is used. Both of these discrepancies would likely be exacerbated in systems where sediment is limited, as in these cases the resistance of the sediment is the only limiting factor in erosion.

Additionally, only a limited range of sedimentary environments are represented by these models. As discussed in section 4.2.1, setting the grain size of the sand fraction to 225 μm means that these models best represent real world deltas with both fine sediment supplies and basin substrates consisting of fine sediments. Systems with fine fluvial inputs were targeted they represent the deltas of many large rivers (as sediment load grainsize tends to decrease with river length; Syvitski and Saito, 2007), though this means that deltas with coarser sediment supplies, such as those forming at the mouths of shorter rivers are not explicitly investigated here. Furthermore, using a finer sand fraction also means that these models all represent deltas underlain by substrates containing little or no coarse material. While this is assumed to be broadly representative of shallow coastal basins with beds composed of muds and silts, this does bring another area of uncertainty in to focus; the lack of reliable field evidence on the grainsize and geotechnical qualities of the sediment underlying deltas. As the author could find little direct quantitative data on the grain size or τ_{ce} of delta substrates, these substrates were based on riverbeds and shallow seas found in non-deltaic environments (see *Figure 4-3:* (Modified from Figure 2-2.) Estimated parameter space of real-world delta substrates, and modelled substrate conditions. Real world examples consist of:- "Sandy" and "Muddy" type shallow coastal sediments described by Joensuu et al. (2018), Glaciomarine till described by Jamieson et al. (2013)*, and similar consolidated Champlain Sea clay described by Ebisa Fola and Rennie, (2010). Model parameters for the previous chapter are included in grey for reference.), and while these environments should be broadly representative of basin substrates, there is some uncertainty around the exact composition of the delta substrates used in this study.

Finally, the scenario for sediment starvation used in these models is an extreme one. Total, instantaneous sediment shutoff would normally be seen only if a dam were constructed directly upstream of the delta, with sufficient capacity to trap all incoming sediment and a small enough length of channel downstream of the reservoir that no significant amount of sediment could not enter the flow before it reached the delta. However, some rivers studied by Vörösmarty *et al.* (2003) have been shown to have experienced sediment load reductions of 95% or more, indicating that some systems may already have conditions close to total sediment loss. Ultimately, though, this model setup was used as an extreme end-member condition to investigate the broader effects of sediment starvation, and while greater range of sediment conditions would have reduced uncertainties around the effects of sediment starvation, this single solution was used to keep models simple, and to keep the overall number of model runs manageable. Future studies could investigate this in more detail by varying the proportion of sediment load lost, the speed at which the loss happens, and by adjusting the grainsize the fluvial input of sediment starved rivers to reflect how coarser sediments settle out of the flow more quickly in reservoirs.

4.5 Conclusion

From the above study it can be seen that in nearly all cases (under the conditions used in this study), the extreme sediment starvation modelled here has a much larger negative effect on deltas than sea level rise, especially in the cases of delta top elevation and land area. Sediment starvation dramatically reduces delta growth, and significantly reduces the mobility of channels, whereas sea level

rise only marginally reduces delta land area and has no significant effect on channel mobility.

Deltas formed over hard substrates (e.g., consolidated mud/glacial till) experience dramatic channel widening, and an increase in the proportion of the delta top occupied by channels, as a result of sediment starvation. This could expose surrounding land or settlements to bank erosion at a much faster rate than would be expected in deltas forming over softer sediment. Deltas forming over more erodible substrates also experience less reduction of channel mobility in the face of sediment starvation, potentially meaning that morphodynamic processes can be continued in these systems by reworking of already deposited delta tops.

Overall, this study shows the importance of considering receiving basin sediment properties, especially in the context of contemporary anthropogenic stresses to deltas such as relative sea level rise and sediment supply reduction. Delta sediment type cannot be considered as a single parameter in determining delta morphodynamics, and instead supplied, delta top and substrate sediment should all be considered separately. The inclusion of this new morphological forcing will give numerical, physical and conceptual delta models more explanatory power to analyse the formation of stratigraphic delta deposits and predict the future behaviour of deltas adapting to the Anthropocene.

4.6 References

Bhuiyan, M. J. A. N. and Dutta, D. (2012) 'Assessing impacts of sea level rise on river salinity in the Gorai river network, Bangladesh', *Estuarine, Coastal and Shelf Science*, Elsevier Ltd, vol. 96, no. 1, pp. 219–227 [Online]. DOI: 10.1016/j.ecss.2011.11.005.

Black, K., Paterson, D. M., Tolhurst, T. J. and Hagerthey, S. E. (2002) 'Working with Natural Cohesive Sediments', *Journal of Hydraulic Engineering*, vol. 128, pp. 2–8 [Online]. DOI: 10.1061/(ASCE)0733-9429(2002)128.

Burpee, A. P., Slingerland, R. L., Edmonds, D. A., Parsons, D. R., Best, J. L., Cederberg, J., McGuffin, A., Caldwell, R. L., Nijhuis, A. and Royce, J. (2015) 'Grain-Size Controls On the Morphology and Internal Geometry of River-Dominated Deltas', *Journal of Sedimentary Research*, vol. 85, no. 6, pp. 699–714 [Online]. DOI: 10.2110/jsr.2015.39.

Caldwell, R. L. and Edmonds, D. A. (2014) 'The effects of sediment properties on deltaic processes and morphologies: A numerical modeling study', *Journal of Geophysical Research: Earth Surface*, vol. 119, no. 5, pp. 961–982 [Online]. DOI: 10.1002/2013JF002965.

Dunn, F. E., Darby, S. E., Nicholls, R. J., Cohen, S., Zarfl, C. and Fekete, B. M. (2019) 'Projections of declining fluvial sediment delivery to major deltas worldwide in response to climate change and anthropogenic stress', *Environmental Research Letters*, vol. 14, no. 8 [Online]. DOI: 10.1088/1748-9326/ab304e.

Edmonds, D. A. and Slingerland, R. L. (2010) 'Significant effect of sediment cohesion on delta morphology', *Nature Geoscience*, vol. 3, no. 2, pp. 105–109 [Online]. DOI: 10.1038/ngeo730.

Erban, L. E., Gorelick, S. M. and Zebker, H. A. (2014) 'Groundwater extraction, land subsidence, and sea-level rise in the Mekong Delta, Vietnam', *Environmental Research Letters*, IOP Publishing, vol. 9, no. 8 [Online]. DOI: 10.1088/1748-9326/9/8/084010.

Ericson, J. P., Vörösmarty, C. J., Dingman, S. L., Ward, L. G. and Meybeck, M. (2006) 'Effective sea-level rise and deltas: Causes of change and human dimension implications', *Global and Planetary Change*, vol. 50, no. 1–2, pp. 63–82 [Online]. DOI: 10.1016/j.gloplacha.2005.07.004.

Eslami, S., Hoekstra, P., Minderhoud, P. S. J., Trung, N. N., Hoch, J. M., Sutanudjaja, E. H., Dung, D. D., Tho, T. Q., Voepel, H. E., Woillez, M.-N. and van der Vegt, M. (2021) 'Projections of salt intrusion in a mega-delta under climatic and anthropogenic stressors', *Communications Earth & Environment*, Springer US, vol. 2, no. 1, pp. 1–12 [Online]. DOI: 10.1038/s43247-021-00208-5.

Ferguson, R. (1987) 'Hydraulic and Sedimentery controlls of Channel Pattern', in Richards, K. (ed), *River Channels: Environment and Process*, Oxford, Blackwell, pp. 129–158.

Fola, M. E. and Rennie, C. D. (2010) 'Downstream Hydraulic Geometry of Clay-Dominated Cohesive Bed Rivers', *Journal of Hydraulic Engineering*, vol. 136, no. 8, pp. 524–527 [Online]. DOI: 10.1061/(ASCE)HY.1943-7900.0000199.

Hackney, C. R., Darby, S. E., Parsons, D. R., Leyland, J., Best, J. L., Aalto, R., Nicholas, A. P. and Houseago, R. C. (2020) 'River bank instability from unsustainable sand mining in the lower Mekong River', *Nature Sustainibility*, vol., no.

Hanebuth, T. J. J., Proske, U., Saito, Y., Nguyen, V. L. and Ta, T. K. O. (2012) 'Early growth stage of a large delta - Transformation from estuarine-platform to deltaic-progradational conditions (the northeastern Mekong River Delta, Vietnam)', *Sedimentary Geology*, Elsevier B.V., vol. 261–262, pp. 108–119 [Online]. DOI: 10.1016/j.sedgeo.2012.03.014.

Herzka, S. Z., Mellink, E., Talley, D. M., Huxel, G. R. and Dayton, P. K. (2013) 'Stable isotope ratios of egg albumen of three waterbird species nesting in the Colorado River Delta indicate differences in foraging ground and isotopic niche breadth', *Aquatic Conservation: Marine and Freshwater Ecosystems*, vol. 23, no. 4, pp. 546–563 [Online]. DOI: 10.1002/aqc.2326.

IPCC (2013) *Summary for Policymakers:*, *Climate Change 2013: The Physical Science Basis. Contribution of Working Group I to the Fifth Assessment Report of the Intergovernmental Panel on Climate Change*, Cambridge University Press, Cambridge, United Kingdom and New York, NY, USA. [Online]. DOI: 10.1260/095830507781076194.

Jamieson, E. C., Ruta, M. A., Rennie, C. D. and Townsend, R. D. (2013) 'Monitoring stream barb performance in a semi-alluvial meandering channel: Flow field dynamics and morphology', *Ecohydrology*, vol. 6, no. 4, pp. 611–626 [Online]. DOI: 10.1002/eco.1370.

Jisan, M. A., Bao, S. and Pietrafesa, L. J. (2018) 'Ensemble projection of the sea level rise impact on storm surge and inundation at the coast of Bangladesh', *Natural Hazards and Earth System Sciences*, vol. 18, no. 1, pp. 351–364 [Online]. DOI: 10.5194/nhess-18-351-2018.

Joensuu, M., Pilditch, C. A., Harris, R., Hietanen, S., Pettersson, H. and Norkko, A. (2018) 'Sediment properties, biota, and local habitat structure explain variation in the erodibility of coastal sediments', *Limnology and Oceanography*, vol. 63, no. 1, pp. 173–186 [Online]. DOI: 10.1002/lno.10622.

Kim, W., Mohrig, D., Twilley, R., Paola, C. and Parker, G. (2009) 'Is it feasible to build new land in the Mississippi River Delta?', *Eos*, vol. 90, no. 42, pp. 373–384.

Kondolf, G. M., Rubin, Z. K. and Minear, J. T. (2014) 'Dams on the Mekong: Cumulative sediment starvation', *Water Resources Research*, vol. 50, no. 6, pp. 5158–5169 [Online]. DOI: 10.1002/2013WR014651.

Krone, R. B. (1999) 'Effects of Bed Structure on Erosion of Cohesive Sediments', *Journal of Hydraulic Engineering*, vol. 125, pp. 1297–1301.

Liu, J. P., DeMaster, D. J., Nittrouer, C. A., Eidam, E. F. and Nguyen, T. T. (2017) 'A seismic study of the Mekong subaqueous delta: Proximal versus distal sediment accumulation', *Continental Shelf Research*, Elsevier Ltd, vol. 147, no. July, pp. 197–212 [Online]. DOI: 10.1016/j.csr.2017.07.009.

Liu, Yilin, Huang, H., Liu, Yanxia and Bi, H. (2016) 'Linking land subsidence over the Yellow River delta, China, to hydrocarbon exploitation using multi-temporal InSAR', *Natural Hazards*, Springer Netherlands, vol. 84, no. 1, pp. 271–291 [Online]. DOI: 10.1007/s11069-016-

2427-5.

Manh, N. Van, Dung, N. V., Hung, N. N., Kummu, M., Merz, B. and Apel, H. (2015) 'Future sediment dynamics in the Mekong Delta floodplains: Impacts of hydropower development, climate change and sea level rise', *Global and Planetary Change*, Elsevier B.V., vol. 127, pp. 22–33 [Online]. DOI: 10.1016/j.gloplacha.2015.01.001.

Minderhoud, P. S. J., Erkens, G., Pham, V. H., Bui, V. T., Erban, L. E., Kooi, H. and Stouthamer, E. (2017) 'Impacts of 25 years of groundwater extraction on subsidence in the Mekong delta, Vietnam', *Environmental Research Letters*, vol. 12 [Online]. DOI: 10.1088/1748-9326/aa7146.

Morton, R. A., Bernier, J. C. and Barras, J. A. (2006) 'Evidence of regional subsidence and associated interior wetland loss induced by hydrocarbon production, Gulf Coast region, USA', *Environmental Geology*, vol. 50, no. 2, pp. 261–274 [Online]. DOI: 10.1007/s00254-006-0207-3.

Morton, R. A., Buster, N. A. and Krohn, M. D. (2002) 'Subsurface Controls on Historical Subsidence Rates and Associated Wetland Loss in Southcentral Louisiana', *Transactions Gulf Coast Association of Geological Societies*, vol. 52, pp. 767–778.

Neumann, J. E., Emanuel, K. A., Ravela, S., Ludwig, L. C. and Verly, C. (2015) 'Risks of coastal storm surge and the effect of sea level rise in the Red River delta, Vietnam', *Sustainability (Switzerland)*, vol. 7, no. 6, pp. 6553–6572 [Online]. DOI: 10.3390/su7066553.

Nienhuis, J. H. and van de Wal, R. S. W. (2021) 'Projections of Global Delta Land Loss From Sea-Level Rise in the 21st Century', *Geophysical Research Letters*, vol. 48, no. 14, pp. 1–9 [Online]. DOI: 10.1029/2021GL093368.

Orton, G. J. and Reading, H. G. (1993) 'Variability of deltaic processes in terms of sediment supply, with particular emphasis on grain size.', *Sedimentology*, vol. 40, pp. 475–512.

Paola, C., Straub, K., Mohrig, D. and Reinhardt, L. (2009) 'The "unreasonable effectiveness" of stratigraphic and geomorphic experiments', *Earth-Science Reviews*, Elsevier B.V., vol. 97, no. 1–4, pp. 1–43 [Online]. DOI: 10.1016/j.earscirev.2009.05.003.

Piliouras, A., Kim, W. and Carlson, B. (2017) 'Balancing Aggradation and Progradation on a Vegetated Delta: The Importance of Fluctuating Discharge in Depositional Systems', *Journal of Geophysical Research: Earth Surface*, vol. 122, no. 10, pp. 1882–1900 [Online]. DOI: 10.1002/2017JF004378.

Sanchez-Arcilla, A., Jimenez, J. A. and Valdemoro, H. I. (1998) 'The Ebro delta: Morphodynamics and vulnerability', *Journal of Coastal Research*, vol. 14, no. 3, pp. 754–772.

Schmitt, R. J. P., Bizzi, S., Castelletti, A., Opperman, J. J. and Kondolf, G. M. (2019) 'Planning dam portfolios for low sediment trapping shows limits for sustainable hydropower in the Mekong', *Science Advances*, vol. 5, pp. 1–12 [Online]. Available at https://www.science.org/doi/epdf/10.1126/sciadv.aaw2175.

Shaw, J. B. and Mohrig, D. (2014) 'The importance of erosion in distributary channel

network growth, Wax Lake Delta, Louisiana, USA', *Geology*, vol. 42, no. 1, pp. 31–34 [Online]. DOI: 10.1130/G34751.1.

Syvitski, J. P. M., Kettner, A. J., Overeem, I., Hutton, E. W. H., Hannon, M. T., Brakenridge, G. R., Day, J. W., Vörösmarty, C. J., Saito, Y., Giosan, L. and Nicholls, R. J. (2009) 'Sinking deltas due to human activities', *Nature Geoscience*, vol. 2, no. 10, pp. 681–686 [Online]. DOI: 10.1038/ngeo629.

Syvitski, J. P. M. and Saito, Y. (2007) 'Morphodynamics of deltas under the influence of humans', *Global and Planetary Change*, vol. 57, no. 3–4, pp. 261–282 [Online]. DOI: 10.1016/j.gloplacha.2006.12.001.

Syvitski, J. P. M., Vörösmarty, C. J., Kettner, A. J. and Green, P. (2005) 'Impact of Humans on the Flux of Terrestrial Sediment to the Global Coastal Ocean', *Science*, vol. 308, no. 5720, pp. 376–380 [Online]. DOI: 10.1126/science.1109454.

Ta, T. K. O., Nguyen, V. L., Tateishi, M., Kobayashi, I., Saito, Y. and Nakamura, T. (2002) 'Sediment facies and Late Holocene progradation of the Mekong River Delta in Bentre Province , southern Vietnam : An example of ... Sediment facies and Late Holocene progradation of the Mekong River Delta in Bentre Province , southern Vietnam : an example', *Sedimentary Geology*, vol. 152, no. February 2017, pp. 313–325.

Tan, X. L., Zhang, G. P., Yin, H., Reed, A. H. and Furukawa, Y. (2012) 'Characterization of particle size and settling velocity of cohesive sediments affected by a neutral exopolymer', *International Journal of Sediment Research*, International Research and Training Centre on Erosion and Sedimentation and the World Association for Sedimentation and Erosion Research, vol. 27, no. 4, pp. 473–485 [Online]. DOI: 10.1016/S1001-6279(13)60006-2.

Vasilopoulos, G., Quan, Q. L., Parsons, D. R., Darby, S. E., Tri, V. P. D., Hung, N. N., Haigh, I. D., Voepel, H. E., Nicholas, A. P. and Aalto, R. (2021) 'Establishing sustainable sediment budgets is critical for climate-resilient mega-deltas', *Environmental Research Letters*, vol. 16, no. 6 [Online]. DOI: 10.1088/1748-9326/ac06fc.

Vörösmarty, C. J., Meybeck, M., Fekete, B. M., Sharma, K., Green, P. and Syvitski, J. P. M. (2003) 'Anthropogenic sediment retention : major global impact from registered river impoundments', vol. 39, pp. 169–190 [Online]. DOI: 10.1016/S0921-8181(03)00023-7.

Waltham, T. (2002) 'Sinking cities', *Geology Today*, vol. 18, no. 3, pp. 95–100 [Online]. DOI: 10.1046/j.1365-2451.2002.00341.x.

Warner, K. (2010) 'Global environmental change and migration: Governance challenges', *Global Environmental Change*, Elsevier Ltd, vol. 20, no. 3, pp. 402–413 [Online]. DOI: 10.1016/j.gloenvcha.2009.12.001.

Zhang, H., Chen, X. and Luo, Y. (2016) 'An overview of ecohydrology of the Yellow River delta wetland', *Ecohydrology and Hydrobiology*, European Regional Centre for Ecohydrology of Polish Academy of Sciences, vol. 16, no. 1, pp. 39–44 [Online]. DOI: 10.1016/j.ecohyd.2015.10.001.

5 Channel incision and interaction with erosion-resistant delta substrates

5.1 Introduction

Previous chapters have used numerical modelling to investigate how deltas interact with their substrate (See Chapters 3 & 4). Both chapters showed that a more erosion resistant substrate led to shallower channels with larger width:depth ratios, and indicated that deltas forming over substrates made mostly of low τ_{ce}, fine sediment had less mobile channels, whereas those with predominantly sand substrates had more mobile channels. The objective of this chapter is to investigate how the channels within a prototype delta (namely Wax Lake Delta), form over a stiff consolidated clay (estimated to be predominantly fine, mid-high τ_{ce}) substrate through assessing the detailed flow and morphodynamics throughout the delta in a set of field studies spanning over a decade, combined with investigations of longer-term dynamics.

In the previous chapters, it was shown that delta morphodynamics are controlled by the interaction of channel beds with basin substrates, and how this influences channel depth. To investigate this, this chapter uses bathymetric data to quantify substrate erosion since delta formation began and investigate the nature of the channel-substrate interface. Multibeam echosounders (MBES) are capable of collecting the sub-meter resolution bathymetry that is necessary for resolving smaller bedforms in three dimensions, and have been used in previous

studies to image submerged bed morphology in large rivers (Parsons et al., 2005), river mouths (Czuba et al., 2011) and delta channels (Hackney et al., 2020). MBES can also collect acoustic backscatter data that can be processed to infer the bed substrate properties, such as bed roughness and material. This chapter uses MBES bathymetry and backscatter to investigate the erosion in to-, and sediment morphodynamics at channel beds that interact with the basin substrate.

Bifurcations have been shown to be critical in determining delta morphodynamics (Edmonds et al., 2011), so this chapter will analyse the dynamics and stability of bifurcations formed over erosion-resistant substrate. Many studies (Edmonds and Slingerland, 2008; Bolla Pittaluga et al., 2003) define bifurcation equilibrium - where water and sediment are split in ratios such that both distributaries are neither aggrading due to excess sediment supply, nor eroding due to deficient sediment supply – as being necessary for bifurcation stability. If bifurcations are not in this equilibrium, the sediment deficient channel would erode and so increase its capacity, while the sediment rich channel would deposit sediment and so slow the flow through it, which would eventually lead to it shutting off and all flow being routed down the dominant channel. As such, stability is defined in terms of a bifurcations ability to return to this equilibrium configuration when exposed to small perturbations (Edmonds and Slingerland, 2008). Salter et al. (2017), expanded on this, showing that consideration of the downstream sink conditions (lengthening and aggradation if the dominant channel) can act as a restoring force, meaning that bifurcations that are not strictly

in equilibrium, could still be in an oscillating-stable condition in which dominance switches between the two distributaries.

Bifurcation instability is driven partially by a feedback in which the dominant channel erodes, and so increases its capacity to transport sediment and water (Kleinhans et al., 2013). As such the erodibility of the bed, and hence the ability of the bifurcation flows to erode downwards would be expected to influence bifurcations stability (bifurcation channels with immobile bed sediment have been found to increase stability; Kleinhans *et al.*, 2008) but few studies have assessed this in detail in the field. Edmonds and Slingerland (2008) used three equilibrium functions of Q_r (the ratio of discharges between bifurcation distributaries) and Θ, (the nondimenstional Shields stress) to explore the stability of bifurcations on deltas forming with fine cohesive sediment supply. This chapter characterises delta bifurcations using Q_r and Θ, with the aim of investigating if delta substrates affect the stability of bifurcations.

Additionally, this study utilises analysis of bedforms and bed morphology to investigate how the WLD interacts with its channel beds, and hance the substrate that underlies it. The type of bedform on present can indicate how much bed load is carried by a channel, and whether the flow is predominantly depositional or erosional. Large, continuous dunes indicate high sediment load (Mazumder, 2003), whereas barchan dunes (individual crescent-shaped bedforms separated by bare bedrock) are known to indicate sediment scarcity (Andreotti et al., 2002).

Bare bedrock channel beds and erosional flutes indicate very low sediment load and bed erosion.

5.1.1 *Wax Lake Delta*

The Wax Lake Delta, Louisiana, USA, is a recently formed delta, prograding into Atchafalaya Bay in the Gulf of Mexico. It is formed in the low energy, microtidal Atchafalaya Bay (mean wave height ≈0.5m, mean tidal range ≈0.35 m), at the mouth of the Wax Lake outlet (WLO) (Figure 5-1). The WLO is a flood-alleviation channel cut between 1938 and 1941 from Grand Lake-Six Mile Lake on the Atchafalaya River to Atchafalaya Bay (Fisk, 1952) to re-route flood flows directly into the Gulf of Mexico in order to reduce flood risk in Morgan City (Nickles and Pokrefke, 1967), which is located on the Atchafalaya river around 25km downstream of where the WLO diverges from the main channel (Figure 5-1*b*).

Between 1917 and 1975, sediment filled the Atchafalaya basin and Grand Lake-Six Mile Lake upstream of the WLO. The deposition of sands here meant that only fine sediment reached the mouth of the outlet (Shaw et al., 2013), and so delta deposition was slow. Significant amounts of sand only reached the outlet mouth when Grand Lake had filled with sediment, and so subaerial delta formation began around 1973 (Shaw et al., 2016), and progressed at a rate of c.1km^2 year^{-1} (Allen et al., 2012). Sediment continued to fill Wax Lake between 1972 and the present day (Figure 5-1 *c*-*e*).

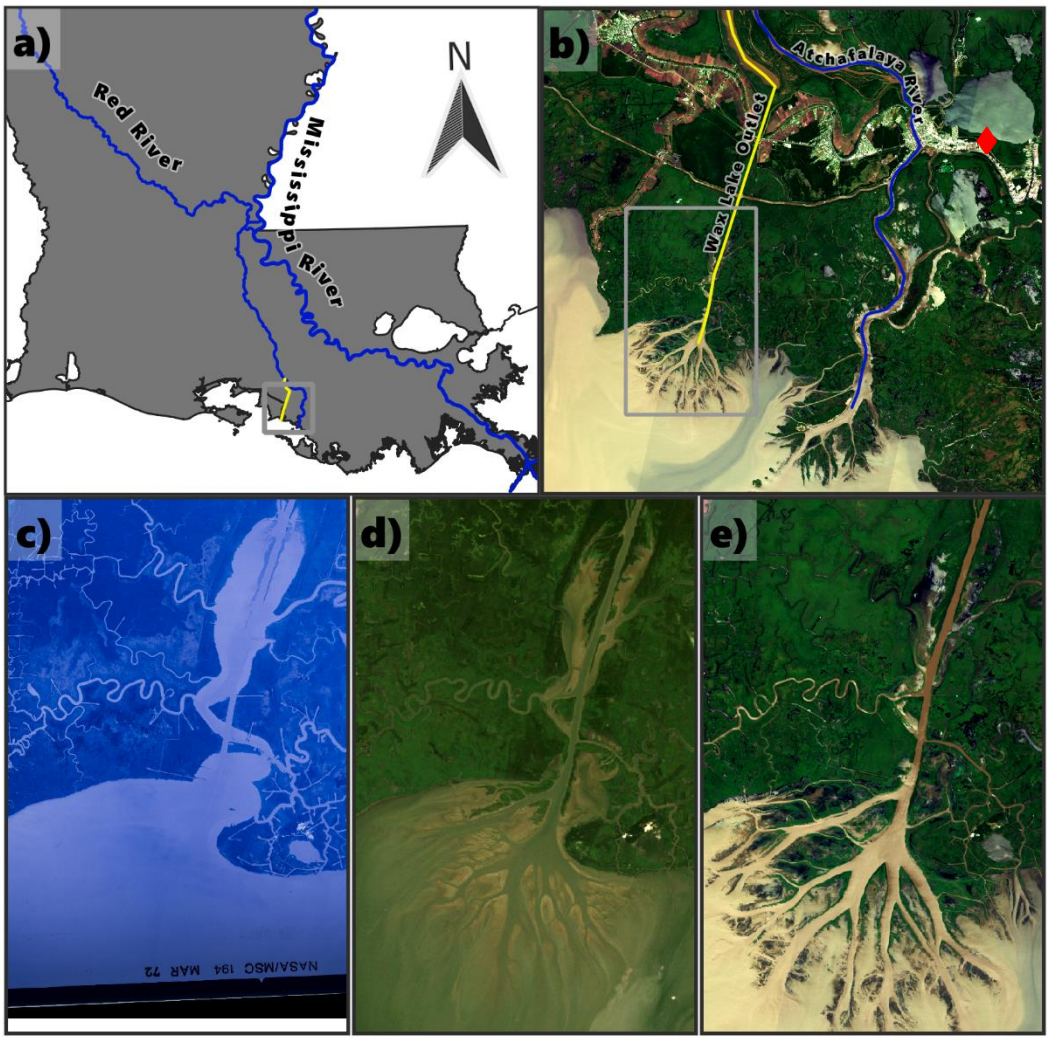

Figure 5-1: Overview of the Wax Lake Outlet and Delta. a) The route of the Mississippi, Atchafalaya and Red Rivers through Louisiana (grey), USA, with the WLO highlighted in yellow. b) Satellite imagery of the lower Atchafalaya system, and the Wax Lake and Atchafalaya Deltas. (Location of Morgan City marked with a red diamond.) c) Aerial imagery of Wax Lake and the WLO on 17/03/1972, prior to delta initiation (Aerial Imagery from USGS Earth Explorer) d) Satellite imagery of Wax Lake Outlet and Delta on 25/08/1986 (Satellite imagery from bands 1-3 of Landsat 5, accessed through USGS Earth Explorer) e) Satellite imagery of Wax Lake Outlet and Delta on 30/04/2020 (Satellite imagery from Sentinel-2)

The current Wax Lake Delta (WLD) consists of primary channels that radiate out from the delta apex channels, as well as multiple smaller channels that branch from primary channels at angles close to 90°, and provide routes for flow on to

island interiors or between primary channels (Shaw et al., 2013). The islands between these channels consist of a subaerial island edge colonised by black willow trees (*Salix nigra*) surrounding a lower intertidal interior covered with underwater or floating vegetation (Olliver and Edmonds, 2017). It had built 100km^2 of subaerial land by 2005 (Kim et al., 2009).

The area around the current location of the WLD has been studied since well before the formation of the delta itself, with initial studies focusing on the viability of building the WLO as part of wider river engineering and diversions on the Mississippi (Fisk, 1952). Subsequent investigations studied the deposition of sediment in the Atchafalaya bay, and the eventual formation of both the Atchafalaya and Wax Lake deltas (Shlemon, 1975; Rouse et al., 1973).

The Wax Lake Delta is a useful example delta for two reasons. First, its whole evolution is within recent history. This, combined with it being part of the drainage system of a major river, has caused its growth to be is well documented from its inception. Secondly, it is one of very few area where new land is being deposited along the Louisiana coast, which has otherwise lost 4833 km^2 of land between 1932 and 2016 (Couvillion et al., 2016) to subsidence and rapid coastal erosion (Morton et al., 2006). These factors make it a good analogue for studying both the early formation and progradation of new deltas, and how land loss in on the Gulf of Mexico coast, and in similar environments, may be slowed or reversed.

Importantly for this study, the Wax Lake delta formed over a basin bathymetry that was recorded by a 1934-5 hydrographic survey (Shaw et al.,

2013). While the consistency of the Atchafalaya Bay bed substrate is not well constrained, the WLD has been found to overlay sediment which is in part made of "tough oxidised Pleistocene clay" (Fisk, 1952. pp. 85). The analysis of Bryant and Trabant, (1972), reported offshore sediments of the Texas-Louisiana Gulf of Mexico to have a vane shear stress of 130 psf (~6.2 kN m^2) at the sea bed, increasing to 200 psf (~9.6 kN m^2) at 5 m. Geological maps suggest that that whole Atchafalaya system in underlain at some depth by the Pleistocene Prairie group (Heinrich et al., 2012), which has been subject to "tens of thousands of years of consolidation, desiccation, oxidation, and erosion" (Kolb and Van Lopik, 1958. pp. 11) and so is likely the "tough oxidised Pleistocene clay" referred to by Fisk (1952). These maps also suggest that sediment of the Teche and Maringouin Mississippi delta lobes are deposited somewhere in between the Prairie group and the modern Atchafalaya-WLD deposit (Heinrich et al., 2012). Though this thesis demonstrates the importance of delta substrate properties for predicting delta behaviour, no exact geotechnical analysis of the sediment underlying the WLD could be found, highlighting the need for future fieldwork to quantify delta substrates.

While not as hard as bedrock found in upland channels, Shaw et al. (2013) argue that the sediment underlying the WLD still behaves as bedrock due to being a distinct, pre-existing sediment to that transported in to the delta, and having many erosional bedforms on its surface. As field studies acknowledging the role of resistant delta substrates and evaluating their role in the determining the morphodynamics are rare, this study seeks to use the WLD as an example to explore how delta interaction with erosion resistant substrates influences channel erosion and deposition, bed level change and bifurcation stability. In light of the

findings from the previous two chapters, Chapter five also seeks to assess the implications of modelling results in Chapters 3 and 4 for real-world systems, by investigating the morphology of a real world delta that is evolving over a resistant substrate with a potentially low sediment input. As such, this chapter utilises fieldwork on the WLD to investigate:

1- How the subaqueous bed elevation of the Wax Lake Delta has changed since its inception, through either erosion of deposition of sediments in channels.
2- How the Wax Lake Delta was interacting with its substrate in 2020, using analysis of the bed morphology to infer erosion or deposition.
3- What the ratios of discharge, sediment transport and channel geometry in delta distributaries reveal about the stability of bifurcations on the delta.

5.2 Methodology

To answer the above research questions, bathymetry, velocimetry and backscatter data from three field campaigns (conducted in the WLD in 2009, 2018 and 2020) was integrated with a suite of historical data.

5.2.1 *Field Data Collection – Wax Lake Delta 2020*

The 2020 survey was performed between the 1st and 7th of March 2020, and covered areas of the delta close to the apex, and in the upper reaches of Main pass to line up with the existing 2009 data (*Figure 5-2a*). During the survey, the discharge of the WLO, measured upstream at Calumet (USGS gauging station LA

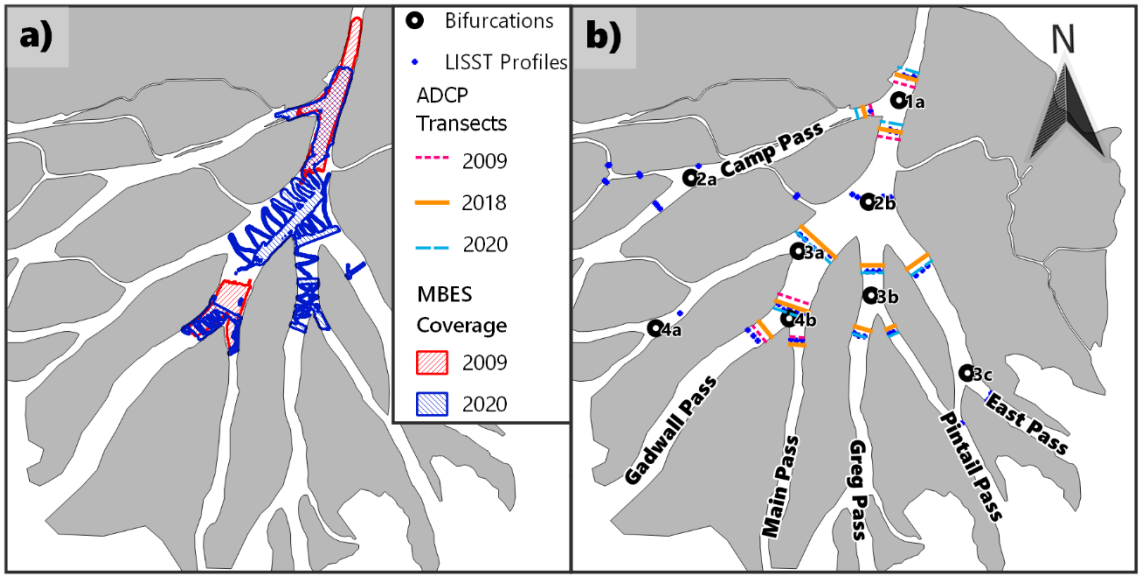

Figure 5-2: Survey locations for the WLD field studies. a) Coverage of multibeam echosounder bathymetry for 2020 and 2009 surveys. b) Locations of diffluences (indicated as number letter combinations, e.g. 2a) targeted in the studies(indicated as number letter combinations, e.g. 2a), laser in-situ scattering and transmissometry (LISST) profiles and acoustic Doppler current profiler transects performed. Other transects where taken during the three surveys, but the shown transects where those that had sufficient coverage across multiple surveys to allow them to be used for the bifurcation analises.

– 07381590, N 29.697°, W91.372°), was 6,392 m^3s^{-1}, close to the peak flow for that year, and exceeding the peak flow seen in many years before then, (see *Figure 5-3*). The bathymetric survey used a Norbit iWMBSh multibeam echosounder (MBES) deployed from a small survey vessel, the *RV Blue Runner,* which recorded both depth soundings and backscatter intensity. This survey vessel also carried a 1200kHz Teledyne Rio Grande acoustic Doppler current profiler (ADCP) to measure flow velocity and suspended sediment concentration, and an Emlid Reach RS2 real-time kinematic differential global positioning system (RTK dGPS) that was used to provide position data for the MBES and ADCP, with both

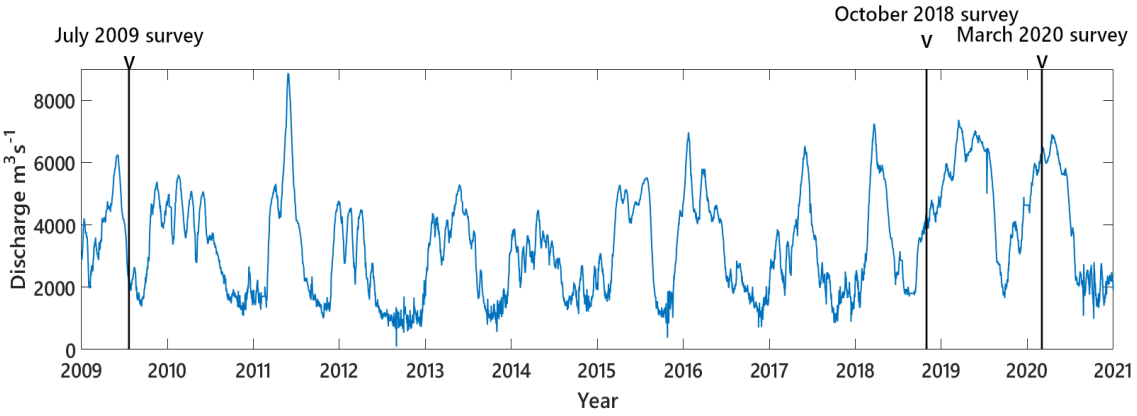

Figure 5-3: Hydrograph of WLO discharge measured at Calumet (N 29.69798645°, W91.3728855°) between 1/1/2009 and 1/1/2020. Note the the longer period of hight flow seen between late 2018 and 2019.

horizontal and vertical accuracies <0.01m while surveying.

The MBES was set to release a frequency modulated pulse with a centre frequency of 400 kHz and a bandwidth of 80 kHz, resulting in each "ping" sweeping from 360 kHz to 440 kHz over 500µs. This frequency was chosen as it gave the best resolution where water depth was shallow, as much of the survey area was (all areas of the survey had a depth <30m, and over much of the survey the depth was <5m). The returning signal was formed by the MBES in to 512

beams, angled such that the returning points where spaces equidistantly over the bed.

The MBES had an across-line resolution of 0.9° (meaning the actual resolution $= 2 \times \text{depth} \times \tan\left(\frac{0.9}{2}\right)$ ≈0.047m at 3 metres depth or ≈0.44m at 28 metres). The system software integrated bottom detection data from the sonar with sound velocity data from a sound velocity probe and three axis orientation data (pitch, roll and yaw) from an inertial motion sensor, both of which are fixed to the sonar head to eliminate offset related errors. Survey swaths were overlapped by 30-50% to ensure coverage and accuracy at the swath fringes.

At regular intervals during the survey, a Norbit 24014-1 WBMS SV Profiler was deployed from the boat to take a profile of sound velocity throughout the whole water column, which could then be used to correct the MBES survey depths.

The ADCP was deployed at 9 transects across the channel, representing the inputs and outlets of 4 bifurcations on the delta (bifurcations 1a, 2b, 3a and 3b). Repeat transects (at least four) were conducted at all locations in order to resolve time-averaged secondary flow characteristics (Vermeulen et al., 2014). ADCP data was collected in Teledyne RD Instruments WinRiver II. This was done to understand how each of these bifurcations was splitting water and sediment discharge between the limbs.

The 2020 field campaign was organised substantially by C.R. Hackney, who also led the deployment of the aDcp. The survey boat was driven by C. Broaddus, of Indianna State University, who also assisted in the deployment of all survey

instruments. The author led the deployment of the MBES. Day-to-day completion of the fieldwork was performed cooperatively by the whole crew. Processing of the aDcp data was completed by C.R. Hackney. MBES processing, and secondary processing and analysis of aDcp data was done by the author, with guidance from C.R. Hackney. This fieldwork was supported by Newcastle University and Indianna State University, and funded by C.R. Hackney's Royal Society International Exchanges Grant (IES\R2\170218).

5.2.2 *Field Data Collection – Wax Lake Delta 2018*

The 2018 survey was conducted between the 29th of October and the 2nd of November, during which time the WLO's discharge was 4,166 m^3s^{-1}. While this was unusually high for the time of year (185% of the 2009-2020 average for that period) it is below the 75th percentile for discharge between 2009 and 2020, and so constitutes only moderate-high flow conditions. The survey consisted of the deployment of the same Teledyne RD Instruments 1200 kHz Rio Grande ADCP as the 2020 surveys for consistency. The ADCP was deployed across 23 transects of the delta channels, which constituted the upstream and downstream boundaries of 8 bifurcations, though only 3 of these matched with sites also surveyed in either the 2009 or 2020 study. The raw data was collected in Teledyne RD Instruments WinRiver II.

A Sequoia LISST-100X, submersible laser diffraction particle analyser was deployed alongside the ADCP at selected transects, to provide the necessary sediment concentration data needed for the ADCP backscatter data to be translated to suspended sediment concentration. The LISST (Laser In-Situ Scattering and Transmissometery) functions by shining a collimated laser through

a known volume of water. Sediment within that water scatters the laser; larger particles scatter it through smaller angles, where smaller particles through larger angles (Agrawal and Pottsmith, 2000). A set of 32 concentric detector rings measure the scattered laser power. Each ring detector measures the light scattered from one of 32 defined log-spaced grain size classes. The distribution of laser power hitting each of the rings and the overall power reaching the sensor is used to calculate sediment grainsize distribution. The power distribution across the detector rings is converted mathematically to an area distribution of particles within the water volume tested by the LISST, which is then converted to a volume for each detector ring (hence grain size bin) by multiplying the area by the median grain diameter of that bin (Agrawal and Pottsmith, 2000).

The LISST recorded constantly while it was lowered slowly from a stationary boat down to the bed, then withdrawn back to the boat. This created sediment concentration-depth profiles that could be compared to ADCP data to convert acoustic backscatter in to sediment concentration.Additionally, five bed samples were taken using a van Veen grab sampler cast from the survey boat while stationary. In some cases, the bed was too hard for the grab to cut deeply into it, but smaller sediment samples were still retrieved by collecting the material that had been scraped off the bottom when the grab landed.

The 2018 field campaign was organised substantially by C.R. Hackney, and D. Edmonds of Indianna State University. E. Oliver (also of Indianna State University) assisted in the deployment of all survey instruments, as well as driving the boat alongside D. Edmonds. The author assisted with aDcp deployment and led the use of the van Veen grab sampler. Day-to-day completion of the fieldwork

was done cooperatively by the whole crew. Processing of the aDcp data was completed by C.R. Hackney, while secondary processing and analysis of aDcp data was done by the author, with guidance from C.R. Hackney. This fieldwork was supported by Indianna State University, and funded by C.R. Hackney's Royal Society International Exchanges Grant (IES\R2\170218).

5.2.3 *Existing Field Data – Wax Lake Delta 2009*

Unpublished data from a 2009 field survey was also used in this study. This data was provided by D.R. Parsons, and originally collected by Parsons, Edmonds and Best. The mean flow over the time of the 2009 survey was 2,197 m^3s^{-1}. The survey was conducted using the survey vessel *R/V Bimini,* which was used to deploy a RESON SeaBat 7125 400kHz MBES. The vessel was also equipped with a Leica 1230 RTK dGPS (horizontal accuracy 0.02m and vertical accuracy 0.02m) to provide position data, a RESON SVP71 sound velocity probe to provide surface sound velocity and a TSS MAHRS gyro-motion sensor to provide three-dimensional, role-pitch-yaw orientation data. This data was integrated with the MBES depth data and recorded in the RESON PDS2000 software for processing.

Additionally, the same Teledyne RD Instruments 1200 kHz Rio Grande ADCP was used to collect flow velocity data for 10 profiles, around two bifurcations (1a and 4b). The raw data was collected in Teledyne RD Instruments WinRiver II as per the details provided for the 2022 surveys.

5.2.4 *Bed Grainsize Analysis*

Bed sediment samples from the 2018 field campaign were returned to be processed in a laboratory at the University of Hull using a Malvern Mastersizer

2000 laser diffraction particle size analyser. Each bulk sample was mixed thoroughly into a slurry with a little water to homogenize the sediments. A subsample of the bulk sample was then ultrasonically dispersed in ~1L of deionised water and fed into the particle size analyser by a Malvern Hydro 2000MU dispersion and sampling unit. Each subsample was run three times, and two of the bulk samples where sub-sampled twice to check that results where repeatable and that the samples had been homogenised sufficiently. The results were exported in to- and analysed using GRADISTATv8 (Blott and Pye, 2001).

5.2.5 *Data Processing - Bathymetry*

The raw MBES data was processed in Caris HIPS & SIPS 10.4, and all soundings where corrected for speed of sound variation through the water column using the sound velocity profiles taken during the survey. The data was adjusted for the altitude of the boat by applying tide data taken from Amerada Pass, Louisiana (*NOAA Tides & Currents, Station 8764227*) at the mouth of the Atchafalaya River, and referenced to the NAVD88 height datum in order for other bathymetry data to be easily comparable (see section 5.2.9: Other Data). All navigation, inertial motion and bottom detection data was visually cleaned to remove erroneous data points. Bathymetry was then gridded into a 0.1m resolution digital elevation model.

5.2.6 *Data Processing – Bed Backscatter*

Bed sediment backscatter intensity data was also processed in Caris HIPS & SIPS 10.4, as a way of estimating the properties of the deltas underlying sediment from its reflectiveness. The raw backscatter intensity data was combined with the

bathymetry data to account for angle-of-incidence based differences in the backscatter, and the adjusted intensity was gridded on a 0.5m raster.

To increase accuracy, a beam pattern for the sonar was generated by the CARIS HIPS &SIPS software on flat, homogenous area of the survey. While this calibration was not sufficient to give absolute backscatter intensity data accurate enough to estimate bed grain size from, a comparative approach could still be used that could give a relative value, with higher intensity (brighter) regions representing harder, more reflective bed material than lower intensity (duller) regions. In this study, it is assumed that less reflective regions are unconsolidated silts, and more reflective regions are the resistant clays that underlay the delta.

5.2.7 *Data Processing – Current profiles*

Raw data from the ADCP surveys were exported from WinRiver II in ASCII format by C.R. Hackney. Using the USGS Velocity Mapping Toolbox v4.09 (VMT; Parsons *et al.*, 2013), the ADCP ASCII files for multiple passes of the same transect were converted in to a single cross channel velocity profile for each transect, which were exported form VMT as a .mat file by the author. These .mat files were then imported into Matlab, where total discharges where calculated by multiplying the flow speed in each ADCP bin by the area of the bin to find the discharge of each bin, then summing the discharges of all bins in the transect.

5.2.8 *Data Processing – Sediment Concentration and Discharge*

To measure suspended sediment transport across a whole cross section of a delta channel, a method is needed that estimates suspended sediment concentration acoustic backscatter from ADCP transects. Szupiany *et al. (*2012)

estimated suspended sand concentration using an exponential function. However, since the average sediment grainsize was much finer in the WLD (an average D_{50} of 44.3 µm, see section 5.3.3), calibration using LISST measurements was instead used. This calibration was provided by C.R. Hackney from the 2018 field survey. This method, where the LISST sediment concentration profile data is plotted against the water column acoustic backscatter from a co-located ADCP transect, has been used previously to resolve sediment pulses over bedforms (Shugar et al., 2010). A sound pulse from an acoustic instrument reflects off sediment particles in the water column, so increasing sediment concentration increases the acoustic backscatter. Because of this, a linear relationship could be found between the sediment concentration and acoustic backscatter data which

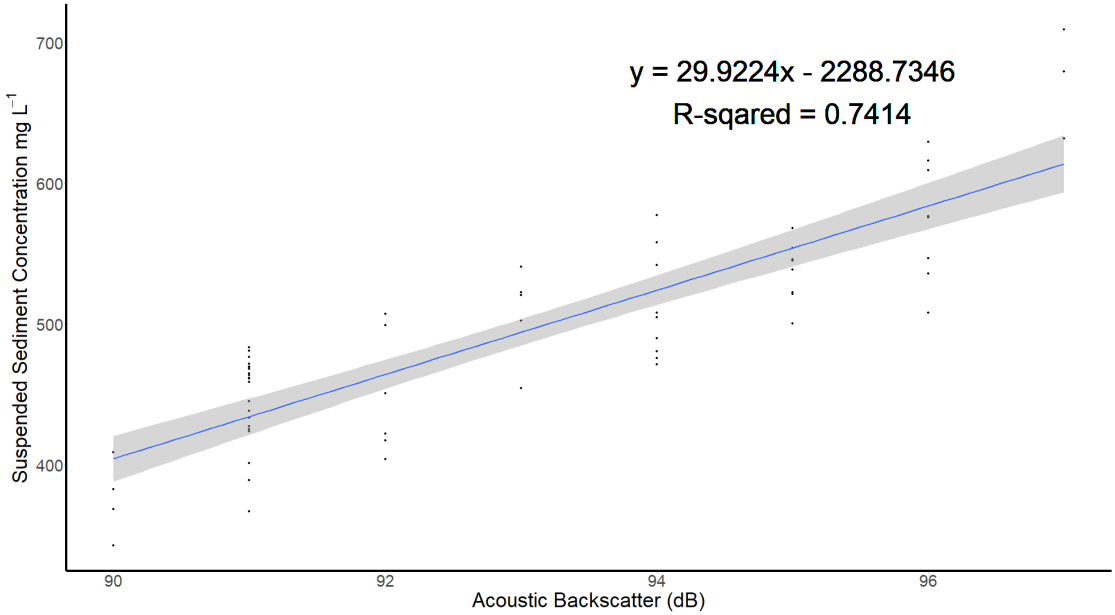

Figure 5-4: Linear relationship for calibrating ADCP acoustic backscatter with LISST suspended sediment distribution, with 95% certainty intervals shown in grey.

could be used to estimate suspended sediment concentration from ADCP backscatter *(Figure 5-4)*.

Using this relationship, the acoustic backscatter data from each transect was converted into a suspended sediment concentration profile in Matlab. This suspended sediment concentration could them be used to analyse the partitioning of sediment within a channel or multiplied by the discharge at each ADCP bin (see section 5.2.7) and summed to give total sediment discharge for that channel.

5.2.9 *Other Data*

Pre-delta bathymetry was provided by John Shaw in the form of DEM constructed from bathymetric measurements collected from 1934-1935 by the National Oceanic and Atmospheric Administration (Shaw et al., 2013). Due to its age the methods used to collect this data is unclear, and without accurate GPS positioning and depth sounding techniques it is unlikely that the vertical accuracy is better than 0.1-1m. However, as no better bathymetric data predating the delta could be found by the author, this data is used, and its potentially high uncertainty taken into account. This data was converted to the MSL_{2000} datum by Shaw, Mohrig and Whitman (2013) by applying a -0.48m adjustment for sea level change since 1935. From this it was converted to the NAVD88 datum with a -0.12m adjustment to all elevations.

Additional channel discharges for transects around bifurcations 1a, 3a and 4b were taken from Hiatt (2013), to provide extra temporal resolution for bifurcation discharge split calculations. These data were collected using a 1Hz Teledyne RD StreamPro ADCP between 20/07/2012 and 24/07/2012.

5.2.10 *Bed Level Change*

To assess how the delta had eroded or deposited sediment though its formation, digital elevation models of difference (DEMs of difference, or DEMoD) were made. This was done by first normalizing all elevation data to the same elevation datum (NAVD88, see above) and then by subtracting the elevation model of one period from that of a more recent period, giving the elevation change between those two times. This was done using QGIS 3.16.3-Hanover, for the periods 1935-2020 and 2009-2020.

Due to uncertainties about the accuracy of the elevation datum for the 2009 survey, DEMs of difference for the period 2009-2020 where instead normalized, by adjusting the mean elevation of the 2009 DEM to the same as that of the 2020 data. To do this, both DEM's were clipped to the area that they overlapped, and then the mean elevation of each of these clipped DEMs was calculated. The difference between the means was then subtracted from the clipped 2009 DEM, such that both DEMs had the same mean elevation. The DEM of difference was then made from the clipped 2020 data and the adjusted 2009 data. This method means that the absolute change between areas could not be examined, but the relative change could, which is still potentially useful for determining areas of deposition and erosion.

To be able to analyse the 1935-2020 DEM of difference more thoroughly, this study attempted to account for uncertainties within the DEMoD by calculating a minimum level of detection, LoD_{min}, for each DEM cell. This was defined as the magnitude of change above which there was 95% confidence, as calculated with a Student's t-test and the combined local standard deviation of

each of the original DEMs. This was done following a method similar to that of Milan et al. (2011), but adapted for MBES data.

Initially, for both MBES datasets, a topographic variability V_{elev} surface was created by calculating the standard deviation of a 1.5m (3x3 cell) moving window centred on each cell. Additionally, a co-located surface of point cloud error - quantified as the standard deviation error of the depth soundings around the averaged elevation – was exported from CARIS Hips & Sips. V_{elev} was binned into 0.05m classes, then for each class, the mean standard deviation of error was calculated for all elevation cells contained within that topographic variability class. This was used to plot a V_{elev} vs. standard deviation of error (SDE) graph (Figure 5-5) to which a curve was fitted. For the 2009 data, a power law equation had to be

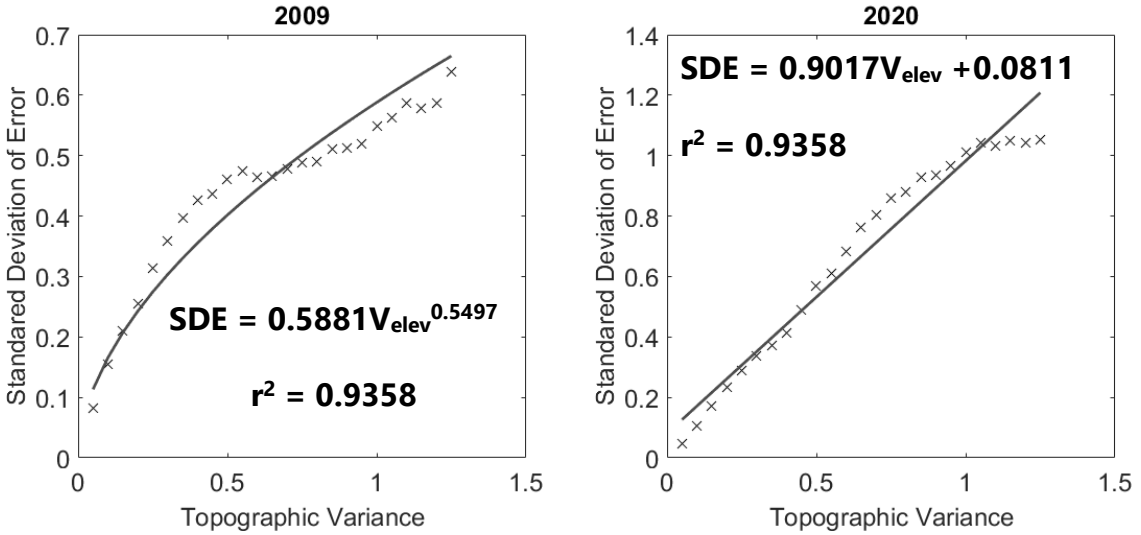

Figure 5-5: Standard deviation of error plotted against topographic variance for both the 2009 and 2020 bathymetric data, with trendlines.

used to produce a sufficiently low r^2 value (SDE = $0.5881V_{elev}^{0.5497}$; r^2 = 0.9358). A linear relation was found to be sufficient for 2020 data (SDE = $0.9017V_{elev}$ +0.0811; r^2 = 0.9599). These relationships where then applied to topographic variability surfaces, creating calculated spatial error surfaces.

From the two error surfaces, LoD_{min} was calculated from these surfaces using the equation:

$$\mathrm{LoD}_{\min} = t\sqrt{Error_{2009} + Error_{2020}} \qquad \textit{(Equation 5-1)}$$

Where t is the critical t value for a 95% confidence interval, and $Error_{2009}$ and $Error_{2020}$ are the calculated spatial error surfaces.

Finally, LoD_{min} was subtracted from the DEMoD to give an adjusted surface that shows only elevation change that was sufficiently large to indicate morphological change rather than error (to 95% confidence). As LoD_{min} was positive everywhere, but the DEMoD contained both negative and positive values, simple subtraction would not have given a satisfactory result. As such an equation that satisfies the below conditions was sought:

$$Adjusted\ dz = \begin{cases} dz - \mathrm{LoD}_{\min} & if\ dz > \mathrm{LoD}_{\min} \\ 0 & if -\mathrm{LoD}_{\min} < dz < \mathrm{LoD}_{\min} \\ dz + \mathrm{LoD}_{\min} & if\ dz < -\mathrm{LoD}_{\min} \end{cases}$$

(Equation 5-2)

To satisfy this, Eq. 5-3 was used:

$$Adjusted\ dz = dz - minimum(abs(dz), \mathrm{LoD}_{min}) * \frac{dz}{abs(dz)} \qquad \textit{(Equation 5-3)}$$

5.2.11 *Bed Characterisation*

Using both the bathymetric and backscatter intensity data from 2020, channel bedforms were characterized manually in QGIS 3.16.3-Hannover, and their locations marked with polygons. Bedforms were characterised manually, by drawing vector lines from apex to base and measuring length, or side to side and

measuring width. “Bedform continuity” was defined using acoustic backscatter data to see if sediment reflectance was continuous between bedforms (indicating bedform sediment covered the whole bed) or discontinuous between bedforms (suggesting that patches of the substrate were exposed between bedforms). After this, individual bedforms or patches of bedforms were characterised visually by bedform type (dunes or ripples, barchan dunes, scours etc.), and sediment reflectivity compared to the surrounding sediment (dull, bright). These where then grouped in to three categories; sediment rich bedforms (bedforms that are present in channels with high bedload transport, such as large, continuous flow-parallel bedforms), sediment poor bedforms (bedforms associated with low bedload transport and sediment starved channels, such as barchan dunes) and erosional bedforms (such as scours). This data could then be compared with water column backscatter and flow velocity data and interpreted in terms of the sediment morphodynamics of the delta system.

5.2.12 *Bifurcation Characterisation*

Flow velocity and sediment concentration data from sections 5.2.7 and 5.2.8 were combined to give total discharge (Q_f) and suspended sediment discharge (Q_{ss}) values for each of the transects. For each bifurcation, these values could then be used to quantify how sediment and water are split between the arms of that bifurcation with the equation (Edmonds and Slingerland, 2008) :

$$R_Q = \frac{Q_1}{Q_2} \tag{5-1}$$

Where R_Q is the discharge for the bifurcation, Q_1 and Q_2 are the discharges of the largest and smallest distributaries, respectively. A similar equation is used for suspended sediment.

$$R_S = \frac{Q_{S1}}{Q_{S2}} \tag{5-2}$$

Where R_S is the discharge for the bifurcation, Q_{S1} and Q_{S2} are the suspended sediment discharges of the largest and smallest distributaries, respectively. Unlike many other distributary systems, the WLD features a prominent three-legged trifurcation. As such, the above formulas fail as a comparison method because the middle distributary is ignores. Due to this, the above formulas are used for all other bifurcations to allow comparison with previous studies (Edmonds and Slingerland, 2008; Bolla Pittaluga et al., 2003), and the trifurcation is analysed separately as a special case.

Additionally, for the analysis of bifurcation stability (after Edmonds and Slingerland, 2008), Shields stress, Θ, in the channel upstream of each bifurcation was calculated:

$$\Theta = \frac{\tau_{bed}}{(\rho_s - \rho)\mathrm{g}D_{50}} \tag{5-3}$$

Where τ_{bed} is the bed shear stress (Nm^{-2}), ρ_s and ρ are sediment and water density respectively (kgm^{-3}), g = $9.81ms^{-2}$ is acceleration due to gravity and D_{50} is the median bed sediment grain size. Measurement of bed sediment samples was conducted for the 2018 survey using a laboratory laser diffraction particle size analysers (see section 5.2.4), and the mean D_{50} across all bed samples, 31.9 μm, was used.

τ_{bed} was estimated from the ADCP data, using the depth-averaged velocity method of Wilcock (1996). In this method, the depth averaged velocity, U (ms^{-1}) can related to bed velocity, u^*:

$$\frac{U}{u^*} = \frac{1}{\kappa}\ln\left(\frac{h}{e\ z_0}\right) \quad (5\text{-}4)$$

Where h is local flow depth, κ ≈0.4 is von Kármán's constant, e is Euler's number approximated to 2.71828, and z_0 is a small height above the bed where u = 0. In this study, we use $z_0 \approx 0.1D_{84}$ following Sime, Ferguson and Church (2007). Using the D_{84} calculated from grainsize analysis of the 2018 bed samples, this gives a giving an estimated z_0 of 9.86×10^{-7}m. Wilcock (1996), relates u^* to τ_{bed} using the equation:

$$u^* = \left(\frac{\tau_{bed}}{\rho}\right)^{0.5} \quad (5\text{-}5)$$

Following Sime, Ferguson and Church, (2007), $\frac{U}{u^*} = \frac{1}{\kappa}\ln\left(\frac{h}{e\ z_0}\right)$ (5-4) can be rearranged and substituted in to (5-5) to give:

$$\tau_{bed} = \rho C_d U^2 \quad (5\text{-}6)$$

Where C_d, the coefficient of drag equals:

$$C_d = \frac{\kappa}{ln^2\left(\frac{h}{e\ z_0}\right)} \quad (5\text{-}7)$$

In this study, the shear stress was calculated for each horizontal ADCP ensemble, to give a channel transect of shear stresses. The depth-averaged mean for each ensemble was used as U, and the ADCP derived flow depth was used as h. Due to the large local variation seen in the ADCP velocity data, the data where smoothed using a 5m moving average. The maximum τ_{bed} in the channel was then used to calculate Θ. This was done for all bifurcations on the delta with

sufficient available ADCP data (*Figure 5-2*: Survey locations for the WLD field studies. a) Coverage of multibeam echosounder bathymetry for 2020 and 2009 surveys. b) Locations of diffluences (indicated as number letter combinations, e.g. 2a) targeted in the studies(indicated as number letter combinations, e.g. 2a), laser in-situ scattering and transmissometry (LISST) profiles and acoustic Doppler current profiler transects performed. Other transects where taken during the three surveys, but the shown transects where those that had sufficient coverage across multiple surveys to allow them to be used for the bifurcation analises.

5.3 Results

5.3.1 *Bed Morphology*

To evaluate how the WLD is interacting with its bed, this section utilises high resolution bathymetry is used to observe bed morphology and bedforms with the

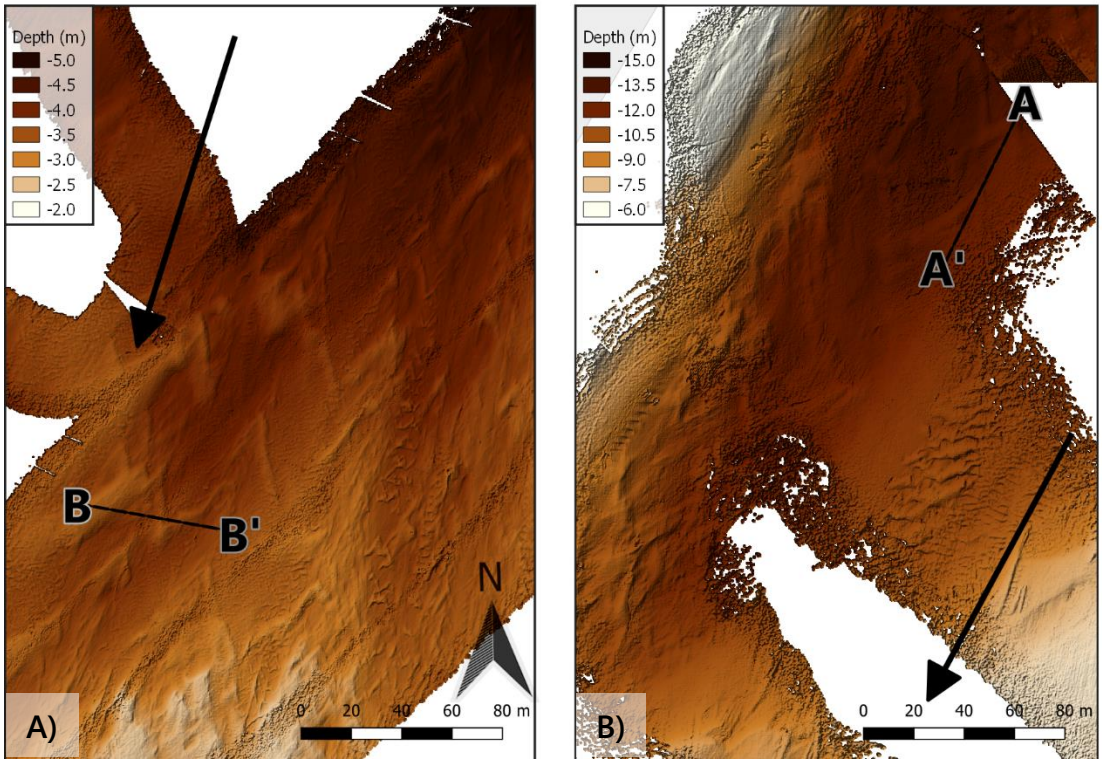

Figure 5-6: Bathymetry of the bed areas in front of the main channel outlet (see figure 5-2). Profiles of transects A and B can be seen in figure 5-7.

aim of identifying areas of erosion, sediment scarcity and sediment deposition. The area of the delta at the mouth of the dredged channel is covered with isolated bedforms moving over a bed that is either smooth or marked with erosional marks (*Figure 5-6*). The erosional marks have widths around 1m, depths of approximately 0.05-0.1m and lengths of many tens of metres. Small trains of barchan dunes (length 5-10m, width ~5m) populate some low-elevation troughs in the bed.

Larger (up to 30m width and length), low relief (0.5m, see *Figure 5-7 a & b*) chevron shaped bedforms cover much of the rest of this area. In *Figure 5-7a*, it can be seen that these bedforms are prograding up a shallow gradient (~1:80), and have a relatively steep stoss (mean angle = 4.59°, σ = 1.68°) and very shallow gradient lee (mean angle = 1.90°, σ = 0.96°). The chevron bedforms were also observed to have a considerably higher backscatter intensity than the channel bed, suggesting that they are formed from a different material (*Figure 5-8*). This material is more sonically reflective than the bed, which is likely made of consolidated mud "bedrock", as demonstrated by the erosive marks mentioned above, though the exact material which the dunes are made from is not known (see section 5.4.1) it is likely sand draping the basin muds.

Just downstream from the end of the dredged channel, the main delta channel splits in to three. The west-most channel has a width of ~925m, and its bed is characterised by a large central sediment bar covered by short (~5m) wavelength flow-parallel bedforms (Figure 5-9a). To the east of this is a ~50m margin of smooth bed or barchanoid dunes between the bar and the channel bank. While the survey did not cover the area to the west entirely, single-line zigzag passes

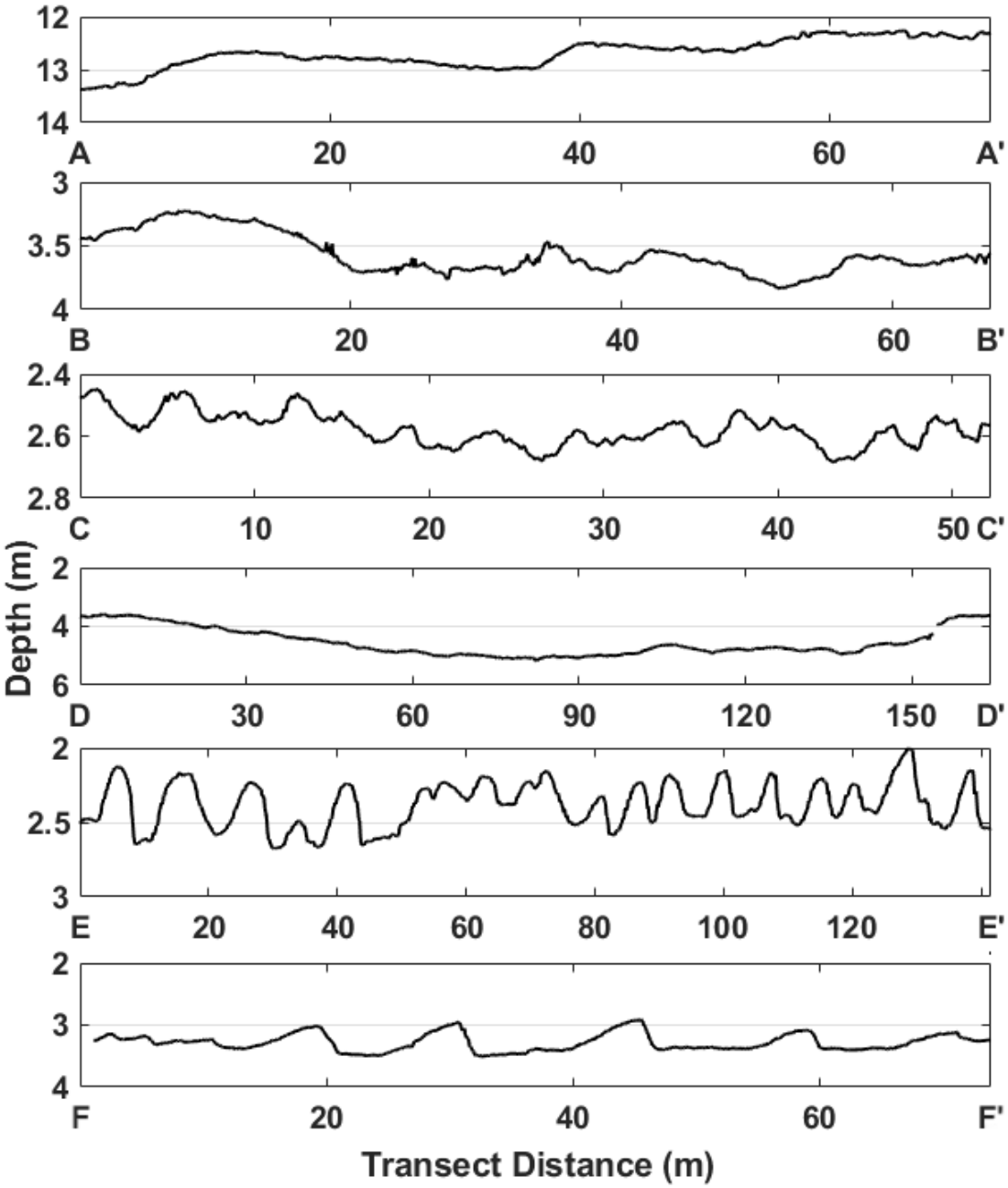

Figure 5-7: Elevation Transects A) Chevron Bedforms at the dredged channel mouth [Figure 5-6] B) Transverse transect across Chevron Dunes [Figure 5-6] C) Longitudinal Transects across a Barchanoid dune train in the middle channel of the trifurcation [Figure 5-9] D) Flow-parallel transect the large scour near the W bank of the 4b bifurcation [Figure 5-10] E) Longitudinal transects along barchanoid dunes in the W leg of the 4b bifurcation [Figure 5-10] F) Longitudinal transect along flow-transverse ripples in the E leg of the 4b bifurcation [Figure 5-10]. Flow direction is left to right for all transects except B and C, which is perpendicular to the flow direction.

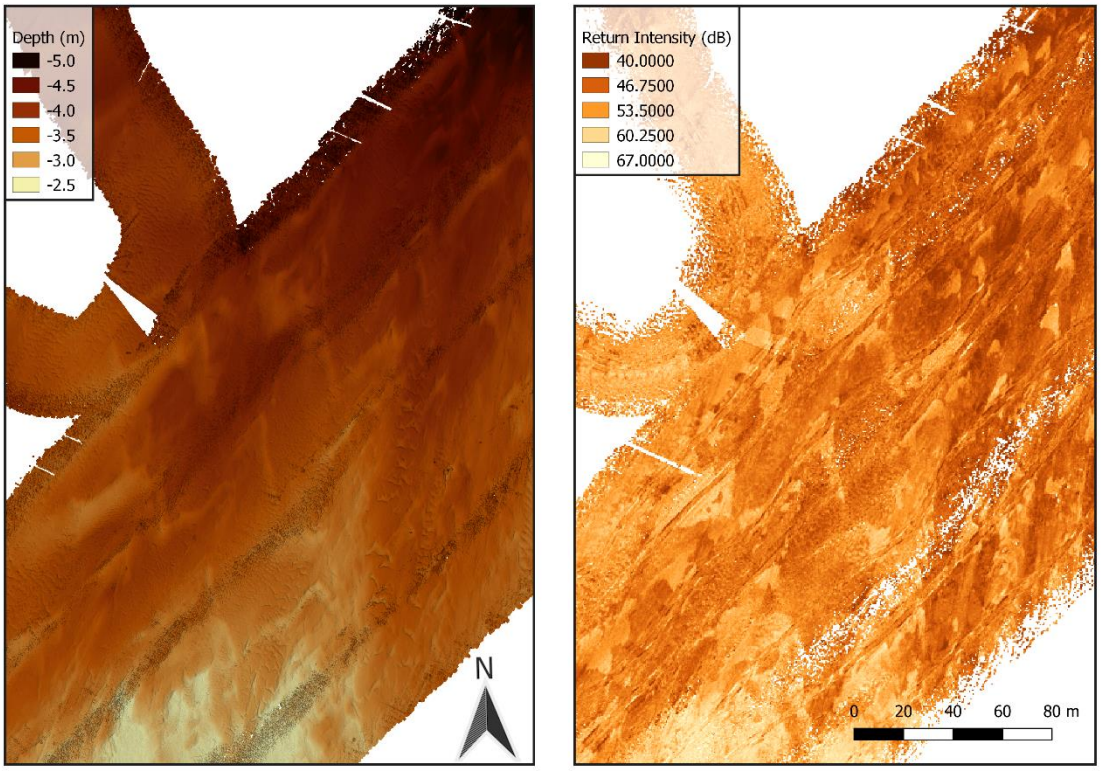

Figure 5-8: Comparison figure of Bathymetry and acoustic backscatter intensity at the mouth of the dredged channel

show a much wider area of planar, bedform-free bed, at least 200m wide (Figure 5-9a).

The middle channel is around half the width of the western leg, at ~400m, and contains largely a clear bed, with groups of isolated barchan dunes in the western 300m of the channel. The eastern 100m of the channel is largely devoid of bedforms apart from some erosional scour marks near the eastern bank. Near the western bank, a deeper section of the channel is filled with barchanoid dunes with much denser spacing than those seen in the channel centre (*Figure 5-9b*).

The east channel is also approximately 400m wide and is characterised by its lack of sediment bedforms. The centre of the channel, however, is marked with multiple, flow parallel troughs which are around 2-4m wide and up to 0.1m deep (*Figure 5-9*c). A major bifurcation (4b, see *Figure 5-2b*) downstream of the western

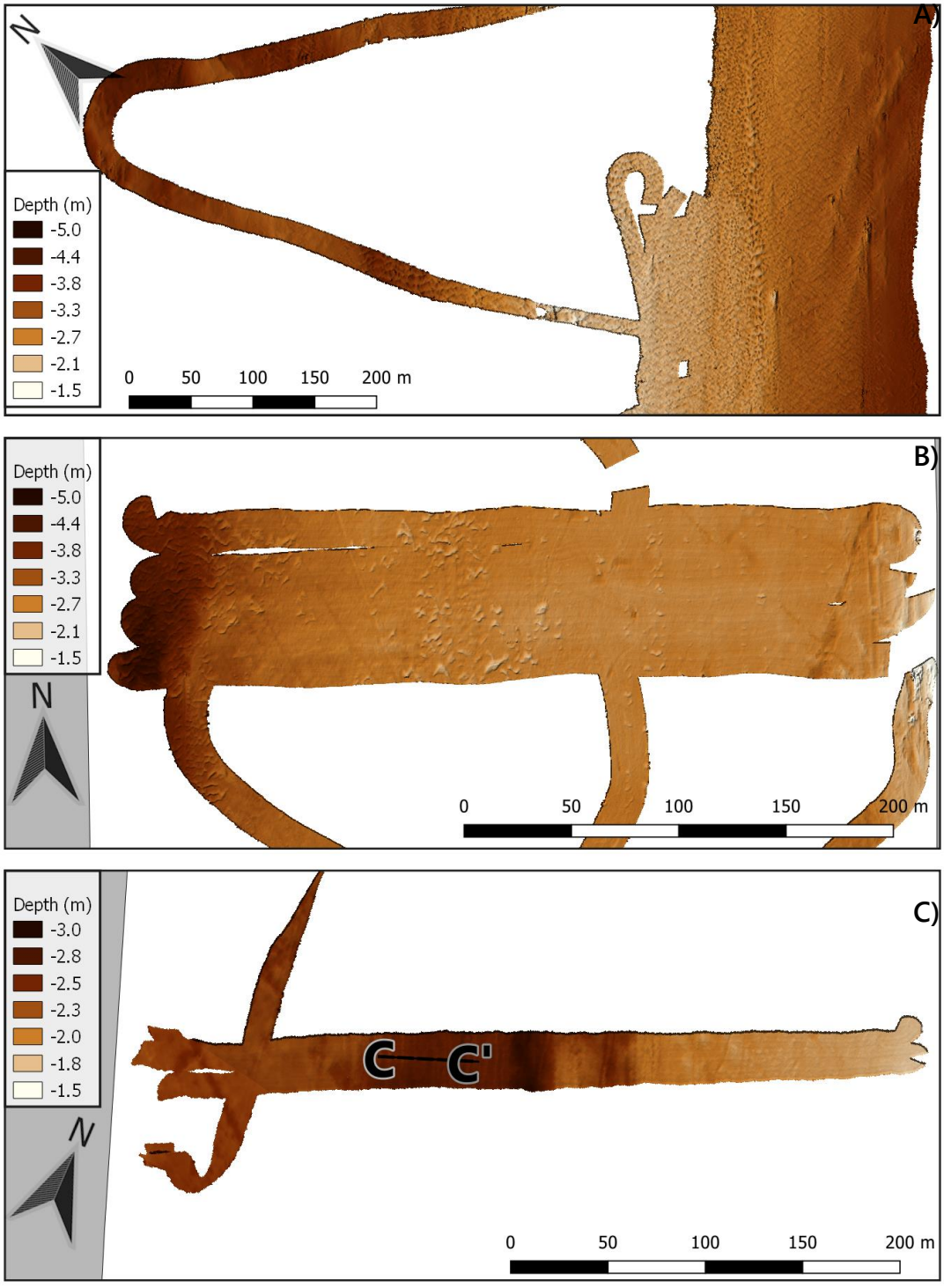

Figure 5-9: Bathymetry of channels flowing out of main trifurcation (2b, see figure *Figure 5-2b*) A) Main Pass, the western leg of 2b, B) the northern end of Greg pass, the central leg of 2b, and C) East pass, the eastern leg of 2b. Profile of transect C, showing erosional flutes can be seen in figure 5-7.

leg of the trifurcation was also surveyed. The west channel of this bifurcation was wider (around 380m) and deeper than the east channel (around 280m in width, see *Figure 5-10*). Near the west bank, just upstream of the bifurcation, is a 75m wide, 2m deep scour with a low-gradient upstream slope and an irregular downstream edge (*Figure 5-7d*) which consists of long, very low gradient erosional channels up to 200m long, between steep ridges of uneroded bed material.

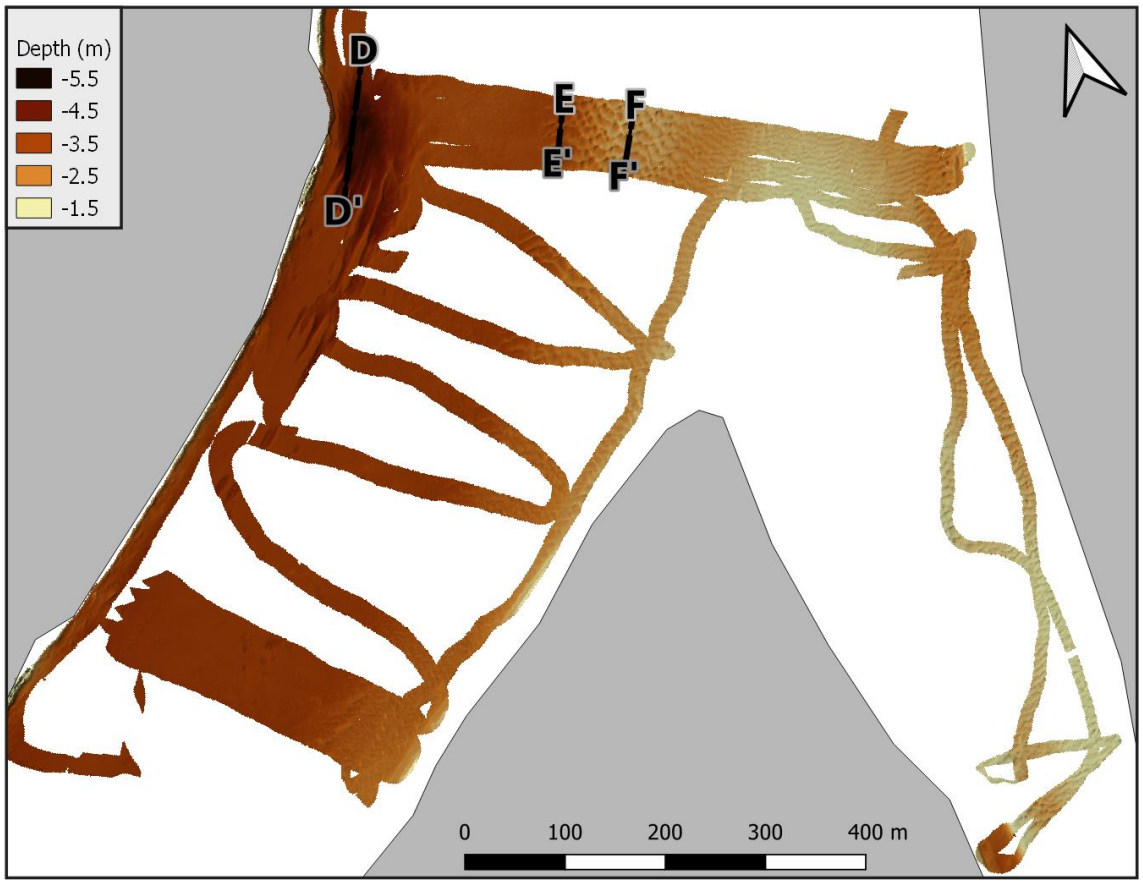

Figure 5-10: Bathymetry of bifurcation 4b, downstream of the west channel of the trifurcation (see *Figure 5-2*b). Profiles of transects D, E and F can be seen in figure 5-7, showing long-profiles of, respectively; the deep scour on the west bank of the channel, the flat bed-dune transition zone and the dune field central to the channel.

Immediately east of the scour is a 100m wide section of channel bed with a depth of around 3.3m, that is either smooth or covered in sparse, low (around 0.1m high) barchanoid bedforms (*Figure 5-10*). The rest of the channel is shallower (1.6-2.8m deep) and covered by larger (30-50cm high; *Figure 5-7f*) flow-parallel bedforms, with some separated barchanoid dunes on the western fringe (*Figure 5-7e* and *Figure 5-10*). The majority of the largest bedforms move down the east channel, causing much of its width to be occupied by these bedforms (much of this is not shown on *Figure 5-10*, as a large section of the channel was too shallow to survey). Downstream survey patches on the west leg, however, show a channel bed largely devoid of bedforms other than some lower amplitude (0.2-0.3m) barchanoid bedforms near the eastern bank.

An ADCP transect just upstream of bifurcation 4b (*Figure 5-11*) shows that the highest velocity flow (~1-1.2 ms^{-1}) was aligned with the western channel margin, upstream of the location of the scour. To investigate the reason for the formation of this scour, the Shields stress was calculated for a sub-section of the 2018 ADCP transect directly upstream of the centre of the eastern channel. This was found to have a value of $\Theta = 0.2465$, 75% higher than the average Shields stress for the whole transect ($\Theta = 0.1407$). A second area of higher flow velocity aligned with the eastern margin, co-located with a peak in suspended sediment concentration of up to 803 mg L^{-1} over the dunes in the eastern part of the channel. Suspended sediment concentration is much lower in the western half of the bifurcation, between 400-500 mg l^{-1}. Combined with the distribution of bedforms, this demonstrates the drivers of bifurcation instability (Kleinhans et al., 2013); one sediment under-supplied, erosive distributary incises to increase its

capacity, while the other, sediment-rich distributary deposits sediment and decreases its capacity.

Bed characterization (*Figure 5-12*) shows that in general, sediment scarcity of the bedforms increases eastward; the western channel of the trifurcation contains sediment rich bedforms (e.g., large, flow parallel dunes) while the eastern channel shows marks of erosion, and very few sedimentary bedforms. In the more distal bifurcation 4b, the same pattern can be seen reversed, with sediment rich beds at the eastern side and erosive beds at the west. Overall, 38.0% (260,006 m^2) of the surveyed bed was found to be covered in erosional bedforms, and 23.2% (158,818 m^2) was covered with sediment poor bedforms such as sparse barchan dunes and sand ribbons. As such, only 38.8% (265,624 m^2) of the surveyed delta bed was covered in bedforms indicative of a healthy sediment supply. This demonstrates that the fashion in which channels in the WLD interact with the underlying substrate varies spatially, and is erosive in many places.

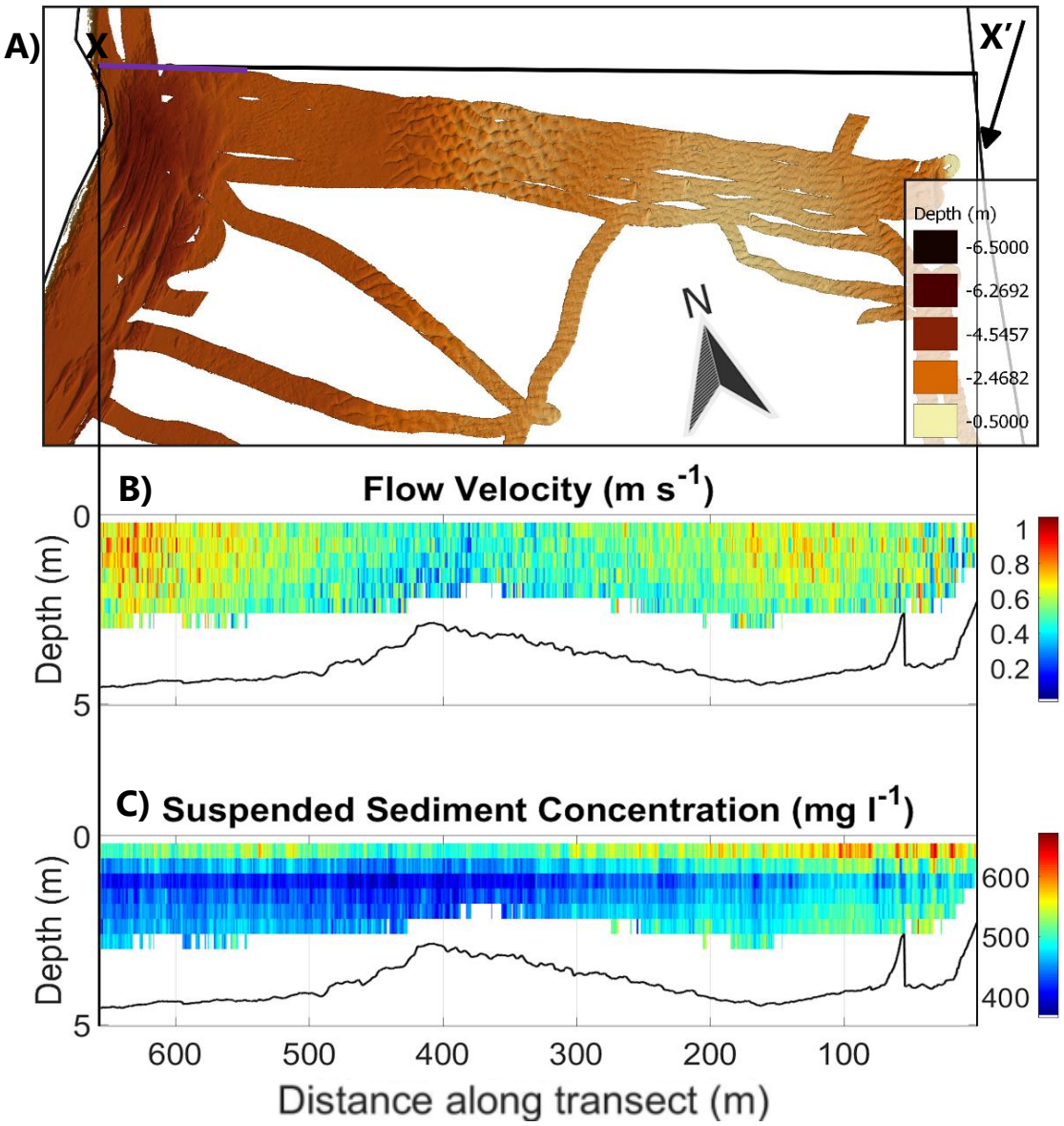

Figure 5-11: Comparison of A) bathymetry (2020), B) flow velocity across transect X and C) suspended sediment concentration data (2018) across transect X at the channel upstream of bifurcation 4b. Shields stress was measured across transect X and separately for the section of transect X highlighted in purple (see text above).

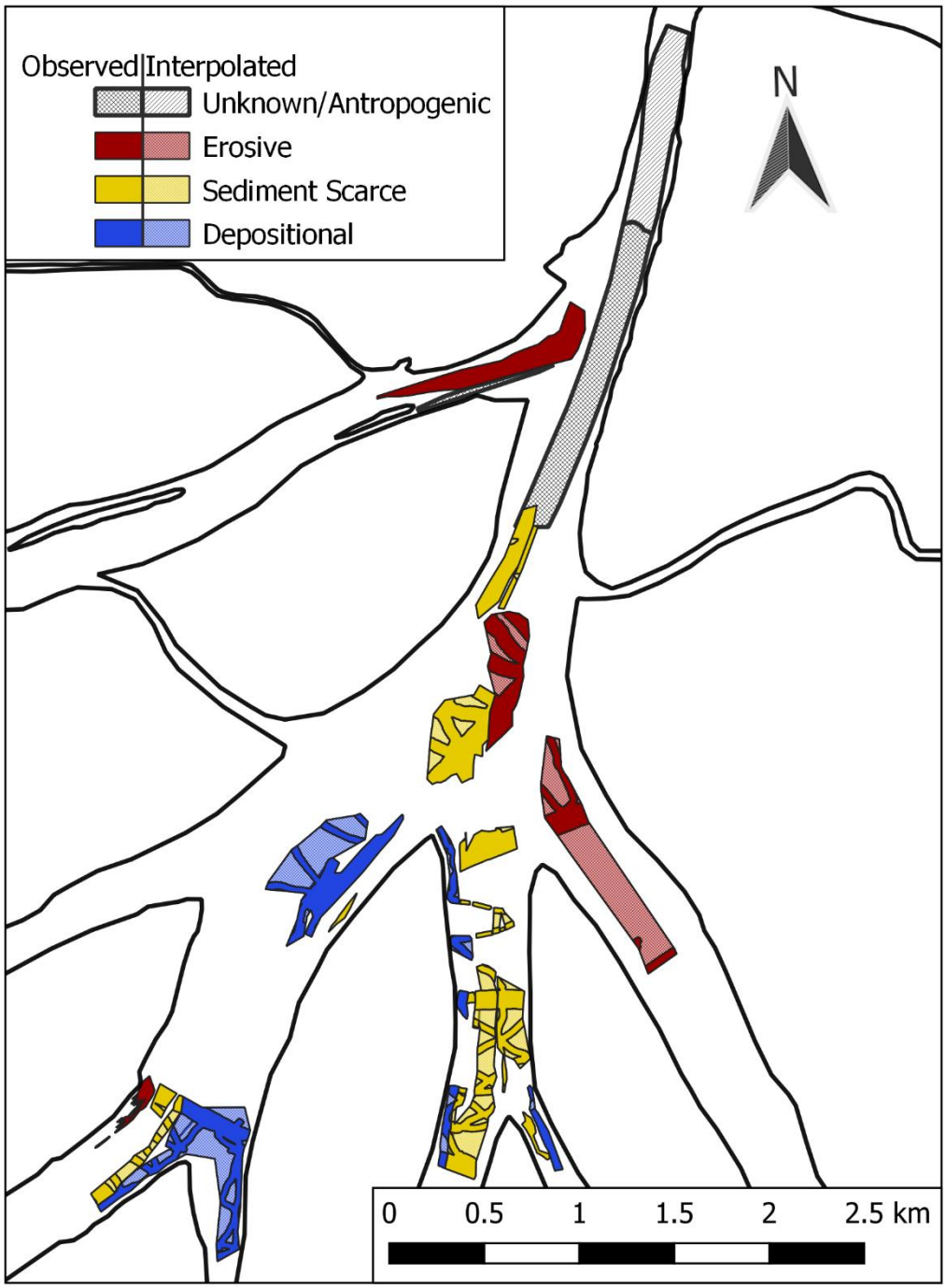

Figure 5-12: Characterization of the bed, of the delta in 2020. Dark areas are categorised directly by observed bathymetry and backscatter data, paler areas are interpolated from characterization in the observed areas.

5.3.2 *Bed Level Change*

To investigate how the bed elevation of the WLD has changed over time, two DEMoDs were created to show the morphological change between 1935-2020, and 2009- 2020. The DEM of difference between pre-delta (1935) and 2020 bathymetry (*Figure 5-13*), it can be seen that areas of deposition within the surveyed channels are rare and are largely limited to the channel margins. Erosion is widespread, with rates as high as 4.9m (an average of 0.056 m y^{-1} if erosion is assumed to have happened consistently since 1935) in the trifurcation, at the mouth of the dredged channel (*Figure 5-13*). Higher bed change (up to 6.7 m) is shown in *Figure 5-13*, but this is within, or close to the dredged channel, so is likely caused by human excavation rather than erosion by the channel. Erosion in the surveyed parts of the eastern channels (East, Pintail and Greg passes) has low magnitudes of 0.78-1.64 m (0.008-0.019 m y^{-1}). Western channels have a mix of erosion and deposition. The area of bare bed in the western distributary of bifurcation 4b has been eroded down to a depth of 1.74 m below pre-delta levels (~0.020 m y^{-1}), whereas the east leg has aggraded by as much as 1.33 m (~ 0.015 m y^{-1}). Due to the high uncertainty around the 1935 data, the smaller changes in depth (< ±c.1 m) may be a result of inaccuracies in the data rather than actual erosion or deposition. Notably, however, the scour in the west distributary has deepened by 3.6 m, (well above the likely uncertainty of the 1935 data) at rate of at least 0.031 m y^{-1}. Additionally, as the scour was not present in the 2009 survey (see *Figure 5-14*), the rate of erosion is likely much higher than this. There is a large area of

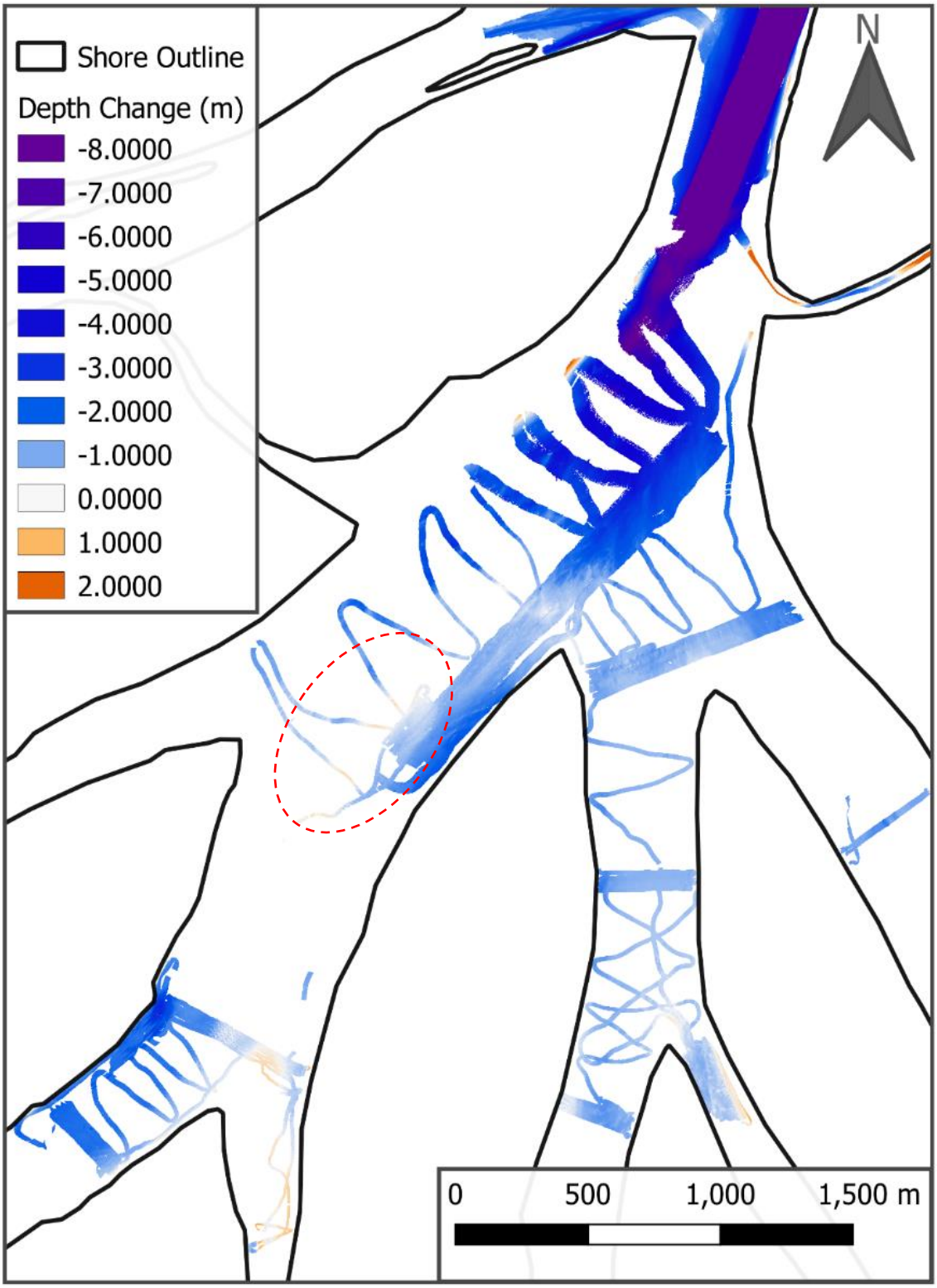

Figure 5-13: DEM of difference between pre-delta (1935) and 2020 bathymetry. Circled is deposition of central bar in west leg of trifurcation.

Figure 5-14: Comparison between the a) 2009 and b) 2020 bathymetry of bifurcation 4b, and c) the relative DEM of difference, which has been adjusted for uncertainty by subtracting the LoD_{min} (see section 5.2.10). *Note the uncertainty around the datum elevation of a.

deposition (c.150m wide and over 400m long) in the centre of the west channel in the trifurcation (*Figure 5-13* – red dashed circle).

Due to uncertainties around the elevation datum of the 2009 data, DEMs of difference for 2009-2020 represent relative change in bed topography, rather than absolute change in bed elevation (see section 5.2.10). The main areas of erosion between 2009 and 2020 in the upper channel are the boundaries of the dredged outlet (See *Figure 5-15a*). This suggests that the outlet channel is being widened, likely as the steep, human-made channel sides collapse. Structures at

the base of the wall resemble fallen blocks of bed material (see *Figure 5-16*), which would support the hypothesis of dredged channel wall collapse.

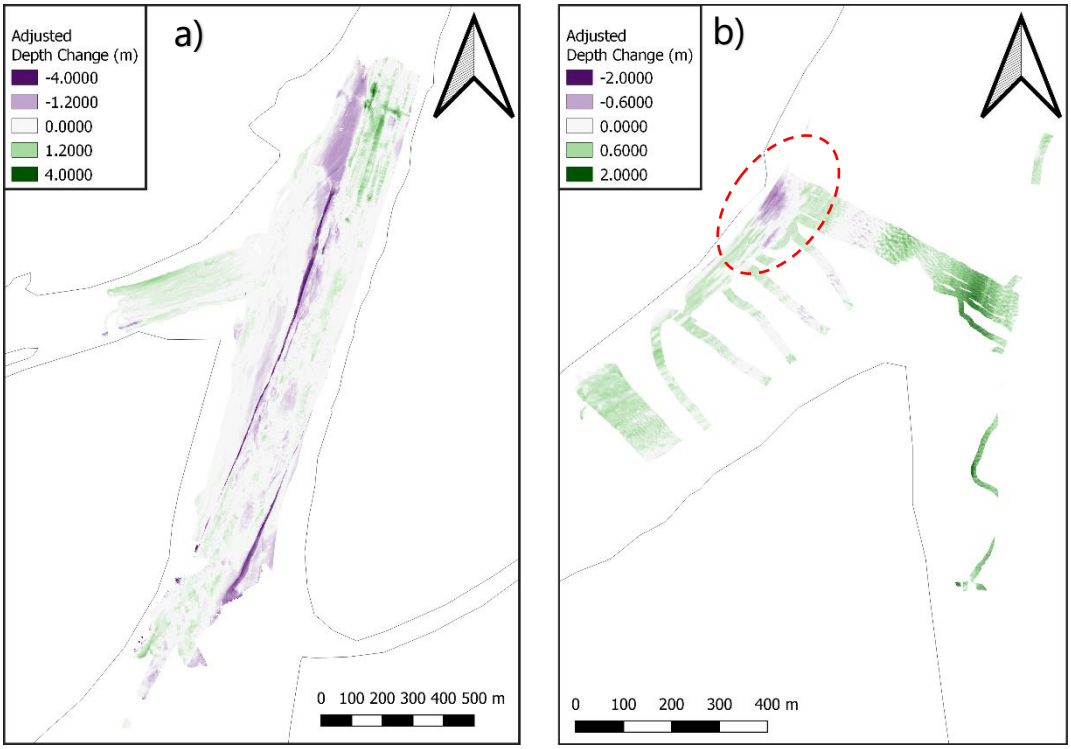

Figure 5-15: 2009-2020 DEM's of difference for A) The main outlet near Camp Island and B) Bifurcation 4b. Note the dramatic depth change at the margins of the dredged channel, likely a result of the side walls collapsing. In both figures, adjustment had been made for uncertainty by subtracting the LoD_{min} (see section 5.2.10), so white areas within the DEMoD indicate no significant change.

In the lower bifurcation, sediment is being deposited in the eastern leg of the channel but eroded from most areas of the western channel, especially in the ~1.5m deep scour that has developed near the western bank (see Figure 5-15b, circled, and *Figure 5-14*b). The area of smooth and sparsely covered bed seen in the west leg of the bifurcation in 2020 was covered in flow parallel dunes in 2009 (*Figure 5-14*).

The above data indicate that, at least at the level of detail achievable with this data, significant erosion and deposition is spatially constrained to small areas

of scour, collapse or aggradation of non-dominant bifurcation distributaries. This seems to be in contrast to the previous section (section 5.3.1), where erosive interactions with the bed were found to be more widespread. This indicates that the cohesive substrate may be affecting the dynamics of channel erosion in this field site.

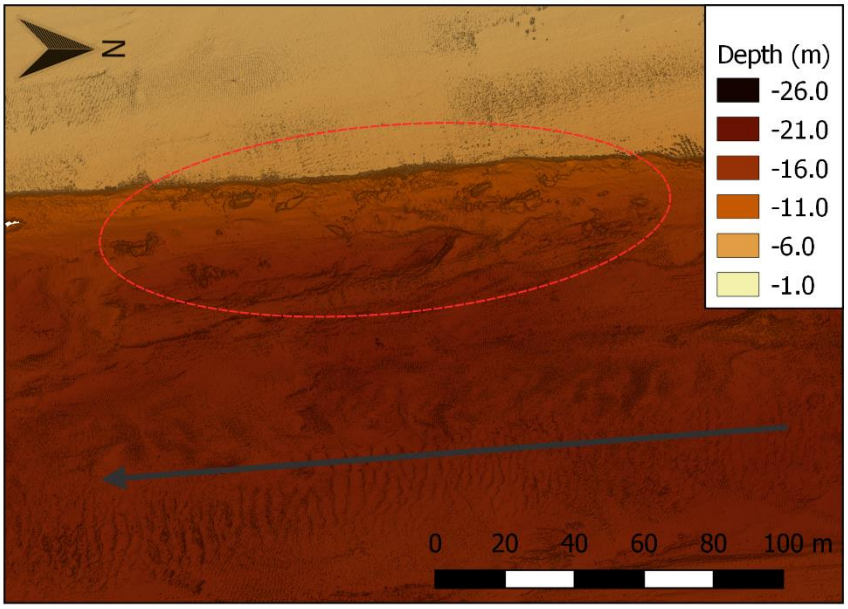

Figure 5-16: Bathymetry of an area of the dredged channel wall, showing blocks of bed material (5-10m in length, 2-3m wide and 0.5-1m tall) at the base of the wall.

5.3.3 *Flow and Sediment Distribution*

To analyse how bifurcations are changing through time in the WLD, the proportional divisions of sediment and flow within distributaries was analysed across multiple field campaigns. For context, data from the LISST samples taken in 2018 suggest that the suspended sediment supplied to the delta was silt and very fine sand. The mean D50 of all LISST profiles was 44.3 µm (σ = 5.1 µm), while the mean D16 and D84 where 14.3 µm and 107.8 µm respectively.

Due to the nature of the trifurcation (diffluence 2a, see figure 5-2b), normal mathematical methods for bifurcation categorisation are ineffective. As data it are displayed here separately. 2018, both sediment and water discharge are split in approximately the same ratios in the trifurcation (61.8%, 22.9% and 15.3% for water and 61.8%, 23.4% and 14.8% for sediment, for west, central and east

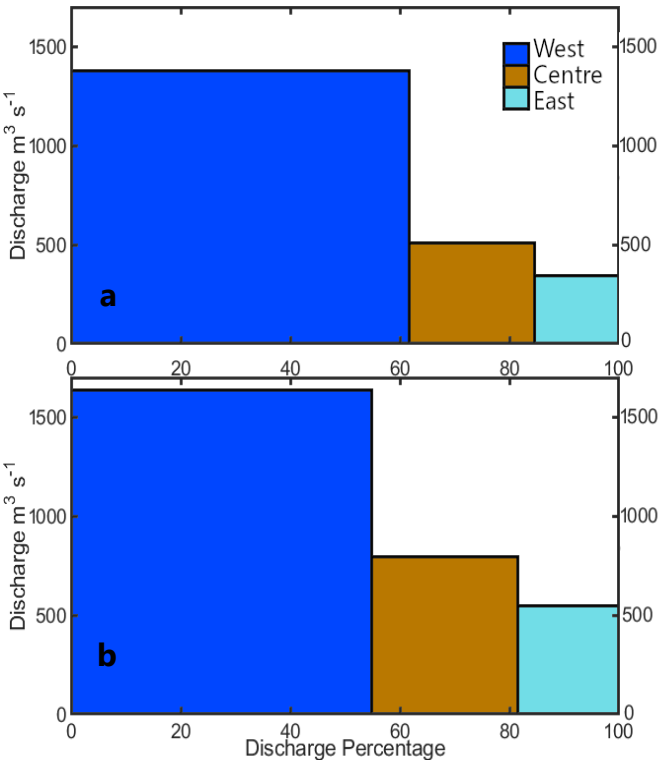

Figure 5-17: Water discharge partitioning in the central trifurcation for a) 2018 and b) 2020

distributaries respectively), with more than half of sediment and water flowing down the large western channel (Figure 5-17). In 2020, discharge to the delta was higher (6,392 m^3s^{-1} vs 4166 $m^3 s^{-1}$), and distribution of water to the smaller centre and east channels was proportionally higher (54.9%, 26.7% and 18.4% for west, central and east distributaries respectively). A similar, but stronger trend was seen with suspended sediment transport (Figure 5-18), with the proportion of

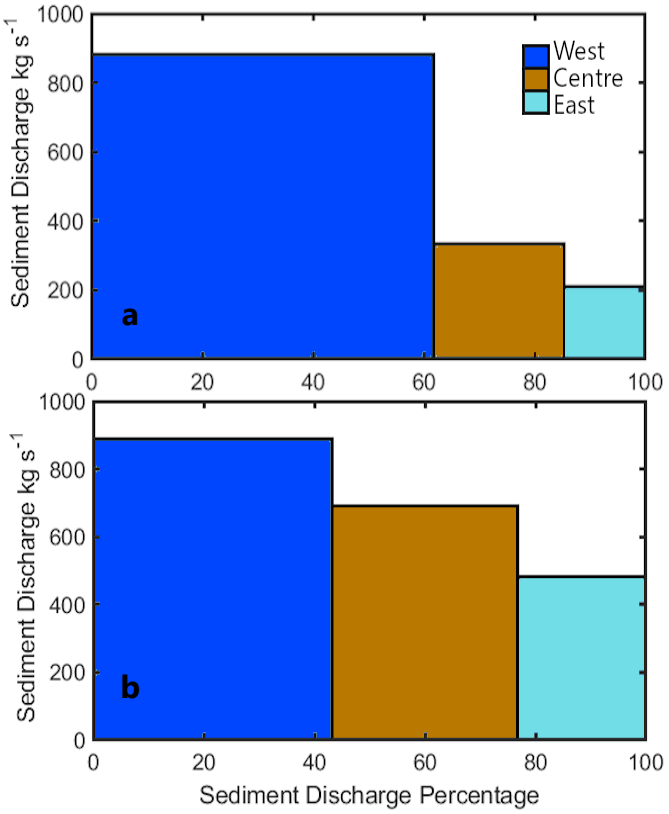

Figure 5-18: Sediment discharge partitioning in the central trifurcation for a) 2018 and b) 2020

sediment being routed down the west channel falling to 43.1%, and the proportion of sediment down the centre and east channels increasing to 33.5% and 23.3%.

Using the discharges of the distributaries of all other diffluences, both sediment and water asymmetries were calculated to investigate bifurcation dynamics. The asymmetry (Q_r) of the bifurcation closest to the delta apex (bifurcation 1a) was found to be decreasing across all years for which data was

available, from 16.7 in 2009 to 7.8 in 2020 (Figure 5-20). In contrast, the furthest downstream bifurcation increases Q_r from 3.0 to 6.0 between 2009 and 2018. The remaining bifurcations change much less dramatically; 3a decreases from 2.16 to 1.42 (2012-2018), then increases again to 1.68 by 2020, and the asymmetry of 3b does not change significantly. Sediment Q_r follows the trends of water Q_r in all recorded years.

Figure 5-19 suggests that the above changes are not driven entirely by differences in discharge. Q_r in bifurcation 1a continues to decrease, even when incoming discharge decreases between 2012 and 2018. Similarly, bifurcation 4b undergoes little change in Q_r, despite an increase in upstream discharge of >100% between 2009-2012, but experiences a doubling in Q_r between 2012-2018, despite negligible change in upstream discharge. This data does not show any clear trend in bifurcation symmetry, or evolution though time. As such, to address the objectives of this chapter, more complex mathematical analysis is discussed in section 5.4.4.

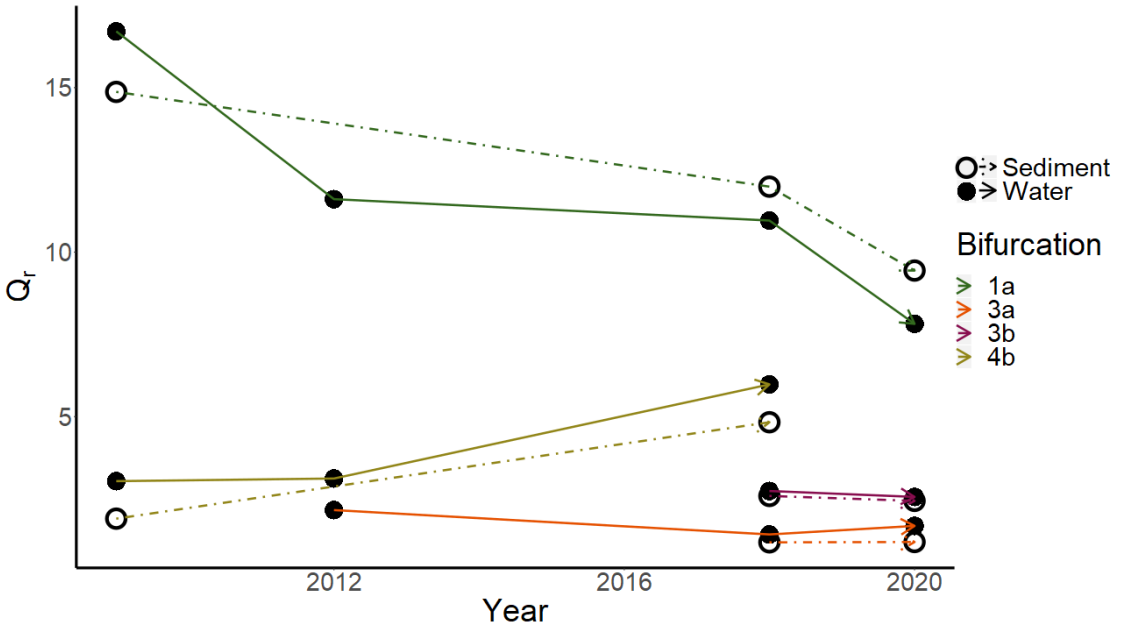

Figure 5-20: Evolution of bifurcation distributary water and sediment discharge ratio between three surveyed years. Adittional water discharges for some bifurcations drawn from *Hiatt 2012*

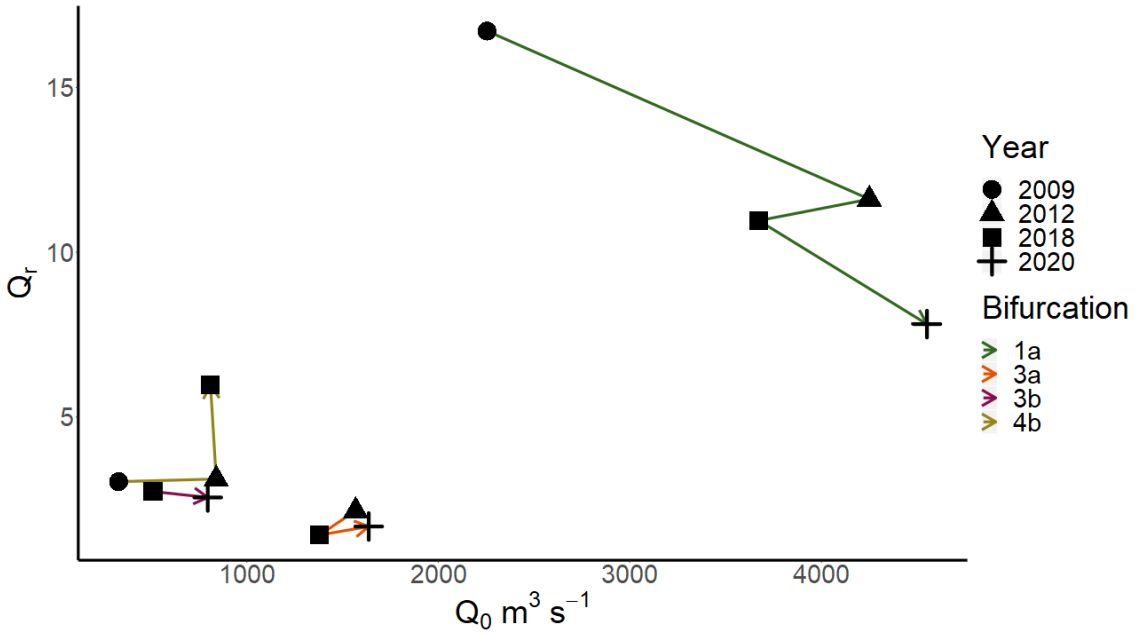

Figure 5-19: Q_r plotted against channel discharge just upstream of the bifurcation.

5.4 Discussion

5.4.1 *Dynamics at outlet channel mouth*

The chevron shaped bedforms seen in Figure 5-6 (detail in figure 5-21a) are not commonly observed, and as such, knowing what flow and sedimentary regime has led to their formation is not straight forward. From the data collected, it can be seen that they are large (up to 30m long and 30m wide) compared to nearby bedforms, though the length of the deposited sediment, measured along the downstream axis, is only 8-12m. They are composed of a different, more acoustically reflective material than the surrounding bed, which is covered in erosional marks and small, sparse sediment bedforms, suggesting that the flow in this area is limited in bedload sediment.

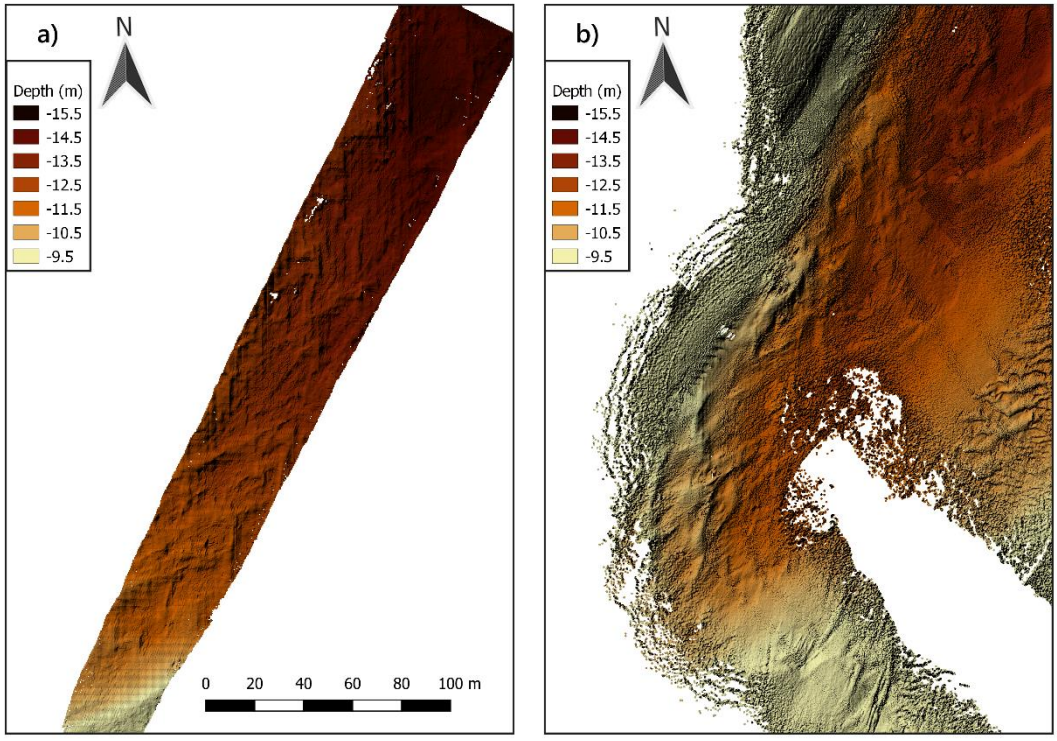

Figure 5-21: Comparison of the same patch of chevron bedforms in a) 2009 and b) 2020

These bedforms were present in the 2009 survey, though only a small patch was within the survey area (*Figure 5-21*), and confidence of the positioning of this survey was low, so direct comparison between 2009 and 2020 is not possible. However, the bathymetry does suggest that they have existed since at least 2009, and have moved since then. In 2018, the local flow speed over these bedforms was ~1.2ms^{-1}, though at the time of the 2020 survey it may have been greater as river discharge was higher at this time. The wavelength of the bedforms is difficult to estimate, as they are isolated and irregular, but measurement of 21 of these bedforms gave an average along-flow length of 15.3 m (**σ** = 6.7 m).

The study of Andreotti *et al.* (2012) presents a theoretical explanation for the formation of a number of bedforms, including chevrons or rhomboids, and attempts to constrain the hydrodynamic conditions that dictate the transition from ripples to chevrons. This study classified sedimentary and flow conditions using a number of metrics, H (flow depth), k (wavenumber = $\frac{2\pi}{Wavelength}$) and L_{sat}, the saturation length, which corresponds to the distance a sediment grain travels horizontally before settling out. Using the metrics described by Andreotti *et al.* (2012), the chevrons observed in WLD were found to have a rescaled wavenumber value (kH = wavenumber x flow depth) of between 0.15-0.5, and angles-to-flow (α) of 60-70°. When compared to the plots in Andreotti *et al.*'s study, these values are seen to be close to the optimum for the growth of chevrons with a L_{sat}/H value of 1-10 (i.e., the bedforms are likely formed by a flow that takes between 1 and 10 channel depths to redeposit sediment after erosion), suggesting a moderately turbulent flow, or fine, easily suspended sediment, which is consistent with the

mean grainsize found during the 2018 survey by LISST profiles (38.7µm). The plots also indicate that these bedforms are very close to the transition point to ripples.

In agreement with the above, Andreotti *et al.* (2012; pp. 114) state that, to create chevrons in a flume, "…H [water depth] must be small if bedload is dominant…" or the sediment must be "fine particles transported in suspension". As some of these bedforms occur at a water depth of >10m, and they all occur in places where the channel is bedload poor, the latter is more likely to be the case. This would suggest that these bedforms are forming under flows capable of transporting the material from which they are made in suspension.

However, Andreotti *et al.* (2012; pp. 124) summarised that "chevrons are long enough to disturb the flow over its entire depth. The flow dynamics is then controlled by the free surface." As mentioned above, many of these bedforms are found in deep water, and it seems unlikely that they will interact with the free surface in anything other than a very subtle way.

Maxwell and Haynes (1989) observed chevron shaped dunes in the Selima sand sheet in south-western Egypt (see *Figure 5-22*a). The chevrons seen where very large compared to the ones seen in this study (130-1200m wavelength), but of lower elevation (0.1-0.3m). These bedforms were interpreted by the author to be the cores of much higher amplitude bedforms, with the visible lighter sediment patches described as sand collecting in the lee of these bedforms. As the flow in the WLD is eroding in to pre-existing sediment, it is possible that the remnants of pre-delta bedforms exist there. However, the movement of the chevrons since 2009 would suggest that they are active and modern, rather than fossilised remains of older bedforms.

Chevron shaped, subaerial dunes found in the coastal areas of Australia, Madagascar and the Bahamas have been the subject of ongoing debate, with studies arguing for aeolian processes, storm waves and impact-induced tsunamis as an origin (Spiske et al., 2020; Vimpere et al., 2019). However, in all of these explanations, the bedforms are sited with down-flow facing apexes, in contrast to what is seen in this study, so the mechanisms presented for those origins are likely not relevant here.

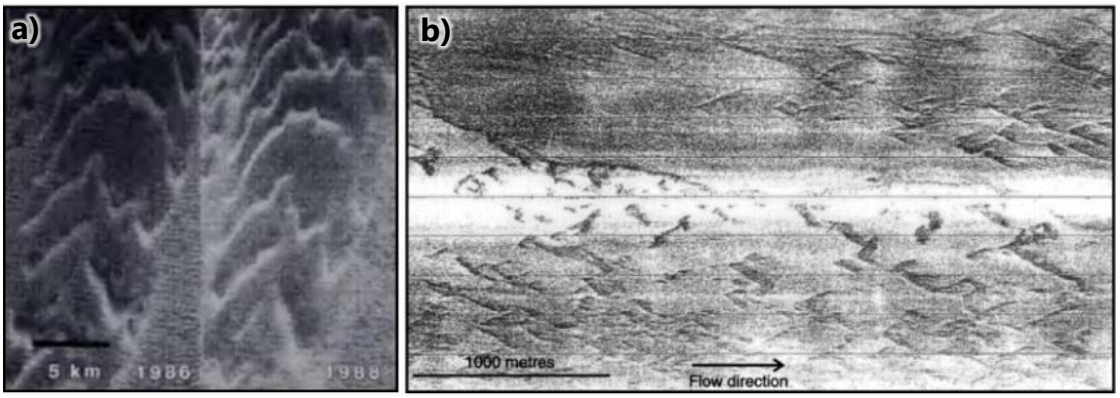

Figure 5-22: Examples of chevron dunes found in field studies, in a) Satellite photography of the Selima sand sheet, Egypt (Maxwell and Haynes, 1989) b) long-range side-scan sonar imagery of the Lower Valencia Fan, northwest Mediterranean (Morris et al., 1998 (note that in this image, dark colours indicate high backscatter).

Morris *et al.* (1998) found bedforms of a similar shape in the Lower Valencia submarine fan, at approximately 2.9km depth (see *Figure 5-22*b). These bedforms where described as "…V-shaped bodies, up to 200m across (limb to limb), up to 300m long, and approximately 2m in amplitude" (Morris et al., 1998. pp. 165) making them around ten times the size of those found in this study. The authors observed the bedforms to have "…sharp upfan-facing and diffuse downflow-facing edges…" (Morris et al., 1998. pp. 165) much like the ones found in the WLD, and also observed them to be high acoustic backscatter areas, which they

attribute to them being made of course sediment or high surface roughness. They interpret these to be deposited from the bedload of a mud dominated, supercritical turbidity current. Much like the ones seen in this study, the bedforms described by Morris *et al.* (1998) are also formed a sufficient depth to be unaffected by the water surface. However, it is likely that these bedforms formed under supercritical flow for at least some time. In the case of the chevrons in the WLD, the flow was only ~1.2ms^{-1} at the time of the survey, and as the 2020 survey was conducted during flood conditions, it seems unlikely that flow velocity ever exceeds this by much. In a water depth of 10m, this gives a Froude number of $\boldsymbol{Fr} = \frac{1.2}{\sqrt{9.81 \times 10}} = 0.1211$, demonstrating that flow here is sub-critical.

While they do give some insight in to the nature of the chevron bedforms seen at the mouth of the subaqueous channel in the WLD, none of the above studies can fully explain their formation. However, these bedforms are isolated to a small area of the delta where the water and sediment leaving the dredged channel is coming in to contact with and adverse gradient (shallowing downstream) at the same time as it is leaving the lateral confinement of the delta's feeder channel. These conditions are likely leading to simultaneous vertical flow convergence and horizontal flow divergence. This, combined with the variable discharge and bedload transport, presents an unusual hydrodynamic environment that is beyond the scope of the above studies, but which is capable of making bedforms with morphological and environmental similarities to the ones the studies found.

While exactly constraining these bedforms is very difficult without further work, this study may suggest that they are made of sediment transported in

suspension (Andreotti et al., 2012) and made of more reflective sediment than the bed, much like those in the study of Morris *et al.* (1998). While consolidated muds are of high reflectance, reworked muds are likely to be much lower reflectance. Collier and Brown (2005) found a positive correlation between grainsize and backscatter intensity in side-scan sonar data. This would suggest that the chevron bedforms are constructed of a coarse material that is still capable of being carried in suspension, at least when the WLD is at high discharge. This material may then be deposited) further up the delta (e.g., in the east distributary of bifurcation 4b as channels shallow and flow velocities decrease. However, further study, with more targeted ADCP measurements and bed sampling, and repeated MBES surveys for dune tracking, would help to better constrain the nature of these bedforms.

5.4.2 *Discussion of bifurcation 4b dynamics*

As discussed in section 5.3.3, the majority of both water and sediment discharges (83 and 86% respectively) are funnelled down the western channel of bifurcation 4b, though the sediment concentration of the sediment flowing down the eastern channel is higher. The eastern channel bed is also seen to be covered in a field of large flow parallel bedforms, while the western channel is largely devoid of bed sediment in the 2020 survey (though was covered in similar bedforms in 2009) and has a large scour that suggests that it has been exposed to intense erosion at some point between 2009 and 2020 (*Figure 5-14*).

The channel above this bifurcation has a shallow curve, which has been shown by Kleinhans *et al.* (2008) to cause the bifurcation leg on the outside of the curve to be favoured with water discharge and the leg on the inside to be

favoured with sediment. The bend here may also be sufficient to generate a secondary helical flow (such as that described in tidal channels by Finotello et al., 2020) and deflect flow near the bed, and hence bedload, towards the inner (eastern) channel. While this is not seen in the 2020 ADCP transect, this helical pattern could be occurring upstream, before the morphology of the channel splits the flow in two (something that can be seen in *Figure 5-11*).

There is high sediment concentration in the eastern channel (especially near the bed, see *Figure 5-11*), despite the low sediment discharge there, suggesting that the slower moving, thinner channel is gradually transporting sediment by bedload. Inversely, the lower sediment concentration, higher discharge western channel likely transports most of its sediment in suspension in faster flowing water, and is erosional rather than depositional. This regime is likely caused, or at least aided by the reduction of flow down the east channel increasing flow down the west, which has led to the increasing erosive energy there removing the flow parallel bedforms seen in 2009, and carving the deep scour seen in 2020.

This trend shows that the western channel is becoming even more dominant over time, which is supported by the consistent increase in Q_r seen in *Figure 5-20*. This increasing trend in asymmetry suggests that the morphodynamics of this bifurcation is evolving towards a state where the bifurcation fully avulses and Main Pass is entirely abandoned unless downstream forcing is able to provide a sufficient restoring force to prevent this (Salter et al., 2017). A more detailed, general discussion of the relationship between asymmetry and stability is presented in section 5.4.4. Further, more regular field study at this bifurcation would help to predict if full avulsion will occur, quantify the impacts of such an

event on the distributary network, and act as an analogue for theoretical studies of unstable bifurcations.

5.4.3 *Discussion of central trifurcation dynamics*

As discussed in section 5.3.3, sediment and water discharge is highest in the western channel, and lower in the central and eastern legs. The bedforms in these channels fit this pattern of eastward-decreasing sediment supply: the western channel contains a central sediment bar (one of the few areas of deposition within the channels; *Figure 5-13*), the centre channel shows isolated barchan dune trains and sand ribbons indicative of a sediment poor system, and the eastern channel is largely devoid of sedimentary bedforms, but is has extensive erosional marks. The trend in sediment partitioning suggests that this split may have been even more extreme in 2018, but has become more equal by 2020 (*Figure 5-17*).

A possible explanation for this split is the pre-delta bathymetry. The western channel has formed in water with a depth of 2.1m, while the centre and eastern channels formed at a depth of 1.6m and 0.7m respectively. As a result, the western leg would be expected to be favoured early in the formation of the delta, and as a result sediment transport capacity grew in the western leg while decreasing in the central and eastern legs (Iwantoro et al., 2021). However, decreasing sediment transport capability is commonly the result of sedimentation in the channels decreasing flow depth and velocity, and little sedimentation has occurred in the east and central channels. Instead, their relatively lower sediment and water conductance is a result of smaller width, and shallower depth as a result of the initial bathymetry of the area. These two channels have also eroded vertically less than the larger western channel (bed change is ~1m, as opposed to 2-3m in the

western channel, see *Figure 5-13*) despite them being originally shallower. It is possible that in deltas forming over resistant sediment, bifurcation asymmetry can be maintained not by sedimentation in the minor channel(s) but by reduced erosion causing these channels to stay relatively shallow relative to the dominant channel which is large enough to more regularly contain flows capable of eroding the substrate.

5.4.4 *Bifurcation stability*

Edmonds and Slingerland (2008) created three equilibrium solutions for bifurcations on deltas; one symmetrical solution in which water and sediment are split evenly between distributaries with the same downstream water surface height, *Figure 5-23*A; an asymmetric solution where sediment and water are split unevenly between distributaries with the same downstream water surface height *Figure 5-23*B; and another asymmetrical solution where downstream water

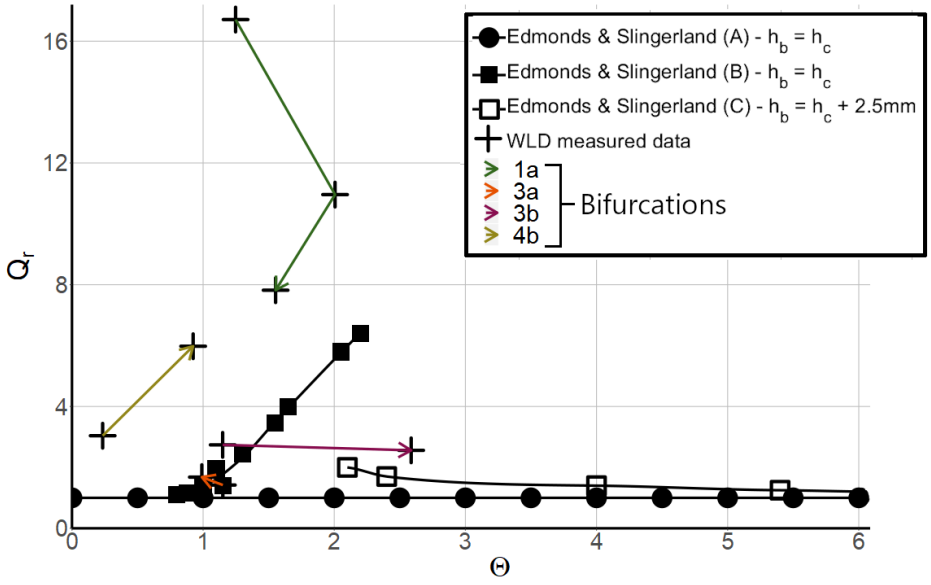

Figure 5-23: Reproduction of the equilibrium diagram of fine grained, cohesive deltaic bifurcations from *figure 7* of Edmonds and Slingerland (2008), with estimated values from the WLD plotted over the original equilibrium functions.

surfaces are unequal. In their study, Edmonds and Slingerland (2008) also compared these equilibrium solutions to measured bifurcations on the Mossy Delta, Saskatchewan, Canada, and found good agreement between the two.

If the same is done for the bifurcations surveyed in this chapter (*Figure 5-23*), it can be seen that the bifurcations surveyed do not all fall within the bounds of Edmonds and Slingerland (2008). While some of the bifurcations plot close to the asymmetric, $h_b=h_c$, solution (*Figure 5-23B*), others, such as 1a and 4b, plot some way off this solution. Instead, these bifurcations fall into the section of the graph to the left of the asymmetric $h_b=h_c$, solution (*Figure 5-23B*), and occupy a space with the same or higher values of Q_r and lower values of Θ.

It was already stated by Edmonds and Slingerland (2008) that some drivers (width:depth ratio and the upstream Chezy coefficient) can change the location of these stable equilibrium configurations. It is conceivable that other drivers, such as bed sediment supply (suggested to be lacking in the WLD; Section 5.3.1 and Shaw, Mohrig and Whitman, 2013) and bed erodibility, could do the same (discussed further in section 6.2). Section 4 showed that higher substrate resistance would be expected to increase width:depth ratio, which Edmonds and Slingerland (2008) found would move the location of the asymmetric, $h_b=h_c$, curve (*Figure 5-23*b) to higher values of Q_r for a given Θ, closer to the high Q_r values seen in bifurcation 1a. Additionally, Iwantoro et al. (2021) show that increased width:depth ratios can move the location of equilibrium solutions in sand-dominated bifurcations towards lower values of Θ. While the sediment grainsize used the equilibrium diagrams shown in that study was courser than that in the

WLD, this would help to explain why the bifurcations seen in this chapter are grouped around lower values of Θ.

Figure 5-23 also shows that the two bifurcations that plot closest to Edmonds and Slingerland's (2008) equilibrium functions (3a and 3b) could be interpreted as being more stable, as both undergo only small changes in Q_r, despite 3b experiencing a large increase in upstream shear stress, Θ. In contrast, bifurcations 1a and 4b plot further form these equilibrium functions, and show large changes in Q_r with only relatively small changes in Θ. Additionally, the asymmetry of bifurcation 1a decreased across all three sampling periods, regardless of the change in Θ (positive in 2009-2018 but negative 2018-2020) which could suggest it is evolving towards a more stable equilibrium.

The modelling study of Salter et al. (2017) showed that downstream drivers can act as a restoring force in bifurcations, preventing complete avulsion and causing the ratio of discharges to oscillate even when upstream conditions are constant. This could mean that bifurcations that are not within an equilibrium solution defined in the above studies could either be pushed towards stability (potentially seen in bifurcation 1a), or have its progression towards avulsion slowed by downstream drivers. This suggests that bifurcations that do not plot close to predefined stable equilibrium solutions are not necessarily unstable. Additionally, previous modelling studies show that the exact location of equilibrium solutions can be changed by bed sediment grainsize (Iwantoro et al., 2021; Bolla Pittaluga et al., 2015), upstream channel slope (Iwantoro et al., 2021) width:depth ratio (Iwantoro et al., 2021; Bolla Pittaluga et al., 2015; Edmonds and Slingerland, 2008) and upstream bed flow resistance (Edmonds and Slingerland,

2008). Because many of these factors are both unconstrained, unsteady, and heterogeneous in the WLD, and because (as discussed above) deviation from an equilibrium solution does not necessarily indicate instability, this thesis does not attempt to define a new equilibrium solution to cover the studies deltas.

5.4.5 *Uncertainty*

Within the 1935 data, due to its age and lack of supporting metadata, uncertainty is likely high, on the order of 0.1-1 metres. As such, changes less than around a meter are treated in the synthesis of this dataset as highly uncertain. However, even with these caveats, it is clear that the Wax Lake Outlet has caused erosion into the substrate in areas close to the mouth of the outlet and in proximal channels. In areas where the change in depth is low, the only conclusion that is drawn is that bed change small or negligible, likely involving the erosion or deposition of surficial sediment rather than large scale incision into the substrate, which this study in concerned with, or land building.

Some uncertainties also exist within the more recent bathymetric surveys. A major uncertainty exists relating to the elevation datum used for the 2009 bathymetric survey, and as such the DEMoD for 2009-2020 was constructed by subtracting the differences in mean elevation between the two DEMs and investigating relative rather than absolute change. Furthermore, intrinsic uncertainty exists within the collection of all bathymetric data, but steps were taken during all of the surveys to minimise these uncertainties. Inaccuracies with GPS measurements were reduced by using Real Time Kinematic dGPS systems with accuracies of < 0.02 m. Variations in the sound velocity of water can lead to inaccuracies in the calculation of water depth, but these were minimised by

taking constant sound velocity measurements at the sensor head that were integrated into the data acquisition, as well as regular sound velocity profiles with a separate probe that could be used to correct the data in post processing. Additionally, bending and twisting of the survey pole that holds the MBES system could cause uncertainty in the data by dynamically changing the offsets between the GPS antenna, Inertial Motion Unit (IMU) and sonar head. These errors are expected to be reasonably small due to the use of stiff survey poles, and even smaller in the 2020 survey as the system used has its IMU located within the same housing as the sensor head, hence no movement is likely. Pole movement was further reduced by thoroughly securing the system to the survey boat with tight fore, aft and lateral straps.

To analyse and account for as much of the remaining uncertainty as possible, the local standard deviations between the depth sounding point cloud and the resulting DEM for 2009 and 2020 where combined to give an estimated minimum level of detection (LoD_{min}; see Section 5.2.10). LoD_{min} was found to be mostly < 0.4 m everywhere except the deep water in the centre of the dredged channel (*Figure 5-24*). LoD_{min} is low in critical areas, for example the scour and the area of deposition in the eastern leg of bifurcation 4b where deposition has been identified (*Figure 5-15*b).

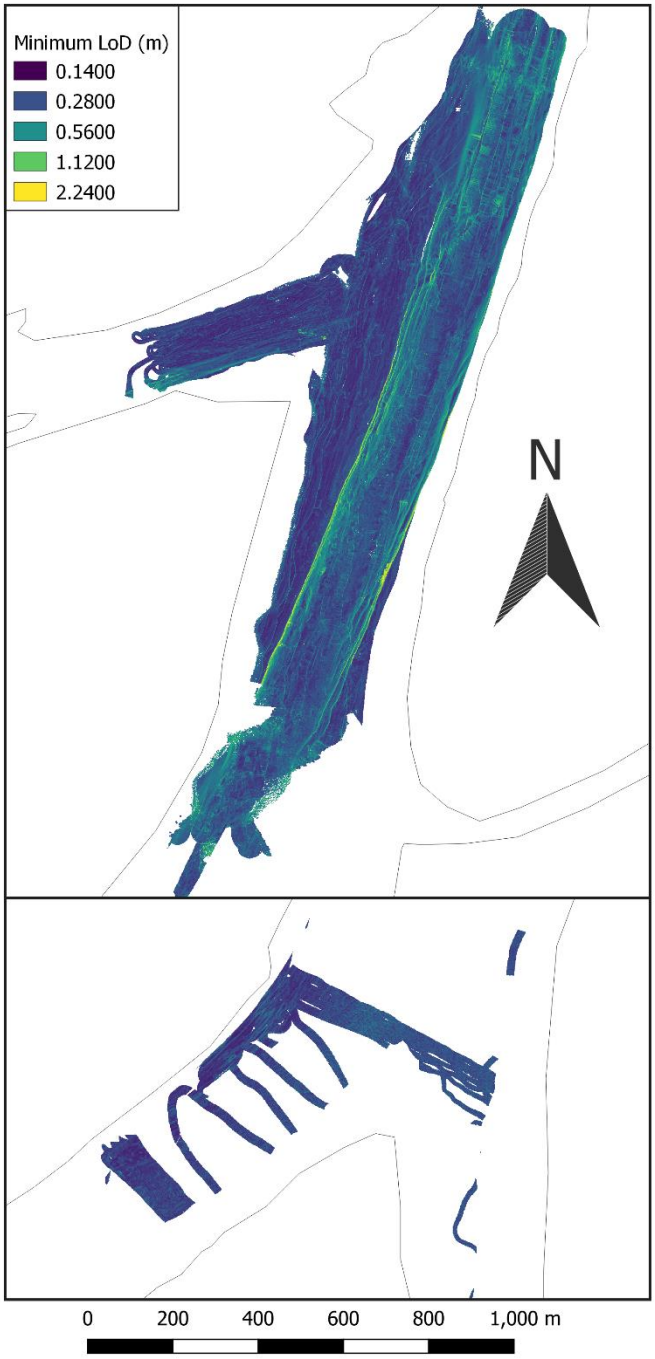

Figure 5-24: The minimum limit of detection, LoD_{min}, of the 2020-2009 DEMoD, for a) the main channel and b) bifurcation 4b.

5.5 Conclusion

This chapter has shown that the bed morphology of the Wax Lake Delta has changed only moderately since its inception, likely as a result of the tough underlying clay reducing the channels' ability to incise downward to increase their capacity. As a result, flow speed remains high in smaller channels, making them less likely to deposit sediment quickly, and hence reduce their own capacity. This could stabilise bifurcations on deltas with resistant underlying sediment, or at least slow the evolution of bifurcations towards channel cutoff.

A variety of both erosional and depositional bedforms were found in the surveyed areas, and their distribution suggested that most channels are either erosional or sediment poor, with deposition limited to areas of the delta downstream of the dominant western trifurcation distributary. Discharge ratios from bifurcation legs suggest that the division of water and sediment through the bifurcations is changing over time, though further monitoring of these division ratios would be necessary to extract the temporal change from the effects of the varying discharge of the Wax Lake Outlet.

Overall, the much WLD system displays signs of being bed sediment limited or erosive in many of its channels. However, the delta is known to be one of the fastest prograding areas of the southern USA coast, suggesting that sediment must be being transported to the distal parts of the delta where it can be deposited to form new land. This could be a result of sediment reaching the delta only in isolated events separated by periods of low sediment supply, or because the delta system is capable of building land with sediment transported in

suspension at only a fraction of its overall capacity, but determining this would once again require further, more regular study of the delta system.

5.6 References

Agrawal, Y. C. and Pottsmith, H. C. (2000) 'Instruments for particle size and settling velocity observations in sediment transport', *Marine Geology*, vol. 168, no. 1–4, pp. 89–114 [Online]. DOI: 10.1016/S0025-3227(00)00044-X.

Allen, Y. C., Couvillion, B. R. and Barras, J. A. (2012) 'Using Multitemporal Remote Sensing Imagery and Inundation Measures to Improve Land Change Estimates in Coastal Wetlands', *Estuaries and Coasts*, vol. 35, no. 1, pp. 190–200 [Online]. DOI: 10.1007/s12237-011-9437-z.

Andreotti, B., Claudin, P., Devauchelle, O., Durán, O. and Fourrière, A. (2012) 'Bedforms in a turbulent stream: Ripples, chevrons and antidunes', *Journal of Fluid Mechanics*, vol. 690, pp. 94–128 [Online]. DOI: 10.1017/jfm.2011.386.

Andreotti, B., Claudin, P. and Douady, S. (2002) 'Selection of dune shapes and velocities part 2: A two-dimensional modelling', *European Physical Journal B*, vol. 28, no. 3, pp. 341–352 [Online]. DOI: 10.1140/epjb/e2002-00237-3.

Anon (n.d.) 'Observed Water Levels at 8764227, LAWMA, Amerada Pass, LA', *NOAA Tides and Currents* [Online]. Available at https://tidesandcurrents.noaa.gov/waterlevels.html?id=8764227&units=metric&bdate=20200228&edate=20200305&timezone=GMT&datum=STND&interval=6&action (Accessed 19 November 2021).

Blott, S. J. and Pye, K. (2001) 'Gradistat: A grain size distribution and statistics package for the analysis of unconsolidated sediments', *Earth Surface Processes and Landforms*, vol. 26, no. 11, pp. 1237–1248 [Online]. DOI: 10.1002/esp.261.

Bolla Pittaluga, M., Coco, G. and Kirwan, M. L. (2015) 'A unified framework for stability of channel bifurcations in gravel and sand fluvial systems', *Geophysical Research Letters*, vol. 42, no. 18, pp. 7521–7536 [Online]. DOI: 10.1002/2015GL065175.

Bolla Pittaluga, M., Repetto, R. and Tubino, M. (2003) 'Channel bifurcation in braided rivers: Equilibrium configurations and stability', *Water Resources Research*, vol. 39, no. 3, pp. 1–13 [Online]. DOI: 10.1029/2001WR001112.

Bryant, W. R. and Trabant, P. K. (1972) 'Statistical Relationships Between Geotechnical Properties of Gulf of Mexico Sediments', *Offshore Technology Conference*, vol. Paper Numb.

Collier, J. S. and Brown, C. J. (2005) 'Correlation of sidescan backscatter with grain size distribution of surficial seabed sediments', *Marine Geology*, vol. 214, no. 4, pp. 431–449 [Online]. DOI: 10.1016/j.margeo.2004.11.011.

Couvillion, B. R., Beck, H., Schoolmaster, D. and Fischer, M. (2016) 'Land Area Change

in Coastal Louisiana (1932 to 2016)', *U.S. Geological Survey Scientific Investigations Map 3381* [Online]. Available at https://doi.org/10.3133/ sim3381.

Czuba, J. A., Best, J. L., Oberg, K. A., Parsons, D. R., Jackson, P. R., Garcia, M. H. and Ashmore, P. (2011) 'Bed morphology, flow structure, and sediment transport at the outlet of Lake Huron and in the upper St. Clair River', *Journal of Great Lakes Research*, Elsevier B.V., vol. 37, no. 3, pp. 480–493 [Online]. DOI: 10.1016/j.jglr.2011.05.011.

Edmonds, D. A., Shaw, J. B. and Mohrig, D. (2011) 'Topset-dominated deltas: A new model for river delta stratigraphy', *Geology*, vol. 39, no. 12, pp. 1175–1178 [Online]. DOI: 10.1130/G32358.1.

Edmonds, D. A. and Slingerland, R. L. (2008) 'Stability of delta distributary networks and their bifurcations', *Water Resources Research*, vol. 44, no. 9, pp. 1–13 [Online]. DOI: 10.1029/2008WR006992.

Finotello, A., Ghinassi, M., Carniello, L., Belluco, E., Pivato, M., Tommasini, L. and D'Alpaos, A. (2020) 'Three-Dimensional Flow Structures and Morphodynamic Evolution of Microtidal Meandering Channels', *Water Resources Research*, vol. 56, no. 7, pp. 1–22 [Online]. DOI: 10.1029/2020WR027822.

Fisk, H. N. (1952) *Geological Investigation of the Atchafalaya Basin and the Problem of Mississippi River Diversion: Volume 1*,.

Hackney, C. R., Darby, S. E., Parsons, D. R., Leyland, J., Best, J. L., Aalto, R., Nicholas, A. P. and Houseago, R. C. (2020) 'River bank instability from unsustainable sand mining in the lower Mekong River', *Nature Sustainibility*, vol., no.

Heinrich, P., Snead, J., Peele, R. H., Massom, M. B., Renken, K. A., Paulsell, R. L. and Pond, L. G. (2012) 'Atchafalaya Bay 30 x 60 Minute Geologic Quadrangle', *Louisianna Geological Survey*.

Hiatt, M. R. (2013) 'A network-based analysis of river delta surface hydrology : An example from Wax Lake Delta', *PhD Thesis* [Online]. Available at https://repositories.lib.utexas.edu/handle/2152/22850.

Iwantoro, A. P., van der Vegt, M. and Kleinhans, M. G. (2021) 'Effects of sediment grain size and channel slope on the stability of river bifurcations', *Earth Surface Processes and Landforms*, pp. 1–15 [Online]. DOI: 10.1002/esp.5141.

Kim, W., Mohrig, D., Twilley, R., Paola, C. and Parker, G. (2009) 'Is it feasible to build new land in the Mississippi River Delta?', *Eos*, vol. 90, no. 42, pp. 373–384.

Kleinhans, M. G., Ferguson, R. I., Lane, S. N. and Hardy, R. J. (2013) 'Splitting rivers at their seams: Bifurcations and avulsion', *Earth Surface Processes and Landforms*, vol. 38, no.

1, pp. 47–61 [Online]. DOI: 10.1002/esp.3268.

Kleinhans, M. G., Jagers, H. R. A., Mosselman, E. and Sloff, C. J. (2008) 'Bifurcation dynamics and avulsion duration in meandering rivers by one-dimensional and three-dimensional models', *Water Resour. Res.*, vol. 44, p. W08454.

Kolb, C. and Van Lopik, J. (1958) 'Geology of the Mississippi River Deltaic Plain – southeastern Louisiana', vol. TR#3-483, no. 3, pp. 3–482.

Maxwell, T. A. and Haynes, C. V. (1989) 'Large-scale, low-amplitude bedforms (Chevrons) in the Selima sand sheet, Egypt', *Science*, vol. 243, no. 4895, pp. 1179–1182 [Online]. DOI: 10.1126/science.243.4895.1179.

Mazumder, R. (2003) 'Sediment transport, aqueous bedform stability and morphodynamics under unidirectional current: A brief overview', *Journal of African Earth Sciences*, vol. 36, no. 1–2, pp. 1–14 [Online]. DOI: 10.1016/S0899-5362(03)00018-6.

Milan, D. J., Heritage, G. L., Large, A. R. G. and Fuller, I. C. (2011) 'Filtering spatial error from DEMs: Implications for morphological change estimation', *Geomorphology*, Elsevier B.V., vol. 125, no. 1, pp. 160–171 [Online]. DOI: 10.1016/j.geomorph.2010.09.012.

Morris, S. A., Alexander, J., Kenyon, N. H. and Limonov, A. F. (1998) 'Turbidites around an active fault scarp on the Lower Valencia Fan, northwest Mediterranean', *Geo-Marine Letters*, vol. 18, no. 2, pp. 165–171 [Online]. DOI: 10.1007/s003670050064.

Morton, R. A., Bernier, J. C. and Barras, J. A. (2006) 'Evidence of regional subsidence and associated interior wetland loss induced by hydrocarbon production, Gulf Coast region, USA', *Environmental Geology*, vol. 50, no. 2, pp. 261–274 [Online]. DOI: 10.1007/s00254-006-0207-3.

Nickles, C. R. and Pokrefke, T. J. J. (1967) *Wax Lake Outlet Control Structure Atchafalaya River - Hydraulic Model Investigation*, *US Army Corps of Engineers Techincal Report HL-88-29*.

Olliver, E. A. and Edmonds, D. A. (2017) 'Defining the ecogeomorphic succession of land building for freshwater, intertidal wetlands in Wax Lake Delta, Louisiana', *Estuarine, Coastal and Shelf Science*, Elsevier Ltd, vol. 196, pp. 45–57 [Online]. DOI: 10.1016/j.ecss.2017.06.009.

Parsons, D. R., Best, J. L., Orfeo, O., Hardy, R. J., Kostaschuk, R. and Lane, S. N. (2005) 'Morphology and flow fields of three-dimensional dunes, Rio Paraná, Argentina: Results from simultaneous multibeam echo sounding and acoustic Doppler current profiling', *Journal of Geophysical Research: Earth Surface*, vol. 110, no. 4, pp. 1–9 [Online]. DOI: 10.1029/2004JF000231.

Parsons, D. R., Jackson, P. R., Czuba, J. A., Engel, F. L., Rhoads, B. L., Oberg, K. A., Best, J. L., Mueller, D. S., Johnson, K. K. and Riley, J. D. (2013) 'Velocity Mapping Toolbox (VMT): A processing and visualization suite for moving-vessel ADCP measurements', *Earth Surface Processes and Landforms*, vol. 38, no. 11, pp. 1244–1260 [Online]. DOI: 10.1002/esp.3367.

Rouse, L. J., Roberts, H. H. and Cunningham, R. H. W. (1973) 'Satellite observation of the subaerial growth of the Atchafalaya Delta , Louisiana', pp. 405–408.

Salter, G., Paola, C. and Voller, V. R. (2017) 'Control of delta avulsion by downstream sediment sinks', *Journal of Geophysical Research: Earth Surface* [Online]. DOI: 10.1002/2017JF004350.

Shaw, J. B., Ayoub, F., Jones, C. E., Lamb, M. P., Holt, B., Wagner, R. W., Coffey, T. S., Chadwick, J. A. and Mohrig, D. (2016) 'Airborne radar imaging of subaqueous channel evolution in Wax Lake Delta, Louisiana, USA', *Geophysical Research Letters*, vol. 43, no. 10, pp. 5035–5042 [Online]. DOI: 10.1002/2016GL068770.

Shaw, J. B., Mohrig, D. and Whitman, S. K. (2013) 'The morphology and evolution of channels on the Wax Lake Delta, Louisiana, USA', *Journal of Geophysical Research: Earth Surface*, vol. 118, no. 3, pp. 1562–1584 [Online]. DOI: 10.1002/jgrf.20123.

Shlemon, R. J. (1975) 'Subaqueous Delta Formation - Atchafalaya Bay, Louisiana', in Broussard, M. L. (ed), *Deltas: Models for Exploration*, Houston Geol. Soc, Houston, Texas, United States (USA)., pp. 209–221.

Shugar, D. H., Kostaschuk, R. A., Best, J. L., Parsons, D. R., Lane, S. N., Orfeo, O. and Hardy, R. J. (2010) 'On the relationship between flow and suspended sediment transport over the crest of a sand dune, Río Paraná, Argentina', *Sedimentology*, vol. 57, no. 1, pp. 252–272 [Online]. DOI: 10.1111/j.1365-3091.2009.01110.x.

Sime, L. C., Ferguson, R. I. and Church, M. (2007) 'Estimating shear stress from moving boat acoustic Doppler velocity measurements in a large gravel bed river', *Water Resources Research*, vol. 43, no. 3, pp. 1–12 [Online]. DOI: 10.1029/2006WR005069.

Spiske, M., Garcia Garcia, A. M., Tsukamoto, S. and Schmidt, V. (2020) 'High-energy inundation events versus long-term coastal processes – room for misinterpretation', *Sedimentology*, vol. 67, no. 3, pp. 1460–1480 [Online]. DOI: 10.1111/sed.12524.

Szupiany, R. N., Amsler, M. L., Hernandez, J., Parsons, D. R., Best, J. L., Fornari, E. and Trento, A. (2012) 'Flow fields, bed shear stresses, and suspended bed sediment dynamics in bifurcations of a large river', *Water Resources Research*, vol. 48, no. 11, pp. 1–20 [Online]. DOI: 10.1029/2011WR011677.

Vermeulen, B., Sassi, M. G. and Hoitink, A. J. F. (2014) 'Improved flow velocity estimates frommoving-boat ADCP measurements', *Water Resources Research RESEARCH*, vol. 50, pp.

5375–5377 [Online]. DOI: 10.1002/ 2013WR015152.

Vimpere, L., Kindler, P. and Castelltort, S. (2019) 'Chevrons: Origin and relevance for the reconstruction of past wind regimes', *Earth-Science Reviews*, Elsevier, vol. 193, no. December 2018, pp. 317–332 [Online]. DOI: 10.1016/j.earscirev.2019.04.005.

Wilcock, P. R. (1996) 'Estimating local bed shear stress from velocity observations', *Water Resources Research*, vol. 32, no. 11, pp. 3361–3366 [Online]. DOI: 10.1029/96WR02277.

6 Synthesis

6.1 Thematic Context

This thesis aimed to investigate the effects of receiving basin substrate on the morphodynamics of river deltas. Deltas have a critical role in food security (Foufoula-Georgiou, 2013), carbon cycling (McLeod et al., 2011), coastal resilience (Barbier et al., 2013; Kathiresan and Rajendran, 2005) and biodiversity, but are threatened by a range of anthropogenic factors such as rapid sea level rise (Nienhuis and van de Wal, 2021; Ericson et al., 2006), upstream land use change and sediment trapping (Dunn et al., 2019) and sand mining (Hackney et al., 2020).

Multiple studies have already shown that more cohesive fluvially supplied sediment can lead to deeper, more stable delta channels with high, solid levees (Burpee et al., 2015; Caldwell and Edmonds, 2014; Edmonds and Slingerland, 2010) with implications for morphodynamics, morphology and sedimentology of deltas systems. Geleynse et al. (2011) expanded this to receiving basin substrates and found that a delta substrate made of a higher proportion of fine, unconsolidated sediment (τ_{ce} = 0.5 N m^{-2}) resulted in more vertical erosion, and so deeper, more sinuous channels when compared to a substrate composed primarily of sand. Other than this, however, little attention had been given to the effects of the receiving basin substrate characteristics on delta formation. This thesis has investigated the effects of increasing the cohesivity of substrate sediment (τ_{ce} = 0.25-12.5 N m^{-2}; Chapter 3), and the combined effects of fine sediment cohesivity and dominant sediment grainsize (Chapter 4) in determining delta morphology and morphodynamics.

The numerical models described in previous Chapters show that deltas that form over resistant substrates have higher altitude delta tops and larger areas of subaerial land (as long as they are supplied with sufficient sediment) than those forming over softer sediment. Reducing the τ_{ce} of the cohesive sediment in substrates that consist mostly of fine sediment decreases the mobility of channels (Figure 3-12). However, if the fraction of cohesive sediment is reduced with τ_{ce}, channel mobility increases instead (Figure 4-11), in a similar way to that seen when fluvial cohesive sediment fraction was reduced in the study of Caldwell and Edmonds (2014). This suggests that cohesive sediment proportion is a stronger influence on channel mobility than τ_{ce}, as it is able to overcome the competing effect of τ_{ce}, when both are varied together. Sediment starvation dramatically reduces delta growth and the mobility of channels, but deltas that form over harder substrates, or that had a less cohesive fluvial sediment supply (previous to sediment shut-off) retained channel mobility by reworking already deposited sediment across the delta top.

Chapters 3 and 4 also found that increasing substrate sediment τ_{ce} decreased the depth of delta channels, even when τ_{ce} is increased in parallel with an increase in fines (as in Chapter 4), despite the fact that Geleynse et al. (2011) found increasing fines content in a delta substrate would increase channel depth. This indicates that, in contrast to what was found for channel mobility, τ_{ce} is a stronger influence on channel depth than cohesive sediment content in the supplied fluvial flux.

To draw useful comparison for the modelling study, fieldwork on the Wax Lake Delta (WLD), Louisiana, USA was conducted to investigate how a real delta

formed over a substrate that is known to be composed of consolidated clay (Fisk, 1952). Previous studies have already shown the WLD is morphodynamically controlled to a degree by erosion (Shaw and Mohrig, 2014) at subaqueous channel tips, where tidal ebb currents combine with fluvial flow to allow incision in to the resistant substrate. Previous Multibeam Echosounder (MBES) bathymetric studies have revealed that this substrate is exposed over 85% of the channel bottom area (Shaw et al., 2013), suggesting that the WLD is interacting erosively with this substrate. The same study also demonstrated that bedload in the WLD is supply-limited, making the WLD an example of a delta with a resistant substrate currently influenced by below equilibrium sediment supply, and hence a good test case for some of the deltas modelled in Section 4.

Fieldwork using acoustic Doppler current profiler, Laser In-Situ Scattering and Transmissometery and multibeam echosounder bathymetry was conducted in order to investigate the current state and stability of Wax Lake delta (see Section 5). Bifurcation dynamics where analysed as a real world manifestation of the channel mobility investigated in Section 3 and 4, and both DEMs of difference since delta formation and the sediment dynamics at channel beds were analysed to reveal the erosive or depositional nature of the delta system, for comparison with channel depth and incision calculated from models in earlier chapters. MBES bathymetry revealed that many of the channels in the delta have beds covered in either sparse bedforms or erosional marks, suggesting that much of the surveyed area was lacking in bedload. Relatively small depths of channel bed change since the inception of the delta suggests that erosion into the substrate has been limited. Bifurcations on the WLD were found not to conform to the stable equilibrium criteria outlined by Edmonds and Slingerland (2008), despite not

having changed planform dramatically since at least 2009, indicating that avulsions and major changes in channel dominance have not happened within this time. This suggests that either the equilibrium solutions found by Edmonds and Slingerland (2008) do not cover the full range of stable configurations for bifurcations on the WLD, where a cohesive substrate is present, or that any morphodynamic instability that these bifurcations display has not been able to push them to fully avulse in this time period.

6.2 Bifurcation stability dependence on of sediment supply and substrate resistance

As shown in Chapter 5, many of the channels on the Wax Lake Delta flow over erosive, 'bedrock' surfaces characterised by lack of alluvial cover, erosive flutes, and scours. Even where alluvial cover does exist, in the majority of channels, it is in the form of isolated barchan dunes, separated by uncovered bedrock beds, suggesting that the system, or at least most of the area surveyed, is bedload poor. The study of Shaw et al. (2013) found similar bed features, and quantified the exposed hard clay substrate ('bedrock') as covering 85% of the delta as a whole, and all of some areas (East, Campground and Mallard Passes). Shaw et al. (2013) also found that flow through the delta channels was sediment under-saturated (or supply-limited) by between 1 and 4 orders of magnitude, likewise suggesting that many channels on the WLD are sediment poor.

Additionally, in Section 5, it was found that some of the surveyed bifurcations plotted away from the equilibrium functions presented in Edmonds and Slingerland (2008). This would suggest that these bifurcations are not in a stable equilibrium. However, as the delta has not greatly changed planform since

at least 2009 (earth observation suggests much longer stability >40 years), these bifurcations being very unstable seems unlikely as well. This would suggest that the equilibrium profiles developed by Edmonds and Slingerland (2008) do not account for all of the drivers present in the case of the Wax Lake Delta. It was found in Section 4 that being sediment deficient, and delta growth over a resistant substrate were two factors that strongly increased the timescale of channel movement (and hence, directly impacting stability). Given that Wax Lake Delta is deficient in bedload, and that it is known to have formed with channel bottoms interacting with the underlying stiff, pro-delta muds, it could be possible that bifurcations on this delta are being made stable at Θ and Q_r values other than those found by Edmonds and Slingerland (2008).

Edmonds and Slingerland (2008) did find that some physical characteristics of the bifurcation, such as the upstream width:depth ratio and Chezy coefficient, could affect the positions of the equilibrium solutions. This was supported by the study of Iwantoro et al. (2021), which reiterated the effect of channel width:depth ratio, and highlighted that both sediment calibre and channel slope can change the position of equilibrium solutions. Given this, it seems likely that channel bed erodibility and sediment load could also adjust which values of Θ and Q_r are necessary for bifurcations to be in stable equilibrium.

As shown in Sections 3 and 4, higher substrate resistance decreases the ability of delta channels to deepen by vertical erosion. This erosion is a destabilising mechanism that allows the dominant channel to increase its capacity for water and sediment transport at the expense of the non-dominant channel. It has been demonstrated that when erosion is precluded in bifurcation

distributaries by bed armouring and sediment immobility, bifurcations that would be considered unstable based on mathematical stability analysis can be stable (Kleinhans et al., 2007). This is proposed by Kleinhans et al. (2013) to be a result of an resistant sediment on the bed of the larger channel preventing that channel from becoming bigger and capturing more flow.

As such, bifurcations on deltas forming over very resistant substrates may be more stable, as if erosion is diminished as a driver of instability, sediment deposition in the non-dominant channel and the resulting reduction in discharge capacity, would be the sole mechanism to increase asymmetry. This would be expected to either preclude or slow total avulsion of an unstable bifurcation, or decrease the frequency of oscillation in quasi-stable bifurcations. In bifurcations formed over substrate of moderate erodibility, the threshold for erosion, and hence deepening of the dominant channel, may only be reached during peaks in discharge and erosive power, resulting in these bifurcations being stable unless floods are able to overcome this threshold.

This similar to the concept of geomorphically effective floods proposed by Costa and O'Connor (1995), in which floods are analysed in terms of the time and magnitude of a hydrograph in which flow is above the threshold of erosion for the channel bed, and hence the total energy available to change the stream's morphology (see example *Figure 6-1*). In a bifurcation, increasing bed resistance would raise the erosion threshold, and so reduce the total amount of energy available for erosion, and so the magnitude and frequency of morphodynamic change. It may also lead to deltas forming in which the stability of symmetrical bifurcations is enhanced, as neither of the evenly split channels have enough

erosive power to begin incision, leading them to become stuck in a symmetric, stable state more easily. However the stability of highly asymmetrical channels would remain as predicted, as the large dominant channel still has sufficient erosive power to incise. Furthermore, as *Figure 6-1* demonstrates "flashier" hydrographs with higher peaks that last for shorter periods could potentially produce more morphodynamic change than longer, slightly lower peaks in systems with high thresholds for erosion. These short periods of morphodynamic change may allow one distributary of a symmetrical bifurcation to enlarge enough to make the bifurcation more asymmetric, and hence potentially less stable.

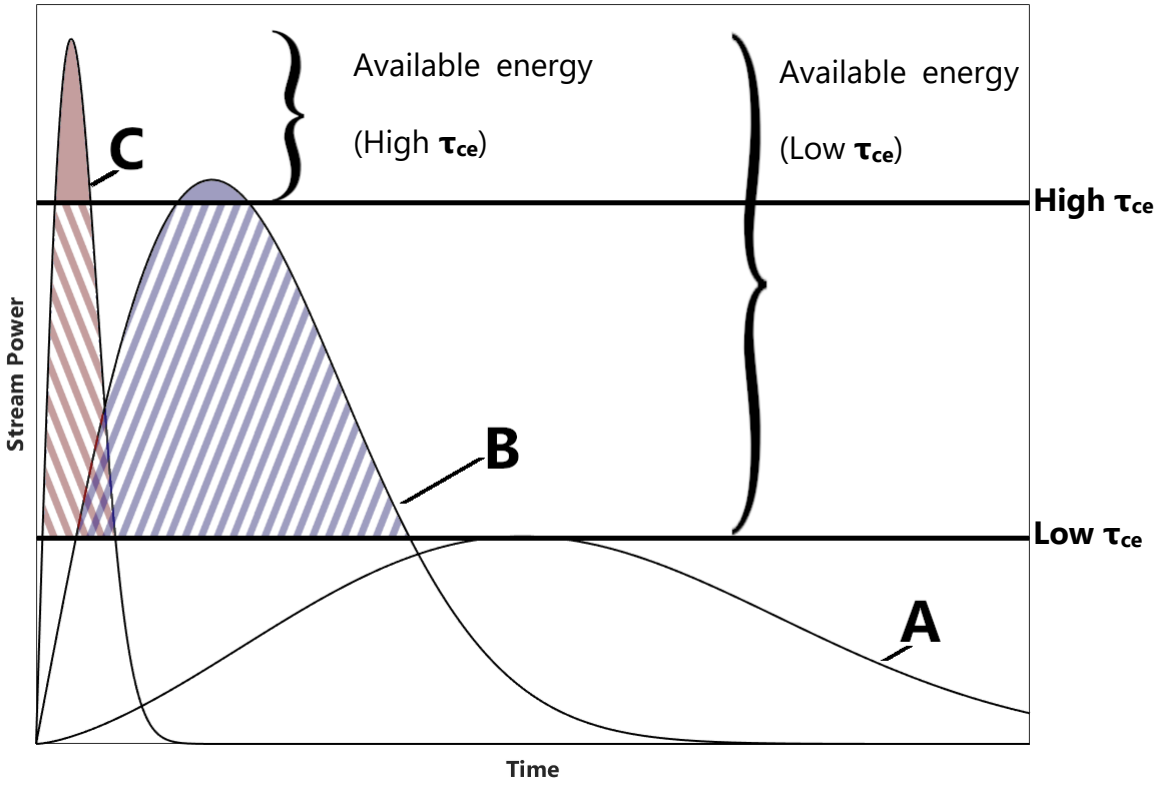

Figure 6-1: Stream power hydrograph demonstrating the concept of Geomorphically Effective Flows, reproduced from Costa and O'Connor (1995), Fig. 11. Solid fill shows energy available for geomorphic change at high τ_{ce}, while diagonal fill shows energy available for geomorphic change at low τ_{ce}.

The deposition of sediment acts as both a driving (through in-channel deposition reducing channel capacity (Kleinhans et al., 2013)) and restoring (as downstream deposition and channel lengthening cause a backwater effect that makes a distributary less favourable (Salter et al., 2017)) force in bifurcation stability. As such, bifurcations that have their sediment supply reduced could experience slower avulsion (in unstable bifurcations) as non-dominant channel beds aggrade, and hence loose capacity, more slowly. Equally, slower channel aggradation downstream of the dominant channel would be expected to reduce the restoring force and decrease the frequency with which a semi-stable bifurcation switched dominant channels. It is possible that this could lead to a semi-stable, switching bifurcation fully avulsing, if sediment supply is not sufficient to cause a backwater effect capable of overcoming the effects of increasing capacity in the dominant distributary.

If sediment supply is shutoff entirely, bifurcations with resistant beds may be forced into becoming stable, as no sediment is being delivered to drive switching behaviours. This would be consistent with the results of models used by Salter et al. (2017), who found that bifurcations could be frozen in a symmetric or asymmetric state by the removal of the effects of sediment deposition by imposing a 'bypass' condition in which all sediment that flowed downstream of the bifurcation was removed from the model instead of being deposited. In Chapter 4 of this study, deltas influenced by sediment starvation were shown to have increased channel residence times and a delta top populated by a higher number of channels (see Figure 4-13). As discussed in section 4.4.1, this could be a result of bifurcations being more stable, increasing channel residence times by fully avulsing less often, which would also increase the number of channels on the

delta top by keeping both distributaries open rather than cutting one off. The reduction in deposition caused by sediment shutoff, as described above, would give a suitable explanation for that finding.

In Chapter 4, deltas with topsets formed of coarser sediment and underlain by less resistant substrate were shown to experience less reduction in channel mobility as a result of sediment starvation, compared to deltas built with finer, more cohesive sediment or underlain by harder substrates. This was attributed to the channels being able to rework the sediment in these cases to continue morphodynamic processes within the channels. Potentially, this could extend to bifurcations as well by replacing allogenic (upstream) sediment no longer supplied from the catchment with autogenic sediment eroded from the upstream channel. The effects of autogenic sediment use in deltas is discussed in more detail below, in Section 6.4.

In summary, this thesis and the studies presented above suggest that both sediment supply reduction and resistant beds reduce the rates of morphodynamics in bifurcations, and so the frequency with which either complete or 'soft' avulsions happen. However, this also predicts that sediment starvation could raise the likelihood of complete avulsion (decrease stability) by removing the restoring force of sediment deposition in the dominant channel. Inversely, resistant substrates lower the likelihood of avulsion (increasing stability) by slowing vertical erosion and capacity gain in the dominant channel, giving more time for sediment deposition cause a backwater effect sufficient to divert flow down the other channel. The increased stability caused by hard substrates and the slowing of morphodynamic processes caused by both the effects

described above could help explain the apparent stability of the WLD despite it not fitting established stability criteria (Edmonds and Slingerland, 2008). As discussed in Section 5, a number of physical factors, including upstream channel aspect ratio, Chezy number, (Edmonds and Slingerland, 2008), sediment grainsize and channel slope (Iwantoro et al., 2021), can change the Θ - Q_r locations of the equilibrium solutions. Many of these properties are unconstrained in the modelling and field studies presented in this study, and sufficient variation in them could generate considerable uncertainty in the position of any equilibrium solutions. As such this thesis does not try to draw a new equilibrium profile, but instead demonstrates the likelihood that both sediment load and channel bottom resistance can move the location of these solutions, much as the above qualities do. More modelling and field studies, focussed on the effects of substrate and sediment supply, are necessary to properly constrain these effects.

6.3 Substrate erodibility: The distinction between cohesive sediment τ_{ce} and sediment cohesive fraction

By comparing the results of Sections 3 and 4, it can be seen that a change in cohesive sediment τ_{ce} of delta substrate does not affect the morphodynamics of a delta (especially channel mobility) in the same way as a change in cohesive sediment τ_{ce} *and* sediment cohesive fraction of delta substrate. This would suggest that sediment cohesive fraction, which was varied in Section 4 but held constant in Section 3, is the driver of this difference in behaviour. Increasing the fraction of cohesive sediment in the fluvial supply to deltas has been shown in a number of modelling studies to reduce channel mobility (Caldwell and Edmonds, 2014; Edmonds and Slingerland, 2010). In these studies, the reduction in channel

movement is attributed to the cohesive sediment forming more stable levees that resist channel avulsion. However, in both of these studies, the basin substrate consisted of the same sediment as the fluvial supply, meaning that the relative effect of substrate and fluvial sediment cannot be distinguished.

In Section 3, delta substrate is held at a constant 80% cohesive sediment, corresponding to deltas close to the highest cohesivity deltas modelled in the studies of Caldwell and Edmonds (2014) and Edmonds and Slingerland (2010) which were found to have low channel mobility. When τ_{ce} is increased, the ability of channels to erode vertically (Figure 3-8), and hence the average channel depth (Figure 3-10) was reduced, and the relative increase in riverbed elevation and hence super-elevation of the channel above the surrounding land was increased. This was interpreted as a forcing which resulted in an increased mobility of channels by increasing the favourability of avulsion.

In Section 4, hard substrates were found to act similarly to those in Section 3; resistant substrates preclude deep incision, increase channel elevation and drive avulsion. However, vertical erosion into the softer, predominantly sand "low resistance" substrate used in Section 4 was found to be more difficult than in to the predominantly fine, low τ_{ce} substrates in Section 3. Sand has a higher critical velocity for initiation of motion and is more easily redeposited as bedload that armours the channel bottom. As a result of this, a shift from "hard" to "soft" beds analysed in Section 4 deepens channels by only ~100% (as opposed to 200-300% as seen in Section 3) and causes them to become thinner, instead of wider as seen in Section 3. It is possible that – as sandy bedload is continually re-deposited and re-eroded, rather than being transported directly to the delta's foreset in wash

load – channels can more easily continue the morphodynamic processes (aggradation, channel lengthening and erosion) that maintain channel mobility and the switching behaviour of bifurcations (Salter et al., 2017). In contrast, within deltas with predominantly fine and low τ_{ce} substrates (presented in Section 3), channels become deep and wide, build strong levees, and avulse rarely, while on deltas with fine and high τ_{ce} substrates (presented in Sections 3 and 4), channels are shallower, and avulsion occurs slightly more frequently as channels are naturally elevated due to limited vertical erosion.

6.4 Implications for the classical Galloway/Orton-Reading Ternary model for deltas

The first model to describe deltas in terms of three competing forces – rivers, waves and tides – was proposed by Galloway (1975). This model was modified by Orton and Reading (1993) to include the morphodynamic effect of sediment grainsize, and how this effect is modulated by tidal and wave energy, in a four membered conceptual model. The effects of fluvial sediment have since been quantified in more detail, both in terms of sediment cohesivity (Edmonds and Slingerland, 2010) and the grainsize distribution (Caldwell and Edmonds, 2014).

The investigations in this thesis highlight that it may be necessary to distinguish between the effects of sediment supplied from the catchment and transported within a channel and the effects of the sediment that the delta topset is made of. The results of Section 4 suggest strongly that these two effects are not the same; when fluvially transported sediment was removed, the effects of sediment cohesive fraction on delta morphodynamics changed, in some cases inverting trends observed in deltas with a constant sediment supply.

These differences may also emerge from the effects of the patterns of sediment deposition, such as deposition of fluvially supplied sediments in bifurcation channels (Kleinhans et al., 2013), at delta mouths (Edmonds and Slingerland, 2007), and on levees. At these locations the impacts are more profound, suggesting that morphodynamics in systems with *allogenic* sediment sources (i.e. sediment sourced mostly from the upstream catchment) are largely dependent on how and where the sediment is deposited. In cases where these systems do erode, it is generally the erosion of recently deposited sediment, such as in mouth bar progradation and dune movement. In the case of sediment poor systems, in which much of the sediment is sourced *autogenically* from within the delta system itself, the controlling factors become erosive and so more dependent on the erodibility of sediment. This may explain the trends seen in Section 4, where an increasing proportion of fluvial cohesivity changed from decreasing width and increasing depth of channels in deltas with constant sediment supply to increasing width and decreasing depth when that sediment supply is removed.

This effect is worth considering as part of the Orton-Reading model, as especially with fine, cohesive sediment, the shear stress or velocity thresholds for deposition and erosion, and hence their behaviours within either a channel or delta topset, can differ by orders of magnitude. Additionally, due to differences in settling velocity and critical velocity for deposition, delta topsets are generally enriched in courser sediment, as it is deposited more proximally while finer sediment is washed further out to distal foresets, meaning the sediment transported in a channel is not always the same as the sediment of the bed and banks of the channel. This highlights that the effects of sediment in a delta is

potentially very different depending on if the system is reliant on allogenic and autogenic sediment.

This thesis has shown that the cohesive proportion and cohesive sediment $\boldsymbol{\tau_{ce}}$ of substrate can set the morphodynamics of deltas and modulate or override the effects of fluvial sediment cohesivity. As not all deltas will form over sediment substrates that are identical to the sediment supplied to them, this factor is also worth considering alongside fluvial and topset sediment represented in the Orton-Reading model. However, as stated in Section 6.3, the relationship between substrate type and morphodynamics is not simple but is made up of the influence both cohesive sediment proportion and cohesive sediment τ_{ce}.

Conceptually, these combined sediment factors could be split across two axes. Firstly, the combined effects of all the sediment present within the delta can be considered in terms of its morphodynamic activity, with sediment more likely to be eroded and deposited repeatedly considered active, and sediment unlikely to go through these processes repeatedly considered inert. For the models conducted within Section 4, those with sand-dominated fluvial supplies (and hence topsets) and softer, sandier substrates could be considered more morphodynamically active systems (the fine sand modelled in these runs is relatively easy to erode, but also frequently deposited, and much of it is carried in bedload), while those with finer, more cohesive fluvial supplies (and hence topsets) and less erodible substrates would be considered morphodynamically inert (the high τ_{ce} mud fraction is difficult for the system to erode, and when it is eroded it is likely carried in suspension to the distal parts of the delta rather than being redeposited) (see Figure 6-2).

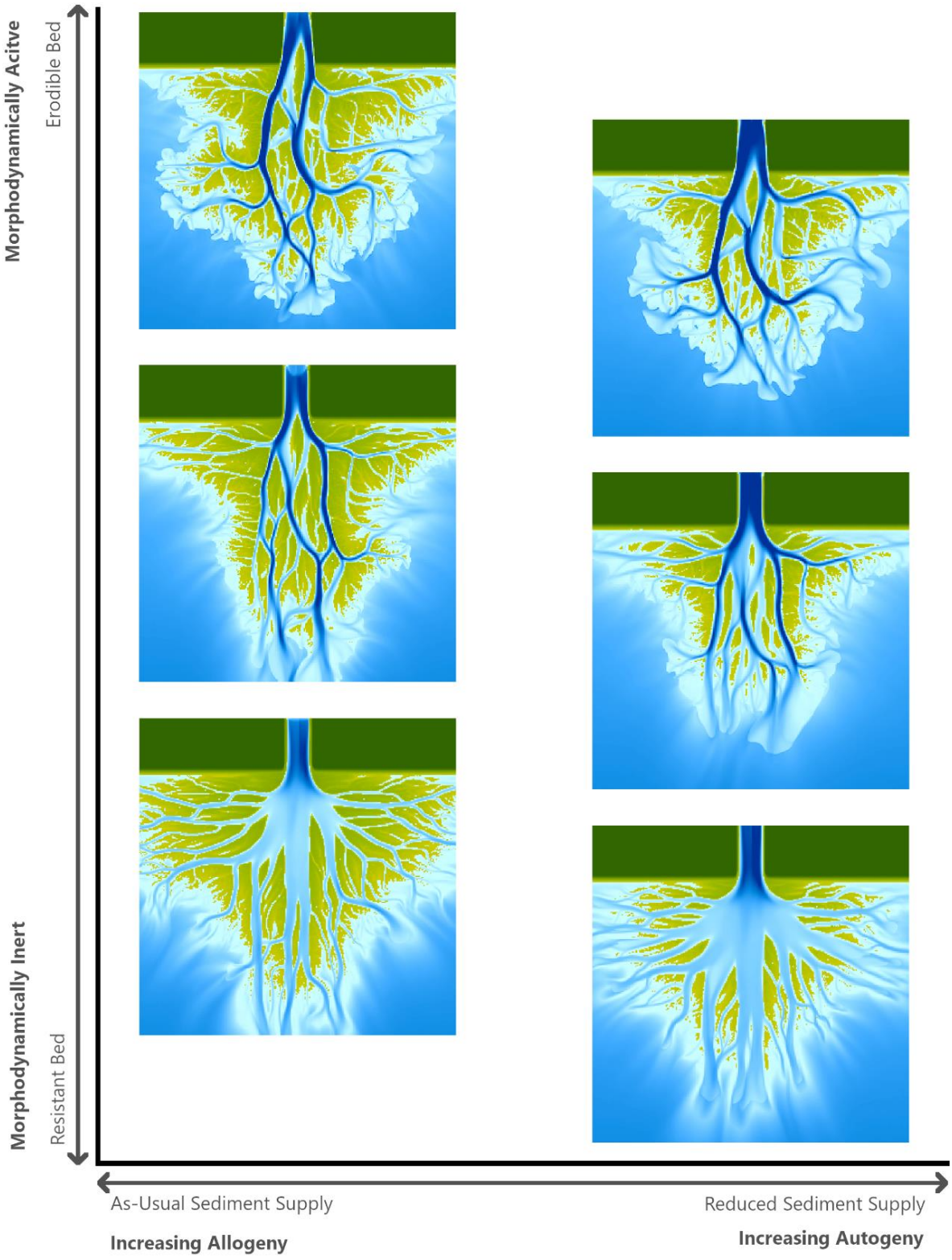

Figure 6-2: *Conceptual diagram of delta morphodynamic pliability against sediment source type.*

Secondly, as mentioned above, deltas with flows that are under-saturated in sediment, such as those undergoing sediment starvation, have excess erosive power and rework sediment already present within them, and so more of their sediment supply is autogenic. Inversely, those with sediment saturated flows mainly deposit sediment as the system progrades rather than eroding, and thus much of the morphodynamically activity on the delta involves allogenically derived sediment (see Figure 6-2). When the systems modelled in Section 4 are assessed in this way, it becomes obvious, from both Figure 6-2 and earlier figures in Section 4 (4-9, 4-10 and 4-11), that more morphodynamically active systems are effected less by a change from allogenic to autogenic sediment than systems that are more morphodynamically inert. This is likely due to the inability of the inert systems to effectively generate autogenic sediment that can continue the morphodynamic processes present on the delta before the allogenic sediment supply was reduced. In light of this, the harder underlying substrate sediment of the WLD, combined with its under-saturated sediment supply (Shaw et al., 2013), suggest that the WLD may be at risk of dramatic morphodynamic change into the future given ongoing changes.

When sediment was added to the Galloway ternary diagram by Orton and Reading (1993), it was considered in the context of its interactions with the other three axes – tides, waves and river input – rather than as an independent axis. Both the interactions discussed in this section expand on this, demonstrating that sediment qualities must be described as multiple axes on this model which differentiate between fine sediment τ_{ce}, and sediment grainsize distribution, and

between sediment in the active channel, on the delta topset and in the substrate. However, these factors are not independent; sediment grainsize has a role in setting the cohesivity and hence τ_{ce} of a sediment, and delta topsets are deposited from fluvial sediment, and are frequently underlain by earlier deposits from the same river system.

Section 4 shows that these factors influence each other by demonstrating the interaction between fluvial cohesivity, and the cohesive sediment fraction and cohesive sediment $\boldsymbol{\tau_{ce}}$, but many of the intricacies of these interactions are still unknown (such as how selective erosion and deposition are affecting the relative grainsize distributions between topset and channel, or how consolidation could change the $\boldsymbol{\tau_{ce}}$ of fine sediments between their initial deposition and becoming overlain by other delta lobes). Due to the uncertainty around, and the nonlinear nature of, these interactions, as well as data paucity around the sediment qualities of delta substrates, this thesis does not attempt to add another axis to the Orton-Reading ternary model, but instead highlights the importance of considering the relative effects of allogenic and autogenic sediment and acknowledges the need for more work in this area to better constrain this.

6.5 Implications for interpreting the sedimentology of ancient deltas

Due to being large, deposition-driven features, deltas are frequently found in the stratigraphic record, and are important as indicators used to reconstruct the paleo-environment of their catchment. As with modern deltas, the sediment underlying them is frequently neglected, despite being arguably easier to assess than in contemporary deltas for a number of reasons. First, unlike features such

as river upstream basin qualities or flow regime, the underlying sediment type can be directly observed, as it is buried, consolidated and likely lithified, hence well preserved beneath the delta. While the exact resilience of the substrate could not be measured (in terms of a τ_{ce} for example), the grain size and material type would be easily attainable and could shed light on the erodibility. Additionally, erosive contacts between the channel and the substrate will also be well preserved, potentially shedding light on the extent of erosion within the channels

All of the delta's modelled in this thesis had shallow basins, such that the channel bottoms where interacting with the basin substrate across most of their length, and as such they all had h/f ratios (the ratio between basin water depth and channel depth) of >1, making them topset-dominated deltas (Edmonds et al., 2011). As most of the morphodynamic effects of delta substrate are caused when channels begin to erode into the substrate, foreset-dominated deltas with h/f <1 are unlikely to be greatly affected by substrate qualities. This excludes, the Cretaceous Last Chance Delta (a well-known fossil delta), as stratigraphic examples of delta-substrate interaction, as it is thought to have formed in a 10-30 m deep basin, and hence be foreset dominated.

Delta deposits that formed over low τ_{ce} fine substrates will have few channels that are incised deeply into their substrates. Infrequent overland flow in these systems could decrease the overall amount of sediment in the topset, which is instead routed to the channel mouths where it is deposited on the delta front. Deltas that formed over low τ_{ce} but more course grained substrates will contain more numerous channels, which Burpee et al. (2015) found led to a more consistent clinoform dip direction by distributing sediment more evenly around

the delta perimeter. These channels would be cut into the substrate, but not as dramatically as those formed over fine and soft substrates. Delta deposits forming over fine, high $\boldsymbol{\tau}_{ce}$ substrates would have channels that eroded only slightly into the substrate. The shallower channels caused by this led to frequent overland flow, and so much of the sediment is deposited on the delta top, rather than the foresets.

Ultimately, assessment of the interaction between paleodeltas and their substrates are difficult to make given preservation and exposure limitations of examples of delta channels incised into pro-delta sediments and reporting of erosional interactions between deltas and their substrates is scarce.

6.6 The effects of uncertainty

River deltas are highly dynamic systems, forming from the convergence of many competing factors. As such, even though this study comprised of 219 numerical model runs and two field campaigns, it cannot account for every type of delta. The deltas modelled here represent ones forming in relatively quiescent basins (in the absence of tides and waves), with variable flow regimes and predominantly fine sediment loads. Additionally, as the resolution of the models was on the order of 10s of metres (30 m and 25 m for the Chapter 3 and 4 models respectively), this represents the minimum size of channels that could be represented by the model, and also identified by the channel finding algorithm. This means that some smaller channels may be unaccounted for. While finer resolution models may have been preferable for simulating these smaller channels, the minimum grid size was limited by computational time and stability considerations.

The numerical modelling in this study was also limited by the use of τ_{ce} as a control on erodibility, and of the Partheneides-Krone bed boundary condition to control the erosion of cohesive sediment. As discussed in sections 2.4.3, 3.4.2 and 4.4.2, the Partheneides-Krone condition neglects the processes of fluid mud mixing and mass erosion in cohesive sediment beds, and uses only a single threshold of erosion controlled solely by the τ_{ce} of the bed material. This means that in situations where bed shear stress is high or when bed strength is low, the simulation will likely underestimate the speed of erosion. In Chapter 4 these conditions where most likely to occur in deltas forming over medium strength substrates as these substrates contained sufficient cohesive sediment for the Partheneides-Krone equation to strongly control erosion, and the cohesive sediment was easily eroded enough to be vulnerable to mass erosion. In chapter three, it is likely that the effect of the Partheneides-Krone formulation was strongest at the centres of channels in lower-mid τ_{ce} substrates, where erosive power sufficiently exceeds bed resistance to create the conditions for mass erosion. This means that models in chapter 3 could have underestimated channel depth.

In Chapter 5, much of the uncertainty existed within the bathymetric surveys, where several factors (e.g. GPS error, water sound velocity, flexure of the survey rig) have likely contributed to variability within the values of depth soundings. However, the design of this study sought to reduce this uncertainty as far as possible, by performing multiple overlapping survey passes and averaging many (frequently >100) sounding points to define the depth of a single DEM grid square, and then to quantify the remaining uncertainty using techniques described in (Milan et al., 2011). This quantification allowed more certain analysis

of bathymetric chance from 2009-2020 by identifying which changes where likely to be products of depth uncertainties, and which were likely to be real morphological changes.

The depth data for 1935, however, likely had much higher uncertainties which could not be quantified, as much of the metadata for the 1935 DEM has been lost. The author could find no record of the collection method or on the expected error of the data. Historical datasets frequently have large uncertainties associated with their use, as a result of the data or metadata being partially lost, being collected using methodologies no longer considered accurate, being referenced to a datum that has moved or been lost, or any combination of the above. However (as is frequently the case with historical datasets used in modern studies) the 1935 dataset offers a unique and important opportunity to compare the current conditions with previous conditions that differ dramatically. As such, this study chose to use the 1935 data while acknowledging the uncertainty of the measurements with a conservative estimate of depth error.

Another limitation of this study comes when comparing the modelled deltas in Chapters 3 & 4 to the field data collected in Chapter 5. Due to the different techniques used, the simulated and real-world deltas were necessarily quantified in different ways; for example, the channel mobility algorithm used velocity and depth data with high temporal resolution to quantify the speed at which channels moved from their positions, but this data was not available for the Wax Lake delta. Equally, the field survey was able to visualise the bedforms within the delta channels, but bedforms are not simulated in Delft3D. Additionally, the delta models were designed to be generic representations of deltas, rather than a

simulation of the Wax Lake Delta, and so direct comparison between these sections is made more difficult by differing boundary conditions and influencing factors in any case. As such, rather than direct quantitative comparison between real and modelled deltas, this study compares them qualitatively.

Additionally, as commented on in section 2.4.3 the critical shear stress of erosion, $\boldsymbol{\tau}_{ce}$, can be measured using a great number of methods, each of which give different results, sometimes varying by orders of magnitude. This compounds the lack of field data for sub-delta sediment resistance found in this study, making quantification of the erodibility of delta substrates highly uncertain. In chapters 3 & 4 of this thesis, this was partially remedied by modelling a high range of $\boldsymbol{\tau}_{ce}$, values, but comparison of the modelled deltas with real-world examples is hindered by this uncertainty.

6.7 Conclusions

This study aimed to show how changing sediment grainsize and $\boldsymbol{\tau}_{ce}$ of fines in delta substrates influenced the morphodynamics, stability and resilience of river deltas in the face of diverse anthropogenic changes. The modelling presented here shows that delta substrates have a dramatic effect on delta morphology, and in many of the modelled cases this influence was greater than that of the fluvial sediment. Deltas formed with morphodynamically 'active' sediment in their substrates and topsets were shown to be more resilient to the loss of their sediment supply than those with formed of morphodynamically 'inert' sediment. Furthermore, it shows that delta sediment type cannot be considered

as a single parameter in determining delta morphodynamics, and instead supplied, delta top and substrate sediment should all be considered separately.

This study highlights the importance of considering receiving basin sediment properties, especially in the context of contemporary anthropogenic stresses to deltas such as relative sea level rise and sediment supply reduction. As sediment supply reduces, the substrate and topset material will become more important in deciding the morphology of deltas. Nienhuis and van de Wal (2021) found that decreasing sediment supply leads to a shift towards tidal and wave driven dynamics – as such, future work exploring how tidal and wave energy interact with delta substrates of different resistances is also likely to be very valuable.

6.8 References

Barbier, E. B., Georgiou, I. Y., Enchelmeyer, B. and Reed, D. J. (2013) 'The Value of Wetlands in Protecting Southeast Louisiana from Hurricane Storm Surges', vol. 8, no. 3, pp. 1–7 [Online]. DOI: 10.1371/journal.pone.0058715.

Burpee, A. P., Slingerland, R. L., Edmonds, D. A., Parsons, D. R., Best, J. L., Cederberg, J., McGuffin, A., Caldwell, R. L., Nijhuis, A. and Royce, J. (2015) 'Grain-Size Controls On the Morphology and Internal Geometry of River-Dominated Deltas', *Journal of Sedimentary Research*, vol. 85, no. 6, pp. 699–714 [Online]. DOI: 10.2110/jsr.2015.39.

Caldwell, R. L. and Edmonds, D. A. (2014) 'The effects of sediment properties on deltaic processes and morphologies: A numerical modeling study', *Journal of Geophysical Research: Earth Surface*, vol. 119, no. 5, pp. 961–982 [Online]. DOI: 10.1002/2013JF002965.

Costa, J. . and O'Connor, J. E. (1995) 'Geomorphically Effective Floods', *Natural and Anthopogenic Influences in Fluvial Geomorphology*, vol. 89, pp. 45–56.

Dunn, F. E., Darby, S. E., Nicholls, R. J., Cohen, S., Zarfl, C. and Fekete, B. M. (2019) 'Projections of declining fluvial sediment delivery to major deltas worldwide in response to climate change and anthropogenic stress', *Environmental Research Letters*, vol. 14, no. 8 [Online]. DOI: 10.1088/1748-9326/ab304e.

Edmonds, D. A., Shaw, J. B. and Mohrig, D. (2011) 'Topset-dominated deltas: A new model for river delta stratigraphy', *Geology*, vol. 39, no. 12, pp. 1175–1178 [Online]. DOI: 10.1130/G32358.1.

Edmonds, D. A. and Slingerland, R. L. (2007) 'Mechanics of river mouth bar formation: Implications for the morphodynamics of delta distributary networks', *Journal of Geophysical Research: Earth Surface*, vol. 112, no. 2, pp. 1–14 [Online]. DOI: 10.1029/2006JF000574.

Edmonds, D. A. and Slingerland, R. L. (2008) 'Stability of delta distributary networks and their bifurcations', *Water Resources Research*, vol. 44, no. 9, pp. 1–13 [Online]. DOI: 10.1029/2008WR006992.

Edmonds, D. A. and Slingerland, R. L. (2010) 'Significant effect of sediment cohesion on delta morphology', *Nature Geoscience*, vol. 3, no. 2, pp. 105–109 [Online]. DOI: 10.1038/ngeo730.

Ericson, J. P., Vörösmarty, C. J., Dingman, S. L., Ward, L. G. and Meybeck, M. (2006) 'Effective sea-level rise and deltas: Causes of change and human dimension implications', *Global and Planetary Change*, vol. 50, no. 1–2, pp. 63–82 [Online]. DOI: 10.1016/j.gloplacha.2005.07.004.

Fisk, H. N. (1952) *Geological Investigation of the Atchafalaya Basin and the Problem of Mississippi River Diversion: Volume 1,*.

Foufoula-Georgiou, E. (2013) 'A vision for a coordinated international effort on delta sustainability', *IAHS-AISH Proceedings and Reports*, vol. 358, no. July, pp. 3–11.

Galloway, W. E. (1975) 'Process Framework for Describing the Morphologic and

Stratigraphic Evolution of Deltaic Depositional Systems', in Broussard, M. L. (ed), *Deltas: Models for Exploration*, Houston, Texas, Houston Geological Society, pp. 87–98 [Online]. Available at http://archives.datapages.com/data/hgssp/data/022/022001/87_hgs0220087.htm.

Geleynse, N., Storms, J. E. A., Walstra, D. J. R., Jagers, H. R. A., Wang, Z. B. and Stive, M. J. F. (2011) 'Controls on river delta formation; insights from numerical modelling', *Earth and Planetary Science Letters*, Elsevier B.V., vol. 302, no. 1–2, pp. 217–226 [Online]. DOI: 10.1016/j.epsl.2010.12.013.

Hackney, C. R., Darby, S. E., Parsons, D. R., Leyland, J., Best, J. L., Aalto, R., Nicholas, A. P. and Houseago, R. C. (2020) 'River bank instability from unsustainable sand mining in the lower Mekong River', *Nature Sustainibility*, vol., no.

Iwantoro, A. P., van der Vegt, M. and Kleinhans, M. G. (2021) 'Effects of sediment grain size and channel slope on the stability of river bifurcations', *Earth Surface Processes and Landforms*, pp. 1–15 [Online]. DOI: 10.1002/esp.5141.

Kathiresan, K. and Rajendran, N. (2005) 'Coastal mangrove forests mitigated tsunami', *Estuarine, Coastal and Shelf Science*, vol. 65, no. 3, pp. 601–606 [Online]. DOI: 10.1016/j.ecss.2005.06.022.

Kleinhans, M. G., Ferguson, R. I., Lane, S. N. and Hardy, R. J. (2013) 'Splitting rivers at their seams: Bifurcations and avulsion', *Earth Surface Processes and Landforms*, vol. 38, no. 1, pp. 47–61 [Online]. DOI: 10.1002/esp.3268.

Kleinhans, M. G., Wilbers, A. W. E. and ten Brinke, W. B. M. (2007) 'Opposite hysteresis of sand and gravel transport upstream and downstream of a bifurcation during a flood in the River Rhine, the Netherlands', *Geologie en Mijnbouw/Netherlands Journal of Geosciences*, vol. 86, no. 3, pp. 273–285 [Online]. DOI: 10.1017/s0016774600077854.

McLeod, E., Chmura, G. L., Bouillon, S., Salm, R., Björk, M., Duarte, C. M., Lovelock, C. E., Schlesinger, W. H. and Silliman, B. R. (2011) 'A blueprint for blue carbon: Toward an improved understanding of the role of vegetated coastal habitats in sequestering CO2', *Frontiers in Ecology and the Environment*, vol. 9, no. 10, pp. 552–560 [Online]. DOI: 10.1890/110004.

Milan, D. J., Heritage, G. L., Large, A. R. G. and Fuller, I. C. (2011) 'Filtering spatial error from DEMs: Implications for morphological change estimation', *Geomorphology*, Elsevier B.V., vol. 125, no. 1, pp. 160–171 [Online]. DOI: 10.1016/j.geomorph.2010.09.012.

Nienhuis, J. H. and van de Wal, R. S. W. (2021) 'Projections of Global Delta Land Loss From Sea-Level Rise in the 21st Century', *Geophysical Research Letters*, vol. 48, no. 14, pp. 1–9 [Online]. DOI: 10.1029/2021GL093368.

Orton, G. J. and Reading, H. G. (1993) 'Variability of deltaic processes in terms of sediment supply, with particular emphasis on grain size.', *Sedimentology*, vol. 40, pp. 475–512.

Salter, G., Paola, C. and Voller, V. R. (2017) 'Control of delta avulsion by downstream sediment sinks', *Journal of Geophysical Research: Earth Surface* [Online]. DOI:

10.1002/2017JF004350.

Shaw, J. B. and Mohrig, D. (2014) 'The importance of erosion in distributary channel network growth, Wax Lake Delta, Louisiana, USA', *Geology*, vol. 42, no. 1, pp. 31–34 [Online]. DOI: 10.1130/G34751.1.

Shaw, J. B., Mohrig, D. and Whitman, S. K. (2013) 'The morphology and evolution of channels on the Wax Lake Delta, Louisiana, USA', *Journal of Geophysical Research: Earth Surface*, vol. 118, no. 3, pp. 1562–1584 [Online]. DOI: 10.1002/jgrf.20123.

7 Conclusion

This study aimed to show how changing sediment grainsize and critical shear stress for erosion, $\tau_{ce,}$ of fines in delta substrates influenced the morphodynamics, stability and resilience of river deltas in the face of diverse anthropogenic changes.

7.1 Summary Conclusions

In Chapter 3, it was shown that deltas that form over high τce substrates have, on average, higher altitude delta tops and larger areas of subaerial land, and as such where likely to be more resilient to changes in relative sea level. The presence of resistant bed substrates was shown to decrease the amount of incision by delta channels and hence the depth channels across delta plains. This was interpreted to cause the water surface to be higher when compared to the surrounding land, and hence make the delta-top gradient more favourable for avulsion. The increased overbank and overland flow from more frequent avulsions in turn lead to more deposition on the delta top and more equitable spread of sediment around the delta perimeter. By contrast, deltas forming over lower τce substrates eroded vertically in to the receiving basin bed, forming large, stable channels with little pressure to avulse, and effectively routed their sediment load to deep waters, leading to smaller, lower and more rugose delta tops.

Further, Chapter 4 addressed questions over the resilience of deltas prograding over differing substrate strengths to perturbations in sediment supply and relative sea level. The results showed that sediment starvation has a much larger impact on the size and morphodynamics of a delta compared to sea-level

rise, and that these impacts were enhanced by substrate strength. Sediment starvation dramatically reduces delta growth and significantly reduces the mobility of channels, whereas sea level rise only marginally reduces delta land area and causes channels to become shallower in deltas forming over low and medium erodibility substrates. Deltas forming over hard substrates (high $\boldsymbol{\tau}_{ce}$, high cohesive content) were found to have shallower, wider channels, and experienced significant channel widening and a dramatic decrease in channel mobility when fluvial sediment supply was removed. Deltas forming over softer substrates (lower $\boldsymbol{\tau}_{ce}$, higher sand content) experienced less reduction of channel mobility in the face of sediment starvation, indicating that morphodynamic processes can be continued in these systems by reworking the delta tops.

Chapter 5 demonstrated that the Wax Lake Delta is sediment limited, and interacts with its substrate chiefly through erosion. Despite this, channel beds have incised into the resistant cohesive substrate only moderately. The chapter proposes that the limited capacity of the system to erode vertically, and its limited sediment supply, may be effecting the behaviour of bifurcations on the delta by modulating the balance of erosion and deposition in the distributary channels.

Chapter 6 discusses and synthesises the implications of the above chapters on the study of deltas forming over substrates of differing resistances. Primarily, it highlights the importance of considering receiving basin properties, especially in the context of contemporary anthropogenic stresses to deltas such as relative sea level rise and sediment supply reductions. Further, the chapter addresses how delta sediment type cannot be considered as a single parameter in determining delta morphodynamics, and instead supplied, delta top and substrate sediment

should be considered separately as they effect delta morphodynamics in different ways and to different degrees, and frequently modulate impacts and perturbations. Considering the complexity of these interactions, Chapter 6 proposes a conceptual model of delta sediment in terms of a morphodynamic activity axis and a sediment autogeny axis. Considered in this way, the results of this thesis show that a switch from allogenic (sourced from upstream) to autogenic (sourced from the delta) sediment control has dramatic impact on the geometry of channels, the frequency with which those channels move and the amount of land that the delta can build for a given sediment flux. Morphodynamically active deltas (i.e. ones capable of remobilising sediment from their bed and topset) are shown to be more resilient to these impacts than morphodynamically inert delta systems.

7.2 Possible Future Work

A range of possible further directions for research could follow on from the methodological and substantive advances made herein.

Further modelling work could explore the relative effects of sediment qualities in the topset and in the fluvial supply in more detail to show how these two factors interact to give the effect normally attributed solely to fluvial supply. In addition to this, a morphodynamic study focussed on single bifurcations (similar to Edmonds and Slingerland, 2008) could be used to directly study the effects of both substrate erodibility and sediment starvation on the stability of these systems. This work could extended to look at other properties of the receiving basin such as depth and receiving basin slope, where the impacts of the characteristics of the substrate would be spatially and temporally modulated.

Modelling must continue to be supported by fieldwork to ensure the accuracy of the modelling studies as well as their applicability to real-world systems. The Wax Lake Delta offers a unique opportunity for field study, as it has been extensively monitored since its inception in the 1940's, forms in to a low tide and wave energy basin which allows easier isolation of fluvial influence, and has already been studied by multiple field (Shields et al., 2019; Bevington et al., 2017; DeLaune et al., 2016; Shaw et al., 2013) remote sensing (Olliver and Edmonds, 2017; Carle and Sasser, 2016; Shaw et al., 2016)] and modelling (Hanegan and Georgiou, 2015) studies. Further bathymetric and velocimetry field studies to provide increased temporal resolution would allow both better comparison to models and more detailed insight in to the stability and dynamics of the bifurcations on the delta.

Additionally, the field study of deltas forming over a range of known substrates would help to support the modelling presented in Chapters 3 and 4, which could necessitate both coring and sub-surface geophysical sensing to better quantify the properties of the substrate, its topography and where it interacts with delta channels. Similarly, a geological and stratigraphic study of ancient deltas could determine and consider the properties of sedimentary layers underlying the delta formation, and whether or not the delta channels had interacted with these substrates. This would allow a more thorough interpretation of the environmental drivers that formed the deposit and improve the understanding of the role of morphodynamics in evolving the stratigraphy.

7.3 References

Bevington, A. E., Twilley, R. R., Sasser, C. E. and Holm, G. O. (2017) 'Contribution of river floods, hurricanes, and cold fronts to elevation change in a deltaic floodplain, northern Gulf of Mexico, USA', *Estuarine, Coastal and Shelf Science*, Elsevier Ltd, vol. 191, pp. 188–200 [Online]. DOI: 10.1016/j.ecss.2017.04.010.

Carle, M. V. and Sasser, C. E. (2016) 'Productivity and Resilience: Long-Term Trends and Storm-Driven Fluctuations in the Plant Community of the Accreting Wax Lake Delta', *Estuaries and Coasts*, vol. 39, no. 2, pp. 406–422 [Online]. DOI: 10.1007/s12237-015-0005-9.

DeLaune, R. D., Sasser, C. E., Evers-Hebert, E., White, J. R. and Roberts, H. H. (2016) 'Influence of the Wax Lake Delta sediment diversion on aboveground plant productivity and carbon storage in deltaic island and mainland coastal marshes', *Estuarine, Coastal and Shelf Science*, Elsevier Ltd, vol. 177, pp. 83–89 [Online]. DOI: 10.1016/j.ecss.2016.05.010.

Edmonds, D. A. and Slingerland, R. L. (2008) 'Stability of delta distributary networks and their bifurcations', *Water Resources Research*, vol. 44, no. 9, pp. 1–13 [Online]. DOI: 10.1029/2008WR006992.

Hanegan, K. and Georgiou, I. (2015) 'Tidal modulated flow and sediment flux through Wax Lake Delta distributary channels : Implications for delta development', vol. 391, no. December 2014, pp. 11–14 [Online]. DOI: 10.5194/piahs-367-391-2015.

Olliver, E. A. and Edmonds, D. A. (2017) 'Defining the ecogeomorphic succession of land building for freshwater, intertidal wetlands in Wax Lake Delta, Louisiana', *Estuarine, Coastal and Shelf Science*, Elsevier Ltd, vol. 196, pp. 45–57 [Online]. DOI: 10.1016/j.ecss.2017.06.009.

Shaw, J. B., Ayoub, F., Jones, C. E., Lamb, M. P., Holt, B., Wagner, R. W., Coffey, T. S., Chadwick, J. A. and Mohrig, D. (2016) 'Airborne radar imaging of subaqueous channel evolution in Wax Lake Delta, Louisiana, USA', *Geophysical Research Letters*, vol. 43, no. 10, pp. 5035–5042 [Online]. DOI: 10.1002/2016GL068770.

Shaw, J. B., Mohrig, D. and Whitman, S. K. (2013) 'The morphology and evolution of channels on the Wax Lake Delta, Louisiana, USA', *Journal of Geophysical Research: Earth Surface*, vol. 118, no. 3, pp. 1562–1584 [Online]. DOI: 10.1002/jgrf.20123.

Shields, M. R., Bianchi, T. S., Kolker, A. S., Kenney, W. F. and Curtis, J. H. (2019) 'Factors controlling storage, sources, and diagenetic state of organic carbon in a prograding subaerial delta: Wax Lake Delta, Louisiana', *Journal of Geophysical Research: Biogeosciences*, pp. 1–17 [Online]. DOI: 10.1029/2018JG004683.

Appendix 1

Code used for finding model cell containing active delta channels for the models run in Section 3:

```
% Originally run in Matlab R2017b
%     Code used to take water velocity, bed elevation and sediment
transport and estimate the position of active delta channels

vMag = %<< Velocity Magnitude, MxNxT matrix, ms^-1
bedLevel = %<< Bed Elevation, MxNxT matrix, m relative to...
                        % model open water bounday level
waterLevel = %<< Bed Elevation, MxNxT matrix, m relative ...
                        % to model open water bounday level
waterDepth = waterLevel - bedLevel; % Water depth...
                        %  calculated from above, m
Qs_bed =  %<< Bedload transport magnitude, MxNxT matrix...
                        %
Qs_sus  = %<< Suspended sediment transport magnitude...
                        % MxNxT matrix,
Qstot = Qs_bed+Qs_sus; % Suspended sediment transport, ...
                        % magnitude calculated from above,
T = size(vMag, 3); %Total number of recorded timesteps...
                        % extracted from above

%% 1. Depth, Velocity and Sediment transport thresholds

DepthThresh = 0.5; % Water Depth threshold (absolute, m)

% Collapse first two matrix dimensions (M & N) into one,
 % then take 95th percentile of each to use as velocity and
 % sediment transport threshold
VelThresh = prctile(reshape(vMag, [302*232,T]), 95);
SedThresh = prctile(reshape(Qstot, [302*232,T]), 95);

%% 2. Make an approximate shoreline mask for the delta

binDepth = bedLevel>0; %Threshold the bed elevation at 0m

% Close the image with a 20 cell disk to remove channels...
deltaTopClose = imclose(binDepth, strel('disk', 20));
% ... and open with a 5 cell disk to remove small islands
shoreMask = imopen(deltaTopClose, strel('disk', 5));

%% 3. Identify "active channel" cells

% Create empty Active Cell matrix
ActiveCells = zeros(size(vMag));
```

```
for t = 1:T % For each recorded timestep

   % Polpulate the Active Cell matirix with cells above
    % the sediment transport and velocity thresholds
   ActiveCells(:,:,t) = (vMag(:,:,t) > VelThresh(t)) &...
                         (Qstot(:,:,t) > SedThresh(t));

end

% Remove cells shallower than water depth threshold
ActiveCells(waterDepth(:,:,t)<DepthThresh)=0;

%% 4. Image processing for channels

% Create empty Channels matrix
ChannelFinal = nan(size(ActiveCells));
% Clip to delta shoreline mask made in 2.
Channels = ActiveCells.*shoreMask;

for t = 1:T % For each recorded timestep

    % Morphological bridging algorithm
     % to connect unconnected channels
    ChannelBrid = bwmorph(Channels(:,:,t),'Bridge', 3);

    % Morphological closing to remove small gaps
    ChannelClose = imclose(ChannelBrid, strel('square',2));

    % Open image to remove objects that represent <1%
     % of total active cells
    ChannelFinal(:,:,t) = bwareaopen(ChannelClose,...
        ceil(sum(sum(ChannelClose))/100));

end
```

Appendix 2

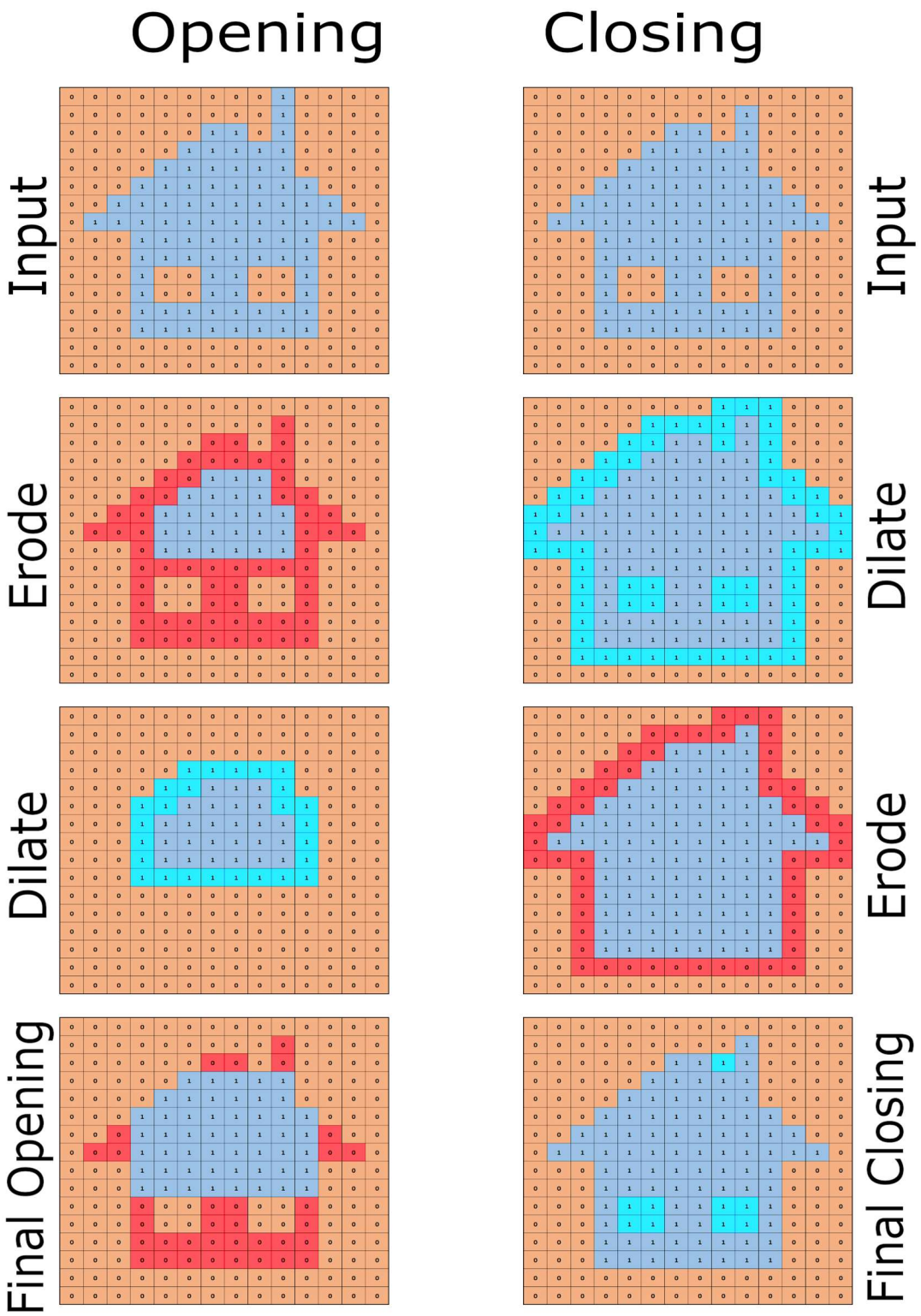

Figure i: Opening and closing operations on a binary image

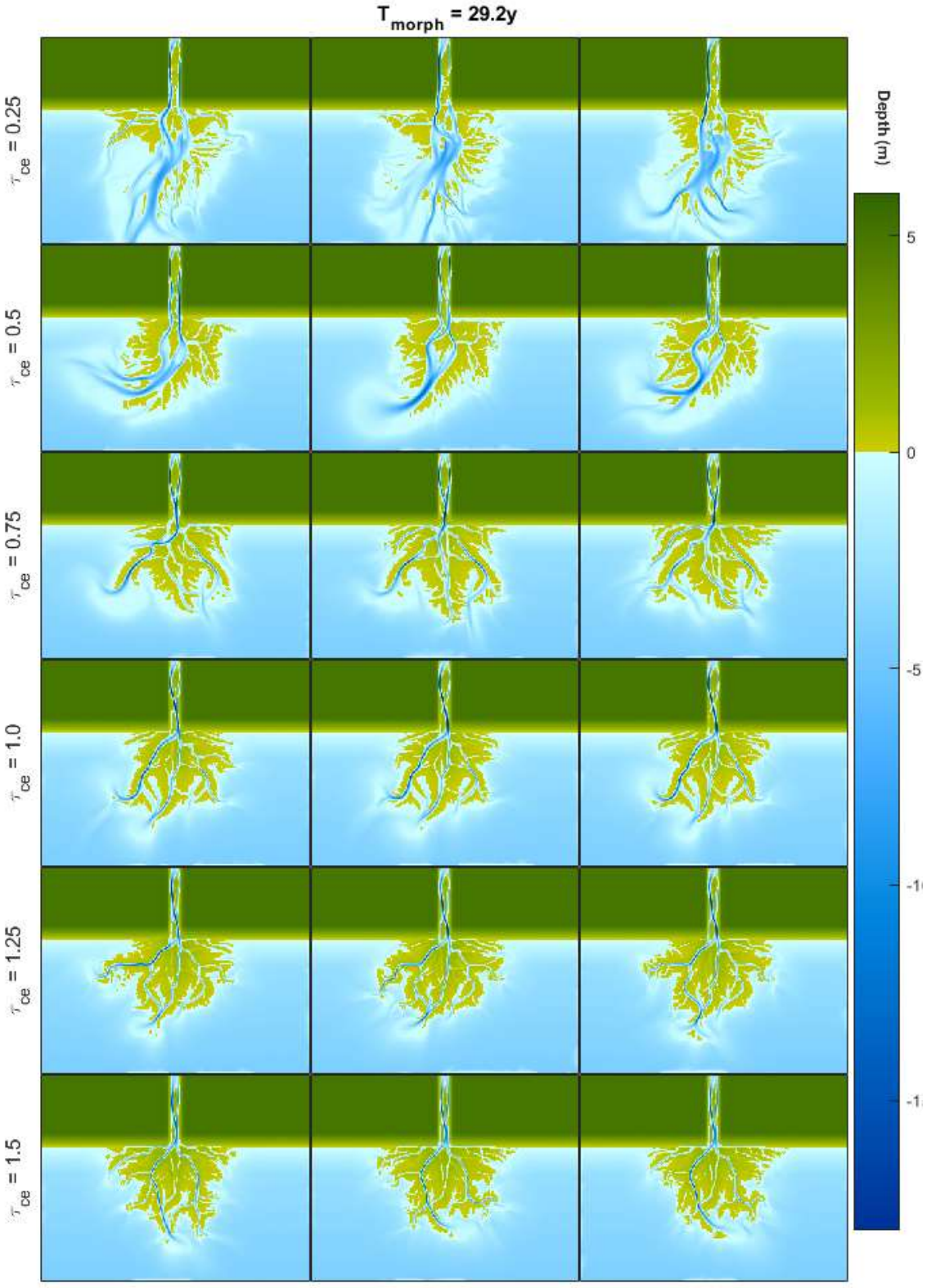

Figure ii: Bathymetry of modelled deltas at end of run.

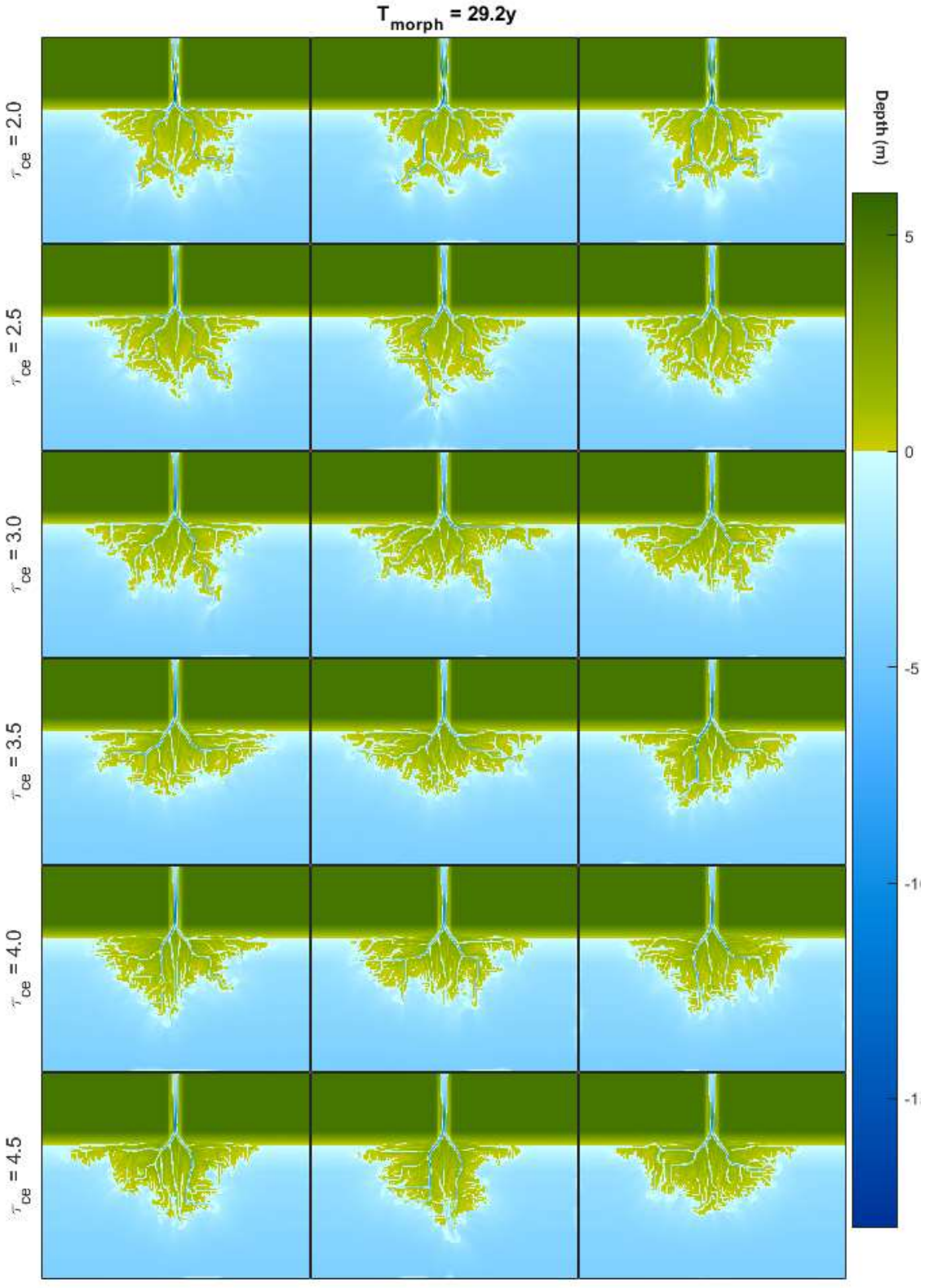

Figure iii: Bathymetry of modelled deltas at end of run, continued

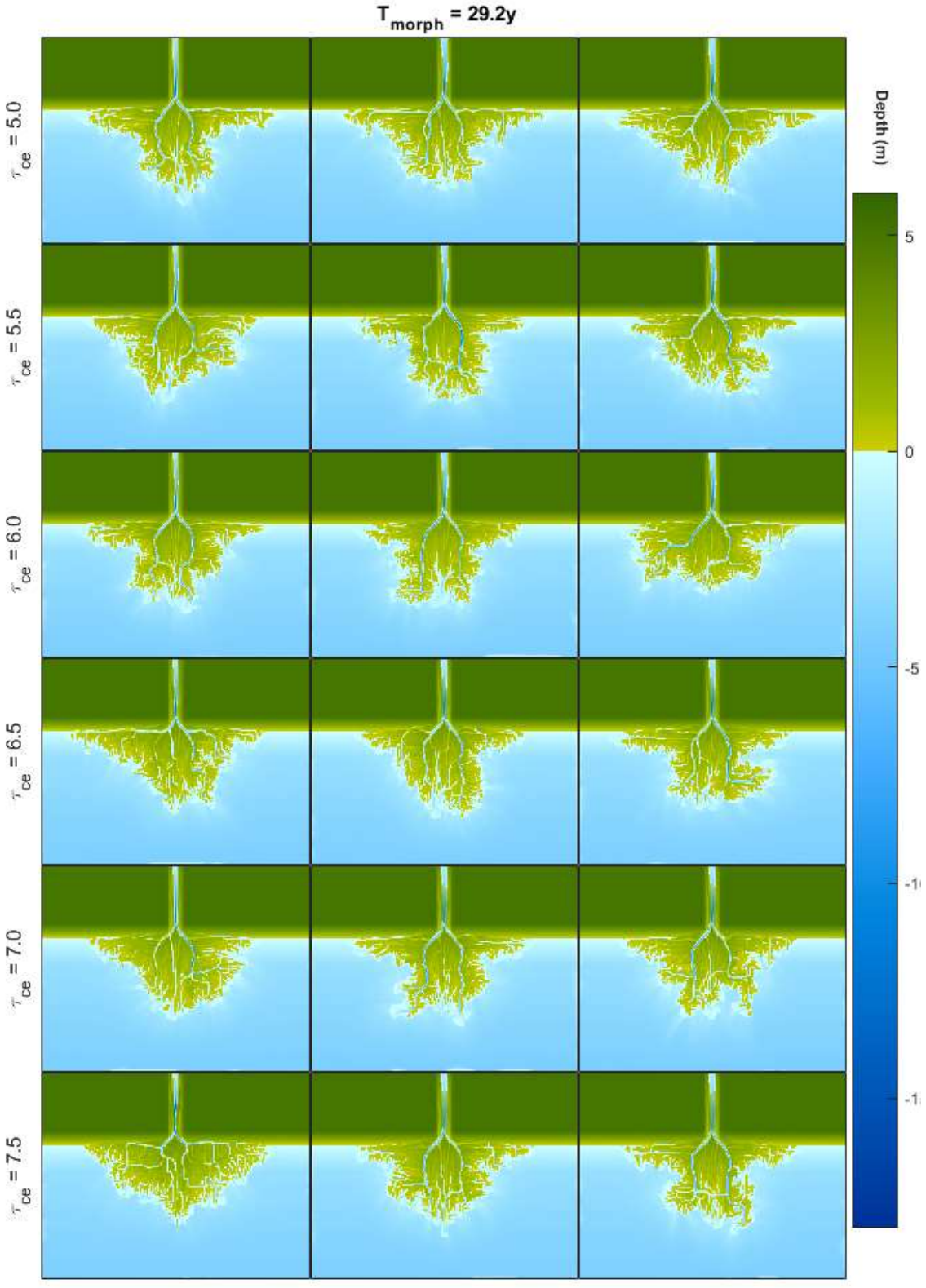

Figure iv: Bathymetry of modelled deltas at end of run, continued

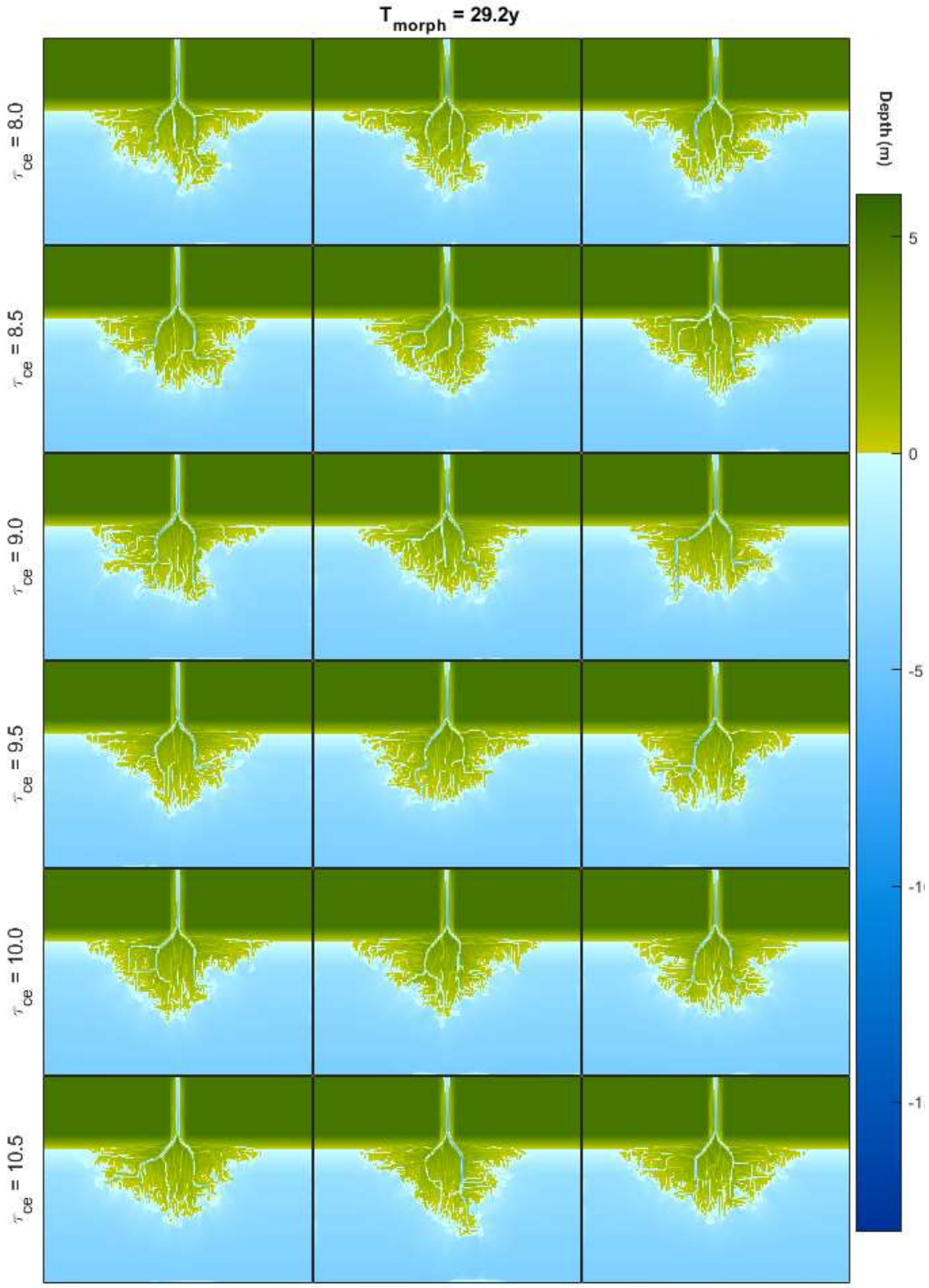

Figure v: Bathymetry of modelled deltas at end of run, continued

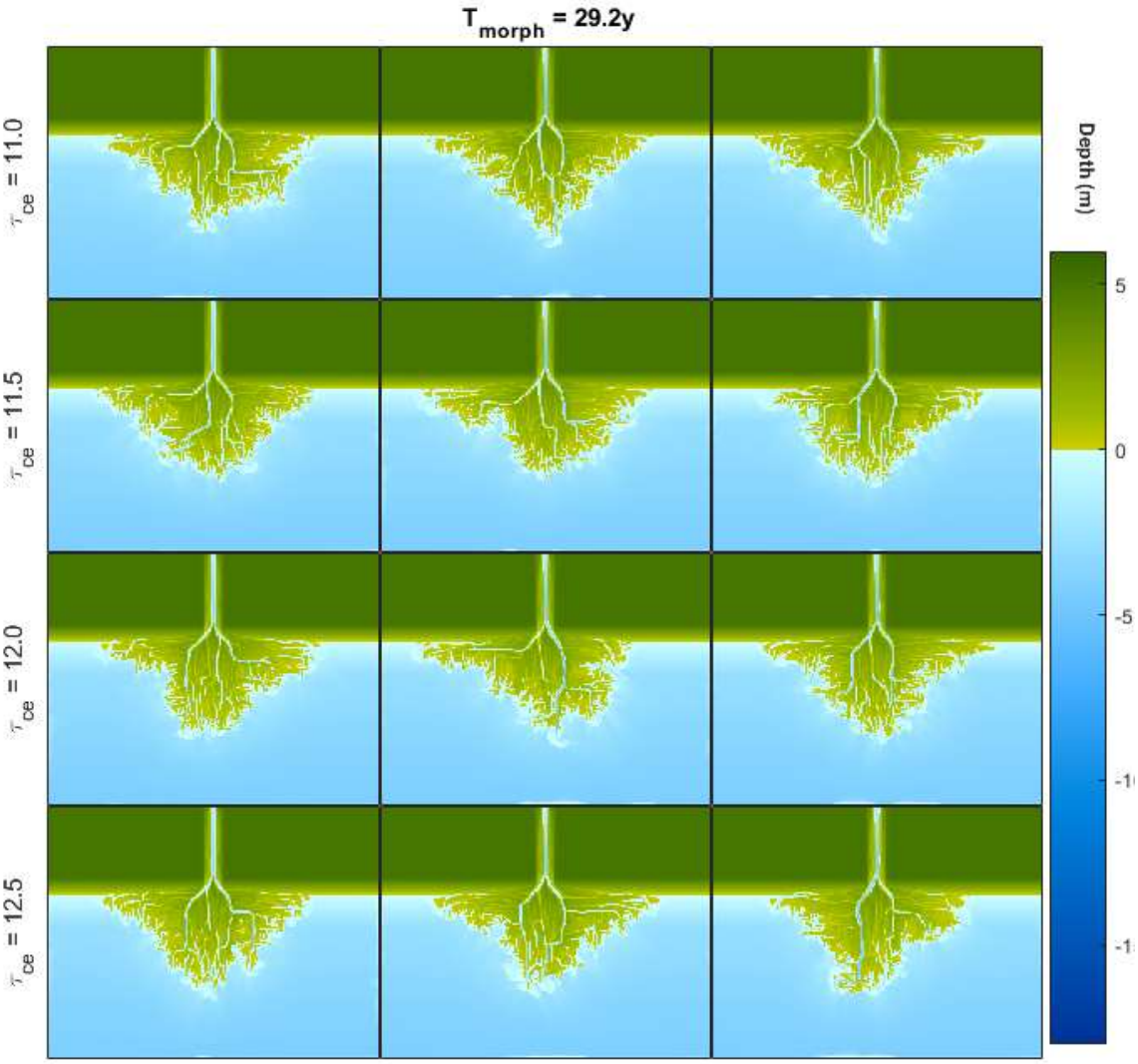

Figure vi: Bathymetry of modelled deltas at end of run, continued

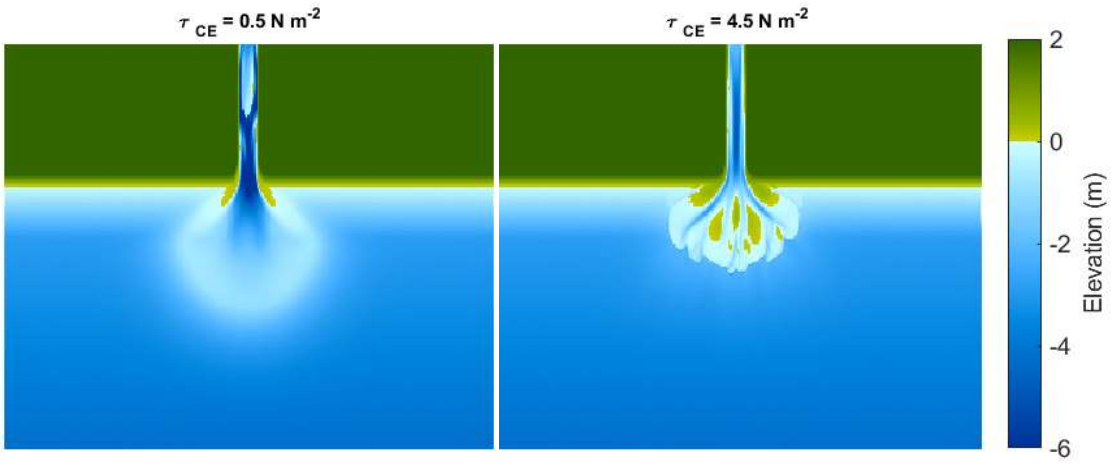

Figure vii: Example of two modelled deltas early in formation. The delta forming over a low τ_{ce} substrate has only deposited a crescent shaped bar, where the dleta forming over a high τ_{ce} substrate has deposited mouth bars and already has multible definable channels.

Appendix 3

Table A1 – Initial model run parameters. Suffixes a, b and c indicate model repeats with new elevation noise filter.

	Low Cohesivity	Moderate Cohesivity	High Cohesivity
Low Resistance	BASERUN_F1B1a BASERUN_F1B1b BASERUN_F1B1c	BASERUN_F2B1a BASERUN_F2B1b BASERUN_F2B1c	BASERUN_F3B1a BASERUN_F3B1b BASERUN_F3B1c
Moderate Resistance	BASERUN_F1B2a BASERUN_F1B2b BASERUN_F1B2c	BASERUN_F2B2a BASERUN_F2B2b BASERUN_F2B2c	BASERUN_F3B2a BASERUN_F3B2b BASERUN_F3B2c
High Resistance	BASERUN_F1B3a BASERUN_F1B3b BASERUN_F1B3c	BASERUN_F2B3a BASERUN_F2B3b BASERUN_F2B3c	BASERUN_F3B3a BASERUN_F3B3b BASERUN_F3B3c

Table A2 – Model run sediment and sea level conditions applied to the initial Base Run conditions.

Initial Conditions	Control Run	Sediment Starvation	0.15m y^{-1} Sea level Rise	Sediment Starvation and Sea Level Rise
BASERUN_F1B1a	NORMRUN_F1B1a	STARVRUN_F1B1a	SLRRUN_F1B1a	SLRSTARVRUN_F1B1a
BASERUN_F1B1b	NORMRUN_F1B1b	STARVRUN_F1B1b	SLRRUN_F1B1b	SLRSTARVRUN_F1B1b
BASERUN_F1B1c	NORMRUN_F1B1c	STARVRUN_F1B1c	SLRRUN_F1B1c	SLRSTARVRUN_F1B1c
BASERUN_F1B2a	NORMRUN_F1B2a	STARVRUN_F1B2a	SLRRUN_F1B2a	SLRSTARVRUN_F1B2a
BASERUN_F1B2b	NORMRUN_F1B2b	STARVRUN_F1B2b	SLRRUN_F1B2b	SLRSTARVRUN_F1B2b
BASERUN_F1B2c	NORMRUN_F1B2c	STARVRUN_F1B2c	SLRRUN_F1B2c	SLRSTARVRUN_F1B2c
BASERUN_F1B3a	NORMRUN_F1B3a	STARVRUN_F1B3a	SLRRUN_F1B3a	SLRSTARVRUN_F1B3a
BASERUN_F1B3b	NORMRUN_F1B3b	STARVRUN_F1B3b	SLRRUN_F1B3b	SLRSTARVRUN_F1B3b
BASERUN_F1B3c	NORMRUN_F1B3c	STARVRUN_F1B3c	SLRRUN_F1B3c	SLRSTARVRUN_F1B3c
BASERUN_F2B1a	NORMRUN_F2B1a	STARVRUN_F2B1a	SLRRUN_F2B1a	SLRSTARVRUN_F2B1a
BASERUN_F2B1b	NORMRUN_F2B1b	STARVRUN_F2B1b	SLRRUN_F2B1b	SLRSTARVRUN_F2B1b
BASERUN_F2B1c	NORMRUN_F2B1c	STARVRUN_F2B1c	SLRRUN_F2B1c	SLRSTARVRUN_F2B1c
BASERUN_F2B2a	NORMRUN_F2B2a	STARVRUN_F2B2a	SLRRUN_F2B2a	SLRSTARVRUN_F2B2a
BASERUN_F2B2b	NORMRUN_F2B2b	STARVRUN_F2B2b	SLRRUN_F2B2b	SLRSTARVRUN_F2B2b
BASERUN_F2B2c	NORMRUN_F2B2c	STARVRUN_F2B2c	SLRRUN_F2B2c	SLRSTARVRUN_F2B2c
BASERUN_F2B3a	NORMRUN_F2B3a	STARVRUN_F2B3a	SLRRUN_F2B3a	SLRSTARVRUN_F2B3a
BASERUN_F2B3b	NORMRUN_F2B3b	STARVRUN_F2B3b	SLRRUN_F2B3b	SLRSTARVRUN_F2B3b
BASERUN_F2B3c	NORMRUN_F2B3c	STARVRUN_F2B3c	SLRRUN_F2B3c	SLRSTARVRUN_F2B3c
BASERUN_F3B1a	NORMRUN_F3B1a	STARVRUN_F3B1a	SLRRUN_F3B1a	SLRSTARVRUN_F3B1a
BASERUN_F3B1b	NORMRUN_F3B1b	STARVRUN_F3B1b	SLRRUN_F3B1b	SLRSTARVRUN_F3B1b
BASERUN_F3B1c	NORMRUN_F3B1c	STARVRUN_F3B1c	SLRRUN_F3B1c	SLRSTARVRUN_F3B1c
BASERUN_F3B2a	NORMRUN_F3B2a	STARVRUN_F3B2a	SLRRUN_F3B2a	SLRSTARVRUN_F3B2a
BASERUN_F3B2b	NORMRUN_F3B2b	STARVRUN_F3B2b	SLRRUN_F3B2b	SLRSTARVRUN_F3B2b
BASERUN_F3B2c	NORMRUN_F3B2c	STARVRUN_F3B2c	SLRRUN_F3B2c	SLRSTARVRUN_F3B2c

BASERUN_F3B3a	NORMRUN_F3B3a	STARVRUN_F3B3a	SLRRUN_F3B3a	SLRSTARVRUN_F3B3a
BASERUN_F3B3b	NORMRUN_F3B3b	STARVRUN_F3B3b	SLRRUN_F3B3b	SLRSTARVRUN_F3B3b
BASERUN_F3B3c	NORMRUN_F3B3c	STARVRUN_F3B3c	SLRRUN_F3B3c	SLRSTARVRUN_F3B3c

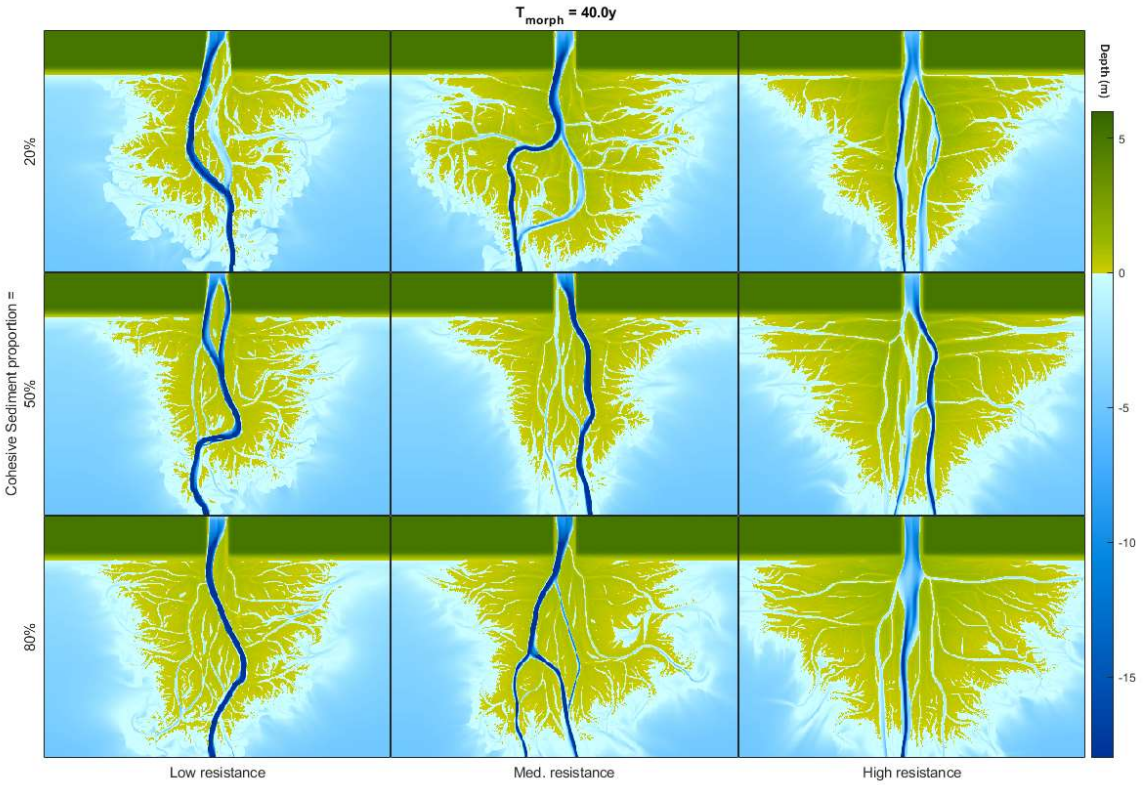

Appendix 3- i: An example of model bathymetry at end of run, showing the effects of channels prograding out of the model domain; the infinite sink there leads to a single, dominant channel with no pressure to avulse.

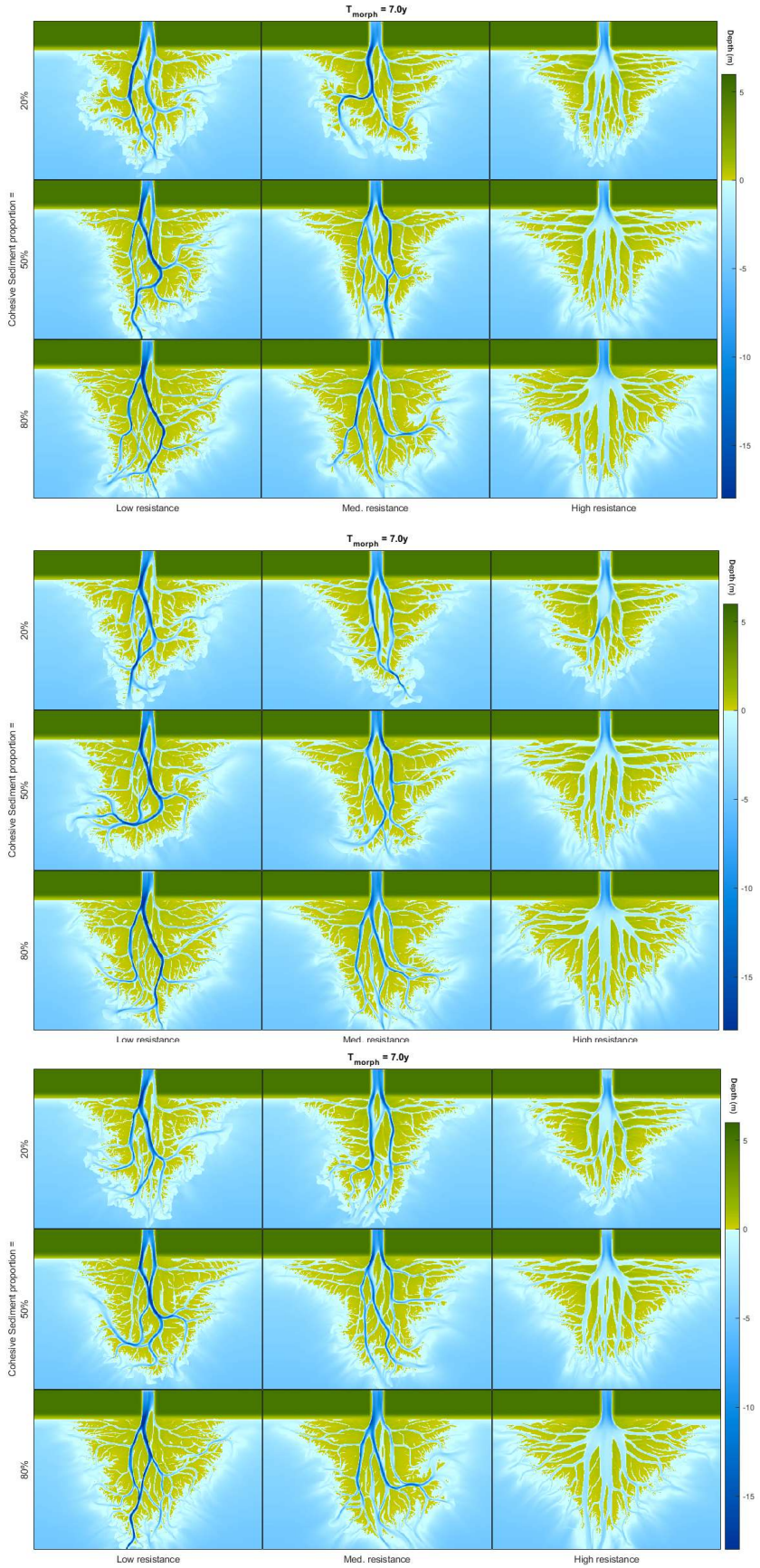

Appendix 3- ii: Bathymetry of all three repeats of each run under control conditions, after 7 morphological years of growth; the time at which they were analysed in the study.

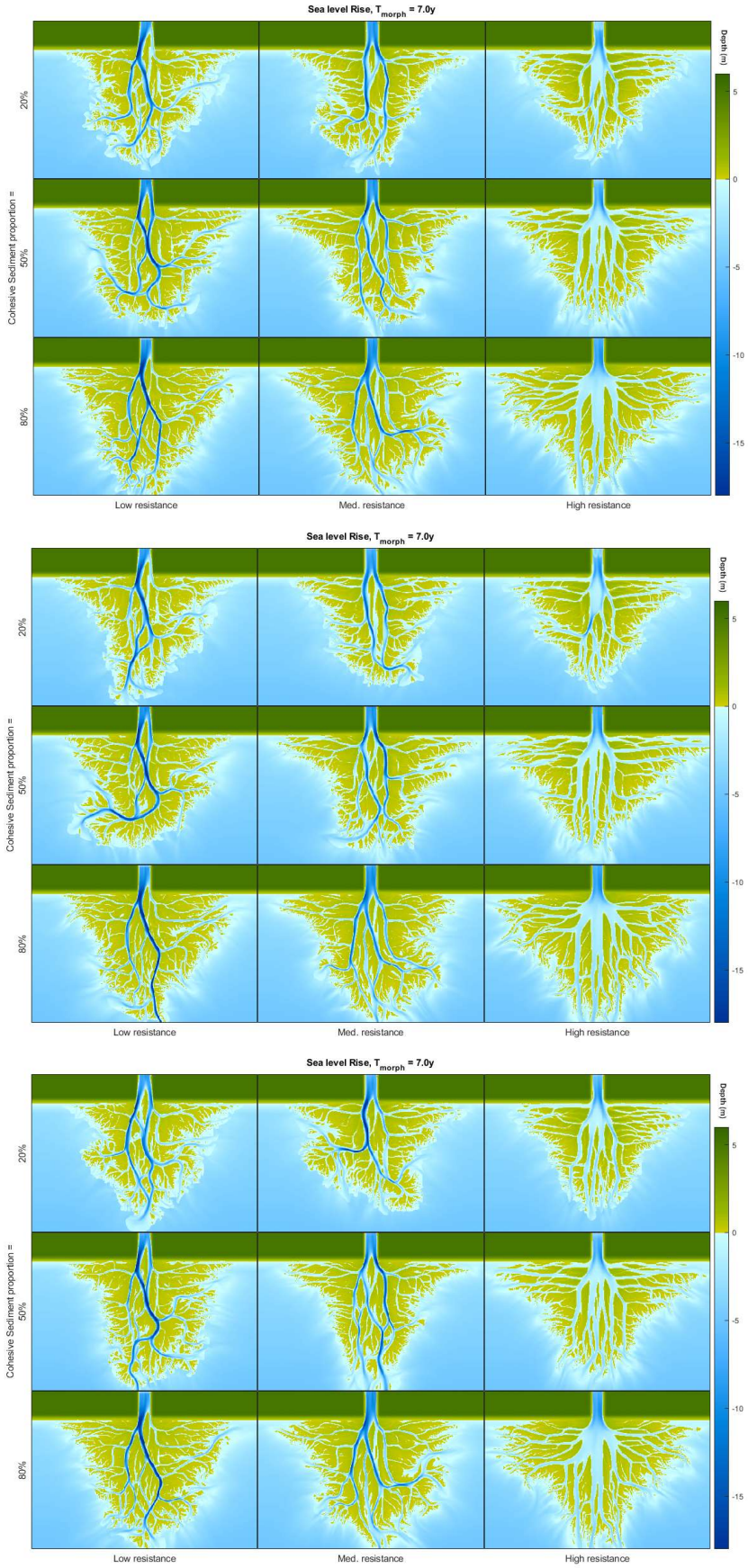

Appendix 3- iii: Bathymetry of all three repeats of each run under 1.5mm y^{-1} sea level rise, after 7 morphological years of growth; the time at which they were analysed in the study.

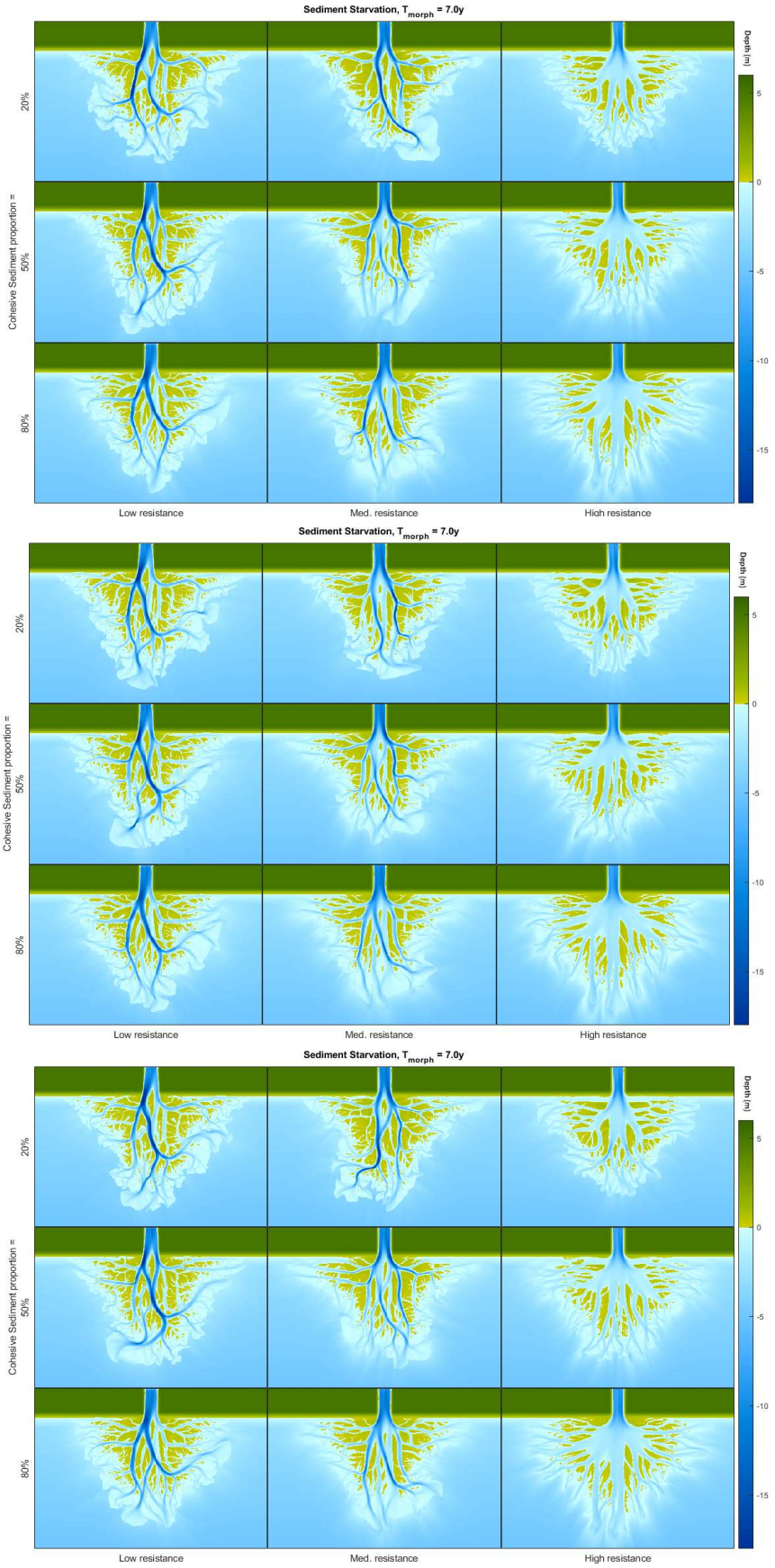

Appendix 3- iv: Bathymetry of all three repeats of each run under fluvial sediment cut-off, after 7 morphological years of growth; the time at which they were analysed in the study.

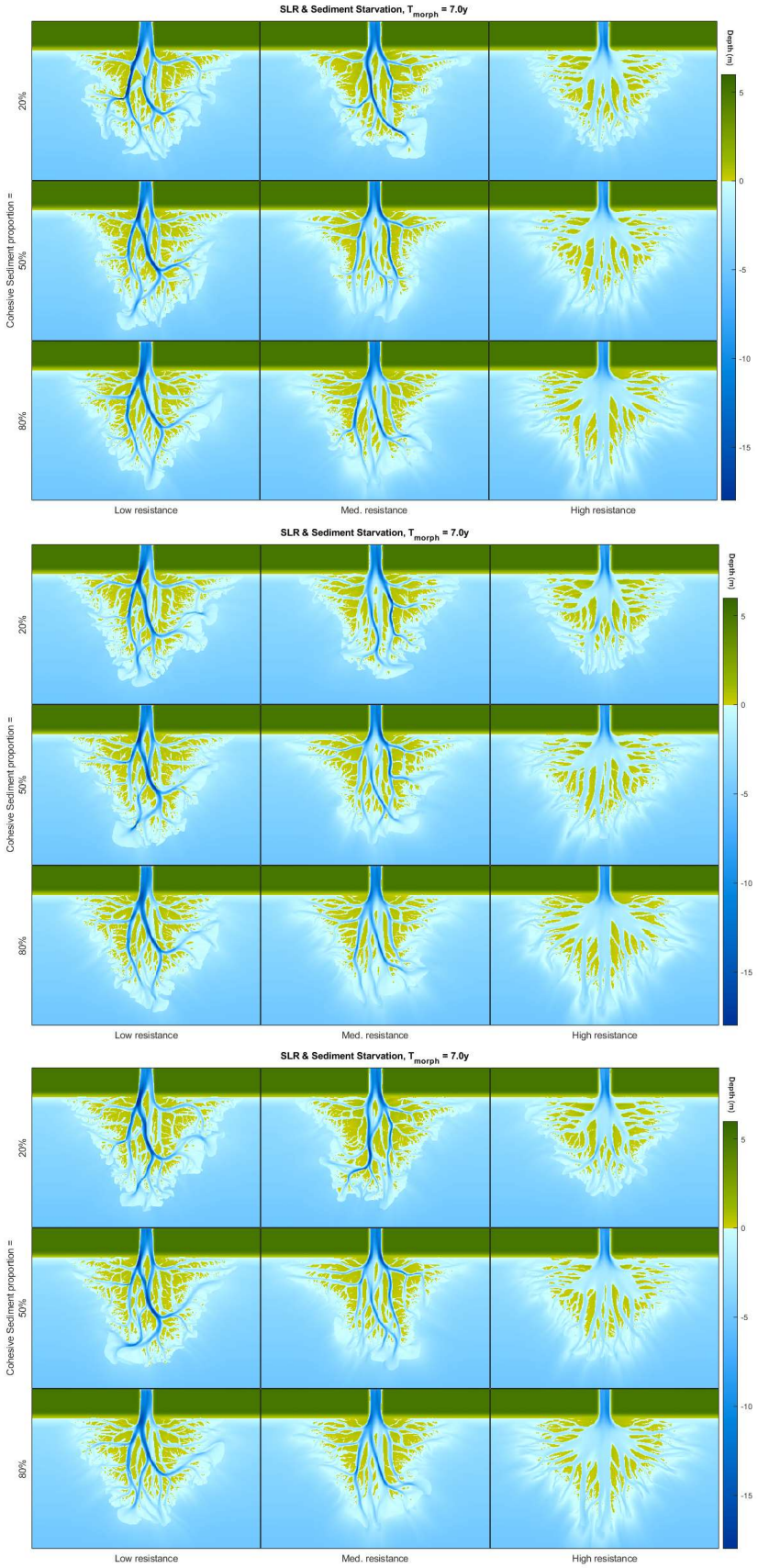

Appendix 3- v: Bathymetry of all three repeats of each run under conditions of both 1.5mm y^{-1} SLR and fluvial sediment shutoff, after 7 morphological years of growth; the time at which they were analysed in the study.

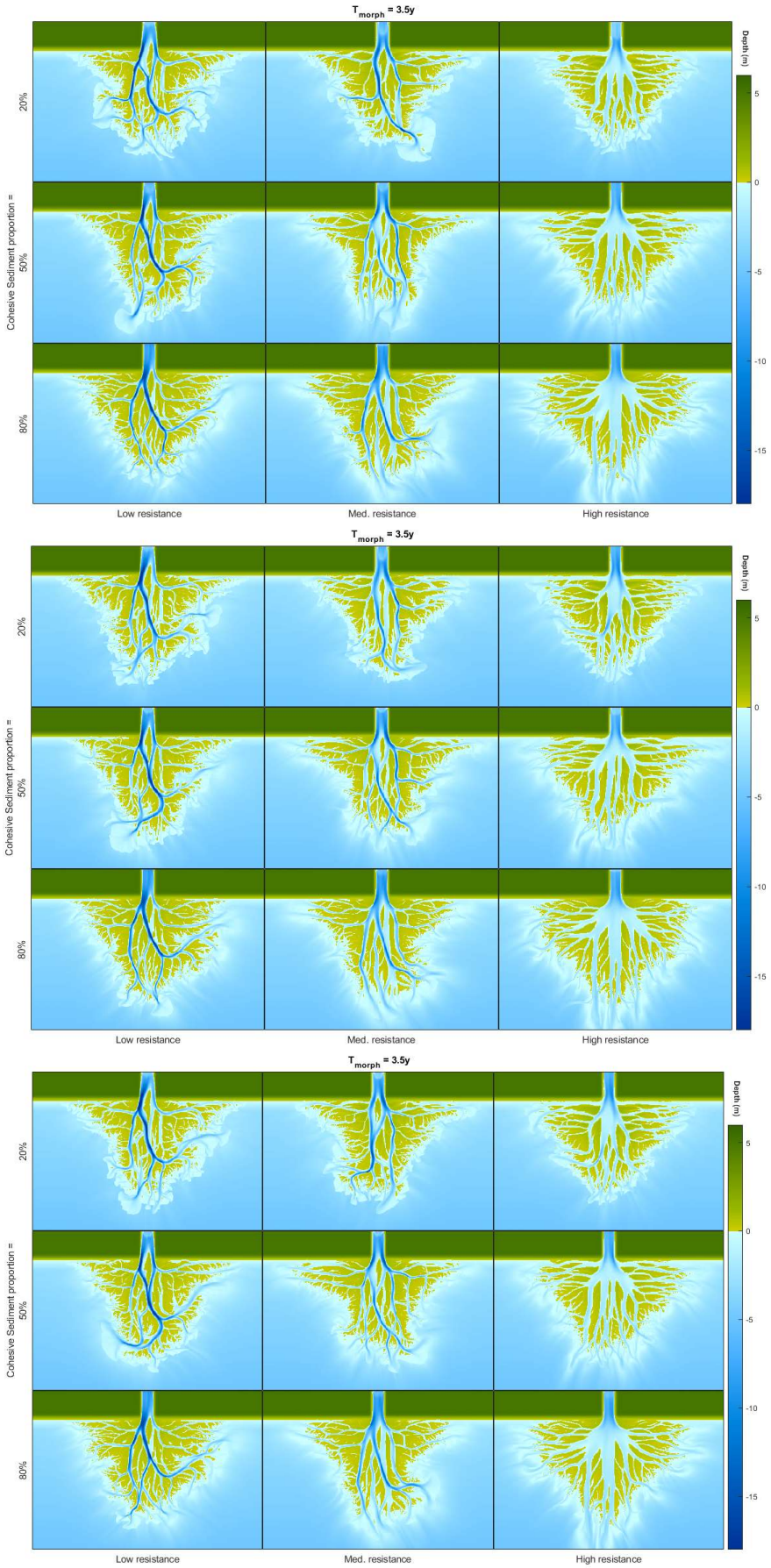

Appendix 3- vi: Bathymetry of all three repeats of each run after 3.5 morphological years of growth; the time at which they were analysed in the study.

Appendix 4

Code used for finding model cell containing active delta channels for the models run in Section 4. Modified from that used in Section 3 (appendix 1) by removing dependence on sediment transport.

```
% Originally run in Matlab R2017b
%     Code used to take water velocity and bed elevation and
estimate the position of active delta channels

vMag = %<< Velocity Magnitude, MxNxT matrix, ms^-1
bedLevel = %<< Bed Elevation, MxNxT matrix, m relative to...
                        % model open water bounday level
waterLevel = %<< Bed Elevation, MxNxT matrix, m relative ...
                        % to model open water bounday level
waterDepth = waterLevel - bedLevel; % Water depth...
                        %  calculated from above, m
T = size(vMag, 3); %Total number of recorded timesteps...
                        % extracted from above

%% 1. Depth, Velocity and Sediment transport thresholds

DepthThresh = 0.5; % Water Depth threshold (absolute, m)

% Collapse first two matrix dimensions (M & N) into one,
 % then take 95th percentile to use as the velocity
 % threshold
VelThresh = prctile(reshape(vMag, [302*232,T]), 95);


%% 2. Make an approximate shoreline mask for the delta

binDepth = bedLevel>0; %Threshold the bed elevation at 0m

% Close the image with a 20 cell disk to remove channels...
deltaTopClose = imclose(binDepth, strel('disk', 20));
% ... and open with a 5 cell disk to remove small islands
shoreMask = imopen(deltaTopClose, strel('disk', 5));

%% 3. Identify "active channel" cells

% Create empty Active Cell matrix
ActiveCells = zeros(size(vMag));


for t = 1:T % For each recorded timestep

   % Polpulate the Active Cell matirix with cells above
    % the velocity threshold
```

```
   ActiveCells(:,:,t) = (vMag(:,:,t) > VelThresh(t));

end

% Remove cells shallower than water depth threshold
ActiveCells(waterDepth(:,:,t)<DepthThresh)=0;

%% 4. Image processing for channels

% Create empty Channels matrix
ChannelFinal = nan(size(ActiveCells));
% Clip to delta shoreline mask made in 2.
Channels = ActiveCells.*shoreMask;

for t = 1:T % For each recorded timestep

    % Morphological bridging algorithm
     % to connect unconnected channels
    ChannelBrid = bwmorph(Channels(:,:,t),'Bridge', 3);

    % Morphological closing to remove small gaps
    ChannelClose = imclose(ChannelBrid, strel('square',2));

    % Open image to remove objects that represent <1%
     % of total active cells
    ChannelFinal(:,:,t) = bwareaopen(ChannelClose,...
        ceil(sum(sum(ChannelClose))/100));

end
```